

**DESIGN, ANALYSIS,
AND PERFORMANCE EVALUATION
OF A POLAR BASED CONTOURING SYSTEM**

Atef E. F. Fahim

A Thesis
in
The Faculty
of
Engineering
and
Computer Science

Presented in Partial Fulfillment of the Requirement
for the degree of Doctor of Philosophy at
Concordia University
Montreal, Quebec, Canada

March 1983

© Atef E. F. Fahim, 1983

ABSTRACT
DESIGN, ANALYSIS,
AND PERFORMANCE EVALUATION
OF A POLAR BASED CONTOURING SYSTEM

Atef E. F. Fahim, Ph.D.
Concordia University, 1983

This thesis presents the design, analysis, and performance evaluation of a polar based contouring system. The system consists of a contour digitizer and an NC machine. The contour digitizer may be a template digitizer or a software digitizer. The combination of the template digitizer and NC machine (TD/NC machine) operates as a copying machine. While the combination of the software digitizer and NC machine (SD/NC machine) resembles in operation a conventional NC system.

The polar contouring system employs an open loop digital control scheme that does not require an on-board computer.

The system offers a number of desirable features over both conventional copying machines and NC systems. Speed scaling, and scaling of contouring speed without the need of reprocessing the contour information are among these features. Furthermore, when operated as an SD/NC machine, the system is capable of tracking a contour with constant speed.

A detailed description of the polar contouring system and the salient features of the prototypes of the template and software digitizers, and of the NC machine that has been built is presented. An analysis of the contouring error due to the incremental approximation of the contour is carried out. An optimization procedure that locates the contour pole with respect to the machine pole for a minimum area error is outlined. Test results of locating the poles of three test contours for a minimum area error are also presented. A dynamic analysis of the NC machine that includes the type of contour, the type and magnitude of the load, and the contouring speed is presented. The results of the analysis indicate that in general, increasing the magnitude of the load or the contouring speed increases the torque required from the axes-drives. It is also shown that the torque increases rapidly with the decrease of the radius of curvature of the contour. The maximum allowable load and contouring speed are shown to be a function of the location of the contour pole with respect to the machine pole. An optimization procedure to locate the contour pole relative to the machine pole is presented for maximizing the allowable limits on load and on contouring speed. A procedure using composite graphs is provided for rapid calculation of the maximum torque required and available from the axes-drives in different contouring operations.

ACKNOWLEDGEMENT

The author appreciates the support and guidance provided by both his supervisors Dr. Seshadri Sankar and Dr. Richard M. H. Cheng.

The author would like also to thank Mr. Roy Blakely, Mr. Dave Hargreaves, and Mrs. Ilana Crawford for their help.

The support provided by the Department of Mechanical Engineering at Concordia University, as well as the scholarships provided by NSERC and the FCAC is acknowledged.

This work was made possible by NSERC grants no. A3685 and A8662, and the FCAC grant no. 042110.

TABLE OF CONTENTS

ABSTRACT	i
ACKNOWLEDGEMENT	iii
LIST OF FIGURES	xi
LIST OF TABLES	xxiii
NOMENCLATURE	xxiv
CHAPTER 1: Introduction	
1.1 : General	1
1.2 : Copying machines	4
1.3 : NC machines.	7
1.4 : Thesis outline	17
CHAPTER 2: CONCEPT AND OPERATION OF THE CONTOURING SYSTEM	
2.1 : Introduction	20
2.2 : Prototype template digitizer	23
2.3 : Software digitizer	38
2.4 : Prototype polar NC machine	48
CHAPTER 3: SALIENT FEATURES, ADVANTAGES AND DISADVANTAGES OF THE POLAR CONTOURING SYSTEM	
3.1 : Introduction	56
3.2 : Method of supplying contour information	57
3.3 : Complexity of controller	58
3.4 : Versatility	59

3.5 : Contouring speed	59
3.6 : Scaling of contouring speed	65
3.7 : Size scaling	67
3.8 : Accuracy of contouring	70
3.9 : Work area	71
3.10: Power utilization of the axes-drives	71
3.11: Reference position	71
3.12: Cost	72

CHAPTER 4: CONTOUR LOCATION FOR MINIMUM CONTOURING ERRORS ON THE POLAR MACHINE

4.1 : Introduction	75
4.2 : Contouring error criterion	76
4.3 : Factors affecting the area error	80
4.4 : An optimization problem for area error minimization	81
4.5 : Selection of an alternate objective function	84
4.6 : Experimental verification of the objective function F_1	94
4.7 : Formulation of the optimization problem	95
4.8 : Optimization algorithm	98
4.9 : Case study results on the suitability of the objective function in predicting the location for minimum area error	99
4.10: Summary	105

CHAPTER 5: DYNAMIC ANALYSIS OF THE POLAR NC MACHINE

5.1 : Introduction	107
5.2 : Kinematic analysis of the NC machine arm and carriage mechanism	108
5.2.1: Case 1: Tool with no offset (zero ra- dius)	110
5.2.2: Case 2: Tool with finite radius	112
5.3 : Dynamic analysis of the polar NC machine	113
5.4 : Torque speed relationship of a stepping motor	119
5.5 : Effect of the contouring speed, load, and contour on the axes-drives torque	121
5.5.1: Inertial load	127
5.5.2: Grinding application	139
5.6 : Effect of relative location between the contour pole and the machine pole on the torque ratios	148
5.6.1: Inertial load	150
5.6.2: Grinding application	155
5.7 : Summary	160

**CHAPTER 6: ANALYTICAL STUDY FOR PARAMETRIC VARIATION
AND OPTIMUM LOADING OF THE NC MACHINE**

6.1 : Introduction	163
6.2 : Effect of inertial load	164

6.2.1: Variable inertial loads with constant contouring speed	164
6.2.2: Constant inertial load with variable contouring speeds	165
6.3 : Effect of dissipative load (Grinding ap- plication)	170
6.3.1: Variable dissipative loads with con- stant contouring speed	170
6.3.2: Constant dissipative load with vari- able contouring speeds	171
6.4 : Effect of changes in the parameters on the location of the maximum torque and torque ratios along the contour	172
6.4.1: Inertial load	175
6.4.2: Grinding application	179
6.5 : Highlights of the analytical parametric study	182
6.5.1: Inertial load	182
6.5.2: Grinding application	183
6.6 : Optimum loading of the polar NC machine	183
6.6.1: Total torque required on both axes in contouring operation	184
6.6.2: Formulation of the optimization prob- lem	192
6.6.3: Results of loading optimization for four test contours	201

**CHAPTER 7: GRAPHICAL PROCEDURE FOR EVALUATING THE LOAD
AND THE LOAD CARRYING CAPACITY OF THE NC
MACHINE**

7.1 : Introduction	205
7.2 : Description and organization of the composite graphs	206
7.2.1: Inertial load	206
7.2.2: Grinding application	209
7.3 : Description of the graphical procedure	218
7.3.1: Inertial load	219
7.3 2: Grinding application	222

**CHAPTER 8: CONCLUSION AND RECOMMENDATION FOR FUTURE
WORK**

8.1 : Conclusion and major highlights	226
8.2 : Recommendation for future work	230

**APPENDIX A: ASSEMBLY DRAWINGS OF THE PROTOTYPE
TEMPLATE DIGITIZER AND NC MACHINE**

A.1 : Assembly drawings of the prototype template digitizer	A.1
A.2 : Assembly drawings of the prototype NC ma- chine	A.4

APPENDIX B: ELECTRIC DIFFERENTIAL MECHANISM

B.1 : Introduction	B.1
--------------------	-----

B.2 : Analysis of the electric differential mechanism	B.2
B.3 : Performance of the electric differential	B.5
B.4 : Control scheme for the electric differential mechanism	B.6

APPENDIX C: SOFTWARE DIGITIZER ALGORITHMS

C.1 : Digitizer algorithm	C.1
C.2 Output algorithm	C.5

APPENDIX D: PERFORMANCE EVALUATION OF THE TEMPLATE DIGITIZER

D.1 : Introduction	D.1
D.2 : Testing circuit	D.1
D.3 Results of testing	D.8

APPENDIX E: ALGORITHMS USED FOR AREA ERROR MINIMIZATION

E.1 : Algorithm for area error calculation	E.1
E.2 : Optimization algorithm for locating the contour pole with respect to the machine pole for minimum area error	E.11

APPENDIX F: STEPPING MOTOR PULL-OUT TORQUE SPEED CHARACTERISTICS

F.1 : Introduction	F.1
--------------------	-----

F.2 : Derivation of the pull-out torque speed
relationship

F.9

F.3 : Experimental verification of the pull-out
torque relationship

F.14

LIST OF FIGURES

CHAPTER 1: INTRODUCTION

Figure 1.1	: 2D, 2½D, and 3D Contouring Operations.	3
Figure 1.2	: Pantograph Copier.	5
Figure 1.3	: Schematic Diagram of a Template Copying Machine/Template Configuration.	8
Figure 1.3	: Schematic Diagram of a Template Copying Machine/Template Configuration.	9
Figure 1.4	: Schematic Diagram of an NC Machine.	14
Figure 1.5	: Velocity Diagram in Contouring Operations.	14
Figure 1.6	: Polar Plotter.	16

CHAPTER 2: CONCEPT AND OPERATION OF THE CONTOURING SYSTEM

Figure 2.1	: Block Diagram of a Polar Contouring System.	21
Figure 2.2	: Schematic Diagram of the Template Digitizer.	24
Figure 2.3.a	: Photograph of the Prototype Template Digitizer.	25
Figure 2.3.b	: Template Digitizer Arm Assembly.	26

Figure 2.3.c : Template Digitizer Angular Shaft Encoder.	27
Figure 2.3.d : Template Digitizer Tracking Roller Mechanism.	27
Figure 2.4 : Sample Template Configurations.	29
Figure 2.5 : Schematic Diagram of the Roller Mechanism.	31
Figure 2.6 : Pictorial Diagram of the Roller Mechanism.	32
Figure 2.7 : Path of the Roller Mechanism for Curved Templates.	34
Figure 2.8 : Sample Shaft Encoder Signals.	36
Figure 2.9 : Conditioning/Combining Circuit for Shaft Encoder Signals.	36
Figure 2.10 : Vector Representation of the Polar System in Contouring.	40
Figure 2.11 : Flowchart of the Digitizer Algorithm.	43
Figure 2.12 : Flowchart of the Output Algorithm.	46
Figure 2.13 : Circuit for Decoding the Software Digitizer Signals.	47
Figure 2.14 : Schematic Diagram of the Prototype NC Machine.	49
Figure 2.15.a: Photograph of the Prototype NC Machine.	50
Figure 2.15.a NC Machine Axes-Drives Arrangement.	51

Figure 2.15.a: NC Machine Arm and Carriage Assemblies.	52
Figure 2.16 : Decoder Circuit for NC Machine Control Signals.	54

CHAPTER 3: SALIENT FEATURES, ADVANTAGES AND DISADVANTAGES OF THE POLAR CONTOURING SYSTEM

Figure 3.1 : Schematic Diagram of the Roller Mechanism in Contouring.	61
Figure 3.2 : Contouring Speed Error Versus V_t .	64
Figure 3.3 : Photographs of Templates Used in Testing.	66
Figure 3.4.a : Size Scaling on the Polar Contouring System.	69
Figure 3.4.b : Logic Circuit for Size Scaling.	69

CHAPTER 4: CONTOUR LOCATION FOR MINIMUM CONTOURING ERRORS ON THE POLAR MACHINE

Figure 4.1 : Error Criteria in the Contouring Operation.	77
Figure 4.2 : Salient Geometric Parameters for the Area Error Calculation.	79
Figure 4.3 : Different Tool Paths When Tracking a Contour.	82
Figure 4.4 : Normalized F_{sum} and ϵ_a Versus γ .	88
Figure 4.5 : Normalized F_{dif} and ϵ_a Versus γ .	90

Figure 4.6	: Normalized Objective Function F_1 Versus γ .	92
Figure 4.7	Effect of the Penalty Factor K/R_m on the Objective Function F_1	93
Figure 4.8	: Theoretical and Experimental Results of the Objective Function F_1 for a Straight Line	96
Figure 4.9	: Topographical Plots of the Objective Function F_1 for the Witch of Agnesi Contour.	100
Figure 4.10	: Topographical Plots of the Objective Function F_1 for the Limacon of Pascal Contour.	101
Figure 4.11	: Topographical Plots of the Objective Function F_1 for the Serpentine Contour.	103

CHAPTER 5: DYNAMIC ANALYSIS OF THE POLAR NC MACHINE

Figure 5.1	Vector Representation of the Polar System in Contouring.	109
Figure 5.2	: Pictorial Diagram of the NC Ma- chine.	114
Figure 5.3	: Free Body Diagram of the NC Ma- chine.	115
Figure 5.4	: Test Contour : Circle.	123
Figure 5.5	: Test Contour : Witch of Agnesi.	124
Figure 5.6	: Test Contour : Limacon of Pascal.	125

Figure 5.7	: Test Contour : Serpentine.	126
Figure 5.8	: Radial Axis Torque Ratio Plots for Circular Contour (Inertial Load).	130
Figure 5.9	: Angular Axis Torque Ratio Plots for Circular Contour (Inertial Load).	132
Figure 5.10	: Radial Axis Torque Ratio Plots for Witch of Agnesi Contour (Inertial Load).	134
Figure 5.11	: Angular Axis Torque Ratio Plots for Witch of Agnesi Contour (Inertial Load).	135
Figure 5.12	: Radial Axis Torque Ratio Plots for Limacon of Pascal Contour (Inertial Load).	137
Figure 5.13	: Angular Axis Torque Ratio Plots for Limacon of Pascal Contour (Inertial Load).	138
Figure 5.14	: Radial Axis Torque Ratio Plots for Serpentine Contour (Inertial Load).	140
Figure 5.15	: Angular Axis Torque Ratio Plots for Serpentine Contour (Inertial Load).	141
Figure 5.16	: Torque Ratio Plots for the Circular Contour (Grinding Application).	143

Figure 5.17	: Torque Ratio Plots for the Witch of Agnesi (Grinding Application).	146
Figure 5.18	: Torque Ratio Plots for the Limacon of Pascal (Grinding Application).	147
Figure 5.19	: Torque Ratio Plots for the Serpentine (Grinding Application).	149
Figure 5.20	: Torque Ratio Plots for Machine Pole at the Location of Minimum Area Error : Witch of Agnesi Contour (Inertial Load).	151
Figure 5.21	: Torque Ratio Plots for Machine Pole at the Location of Minimum Area Error : Limacon of Pascal, Contour (Inertial Load).	152
Figure 5.22	: Torque Ratio Plots for Machine Pole at the Location of Minimum Area Error : Serpentine Contour (Inertial Load).	153
Figure 5.22	: Torque Ratio Plots for Machine Pole at the Location of Minimum Area Error : Serpentine Contour (Inertial Load).	154
Figure 5.23	: Torque Ratio Plots for Machine Pole at the Location of Minimum Area Error : Witch of Agnesi Contour (Grinding Application).	156
Figure 5.24	: Torque Ratio Plots for Machine	

	Pole at the Location of Minimum Area Error : Limaçon of Pascal Contour (Grinding Application).	157
Figure 5.25 :	Torque Ratio Plots for Machine Pole at the Location of Minimum Area Error : Serpentine Contour (Grinding Application).	158
Figure 5.25 :	Torque Ratio Plots for Machine Pole at the Location of Minimum Area Error : Serpentine Contour (Grinding Application).	159

CHAPTER 6: ANALYTICAL STUDY FOR PARAMETRIC VARIATION AND OPTIMUM LOADING OF THE NC MACHINE

Figure 6.1 :	Sensitivity Parameter $\Gamma_R^{(I)}$ Versus V_t	168
Figure 6.2 :	Sensitivity Parameter $\Gamma_\theta^{(I)}$ Versus V_t	169
Figure 6.3 :	Sensitivity Parameter $\Gamma_R^{(G)}$ Versus V_t	173
Figure 6.4 :	Sensitivity Parameter $\Gamma_\theta^{(G)}$ Versus V_t	174
Figure 6.5 :	$d\theta/dM_c$ Versus ρ for the Maximum Angular Axis Torque for an Inertial Load.	178
Figure 6.6 :	Sum of Torques Versus Angular Location for the Circular Contour	

	(Inertial Load).	185
Figure 6.7	: Sum of Torques Versus Angular Location for the Witch of Agnesi Contour (Inertial Load).	186
Figure 6.8	: Sum of Torques Versus Angular Location for the Limacon of Pascal Contour (Inertial Load).	187
Figure 6.9	: Sum of Torques Versus Angular Location for the Serpentine Contour (Inertial Load).	188
Figure 6.10	: Sum of Torques Versus Angular Location for the Witch of Agnesi Contour, Pole at Location of Minimum Area Error (Inertial Load).	189
Figure 6.11	: Sum of Torques Versus Angular Location for the Limacon of Pascal Contour, Pole at Location of Minimum Area Error (Inertial Load).	190
Figure 6.12	: Sum of Torques Versus Angular Location for the Serpentine Contour, Pole at Location of Minimum Area Error (Inertial Load).	191
Figure 6.13	: Sum of Torques Versus Angular Location for the Circular Contour (Grinding Application).	193

Figure 6.14	: Sum of Torques Versus Angular Location for the Witch of Agnesi Contour (Grinding Application).	194
Figure 6.15	: Sum of Torques Versus Angular Location for the Limacon of Pascal Contour (Grinding Application).	195
Figure 6.16	: Sum of Torques Versus Angular Location for the Serpentine Contour (Grinding Application).	196
Figure 6.17	: Sum of Torques Versus Angular Location for the Witch of Agnesi Contour, Pole at Location of Minimum Area Error (Grinding Application).	197
Figure 6.18	: Sum of Torques Versus Angular Location for the Limacon of Pascal Contour, Pole at Location of Minimum Area Error (Grinding Application).	198
Figure 6.19	: Sum of Torques Versus Angular Location for the Serpentine Contour, Pole at Location of Minimum Area Error (Grinding Application).	199

CHAPTER 7: GRAPHICAL PROCEDURE FOR EVALUATING THE LOAD AND LOAD CARRYING CAPACITY OF THE NC MACHINE

Figure 7.1	: Torque Required and Available from the Radial Axis-Drive (Inertial Load).	207
Figure 7.2	: Torque Required and Available from the Angular Axis-Drive (Inertial Load). Part 1 of 2.	209
Figure 7.3	: Torque Required and Available from the Angular Axis-Drive (Inertial Load). Part 2 of 2.	210
Figure 7.4	: Torque Required and Available from the Radial Axis-Drive (Grinding Application). Part 1 of 2.	213
Figure 7.5	: Torque Required and Available from the Radial Axis-Drive (Grinding Application). Part 2 of 2.	214
Figure 7.6	: Torque Required and Available from the Angular Axis-Drive (Grinding Application). Part 1 of 2.	216
Figure 7.7	: Torque Required and Available from the Angular Axis-Drive (Grinding Application). Part 2 of 2.	217

APPENDIX A: ASSEMBLY DRAWINGS OF THE PROTOTYPE

TEMPLATE DIGITIZER AND NC MACHINE

Figure A.1	: Template Digitizer Arm Assembly.	A.2
Figure A.2	: Template Digitizer Carriage Assembly.	A.3

Figure A.3 : Template Digitizer Angular Shaft
Encoder Assembly. A.3

Figure A.4 : Polar NC Machine Arm and Carriage
Assembly. A.4

APPENDIX B: ELECTRIC DIFFERENTIAL MECHANISM

Figure B.1 : Circuit Diagram of an Electric
Differential Mechanism. B.4

Figure B.2 : Torque-Speed Characteristics of an
Electric Differential Mechanism. B.8

**APPENDIX D: PERFORMANCE EVALUATION OF THE TEMPLATE
DIGITIZER**

Figure D.1 : Block Diagram of the Circuits Used
in the Performance Evaluation of
the Template Digitizer. D.2

Figure D.2 : Recording Circuit for the Encoder
Signals. D.4

Figure D.3 : Sampler Circuit for the Recorded
Encoder Signals. D.6

**APPENDIX F: STEPPING MOTOR PULL-OUT TORQUE SPEED
CHARACTERISTICS**

Figure F.1 : Axial View of a D-C P-M Stepping
Motor. F.2

Figure F.2 : Section View of a D-C P-M Step-
ping Motor. F.3

Figure F.3	: Stepping Motor with 5 Teeth on the Rotor.	F.5
Figure F.4	: Drive Circuit for Stepping Motor.	F.5
Figure F.5	: Stepping Motor Rotor Positions in Sequential Stepping.	F.8
Figure F.6	: Stepping Voltage Pattern for Wave Energization.	F.10
Figure F.7	Torque of a Stepping Motor.	F.16

LIST OF TABLES

Table 3.1: Comparison Between Existing Contouring Systems and the Polar Contouring System.	74
Table 4.1: Test Contour Parameters and Results of Optimization for Area Error Minimization.	104
Table 5.1: System/Operating Parameters.	129
Table 6.1: Results of Optimization for Loading Conditions (Inertial Load).	202
Table 6.2: Results of Optimization for Loading Conditions (Grinding Application).	204
Table B.1: Data of the Motors Used in the Electric Differential Mechanism.	B.7
Table F.6: Switching Sequences for D-C P-M Stepping Motors.	F.6

NOMENCLATURE

a_t	acceleration of the NC machine carriage along the tangent to the contour.
$a^{(i)}$	area error between the contour and its approximating curve in the i -th angular resolution.
a_c	acceleration of the NC machine carriage.
a_{cn} , a_{cr}	acceleration of the NC machine carriage normal to the arm and along the arm respectively.
C	radial displacement of the machine pole from the contour pole.
c	projected length of a line along the radial vector.
F_1 , F_2	objective functions for optimization.
F_f	friction force normal to the NC machine arm and due to its support.
F_{cr} , F_{cn}	components of the force opposing the tool, radial and normal to the arm respectively.
F_{sum} , F_{dif}	dimensionless functions made up of N_R and N_θ .
H	template thickness
J_A	mass moment of inertia of the NC machine arm.
J_A	equivalent mass moment of inertia of the

	NC machine arm and angular axis-drive.
K_1	torque transformation factor for the worm worm-gear reducer, including friction losses.
K_2	torque to force transformation factor for the power screw and nut assembly, including friction losses.
K_C	force factor for the grinding operation.
K_T, K_V	torque and voltage constants of the stepping motors.
k_R^o	angular to linear transformation factor for the power screw and nut assembly.
k_θ	speed reduction factor for the worm worm-gear reducer.
L_A	distance between the NC machine pole and the arm support.
L_a	inductance of the stepping motor coils.
l	linear segment of an approximation to a contour.
M'_C	mass of the NC machine carriage.
M_C	equivalent mass of the NC machine carriage, with the power screw and radial axis-drive inertias reflected on it.
N_R, N_θ	number of radial and angular steps representing a line respectively.
N_S	number of teeth on the stepping motor rotor.

- R_a total resistance of the stepping motor coil and drive circuit.
- R_r, R_r^* tracking roller or tool-radius and its nondimensional value with respect to the thickness of the template.
- r radial displacement of the center of the carriage from the machine pole.
- r_1 radial displacement of a point (P) on the contour from the NC machine pole.
- r_c radial displacement of the center of the carriage from the contour pole.
- T_p pull-out torque of a stepping motor.
- $T_{PR}, T_{P\theta}$ pull-out torque of the radial and angular stepping motors respectively.
- T_R, T_θ torque required from the radial and angular axes respectively.
- t time.
- v voltage.
- v_t constant velocity of a point along the tangent to the contour.
- v_x, v_y velocity of the machine tool along the X- and Y-axis respectively.
- v, v^* velocity of the tracking roller at the center of the carriage and its nondimensional value with respect to $2v_t$, respectively.
- v_G velocity of the pressure roller

	tangential to the contour.
α	angle between the radial vector from the contour pole and the tangent to the contour, at a point (P).
α_c	inclination of the grinding force to the work-piece surface.
β	angular displacement of the machine pole from the contour pole.
γ	angle between the machine arm and the tangential vector at a point on the contour; measured from the arm.
ΔA	template digitizer and NC machine angular resolution
$\Delta R, \Delta \theta$	template digitizer and NC machine radial and angular stepping increments, respectively.
Δs	length on the contour corresponding to an angular or radial step.
ϵ_a	area error between the contour and its approximating curve.
ϵ_d	deviation error between the contour and its approximating curve.
θ	angular displacement of the template digitizer or the NC machine arm.
θ_1	angular displacement of a point on the contour with respect to the NC machine pole.

θ_c	angular displacement of the center of the carriage with respect to the contour pole.
λ	lead of the power screw helix.
$\Lambda_1, \Lambda_2, \dots$	equation simplification parameters, grouping parameters.
ρ	radius of curvature at a point on the contour.
τ_1, τ_2, \dots	equation simplification parameters, grouping parameters.
T_R, T_θ	torque ratio, defined as the ratio of the torque required to that available for the radial and angular axes respectively.
ϕ	angle of inclination of the velocity vector tangential to the contour, or of the tangent to the contour.
ω_R, ω_θ	angular velocity of the radial and angular axes-drives respectively, measured in electric degrees.

Note:

- Superscripts (I) and (G) indicate inertial and grinding cases, respectively.
- Subscripts R and θ refer to the radial

and angular axes respectively.

- A "^" on top of a parameter indicates the maximum value of that parameter along the contour.

- A "*" on top of a parameter indicates a nondimensional value of that parameter.

CHAPTER 1

INTRODUCTION

1.1 General

Contouring is defined as an operation of following or tracing the silhouette of an object. This operation is frequently used in many aspects of engineering and manufacturing practices.

Contouring systems are found incorporated into machines that are intended for a wide variety of applications. Some examples where such systems are utilized are:

- **Material removal:** In the manufacturing of turbine blades, cams and a host of similar products turning, milling, and grinding machines are equipped with contouring systems that guide the tool over the required contour.
- **Non-contact cutting:** Various non-contact cutting methods like flame or plasma cutting rely on a contouring system to guide the cutting nozzle over the cutting line.
- **Drafting:** The use of contouring systems in automatic drafting machines is relatively new. With the advent of computer-aided-design (CAD) these machines have become a necessity in modern design offices. In these machines the contouring system guides the drafting pen to produce the required drawing.
- **Clothing industry:** In the clothing industry, sewing ma-

chines are equipped with contouring systems to guide the sewing head over the sewing line (e.g. sewing of a shirt collar).

In general, contouring can be classified as:

- a) spacial ($3D/2\frac{1}{2}D$), where a set of three axes is required to define any point on the contour, and
- b) planar (2D), where a set of only two axes is needed.

Spacial contours may be produced by a series of parallel planar contours each incremented from the previous one along the normal (third axis) to the planes with the tool tilted such that its tangent plane at the cutting point coincides with the tangent plane of the contour. This type of operation, shown in Figure 1.1.a is known as 3D (three dimensional) contouring. Warped and double curved surfaces are examples that require such contouring operations. A less complex operation which approximates the 3D is commonly known as $2\frac{1}{2}D$, and is shown in Figure 1.1.b: In this operation the tool is indexed along the third axis with no tilt adjustment. This operation can be easily performed using planar contouring (2D, shown in Figure 1.1.c) by providing it with an indexing drive along the third axis. The latter three of the above examples are typical of planar contouring.

Some 2D contours can be produced by means of linkage mechanisms. Circles, for example, can be produced by one end of a rod constrained to move with the other end fixed at a point in the plane. References [1] and [2] present a

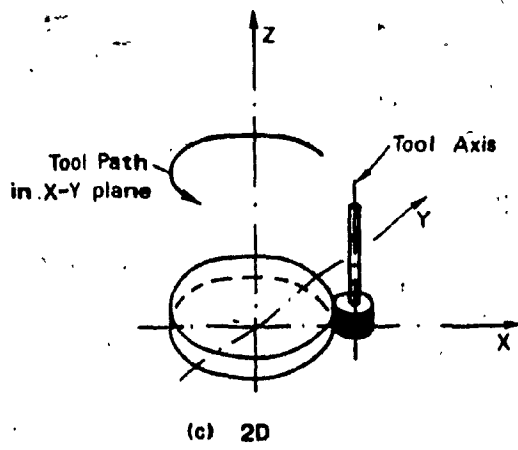
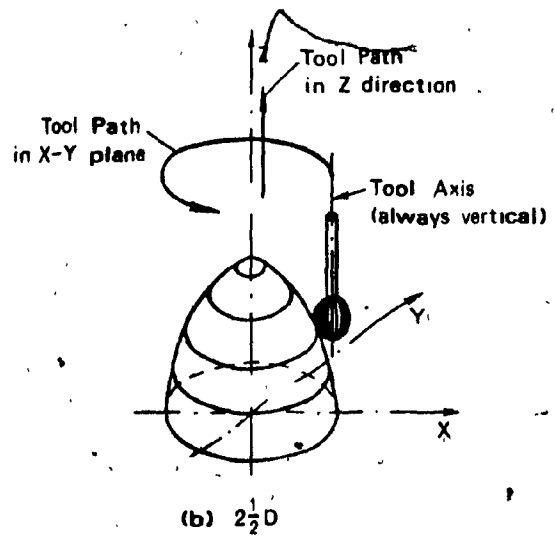
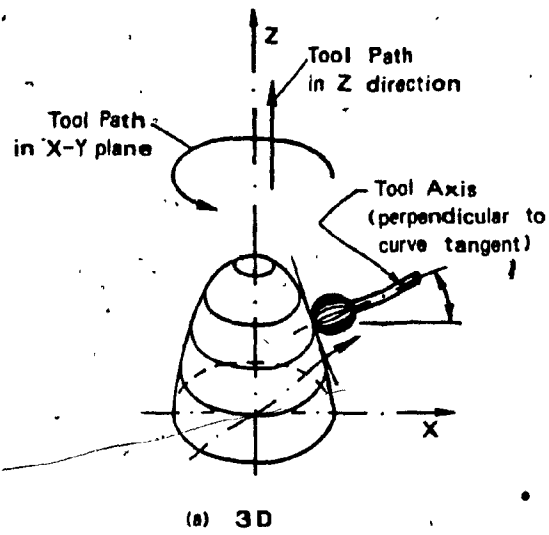


Figure 1.1: 2D, $2\frac{1}{2}D$, and 3D Contouring Operations.

large number of such mechanisms for producing a variety of contours. In general, however, such mechanisms are very complicated in construction. Furthermore, each of these mechanisms is specialized to produce a single family of contours and in general cannot be easily adapted to produce other families. Thus, for a single system to produce any arbitrary contour, it cannot make use of these linkage mechanisms.

A large number of general purpose contouring machines have evolved over the years. These machines require as input some form of information about the contour they have to produce. Depending on the form of input, these machines can be categorized as: a) Copying machines, and b) Numerical control (NC) machines.

1.2 Copying machines

These machines utilize a template of the required contour for their operation. The pantograph copier shown in Figure 1.2 is a pioneer system belonging to this category. With reference to the figure, in its primitive form, the tracer pin is manually guided over a template. By virtue of the design of the pantograph links, the tool traces a curve geometrically similar to the template. The reproduction scale depends upon the position of the tool on the tool arm. The main application of the pantograph copier is in engraving. When large forces are encountered by the tool, as in metal removal applications, high power electric, hydraulic,

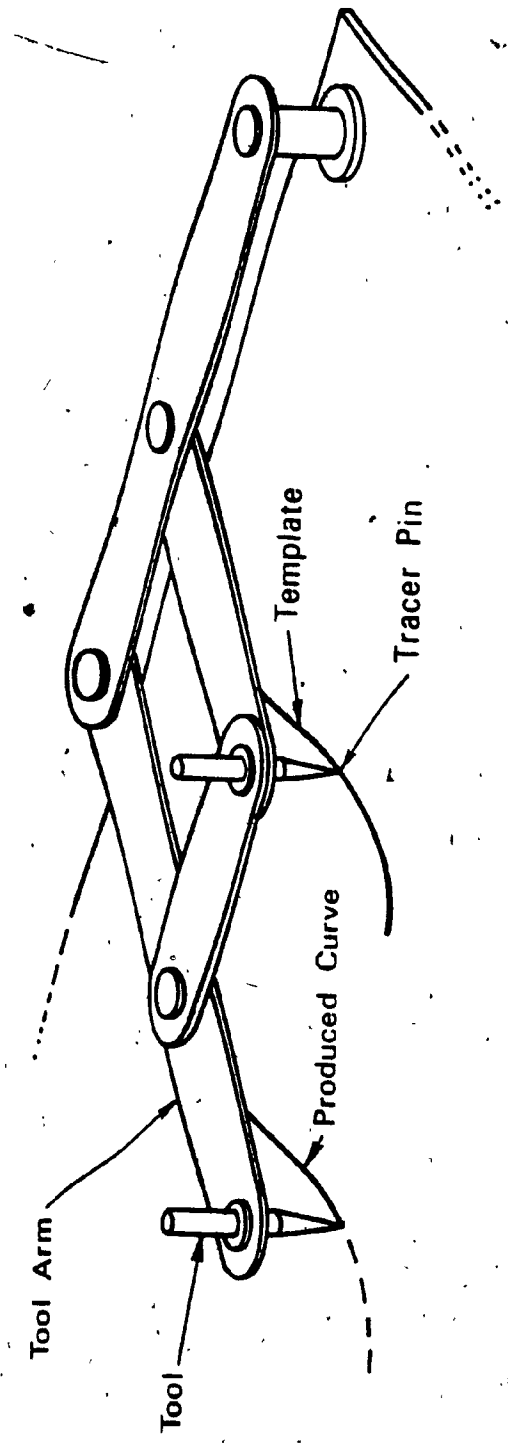


Figure 1.2: Pantograph Copier.

or electro-hydraulic copying machines have to be used. Figure 1.3.a shows a schematic diagram of such a machine. The machine consists of two machine beds, one sliding along the X-axis, the other along the Y-axis. The machine tool is linked to a template follower either directly or through a force amplifier. With reference to Figure 1.3, and with no loss of generality, the template follower may be one of the following types:

a) Passive-type, as shown in Figure 1.3.b, in which the template follower is simply preloaded against the template along the Y-axis. Moving the template along the X-axis causes the Y-axis bed to move back and forth in accordance with the template profile thus producing the copying action. Passive followers can be used only within a small range of template slope angles, the range of angles being a function of the speed of template travel along the X-axis. Reference [3] describes 2D and $2\frac{1}{2}$ D copying machines utilizing such followers. The machine described in the reference utilizes hydraulic servo-controlled amplifier between the tool and the template follower.

b) Active-type followers, shown schematically in Figure 1.3.c, carry a set of two force transducers arranged normal to each other. The transducer signals are utilized to control the X- and Y-axis bed movements. The beds are controlled in such a way that the follower is always kept in contact with the template.

c) A third type of follower utilizes an opto-electronic

sensor to follow a line or edge (silhouette) type template. Reference [4] describes a flame cutting copying machine that uses such a follower. One such sensor is detailed in Reference [5] and shown schematically in Figure 1.3.d. The sensor consists of a circular array of photo-diodes and a single diode at the centre. The control element of the copying machine uses the information from the circular array of sensors to guide the central photo-diode over the silhouette.

d) Powered-type followers are mainly employed in applications where the force opposing the tracking action is low. The clothes manufacturing industry is the largest user of this type of follower. An industrial sewing machine utilizing a powered follower is described in Reference [6]. Figure 1.3.e shows a schematic of a powered follower-cam arrangement. The follower is the shaft of an electric motor that is kept in contact with a magnetized steel template.

References [7] to [10] describe a gyroscopic tracking mechanism where the gyro spin axis acts as a powered follower. The spin axis adheres to the template due to the gyroscopic action. Detailed analysis of the mechanism is given in the references. References [9] and [10] report prototypes that has been satisfactorily tested:

1.3 NC machines.

In its broad meaning, a system is termed numerically controlled if it operates automatically according to a set

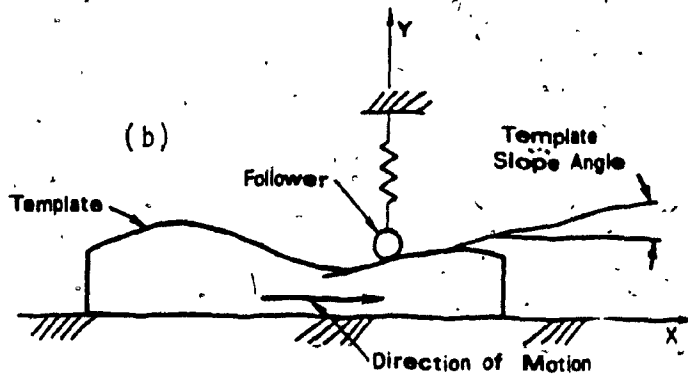
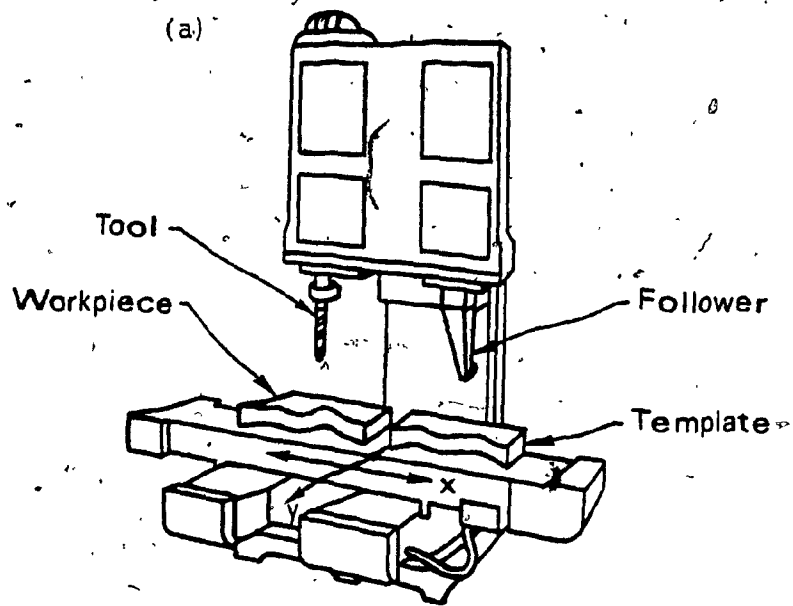


Figure 1.3: Schematic Diagram of a Template Copying Machine/Template Configuration.

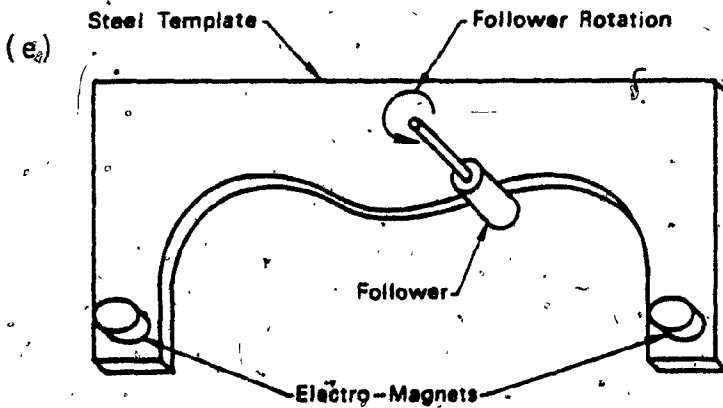
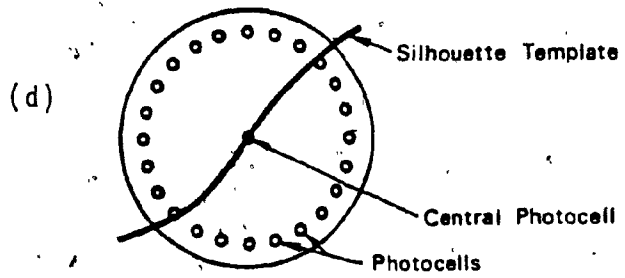
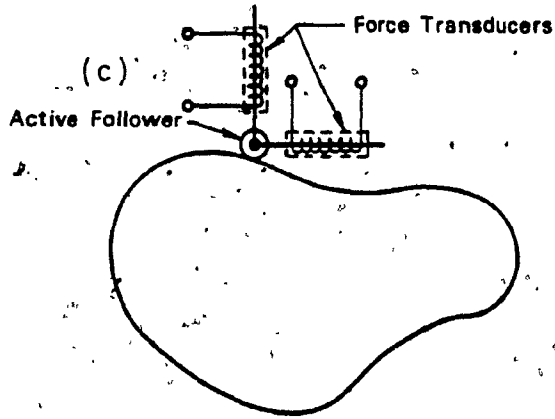


Figure 1.3: Schematic Diagram of a Template Copying Machine/Template Configuration.

of coded instructions fed to it. References [11] and [12] report the first NC machines to have appeared during the 18th century : the Falcon (1728) and Jacquard (1800) looms. According to Reference [11], for the next 150 years the only descendants of these machines were the piano and the barrel organ player. Modern NC machines first appeared around the year 1942, and were developed simultaneously but separately by the Bendix corporation, and by Massachusetts Institute of Technology in collaboration with I.B.M. and Cincinnati Milling Company. The 1942 machines were computer controlled. In the last three decades, due to the rapid development in computers and related technologies, NC machines have proliferated all over the U.S.A. Europe, and Japan, and the term "numerically controlled" has become synonymous with computer controlled machines. Figure 1.4 shows a schematic of an NC machine. These machines look similar to copying machines with the exception of the absence of the template follower, and the presence of a controlling computer. Literature on NC machines is abundant. References [13] to [16] are conference proceedings of engineering societies devoted to the subject. These references report advances in both the hardware and software of NC machines.

NC machines differ from servo controlled machines in that they move in preset increments or resolutions on each of their axes. The axes-drives, however, may themselves be controlled through analog servos. The machine can index

only to those points on its axes that are multiples of the resolutions. Servo controlled machines, however, have an infinite resolution and can move to any location on the axes.

Depending on the capability of NC machines they are classified as: a) Point-to-point, b) Straight path, or c) Contouring NC machines.

a) Point-to-point NC machines are by far the simplest and the most common of the three classes. Here the tool cannot operate while the machine beds are in motion. The machine acts as a positioning table for the work piece and also performs some control functions like tool change and operation. Point-to-point NC machines are mainly used in applications like drilling, tapping, reaming and the like.

b) The tool of a straight path NC machine is in continual operation while the machine beds are in motion. The controller for this type of machine is more complex than that for the previous type, and is capable of coordinating the axes-motors so that the work-piece can move in a straight line in any direction. Recent improvements on these machines allow them to follow circular paths, Reference [11].

c) In the case of NC contouring machines the contour information is in the form of coordinate sets of points on the curve. A large memory is required to store this information. The curve distance between the given points on the contour are much larger than the machine resolution. The controller has to interpolate between the supplied points in

order to smoothen the curve. Furthermore, the controller has to coordinate the velocity of the axes-drives in order to produce constant contouring speed. These two mathematical tasks together with auxiliary control functions, like tool change and operation, necessitate a powerful controller. These controllers are usually built around powerful microprocessor units, and although the ratio of cost to power of microprocessors is dropping rapidly, the cost of controllers is not decreasing appreciably yet. This is due to the high development cost, the small number of units built, and the expense of good control software.

In almost all contouring applications, constant speed of travel along the contour is a highly desirable feature. Reasons for such preference are specific to each application. In flame or plasma cutting applications, for example, constant speeds of travel along the cutting line allow precise gauging of the power required, resulting in savings in cutting energy. For metal removal applications like milling or grinding, the constant contouring speeds would result in a better surface finish and extended tool life. In some contouring applications, as in the clothing industry, speeds of travel along the sewing line must be constant to insure equal stitch lengths. Such a homogeneous stitch is essential both for the strength, as well as for the aesthetic appearance of the product. Some other contouring applications are rather insensitive to the speed of travel along the contour. Drafting pens for example have

reached such a maturity of design that allows them to operate over a wide range of travel speeds. Consequently, there is no constraint of constant contouring speed along contours in drafting applications.

All the commercially available contour following systems utilize a Cartesian system of coordinates for their operation. Referring to Figure 1.5, constant contouring speeds would be achieved if the following mathematical relation is satisfied at every point on the contour:

$$V_t = \left[V_y^2 + V_x^2 \right]^{\frac{1}{2}} = \text{constant} \quad 1.1$$

To satisfy the above relation, the tangent to the contour at every point must be known. In the case of copying machines, finding the tangent direction involves complicated instrumentation which substantially increases the cost of the system. For NC machines, however, the controller approximates the velocity relation to keep the tracking velocity within acceptable tolerance. In the powered type follower systems, the follower is driven at a constant rotational speed and supplies the motive power. Under ideal conditions of no slip, this translates to constant tracking speed along the magnetized template.

Reference [17] describes the prototype of a plotter that utilizes polar coordinates. A photograph of the prototype is shown in Figure 1.6. The plotter consists of a semicircular bed (A). An arm (B) hinged at the centre of

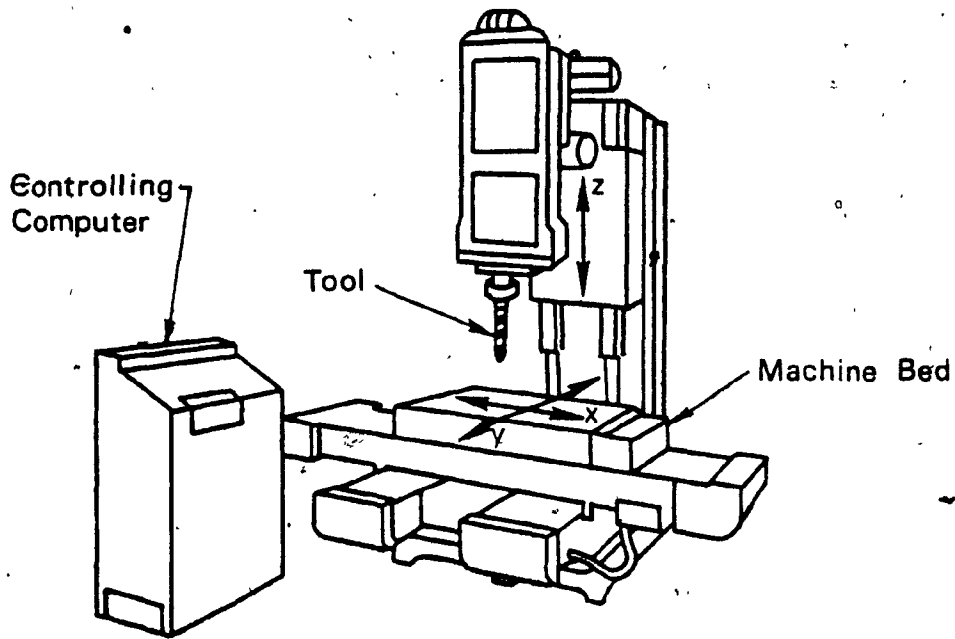


Figure 1.4: Schematic Diagram of an NC Machine.

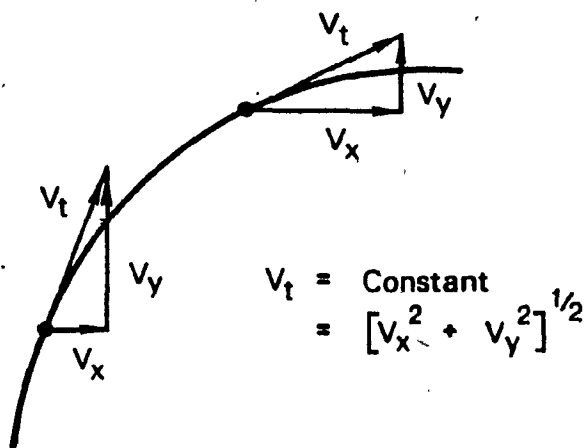


Figure 1.5: Velocity Diagram in Contouring Operations.

the semicircle is powered by means of a cable (C) and pulley arrangement. The arm swings around the hinge (D). A stepping motor (E) drives the cable (C). The arm carries a carriage (F) fitted with the plotting pen and driven by another stepping motor (G) through a cable and pulley system (H). The configuration of this system is shown to be suitable only for plotting applications. No analysis or study of the mechanism is reported.

This thesis is concerned with the planar class of contouring systems, and for the purpose of brevity the terms "contours" and "contouring" will refer to the planar class throughout the text, unless otherwise specified.

The thesis presents a contouring system which utilizes polar coordinates for its operation. The system is comprised of a contour digitizer and an NC machine. Two types of digitizers are discussed: a physical template digitizer, a prototype of which has been built and tested, and a software digitizer which requires as input a mathematical representation or points on the contour. The software digitizer uses a computer which is not on-board the NC machine and does not control its operation on real time basis. The output of both digitizers can either be transmitted directly to the NC machine or can be recorded on magnetic tape for repetitive, or later, use. A prototype of the NC machine has also been built. The machine controller is simple and does not utilize any microprocessors for its operation. The machine is dedicated for contouring appli-



Figure 1.6: Polar Plotter.

cations. Some auxiliary control functions, however, can be added without complication.

1.4 Thesis outline

The thesis discusses the overall philosophy of a polar coordinate based contouring system. The main operational aspects of the system are studied in detail. The study includes synthesis, analysis, and design of the contouring system. A detailed study of the system under kinematic and dynamic conditions is given. Two methods are presented, one for optimally locating a contour within the work space in order to minimize the digitization error, and the other to evaluate the limit of the contouring speed of the system under load. Other studies, concerned with the structural rigidity, vibration, and similar aspects have not been included.

Chapter 2 of the thesis presents first the different configurations of the system. This is followed by a description of two different methods used to digitize contours: the template digitizer, and the software digitizer. Prototypes of a template digitizer and an NC machine have been built. Detailed description of both prototypes, as well as the software digitizer that has been constructed is also presented.

Chapter 3 discusses the main features of the polar contouring system. These features as well as the advantages and shortcomings of the system are itemized and compared

with those of commercially available contouring machines. A summary of the salient points is given in the form of a tabulated comparison at the end of the chapter. Due to the nature of polar coordinates, the system resolution is not homogeneous within the operating area, as a result, an error analysis which is of paramount importance is studied in this chapter.

In Chapter 4 it is shown that an area error criterion is more stringent than the traditional deviation error criterion. A study of this error shows that its magnitude depends upon the position of the contour with respect to the machine pole. The calculation of the area error is too lengthy a process to be used as an objective function in an optimization routine for minimization. An alternate objective function, formulated in Chapter 4, is fast to calculate and is suitable to incorporate in an optimization routine. The results of optimization and some sample calculations of area errors for three test curves are also presented in this chapter.

Chapter 5 deals exclusively with the kinematics and dynamics of the NC machine. The dynamic study is used to determine the load capacity of the machine. The load on the axes-drives depends upon the machining forces as well as on the contour being processed and the contouring speed. The effect of these operational parameters on the torque requirement of the axes-drives is also studied in this chapter. Furthermore it is shown that for a given set of

operating parameters the load on the axes-drives varies with the position of the contour pole relative to the machine pole.

In Chapter 6 a detailed analytical study is conducted to evaluate the effect of variation of operating parameters on the torque of the NC machine axes. An objective function is formulated for minimizing the total torque of the NC machine and equalizing the load imposed on the two axis drives. The objective function is incorporated within an optimization algorithm to locate the relative location of the machine pole from the contour pole. Based on the results of the optimization, a procedure is outlined to increase either the contouring speed or the allowable load on the machine.

In Chapter 7 a graphical procedure is also presented by which both the torques required and available from the two drives can be easily found.

The thesis concludes by outlining the salient features of the contouring system. A summary of the investigations as well as the important findings are given. Recommendations on the future studies towards development of a second generation prototype and eventually, of an industrial system are outlined.

CHAPTER 2
CONCEPT AND OPERATION
OF THE CONTOURING SYSTEM

2.1 Introduction

The configuration of the polar contouring system allows it to operate as a copying system or as an NC system that has very little on-board signal processing. Figure 2.1 shows a block diagram of the contouring system in its different configurations, as well as the flow of signals between the various components. The system is composed of two parts, a contour digitizer and an NC machine. As shown in the figure, the digitizer can be either a template digitizer or a software digitizer. When the contouring system is used for copying, it is configured as a template digitizer/NC machine (TD/NC machine), while when used as an NC system it is configured as a software digitizer/NC machine (SD/NC machine). Contour information for the template digitizer is provided by means of a template of special form. Two forms of templates intended for precision and non-precision work will be discussed later. The software digitizer utilizes a computer to digitize the contour, with the information being in equation form or as a number of discrete points on the contour. The control signals from a digitizer can be directly channeled to the NC machine or recorded on magnetic tape for later use. Recording the control signals prior to use has a number of advantages that will be discussed in

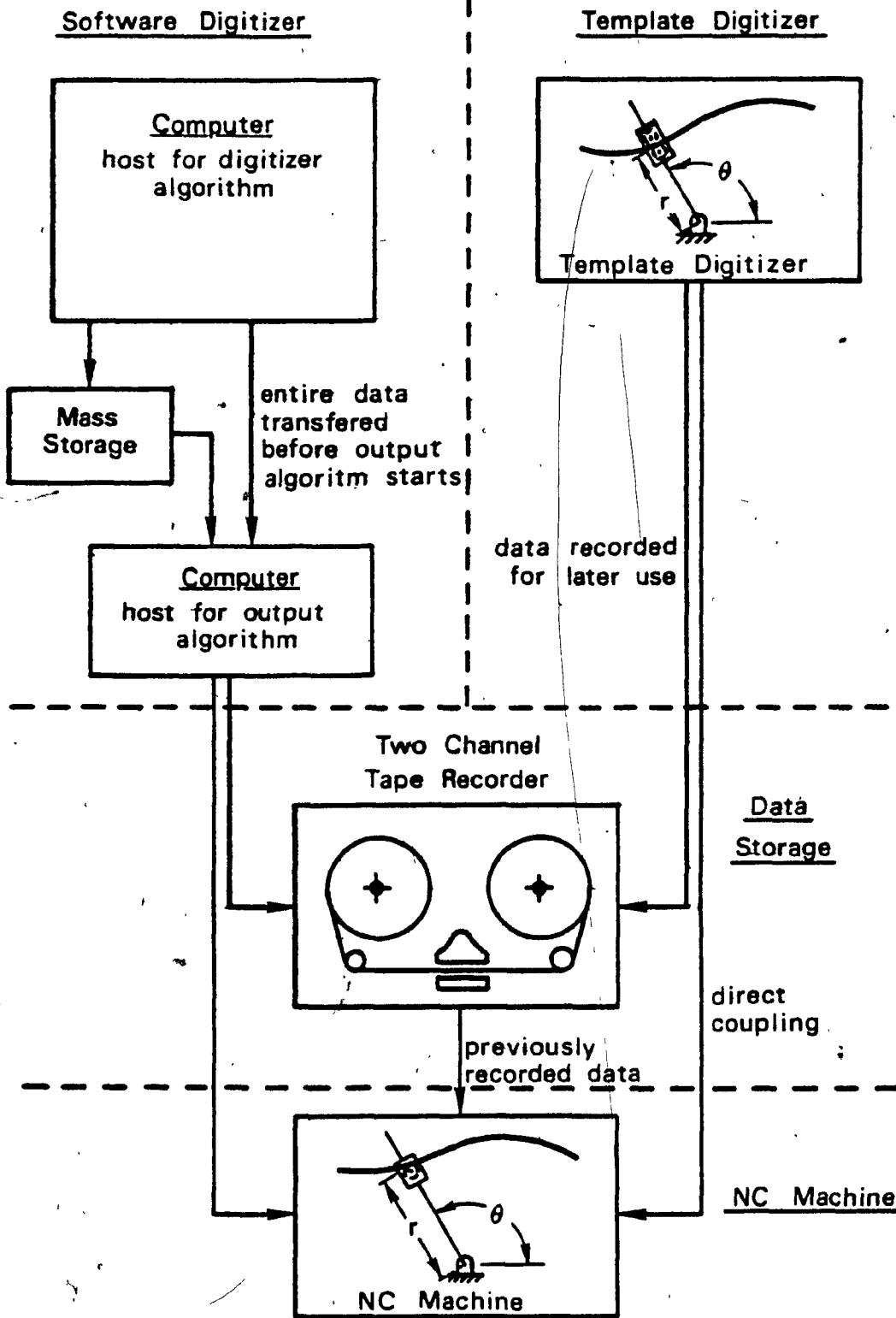


Figure 2.1: Block Diagram of a Polar Contouring System.

detail later. Some of these advantages are:

- a) Ease of scaling the contouring speed by altering the tape playback speed,
- b) A single template digitizer can be used to prepare recorded control signals for more than one NC machine, and
- c) Recording control signals rather than directly channeling them to the NC machine allow software digitizers to run in BATCH mode on computers. In addition, recording the control signals allow small computers to be used as hosts for the digitizer since no speed constraint is imposed on the computation. Furthermore, computer resources are not tied down executing the same commands repeatedly, and can be available for other processes.

For recording and playback of the control signals, a conventional stereo, reel or cassette tape recorder can be used. The speed control circuit on the tape recorder can be modified to allow for variable speed and thus providing speed scaling. Some commercially available recorders are built with such a feature. The output signals from the two recorder channels are conditioned before feeding to the NC machine.

The NC machine accepts the control signals and uses a simple hardware logic circuit to direct them to the appropriate axis-drive.

Prototypes of the various components of the system shown in Figure 2.1 have been built and tested. Detailed descriptions of prototypes of the three main components in

the figure, namely, the template digitizer, the software digitizer, and the NC machine are presented below.

2.2 Prototype template digitizer

A schematic diagram of the prototype template digitizer and correspondingly labelled photographs are shown in Figures 2.2 and 2.3 respectively. With reference to the figures, the platform (A) constitutes the working area of the digitizer. An arm (B) is keyed to a shaft (S) at one end and free to swing within the limits marked by the stops (C) and (C') (not shown on the photographs). The stop (C) on the right, marks the arm's home position or the reference of the angular axis. A digital shaft encoder (D) which translates shaft positions to electric signals is fixed on the shaft in order to indicate the angular position of the arm. A carriage (E) is mounted on the arm and can slide over it. The fully retracted position of the carriage corresponds to its home position, or the reference position of the radial axis. The carriage carries another shaft encoder (F) and a pair of tracking rollers (G) and (G'), of equal radii. These rollers are designed to provide high friction between themselves and the template. Both rollers are powered in order to equally distribute the driving force and reduce the possibility of slip while rolling over the template. The rollers are driven through a power train by two precision, variable speed, DC motors (H) and (H') that are mounted on the carriage. The motors are wired in such a

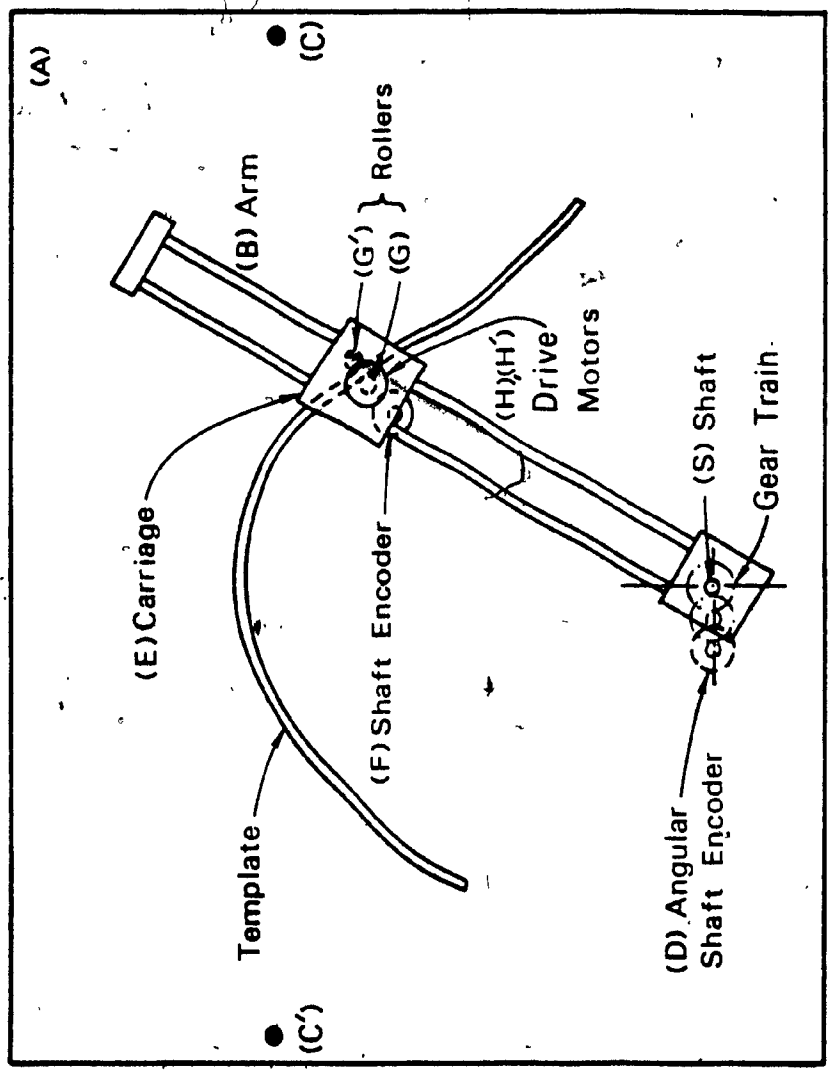


Figure 2.2: Schematic Diagram of the Template Digitizer.

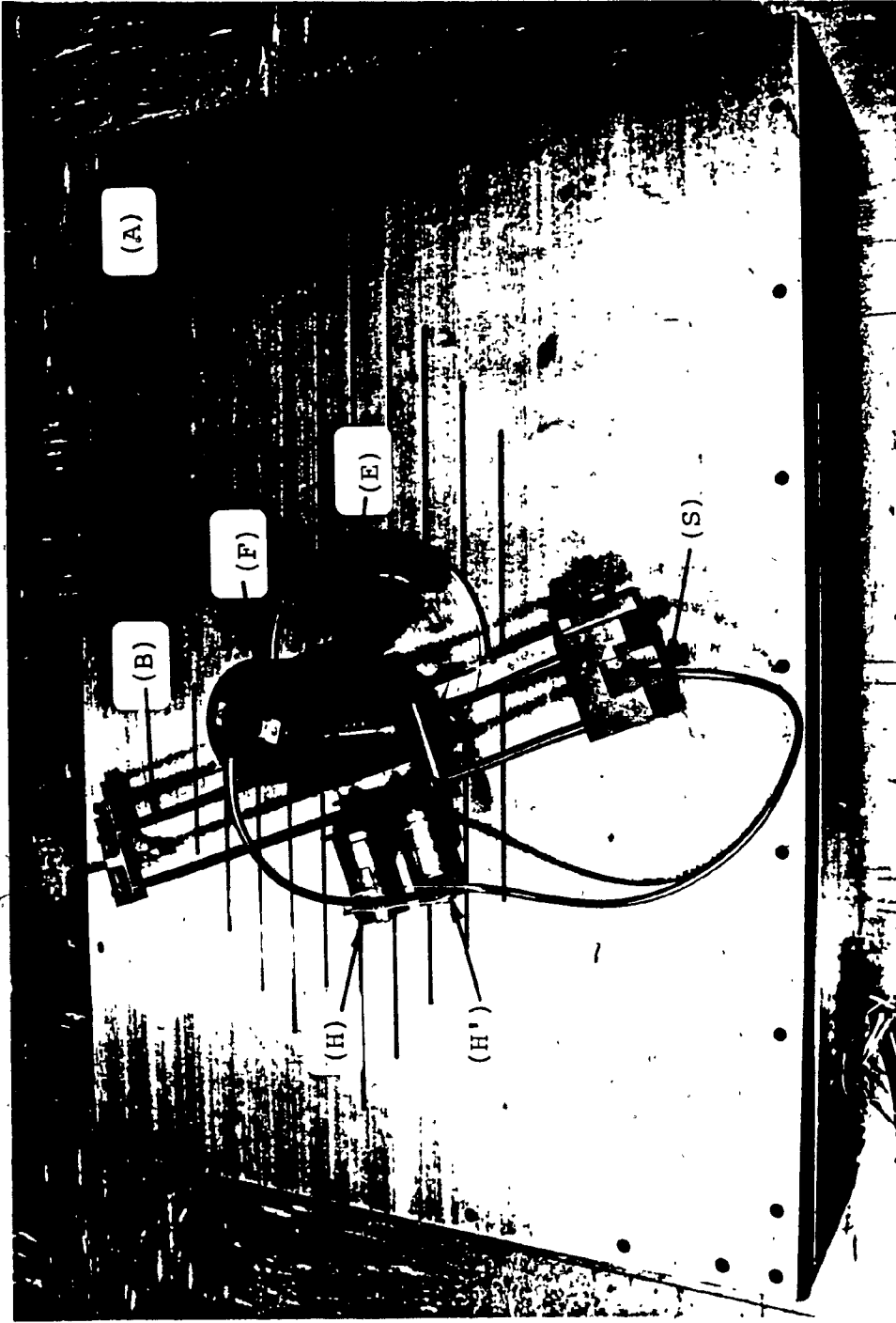


Figure 2.3.a: Photograph of the Prototype Template Digitizer.

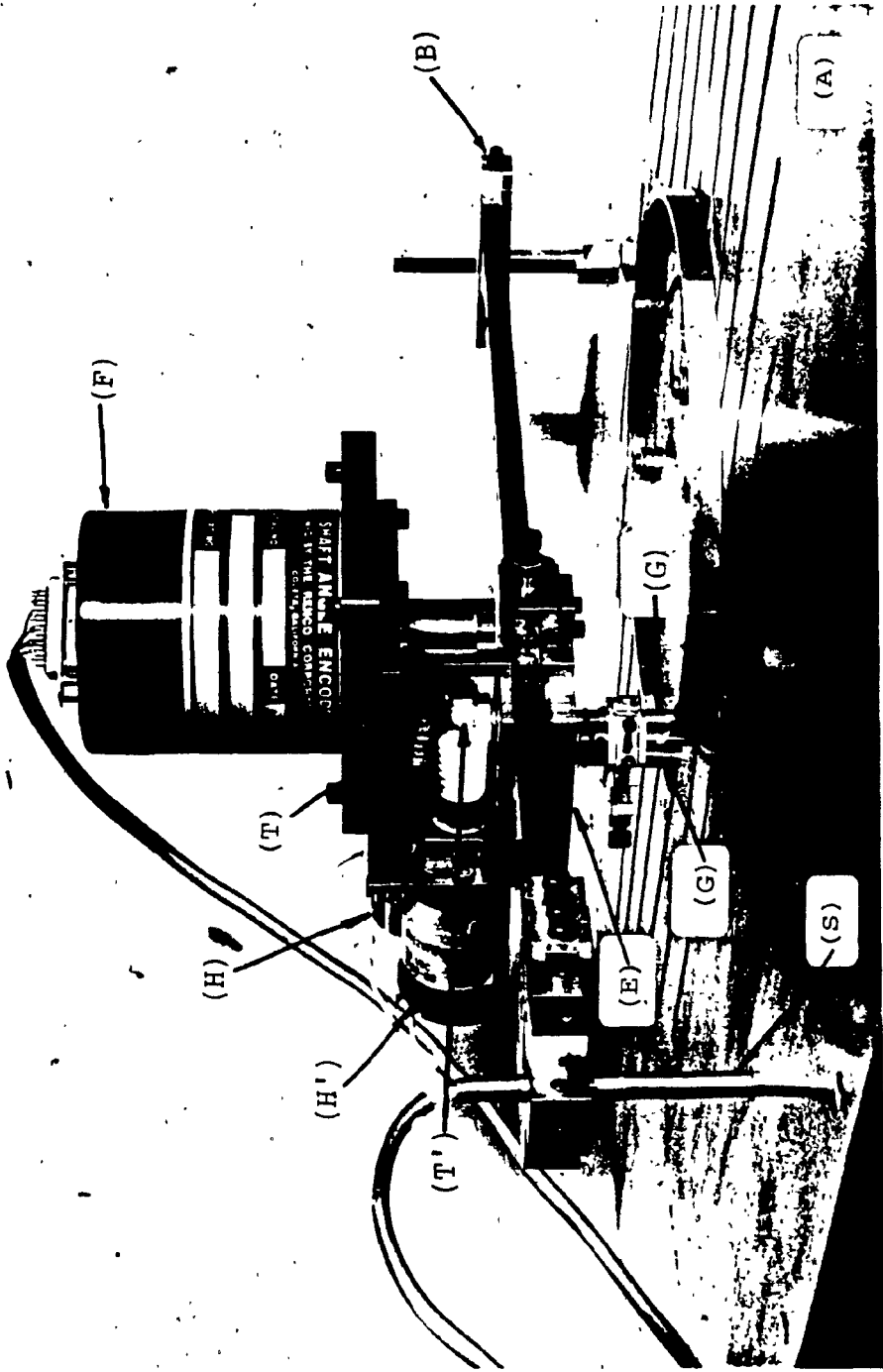


Figure 2.3.b: Template Digitizer Arm Assembly.

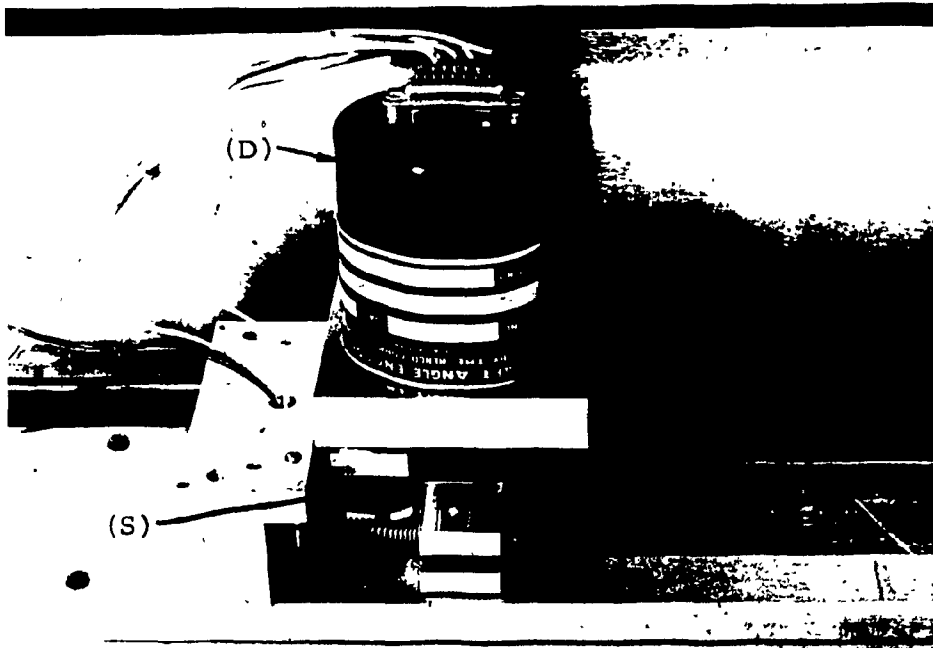


Figure 2.3.c: Template Digitizer Angular Shaft Encoder.

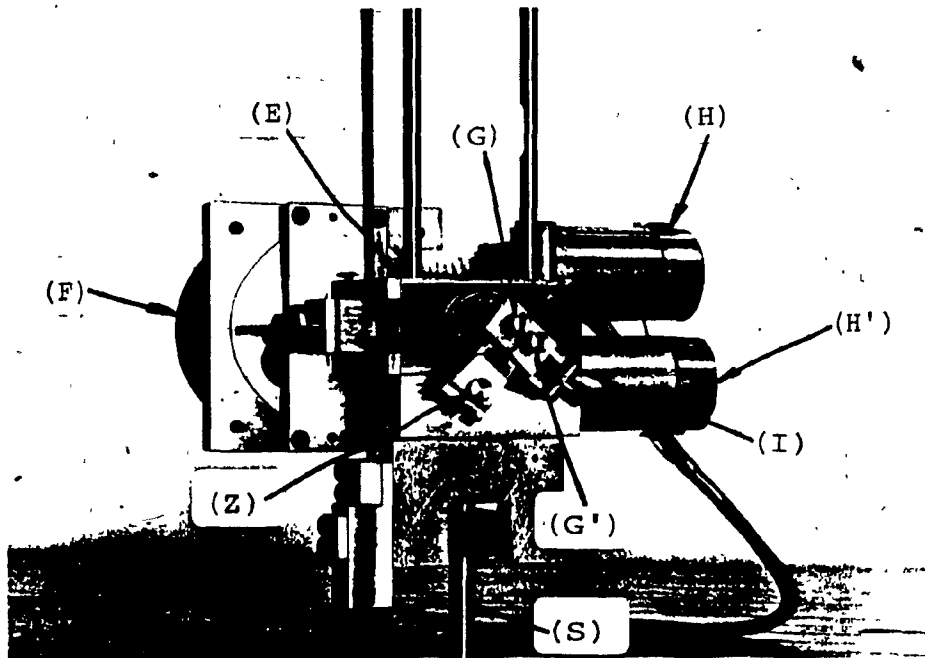


Figure 2.3.d: Template Digitizer Tracking Roller Mechanism.

way so as to produce a mechanical differential effect. The shaft encoder (F) has a friction roller mounted on its shaft. The roller rolls on the arm, and the signals from this encoder indicates the position of the carriage along the arm.

Assembly drawings of the major components of the template digitizer are included in Appendix [A-1].

Figure 2.4 shows two types of templates. The template shown in Figure 2.4.a is formed out of a flexible L-section strip which is fixed along its edge to the working area of the digitizer by means of screws. This type of template is less suited for precision work. The template shown in Figure 2.4.b consists of a raised track machined out of a solid plate, made of metal or otherwise. That side of the track over which the roller (G) rolls is the actual contour that will be produced by the NC machine and must be accurately formed. For no slip between the template and the roller (G), the contouring speed should be directly proportional to the rotational speed of (G).

The rotational speed of the rollers (G) and (G') may be controlled in either of the following two ways:

- a) the rotational speed of (G) can be kept constant through the use of a speed sensor and a feed-back control loop, or
- b) the sum of the two rollers speed is kept constant through the use of a feed-back controller.

Although the former case is preferable, the controller is complex. The controller in the latter case is simple, how-

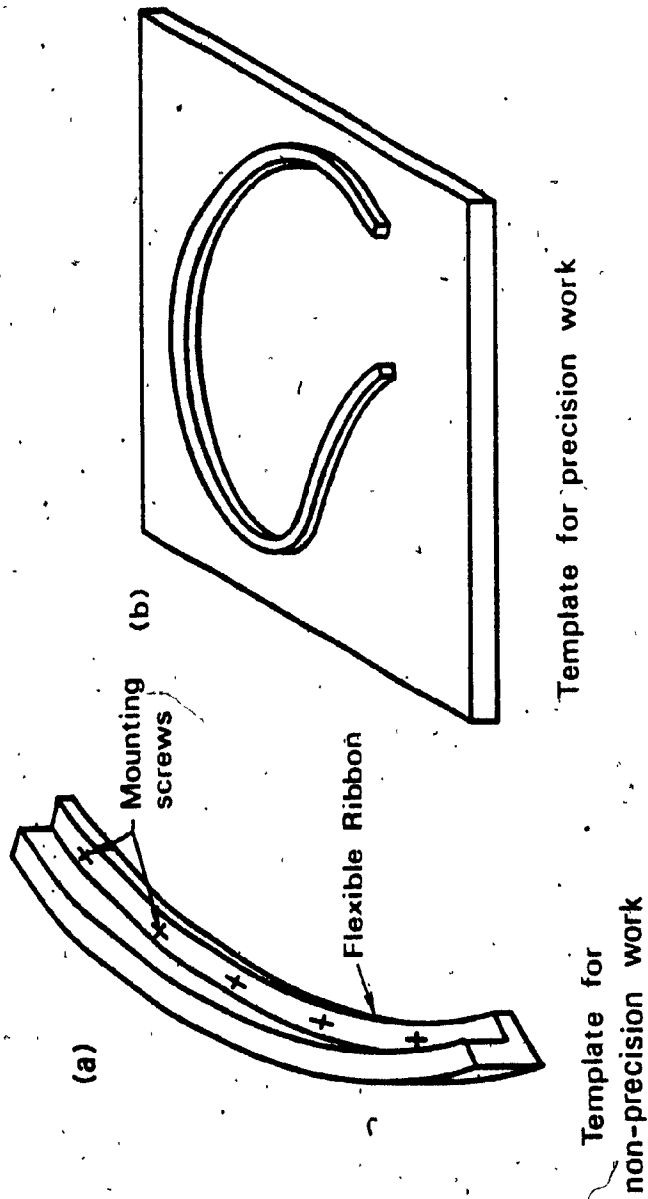


Figure 2.4: Sample Template Configurations.

ever, depending on the contour being tracked, the contouring speed may vary slightly. Detailed analysis of the variation in the contouring speed and the parameters contributing to it are discussed in Section 3.5 of the thesis.

The arrangement of the two rollers is shown schematically in Figure 2.5. Roller (G) is located at the centre of the carriage. An arm (I) swings about the axis of (G) and carries the second roller (G'). Roller (G') can slide on (I) and is spring-loaded against the roller (G) by a spring (J). The tracking roller (G) offsets the centre of the carriage from the template contour by a distance equal to its radius. If the template contour is to be reproduced, the diameter of the roller (G), and (G'), must be identical to that of the working diameter of the tool used on the NC machine.

In order for the carriage to be able to follow closed contours, the arm (I) has to be able to rotate through a full revolution around the axis of roller (G). The power train for the rollers is designed so as not to interfere with arm (I). A perspective drawing of the roller and power train arrangement is shown in Figure 2.6. The arrangement consists of two concentric shafts located at the centre of the carriage. The inner shaft extends beyond the outer one on both ends and has a worm gear (T) and the roller (G) fixed to its upper and lower ends respectively. The outer shaft also has a worm gear (T') fixed to its upper end. On

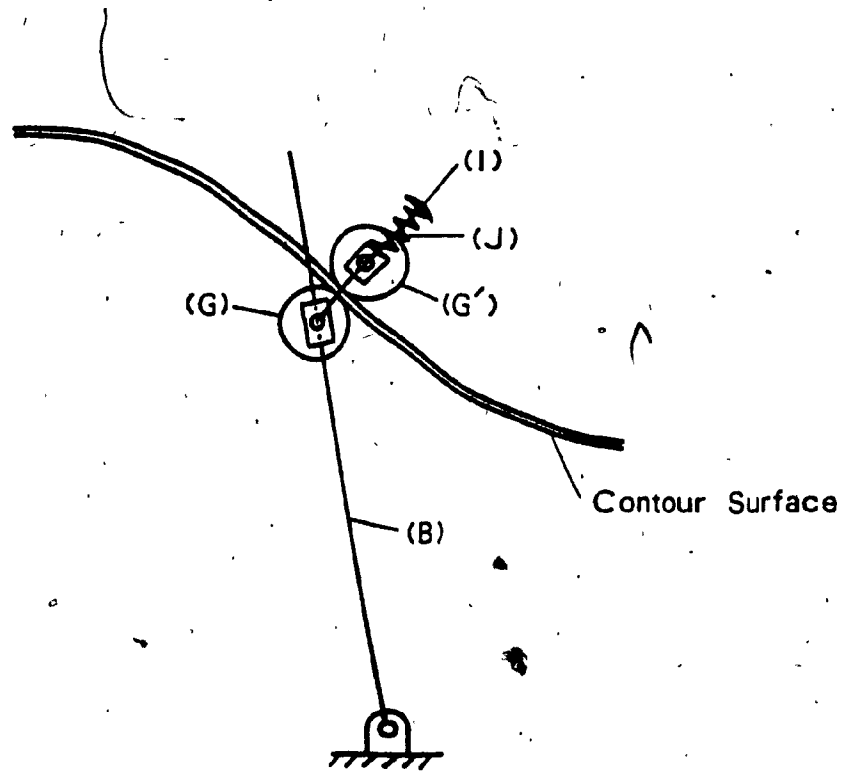


Figure 2.5: Schematic Diagram of the Roller Mechanism.

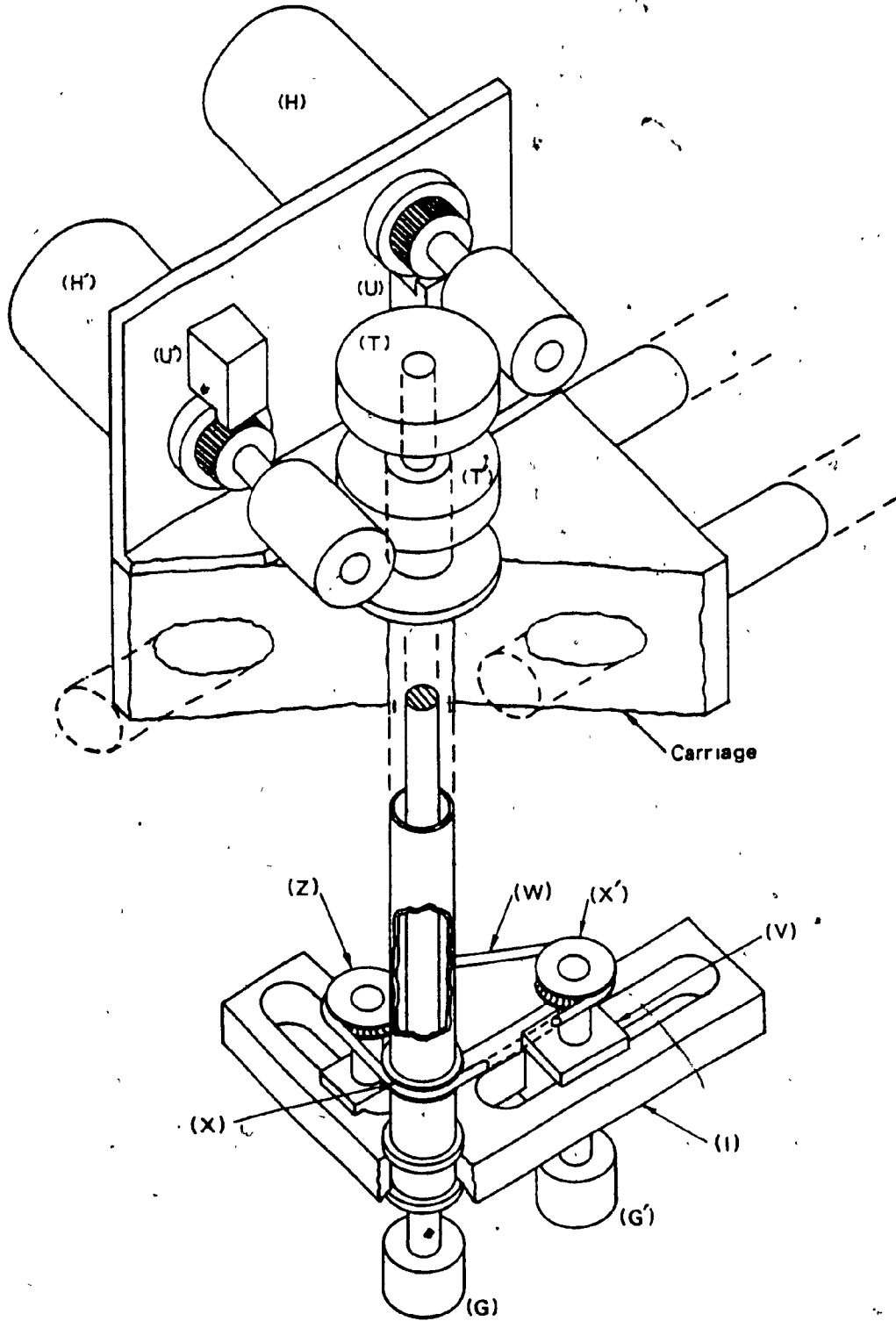


Figure 2.6: Pictorial Diagram of the Roller Mechanism.

its lower end, however, a pulley (X) is mounted followed by the arm (I) as shown. The arm is free to rotate around the outer shaft. A slider (V) slides on (I) and carries another pulley (X') on top and the roller (G') on its bottom side. The roller (G') and the pulley are fixed to rotate together by a short shaft (not shown). The slider is spring-loaded so as to bring the two rollers together. A belt (W) transmits motion between the pulleys (X) and (X'). An idler roller assembly (Z) provide tension on the belt to avoid slip. The worm gears (T) and (T') are meshed to two worms which are driven by two DC motors as shown in the figure. The motor shafts carry two optical shaft encoders (U) and (U') which are used for speed feedback of the rollers (G) and (G').

The two DC motors are series-connected and are powered by a variable voltage power supply. The electro-mechanical relationship of the two motor system is derived in Appendix [B] and resembles in function a conventional gear differential. The importance of driving the rollers through a differential arrangement can be best demonstrated by means of a schematic diagram. Figure 2.7 shows the rollers tracking two possible templates. In Figure 2.7.a the path of roller (G) in the section labelled a-b on the template is shorter than the path of roller (G'). Since both rollers are constrained to move together, the difference in speed resulting from the unequal path lengths is taken up in the differential arrangement thus preventing the rollers from

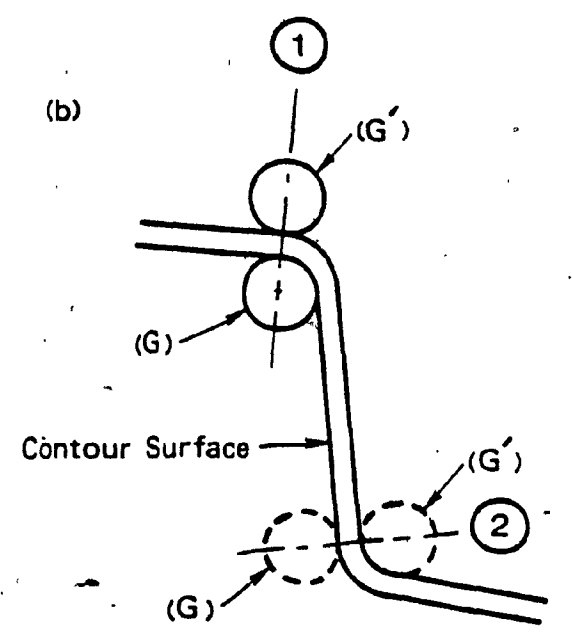
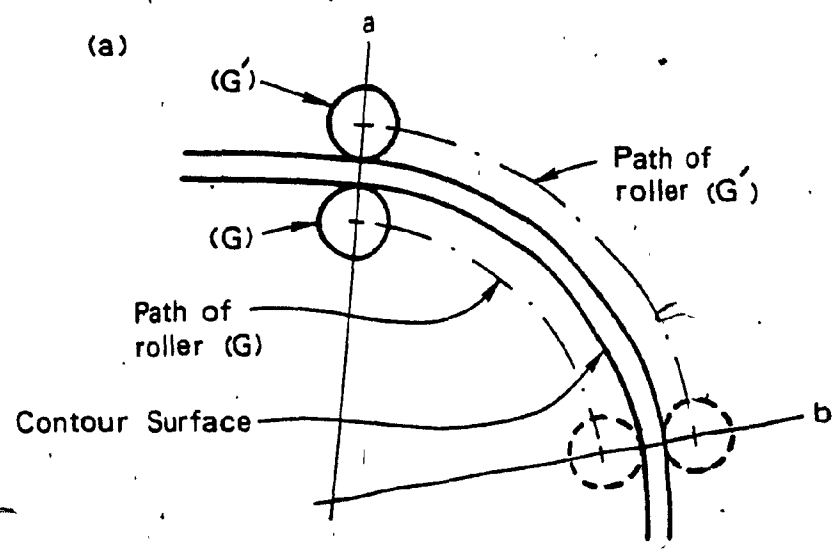


Figure 2.7: Path of the Roller Mechanism for Curved Templates.

slipping. The need for the differential here is analogous to that in the case of the driving wheels of a car when manoeuvring curves. For the template shown in Figure 2.7.b, assuming (G) alone was powered, when the rollers reach the position indicated as (1), the direction of the driving force is such that it does not allow (G') to manoeuvre around the curve and result in wedging and slipping of the roller system. In the event of (G') alone being powered, a similar situation would occur at the position marked (2), with (G) and (G') interchanging their roles. The presence of the differential arrangement allows (G) at position (1) and (G') at position (2) to come to a full-stop while the other roller negotiates the curve.

Each of the shaft encoders used in the prototype generate two logic signals as shown in Figure 2.8. The horizontal axis of the traces represent shaft rotation. With reference to the figure the upper and lower traces indicate Clockwise (CW) and Counter clockwise (CCW) indexations respectively of the encoder shaft. These two signals are combined into one as shown in the figure in order to permit recording the signals from one encoder onto one of the two channels of a commercial stereo tape recorder. The encoders are arranged such that the motion of the carriage away from the pole and rotation of the arm in the CCW direction generate positive going pulses as shown in the figure. The reverse of the above mentioned directions of motion result in negative pulses. The time rate at which the pulses are

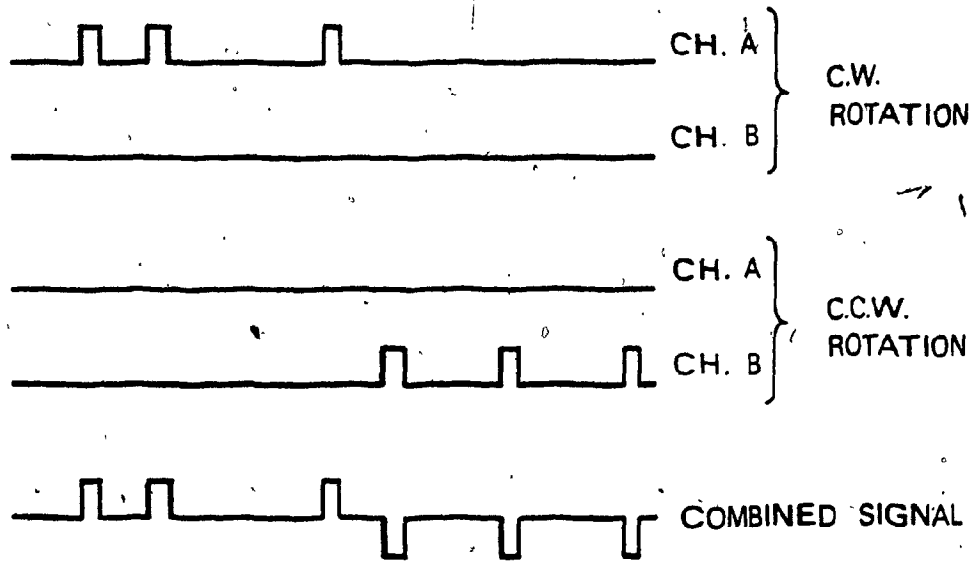


Figure 2.8: Sample Shaft Encoder Signals.

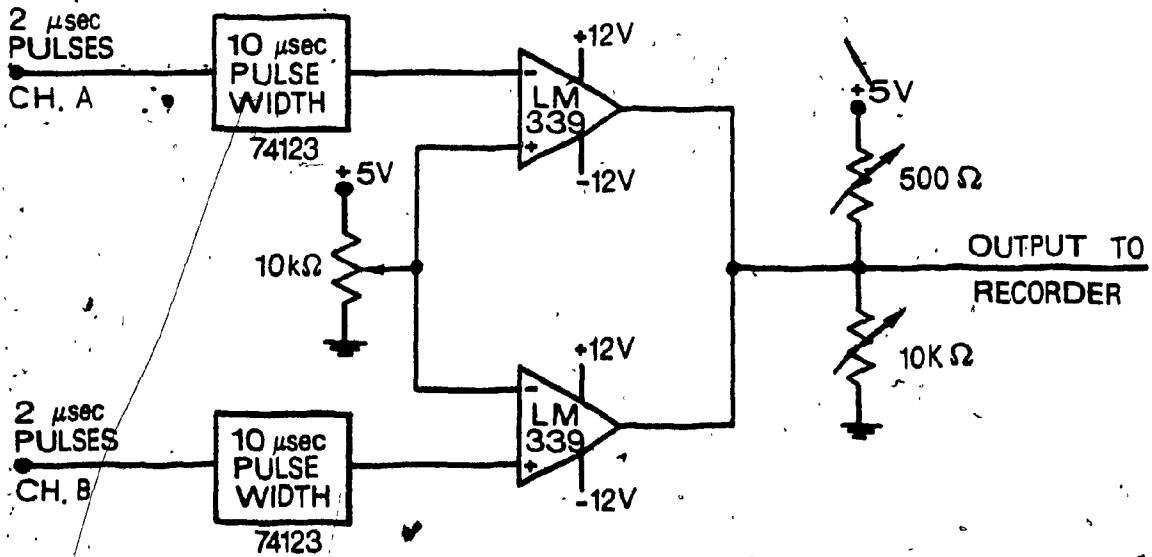


Figure 2.9: Conditioning/Combining Circuit for Shaft Encoder Signals.

generated for the trace in Figure 2.8 corresponds to the speed of motion of the axis. Since the encoder output signals have a pulse width of 2 μ s, which is unsuited for tape recording, the pulse width is first increased to 10 μ s using monostable multivibrators before processing. An operational amplifier circuit shown in Figure 2.9 is used to carry-out this process of signal addition. One of the encoder channels is connected to an inverting amplifier and the other to a non-inverting one. Since the CW and CCW signals cannot occur simultaneously the output of both amplifiers are simply connected together as shown in the figure. One such circuit is provided per axis-drive.

The operation of the digitizer is as follows: the rollers (G) and (G') are forced apart and then released so as to squeeze the raised track of the template in between them. Powering the DC motors through a speed regulator circuit causes the rollers, and hence the carriage, to track the template. As the carriage moves along the template, the shaft encoders generate two series of signals through their associated circuitry, each series corresponding to an axis.

The specifications of the template digitizer prototype are as follows:

Radial resolution : $R=2.54 \times 10^{-3}$ cm. (0.001 inch)

Angular step : $=3.927 \times 10^{-4}$ radians

Angular resolution : varies linearly with the radial displacement from the machine pole, and given by:

$$\Delta A = r \Delta \theta$$

Work area : is a section of an annulus subtended by an angle of 2.8 radians, and inner and outer radii of 7.62 cm. (3 inch) and 33.02 cm. (13 inches) respectively.

2.3 Software digitizer

The software digitizer, shown in Figure 2.1, is made up of two computer algorithms. The first one is a digitizing algorithm written in the FORTRAN language. The second, an output algorithm, is an ASSEMBLER routine responsible for transfer of the data generated by the digitizing algorithm to the output device. As shown in Figure 2.1, the digitizing algorithm requires the contour information, the tracking speed, as well as information about the tool to be used on the NC machine. The algorithm generates a file that is a numerical image of the signals that would be generated by the template digitizer if a template of the same contour was being tracked. This file can be either transferred to a mass storage device or stored in data memory.

When the file representing the whole contour has been generated, the output algorithm is initiated. The output algorithm receives the information from the data file in memory and synchronizes their delivery to the output port with time signals provided by the real time clock of the computer. An electronic circuit is used to combine the in-

formation from two bits on the data lines of the output port into two signals similar to that shown in Figure 2.8.

The digitizer algorithm runs under BATCH mode on time-shared computers, as well as on small and slow computers. The output routine, however, runs under REAL TIME conditions, thus precluding time-shared computers from hosting the algorithm. The file generated by the digitizer can be accessed from the data memory of the time-shared machine through a direct memory access device (DMA), thus eliminating physical memory duplication. Alternatively, the file can be transferred entirely to the memory of the computer hosting the output algorithm. Description of the two algorithms are given below.

Digitizer algorithm:

This algorithm is written in FORTRAN and thus is machine independent. The algorithm solves the geometric relationship of the NC machine as the axes are indexed by one resolution at a time, subject to the constraints imposed by the contour $r_1 = r_1(\theta_1)$ and contour pole location (C, β) . The time interval required to cover one resolution on either axis is calculated from the contouring speed and the path length corresponding to the resolution. Figure 2.10 shows a schematic diagram of a tool of radius R_r tracking a curve $r_1 = r_1(\theta_1)$ whose pole (O_1) is related to the machine pole (O) by vector (C, β) . Two geometric expressions can be formulated, for the point of contact (P) between the tool and the curve, to relate the angular orientation of the arm

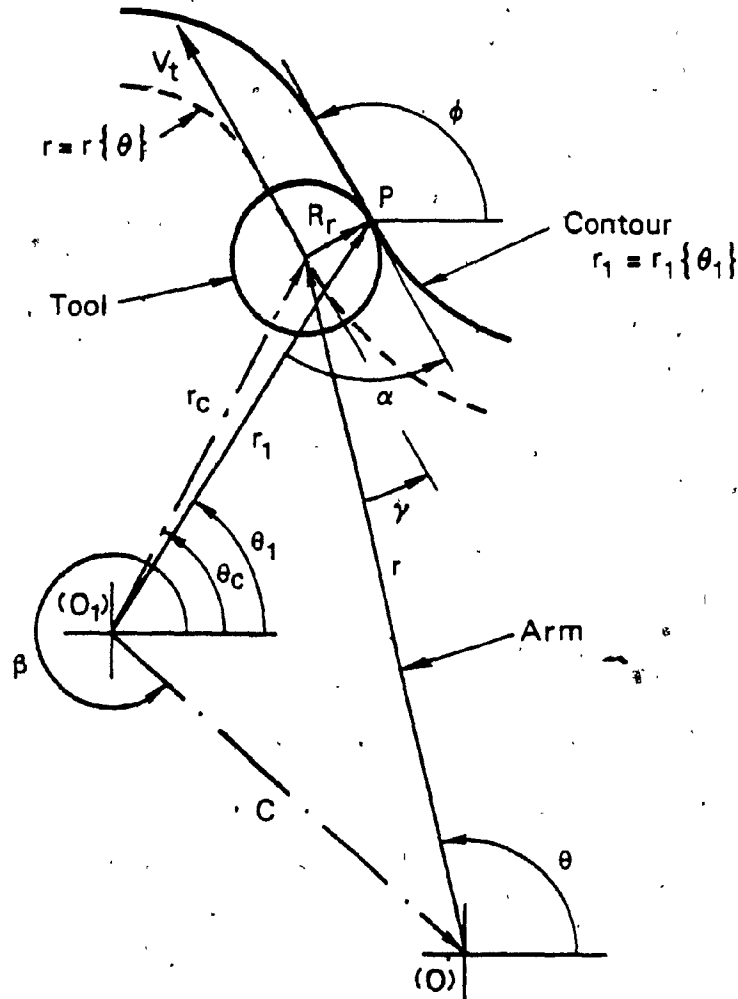


Figure 2.10: Vector Representation of the Polar System in Contouring.

and the radial displacement of the center of the tool r to the angular position of (P) as follows:

$$r_1 \sin(\theta - \theta_1) - C \sin(\theta - \beta) - R_r \cos(\alpha - \theta + \theta_1) = 0 \quad 2.1$$

$$r - \left[C^2 + r_c^2 - 2Cr_c \cos(\theta_c - \beta) \right]^{\frac{1}{2}} = 0 \quad 2.2$$

where,

$$\alpha = \cos^{-1} \left[\frac{dr_1}{d\theta_1} / r_1 \right]$$

$$r_c = \left[r_1^2 + R_r^2 - 2 r_1 R_r \cos\alpha \right]^{\frac{1}{2}}$$

and,

$$\theta_c = \theta_1 - \sin^{-1} \left[R_r \cos\alpha / r_c \right]$$

The distance travelled on the contour (Δs) that results due to indexing of either of the two axes by one resolution is given by:

$$\Delta s = \left\{ \begin{array}{l} \int_{\theta_1 \text{ (initial)}}^{\theta_1 \text{ (final)}} r_1 \{ \theta_1 \} d\theta_1 \text{ For R-axis movement} \\ \int_{r_1 \text{ (initial)}}^{r_1 \text{ (final)}} \theta_1 \{ r_1 \} dr_1 \text{ For } \theta\text{-axis movement} \end{array} \right\} 2.3$$

The time required to cover this length is given by:

$$t = \Delta s / V_t$$

2.4

A simplified flow-chart of the digitizer algorithm is shown in Figure 2.11, and a computer listing of a software implementing the flowchart is given in Appendix [C-1]. With reference to the flow-chart, the algorithm consists essentially of two loops, each corresponding to an axis in the polar system. Starting with one of the axes as determined by IFLAG; say θ , it is indexed by $\Delta\theta$ in a direction determined by the required direction of rotation. Using the new value θ Equation 2.1 is iterated to solve for θ_1 . If no convergence is achieved, the direction of indexation of θ is reversed and the iteration process restarted. Once θ_1 is found, the value of r is calculated from Equation 2.2. The change in r is evaluated, and if found greater in magnitude than the ΔR , the θ loop is abandoned and the radial axis loop is started. For a change less than ΔR , the loop continues by calculating the length of the contour curve in the interval $\Delta\theta$ using Equation 2.3. The time required to cover this interval is then calculated using Equation 2.4. Information about the time, the direction of indexation and the axis indexed are written into the output file. Conditions for the end of the contour, i.e., the stop criterion, are then evaluated and the loop is restarted if the end of the contour is not reached. The loop for the radial axis is exactly similar to that of the angular axis with the axial parameters interchanged as can be seen from

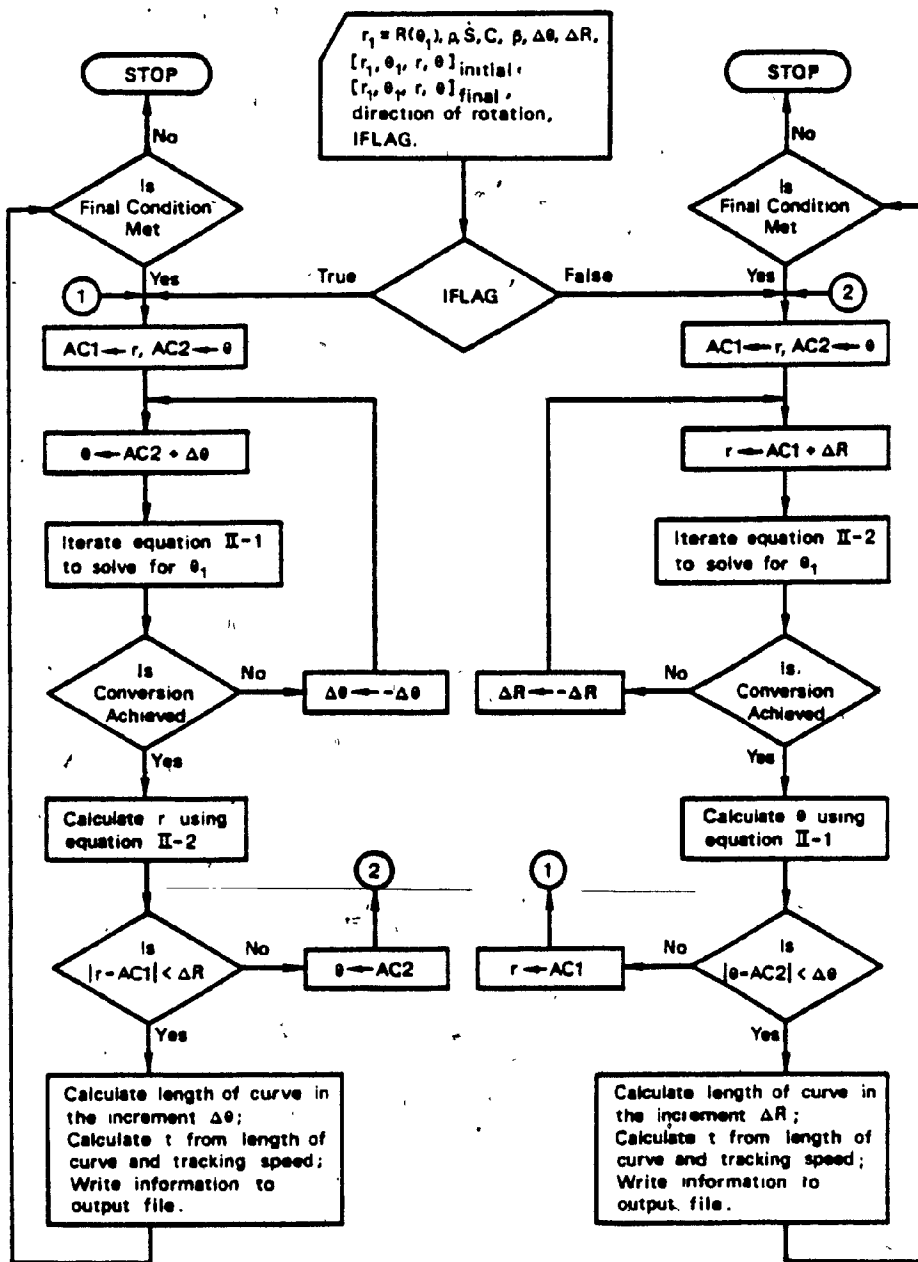


Figure 2.11: Flowchart of the Digitizer Algorithm.

the flow-chart. In this loop, however, the radial displacement r is indexed by ΔR and Equation 2.2 is iterated to solve for θ .

In this algorithm, the contour information can be supplied in equation form or as discrete points on the contour. In the latter case, more points are generated in between those given by using the Cubic Spline interpolator. A description of this interpolation technique is given in Reference [18]. If the analytical expression of the contour $r_1(\theta_1)$ and the first derivative of r_1 with respect to θ_1 are known, then an iterative procedure for finding the solution of Equations 2.1 and 2.2 are carried out using the Newton-Raphson root finding technique [18]. If the first derivative cannot be obtained easily, then the Secant root finding technique [18] is used. Both the above-mentioned root finding techniques require initial guesses to start the iteration process. The immediate previous values of points on the contour are used for such guesses. The integration of Equation 2.3 required to evaluate the length Δs is carried out numerically using a Guassian Quadrature, Reference [18]. The integrand is approximated by a Laguerre Polynomial, whose weights and roots are given in Reference [19].

The generated output file consists of multiple records of two entries each. The first entry is the time required to cover the resolution, and the second indicates the axis indexed and the direction of indexation. The second entry

in the record occupies only two bits in a computer word, with the least significant bit indicating a radial or angular resolution if it is 1 or 0 respectively. The other bit indicates positive or negative direction of indexation, if it is 1 or 0 respectively. Simultaneous indexation of both axes is entered as two successive records with zero time period in between them. For excessively long contours the generated data file is divided into a number of smaller ones with cumulative time entries inserted at their boundaries. These small files are processed one at a time. The cumulative time signals are used to synchronize the appending of these files together.

Output algorithm:

Figure 2.12 shows a flow-chart of this algorithm. The ASSEMBLER code is best suited here due to the high execution speed required and to the simplicity of the algorithm. Computers that can host this algorithm should have access to a real time clock. As shown in Figure 2.12 the algorithm is composed of one simple loop. The loop starts by reading the first entry, which is a time entry, from a record in the data file generated by the digitizing algorithm. The time value is transferred to the clock register. The clock is started, and interrupts the central processor when the time period loaded into its register lapses. The processor then transfers the second entry in the record, axes information, to the output port. The end of file condition is checked and if records still exist on file the loop is re-

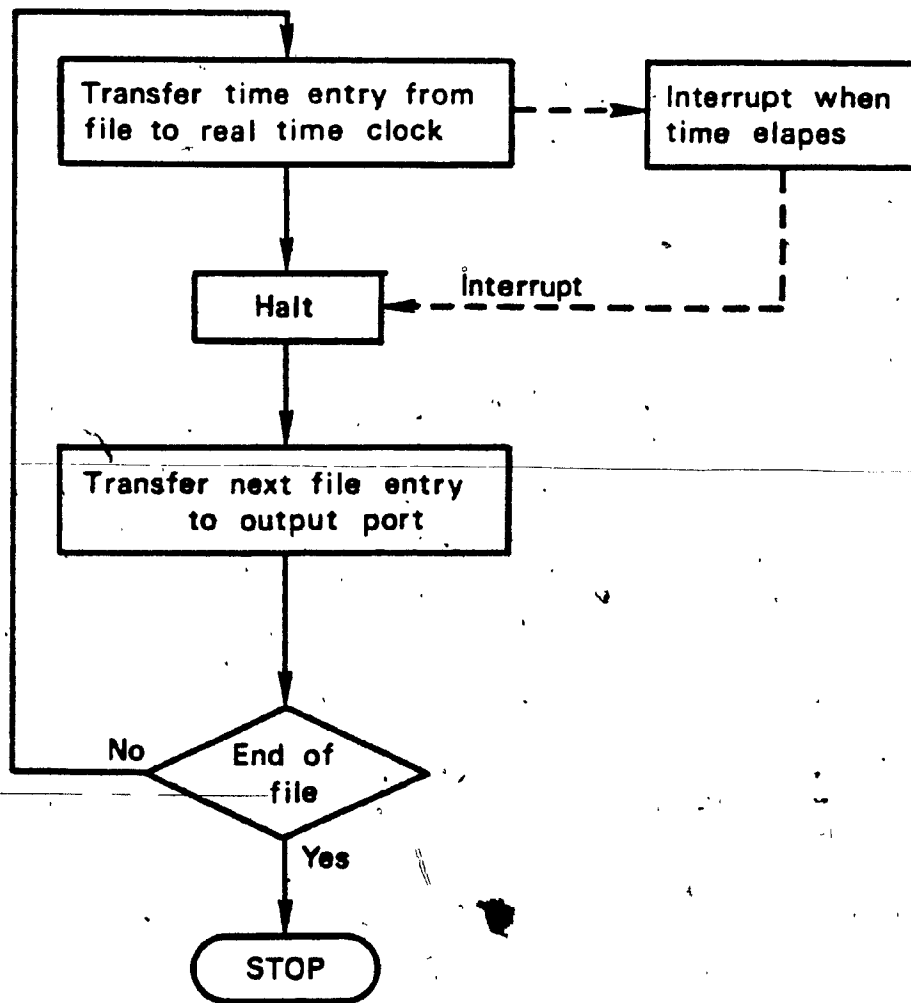


Figure 2.12: Flowchart of the Output Algorithm.

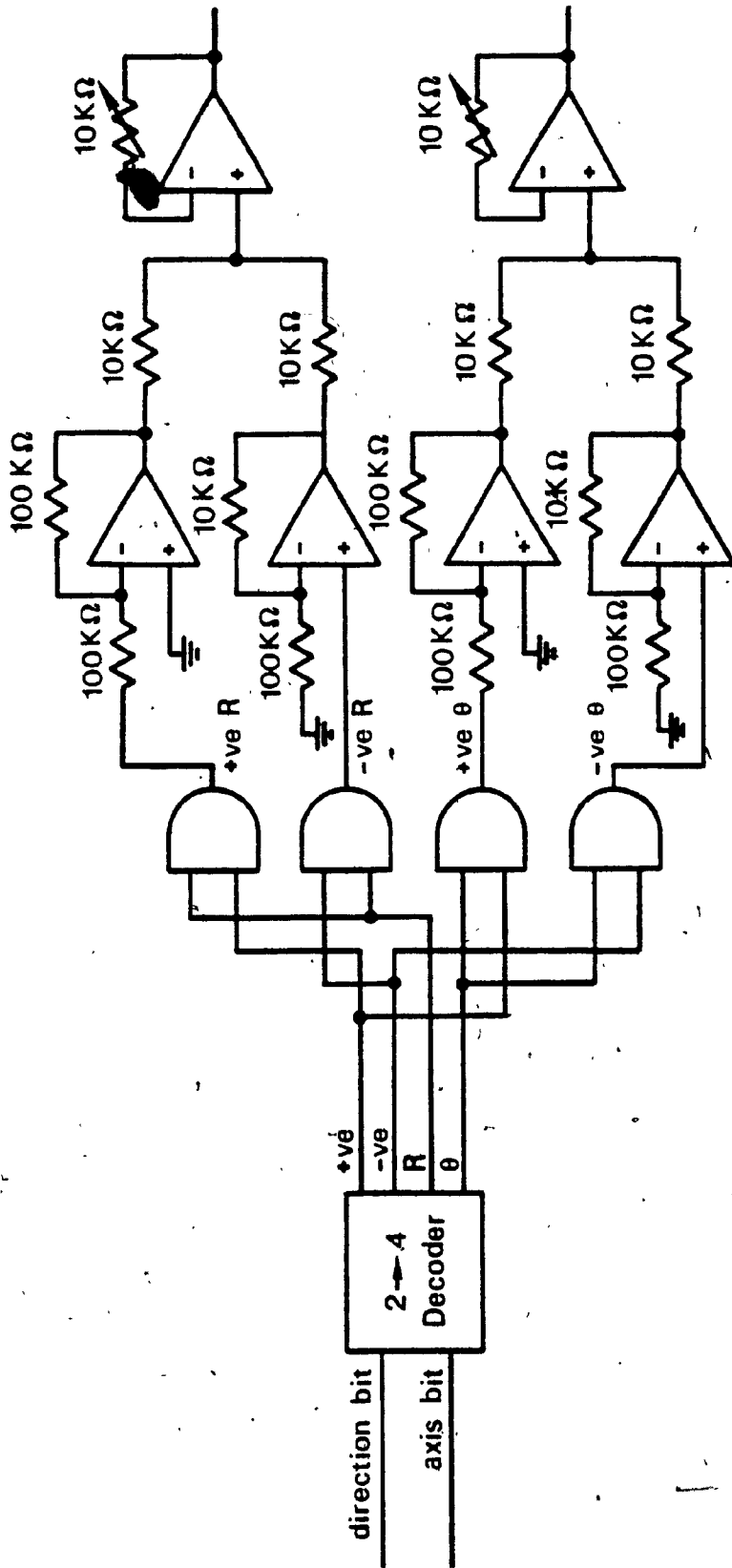


Figure 2.13: Circuit for Decoding the Software Digitizer Signals.

started.

Appendix [C-2] lists a fully documented sample program that has been implemented and tested on a TM-990/189 single board microcomputer. The program is based on the above-illustrated flowchart. A full description of the microcomputer is given in References [20] and [21]. The computer is a 16-bit machine, which allows packing of the time and axis entries in a record into one word, thus making full use of the available memory. With 14-bits available for a time entry, a time period ranging from 0 seconds up to approximately 0.5 sec in steps of 33 μ sec can be achieved. The axes information in the two least significant bits are decoded using the circuit shown in Figure 2.13 into two signals similar to those of Figure 2.8. The circuit uses a 2-to-4 decoder and four AND gates to trigger a bank of four operational amplifiers as shown. The outputs from each pair of amplifiers corresponding to one axis are then summed.

2.4 Prototype polar NC machine

A schematic diagram and labelled photographs of the prototype NC machine are shown in Figures 2.14 and 2.15. With reference to the figures, the prototype resembles the template digitizer described earlier. It consists mainly of a work area (A) and an arm (B) keyed at one end to a shaft (S). The shaft is driven by a stepping motor (C) via a worm-and-gear train (D). The arm is essentially a cantilever pivoted at one end and supported by a unit (E) at the

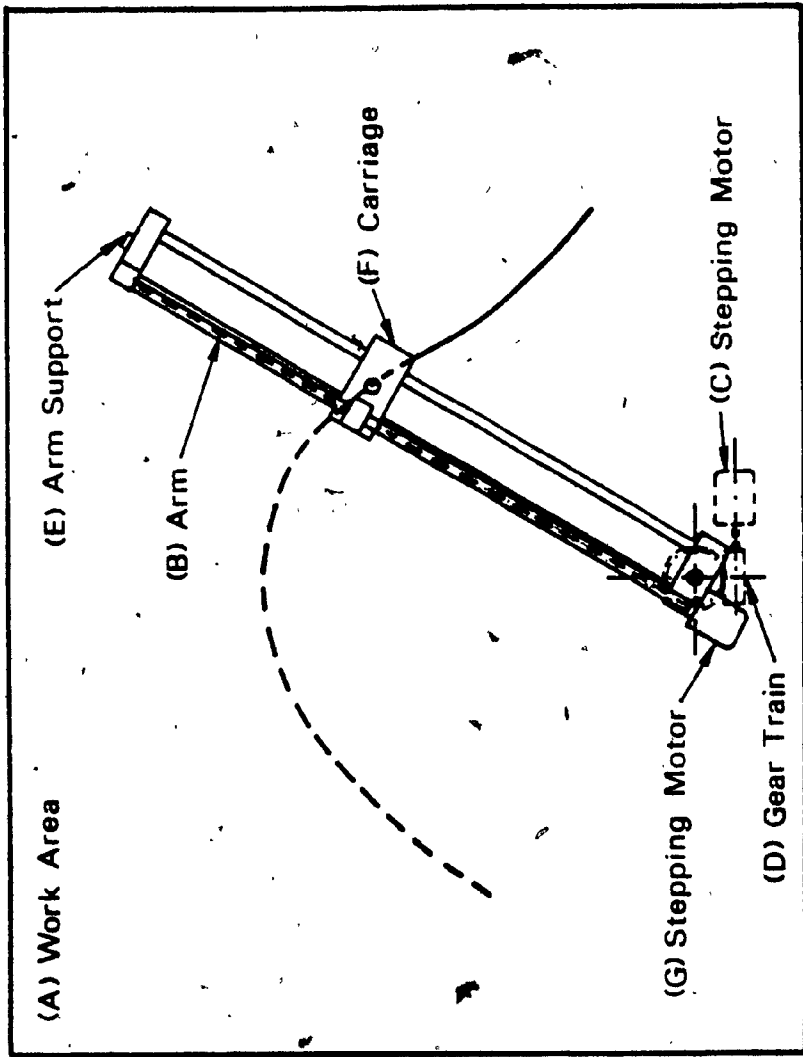


Figure 2.14: Schematic Diagram of the Prototype NC Machine.

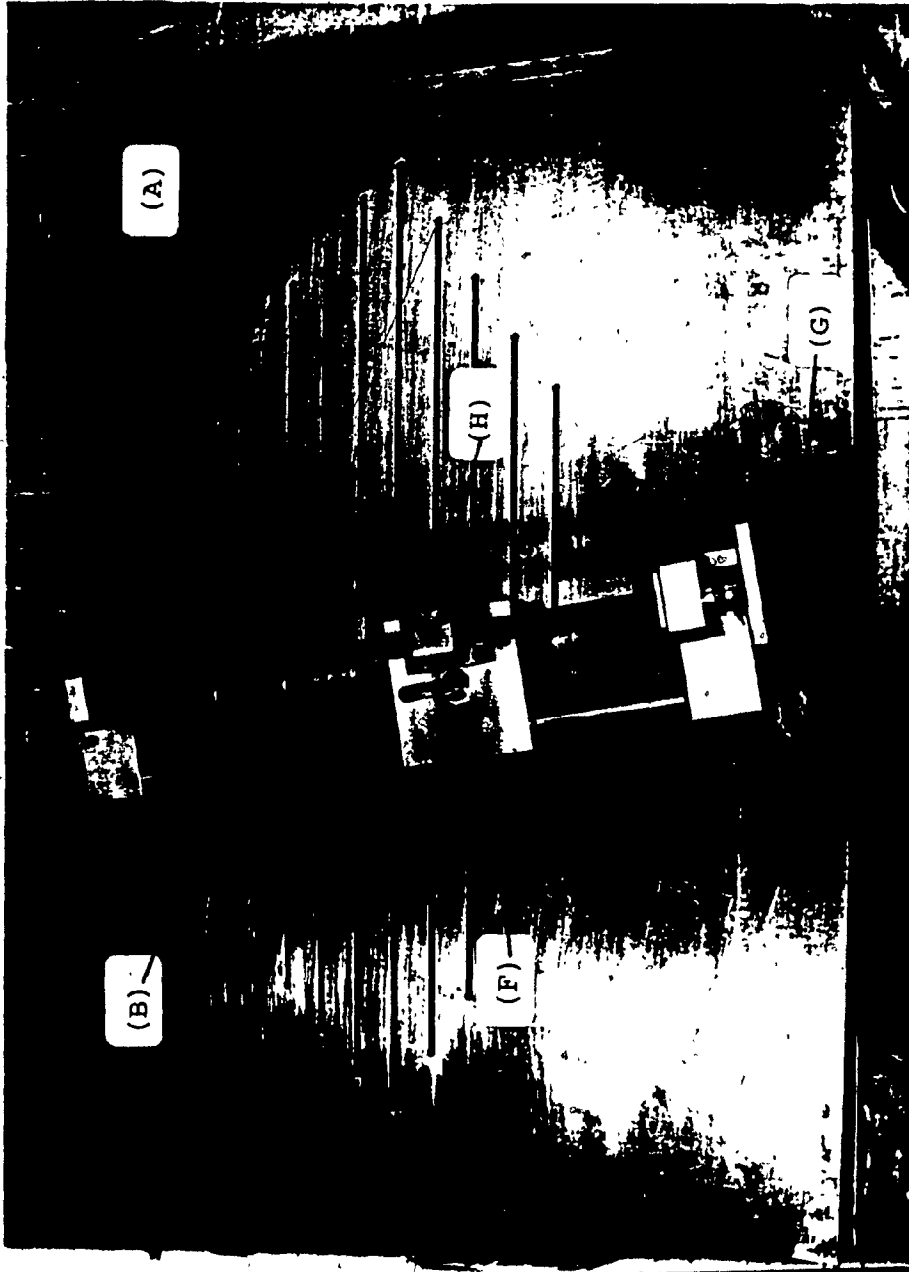


Figure 2.15.a: Photograph of the Prototype NC Machine.



Figure 2.15.c: NC Machine Axes-Drives Arrangement

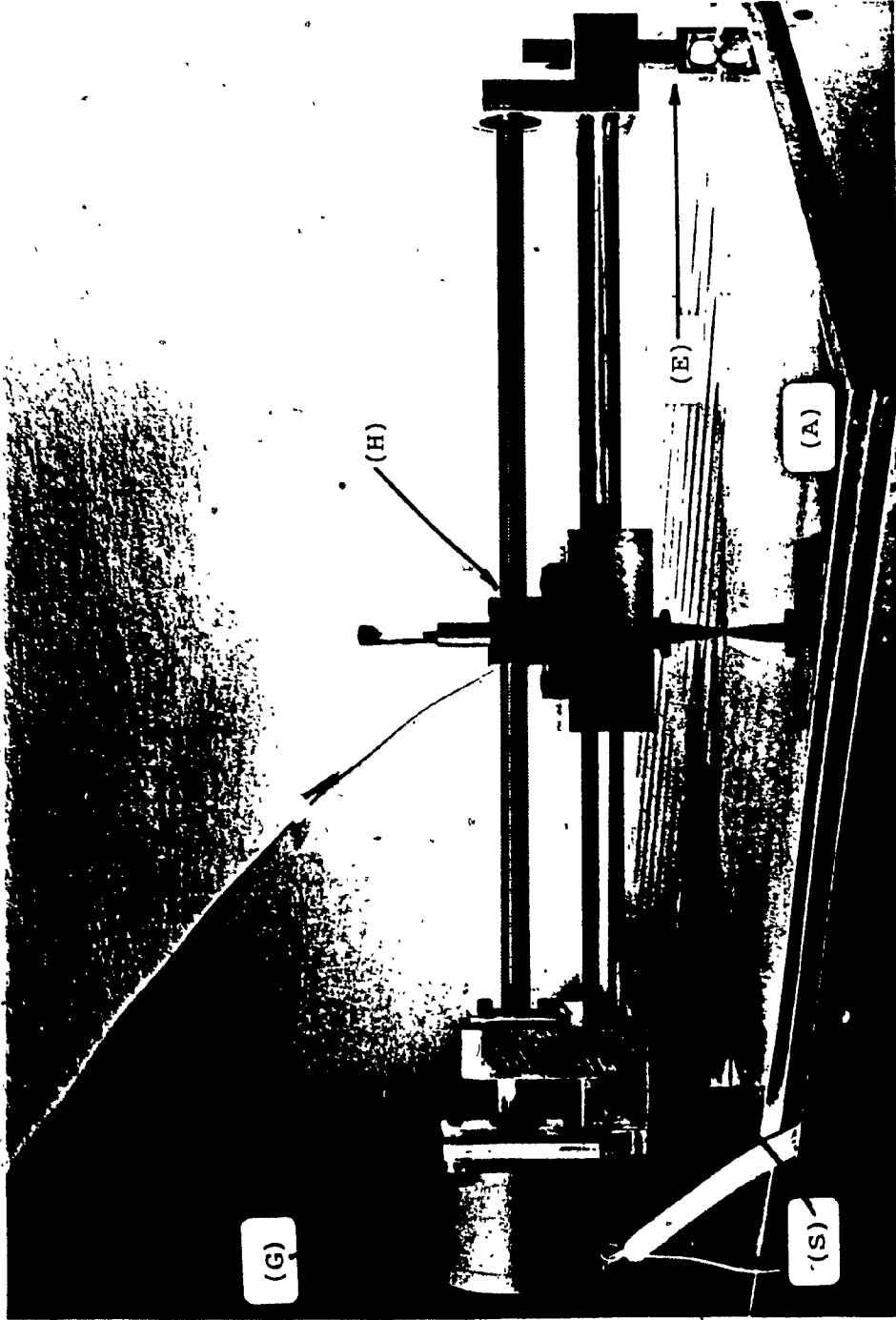


Figure 2.15.b: NC Machine Arm and Carriage Assemblies.

overhanging end. A carriage (F) travels on linear bearings along the length of the arm, being driven by another stepping motor (G) mounted on the arm. The drive force is transmitted to the carriage via a split nut and lead-screw arrangement (H). Within the context of polar coordinates the arm position provides the angular axis while the displacement of the carriage along the arm provides the radial position. The carriage carries the tool. The tool is a pen in the demonstrated prototype. The motion of the arm is limited by the two stops (I) and (I') (not shown on the photographs). The right stop (I) marks the home position of the arm or the angular axis reference. The location of (I) corresponds to the home position of the arm of the template digitizer. The position at which the carriage is at its minimum displacement from the shaft (S) marks its home position, or the radial axis reference. This reference also is identical with the corresponding reference on the template digitizer.

Subassembly drawings of the prototype NC machine are included in Appendix [A-2]. A hardware logic circuit (not shown) uses threshold comparators to decode the two composite incoming signals before channelling them to the two motor drive circuits. Figure 2.16 shows a schematic of the logic circuit used. The two stepping motors can also be driven directly from the encoder signals.

The stepping motors are energized in a "wave" scheme, also known as "half step" scheme, as opposed to the commonly

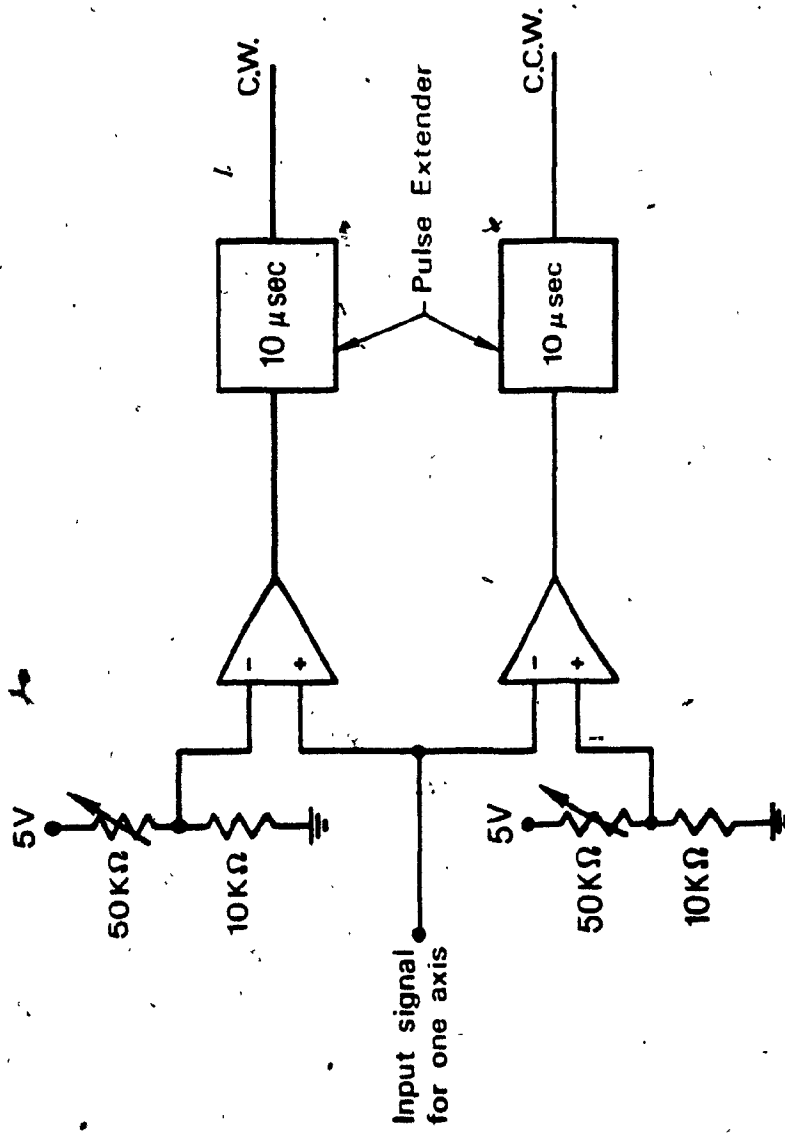


Figure 2.16: Decoding Circuit for NC Machine Control Signals.

used single and double phase schemes. Description of this mode of operation as well as the general description, operation, and characteristics of electric stepping motors can be found in References [22] to [29]. A brief description of the motor is outlined in Appendix [F.1]. The drive circuits required for the wave scheme are more complex than those required for the other two schemes. Further, the output torque of the motor is only 60% to 70% of that attainable when employing two phase energization. The wave mode of operation is used, however, since it offers two important advantages over the other two: the step angle of the motor is half its normal one thus resulting in finer machine resolutions, and secondly, resonance problems inherent to stepping motors are drastically reduced, Reference [22] (pp.228).

The resolution and the size of work area of the NC machine are identical to those of the template digitizer.

CHAPTER 3

SALIENT FEATURES, ADVANTAGES

AND DISADVANTAGES OF THE POLAR CONTOURING SYSTEM

3.1 Introduction

Commercially available contouring systems are either copying machines having analog servos as their controlling element and using a template as a source of contour information or they can be NC machines relying totally on an on-board computer for control and utilizing information in the form of numerical data. The system proposed in this thesis occupies a distinct space in-between these two types of machines. It is numerically controlled, but rather than using an on-board computer for control, it uses a simple hardware logic circuit and timing signals implicit within the contour data. The contour information can originate from a template or from an off-board computer. In the latter case the information is recorded on magnetic tape and then supplied to the machine as described earlier in Chapter 2. Since the system is digitally based, it makes use of recent advances in digital electronics to handle and manipulate the flow of information between its various components. The configuration of the system allows it to be more versatile than copying machines. The system may be equipped with an on-board computer which would make it as versatile and flexible as conventional NC machines in general applications.

In strict contouring applications, the system offers a number of advantages over both types of conventional machines. It should be noted also that the system has some drawbacks, but the advantages outweigh these drawbacks. An itemized comparison between the proposed contouring system and the conventional machines follows. At the end of this chapter a tabulated summary of this comparison is provided in Table 3.11.

3.2 Method of supplying contour information

The method by which the contour information is supplied to the proposed system is among its most outstanding features. As mentioned earlier the system can operate both as a copying machine or as an NC machine. This flexibility allows the system to be used as an NC machine, in applications where the required contour is too complex to be put in template form or where a high degree of accuracy is required. If a template is available, the system may be used as a copying machine. This flexibility is not shared by available systems.

Another outstanding feature of the system is the ease with which digitized contour signals can be recorded and then played back to produce duplicates of the digitized contour. This feature is particularly useful in large volume production where one taped set of data can be duplicated so as to operate several polar contouring machines. Although this ability is shared by commercial NC machines, they have

the drawback of requiring one computer per machine in order to reprocess the data supplied to produce a single contour.

3.3 Complexity of controller

Although the complexity of the controller is transparent to the user it is reflected both in the cost of the system and in its serviceability.

Analog servos in copying machines use complicated precision components for their operation. These servos have reached such a maturity of design that their performance and reliability can be fairly well predicted. Because of their complexity only experienced and well trained personnel can service servo systems. NC machines are by far the most complex contouring machines available. The controlling computer is specially designed for high instruction execution speed and large data storage space. They are also equipped in the majority of cases, with hardware arithmetic units and similar hardware devices to expedite the execution of the interpolation and axes control tasks.

The proposed system-controller is less complex than those available on commercial contouring machines as evident from the descriptions given in the previous chapter. Although no experience has yet been accumulated concerning its reliability and serviceability it is believed that its simplicity should give it an advantage in these areas.

3.4 Versatility

NC machines can in general perform more varied tasks than available copying machines or the proposed contouring system. Tool change, control of cooling fluid in metal removal applications, set-up of the work-piece, and the like are examples of such tasks that can be carried out. More advanced NC machines are even capable of adaptive control, that is, the modification of parameters in the control programs to compensate for changing conditions like tool wear or work-piece temperature rise.

Both conventional copying machines and the proposed contouring system are confined only to contouring applications. Since the proposed system is digitally based it can be equipped with a small computer controller to carry out auxiliary tasks similar to those mentioned above.

3.5 Contouring speed

Most of the available copying machines cannot track a contour at a constant speed. This is mainly due to the lack of information about the direction of the tangent at the point of contact between the template and the tool. An exception to this is the type of copying machines employing powered followers which are mainly used in the clothing industry. NC machines track a contour at approximately constant speed, Reference [12] (pp.25). Depending upon the

percentage of speed regulation, this control process could be the most time demanding task that engages the machine controller.

The proposed system has the capability of tracking a contour at a constant speed when operated with a software digitizer. Since digitization and imbedding of the time-reference into the signal is done prior to the contouring operation itself, the digitizing software is not affected by production time constraints. When these data are recorded and played back on commercial, stereo, magnetic tape recorders with typical tape speed regulation of 0.07%, the maximum contouring speed fluctuation resulting will not exceed 0.14% peak to peak.

For the TD/NC machine, the contouring speed depends upon the control scheme of the tracking rollers (G) and (G') as mentioned in Section 2.2. Using the control scheme whereby the sum of the speeds of the two rollers is kept constant, results in possible variation in the contouring speed as the roller mechanism tracks a contour. This variation depends upon the radius of curvature of the contour at the point of contact with the roller, the radius of the roller, and the thickness of the template. The relation between these parameters is derived as follows: Figure 3.1 shows two rollers each of radius R_r joined together by the link (I) and tracking a contour of uniform thickness H. The rollers contact the two sides of the template at (P) and (P') and are spring loaded against the template. Assuming

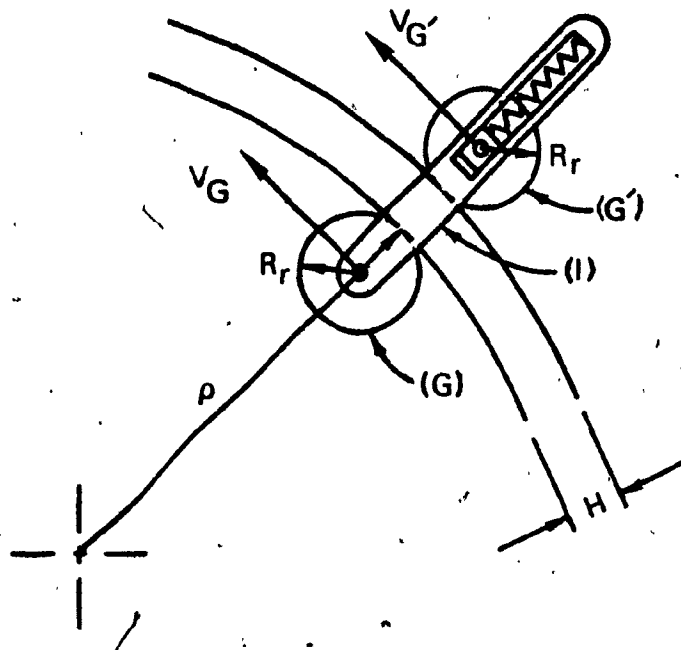


Figure 3.1: Schematic Diagram of the Roller Mechanism in Contouring.

negligible friction in the roller bearings, the equilibrium position of the link (I) is along the normal to the tangent at (P) and (P'). This position is also collinear with the direction of the radius of curvature ρ at (P). The instantaneous direction of motion of the rollers is around the centre of curvature. With reference to the figure the following kinematic relation can be derived:

$$v_{G'} = \frac{v(\rho + H + R_r)}{\rho - R_r} \quad 3.1$$

where v and $v_{G'}$ are the velocities of the rollers (G) and (G') respectively. The roller differential arrangement is driven at a constant angular velocity that would result in the following equation:

$$2V_t = v + v_{G'} \quad 3.2$$

Substituting Equation 3.1 into Equation 3.2 and rearranging yields:

$$v^* = \frac{\rho^* - R_r^*}{2\rho^* + 1} \quad 3.3a$$

$$v^* = \frac{\rho^* + R_r^*}{2\rho^* - 1} \quad 3.3b$$

Equations 3.3.a and 3.3.b are for the cases where the center of curvature of the contour and the roller (G) are on the same side of the contour or on opposite sides respec-

tively.

where v^* is the nondimensional contouring speed with respect to the set speed V_t and is given by: $v^* = v/V_t$,

R^* is the nondimensional roller radius with respect to the template thickness and is given by: $R_R^* = R_R/H$,

and ρ^* is the nondimensional radius of curvature with respect to the template thickness and is given by; $\rho^* = \rho/H$. ρ^* has a minimum value of R_R^* .

Reference [30], (pp.17-1-5), gives the radius of curvature ρ for a curve $r_1 = r_1(\theta_1)$ in polar coordinates as:

$$\rho = \frac{\left[r_1^2 + (dr_1/d\theta_1)^2 \right]^{3/2}}{\left[r_1^2 + 2(dr_1/d\theta_1)^2 - r_1(d^2r_1/(d\theta_1)^2) \right]} \quad 3.4$$

Figure 3.2 shows a plot of the percentage variation in the contouring speeds for different values of R_R^* and ρ^* . The figure shows a high rate of decrease in the percentage error in contouring speed with the increase of ρ^* , particularly so at small R_R^* values. The figure also shows that when the radius of curvature of the contour equals the rollers diameter, the error in contouring speed increase to 100% and 200% for the cases when the center of curvature and the roller (G) are on the same side of the contour and when they are on opposite sides respectively.

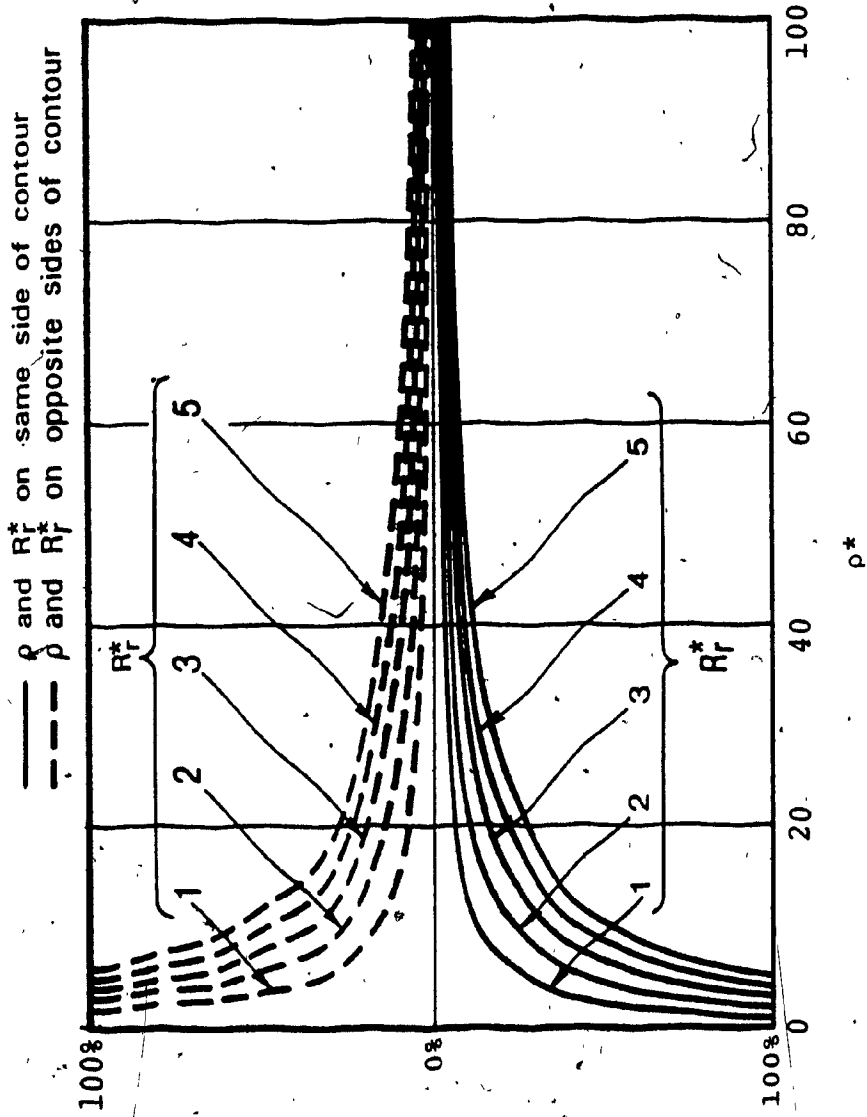


Figure 3,2: Contouring Speed Error Versus ρ^*

For moderately undulating contours, and practical rollers diameter and template thickness, the variation in contouring speed is within acceptable limits. For example, in the case of the prototype template digitizer with rollers diameter and template thickness of 0.3175 cm (1/8 inch), speed varies by less than 10% for a radius of curvature as low as 5 cm (2 inches).

Three templates were digitized on the prototype template digitizer. The signals from the encoders and the time period between them were collected using a hybrid computer as explained in Appendix [D]. The three templates are shown in a photograph in Figure 3.3. The circular template represents the case of constant radius of curvature, while the line template has an infinite radius of curvature. The rectangular template has an infinite radius of curvature along its linear segments and a radius of curvature very close to the radius of the rollers at the corners. An analysis of the collected data showed that upon switching the power supply on, that is to say applying a step velocity input, the contouring speed oscillates for a short length on the template before stabilizing. Imperfections, in the form of indentations, on the rectangular template cause the contouring speed to oscillate again for a short length on the template.

3.6 Scaling of contouring speed

When a contour is digitized, the generated signals are

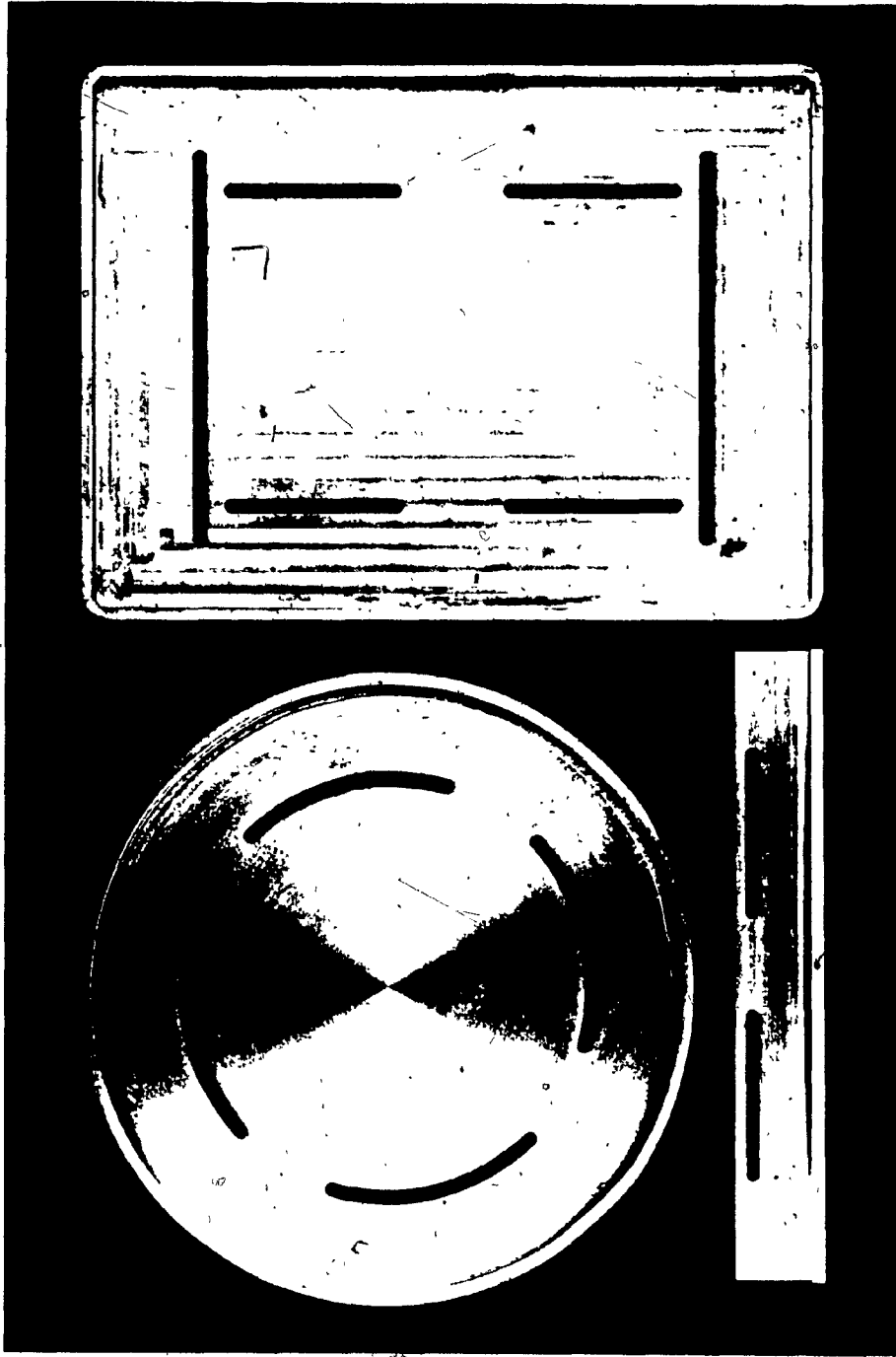


Figure 3.3: Photograph of Templates Used in Testing.

timed so as to reflect a constant contouring speed. Recording these signals on magnetic tape, and then using a different playback speed other than that used for recording, results in a proportional change in the time periods between the signals, and hence in scaling the contouring speed. Scaling of the contouring speed has practical applications in cases where the contouring speed needs to be changed after a contour has been digitized. It also can be made use of as explained in Appendix [D] to collect time period information between the two encoder signals. The procedure consists of recording the signals at a high tape speed and then playing it back at a slow speed. This allows more accurate measuring of the time periods between the signals.

3.7 Size scaling

The majority of commercial copying machines are not capable of producing a contour of different size other than that of the generating template. Copiers that are capable of size scaling are expensive. Available NC machines can generally be programmed to track a contour of different scale than that of the supplied information. In the proposed machine, however, up or down-scaling of the size can be very easily achieved by simply scaling the radial axis only. The angular resolution in polar coordinates is given by:

$$\begin{aligned}\Delta A &= r \Delta \theta \\ &= n_R \Delta R \Delta \theta\end{aligned}$$

3.5

where ΔA is the angular resolution,
 $\Delta \theta$ is the angular step,
 ΔR is the radial step (also the radial resolution),
and n_R is an integer equal to the number of radial resolutions from the machine pole to the carriage position.

The simplicity of scaling here is attributed to the fact that the angular resolution is proportional to the radial resolution, and scaling the radial resolution causes an equivalent scaling of the angular one.

Scaling the radial resolution is achieved by designing the system such that one radial resolution on the NC machine is equivalent to m resolutions on the digitizer. Using a presettable logic counter to intercept the radial signals to the NC machine, and setting it so as to signal the radial axis after every k incoming signals instead of after the usual m , where both m and k are integers, results in scaling the contour by a factor of m/k . Figure 3.4.a shows a simple example where the digitizer radial resolution is four times smaller than that of the NC machine. The counter signals that would result in doubling the contour size as well as those that would halve it are also shown.

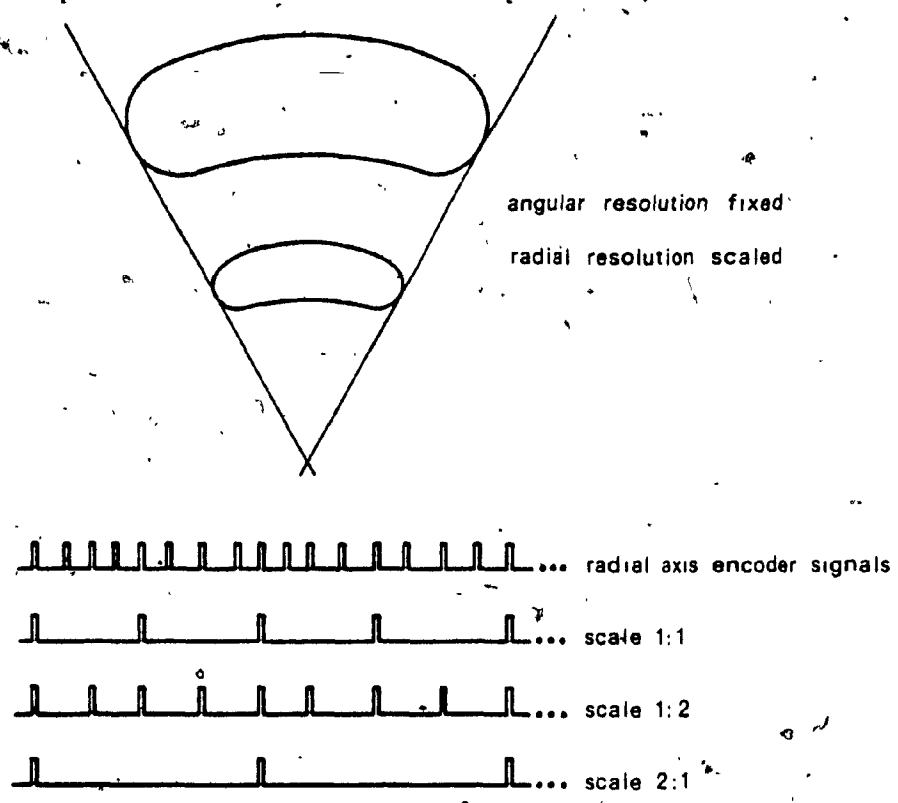


Figure 3.4.a: Size Scaling on the Polar Contouring System.

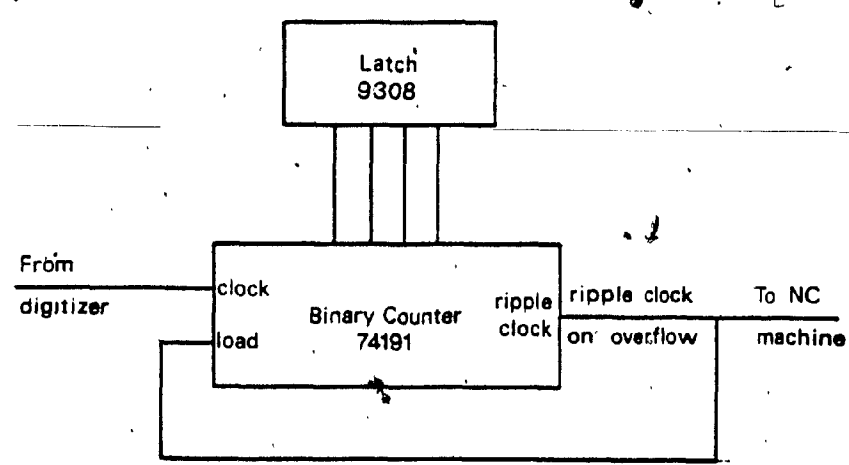


Figure 3.4.b: Logic Circuit for Size Scaling.

Figure 3.4.b shows a single counter chip connected so as to produce scaling factors ranging from 1:4 down to 4:1 when used with the above mentioned example. The circuit is introduced here to emphasize the simplicity of achieving size scaling.

Size scaling is a very practical feature particularly in metal removal applications. The original contour is scaled down after every pass to compensate for the metal removed during that pass. Furthermore, when combined with speed scaling, higher machining speeds can be used for rough cutting passes and lower ones for finishing cuts. These speeds can be produced with the same taped signals.

3.8 Accuracy of contouring

The accuracy of copying machines depends upon the analog servo used to control them, as well as on the load on the axes-drives. NC machines have preselected resolutions, and when operated within their load carrying capacity, the accuracy is limited to one resolution.

Cartesian based NC machines usually have equal resolutions along both axes. The resolution is homogeneous within the work space. The proposed contouring machine has a constant resolution along the R-axis. However, the angular axis resolution varies linearly with the radial position within the work space. This variable angular resolution, although a drawback simplifies size scaling as mentioned earlier.

The upper accuracy bound of a contour produced on the polar NC machine is equal to the maximum angular resolution, and occurs if the contour is machined at the extremity of the work area.

3.9 Work area

Cartesian coordinate based NC machines allow more work area than those using polar coordinates for the same overall machine size.

3.10 Power utilization of the axes-drives

Available copying machines as well as the majority of NC machines utilize feedback loops to guard against errors. This allows the machines to operate at near full torque capacity of the axes-drives. The proposed contouring system operates with an open loop, and thus a reasonable factor of safety on loading must be imposed. Alternately, a method for determining the exact torque required for a given application may be used. By varying the machining parameters, the torque required by the axes-drives is kept below that available from them. A simple method for determining such a required torque will be presented in a subsequent chapter.

3.11 Reference position

The homogeneity of the resolutions in Cartesian based systems allow a contour to be generated anywhere on the work

space from a given set of information. The reference position is simply transferred to the new position. This floating reference feature simplifies setting up of a work-piece for machining.

In the proposed polar system, a contour can be produced only from the same radial displacement used for digitizing it. The reference position of the angular axis, however, can be floating. Setting up of a work piece at the radial reference is a simple task and can be automated.

3.12 Cost

Present trends towards digital controls, inspired by rapid advances in the field of digital electronics are continually reducing the costs of digital systems hardware. This trend, however, is counterbalanced by an ever increasing cost of driver software required for these controllers. The type of software required for these controllers is very specialized due to the complexity of the control task and the high execution speed required to keep up with contouring speeds dictated by production practices. The proposed contouring system eliminates the need for such software since the axes-drives are not controlled directly by a computer even when a software digitizer is employed. This results in a lower cost system. Contouring systems utilizing analog controls are inherently more expensive than the proposed system, owing to the cost of the high precision components required.

A comprehensive cost study would have to include other economic aspects such as production time savings, and maintenance costs. For the production of a large batch of the same contour, the production times for the three systems is expected to be identical. However, as both the ratio of the contouring time to the setting-up time and the number of required parts in a production batch decrease, conventional NC machines would prove more economical. Production time savings by factors as high as 4 or 5 times for such applications have been reported in Reference [11].

The cost of maintenance of conventional NC machines would be higher than those of the other two systems due to the complexity of their controllers. The maintenance costs of available copying machines would be still higher than those for the proposed system, due to the complexity and precision of servo controllers.

TABLE 3.1: Comparison between existing contouring systems and the polar contouring system.

ATTRIBUTES	2,23D COPYING MACHINES	2,23D NC MACHINES	PROPOSED SYSTEM
METHOD OF SUPPLYING CONTOUR INFORMATION	CONTOUR INFORMATION IN THE FORM OF A TEMPLATE	CONTOUR INFORMATION IN THE FORM OF NUMERICAL DATA	CONTOUR INFORMATION IN THE FORM OF A TEMPLATE OR NUMERICAL DATA
SIMULTANEOUS USE OF THE CONTOUR INFORMATION ON OTHER MACHINES	NOT POSSIBLE	CONTOUR INFORMATION CAN BE SUPPLIED ON PUNCHED, OR MAGNETIC TAPE TO OTHER MACHINES	DIGITIZED CONTOUR SIGNALS CAN BE RECORDED, DUPLICATED AND REUSED ON OTHER MACHINES
COMPLEXITY OF CONTROLLER	PRECISION SERVO CONTROLLER	COMPLEX COMPUTER BASED CONTROLLER	SIMPLE HARDWARE LOGIC CONTROLLER
VERSATILITY	CONFINED TO CONTOURING APPLICATIONS	VERSATILE; CAPABLE OF TOOL CHANGE; INITIAL SET UP OF WORK-PIECE AND THE LIKE	CONFINED TO CONTOURING APPLICATION; EASY TO EQUIP WITH COMPUTER CONTROLLER TO CARRY OUT AUXILIARY CONTROL TASKS
CONTOURING SPEED	NOT CONSTANT	SMALL VARIATION; CAN BE MADE CONSTANT FOR SLOW CONTOURING SPEEDS	CONSTANT IN CASE OF SOFTWARE DIGITIZER; SMALL VARIATIONS SUBJECT TO CONTOUR IN CASE OF TEMPLATE DIGITIZER
CONTOURING SPEED SCALING	THE CONTOURING PROCESS HAS TO BE INITIATED AT THE NEW SPEED	THE COMPUTER CONTROLLER HAS TO REPROCESS THE CONTOUR INFORMATION SUBJECT TO THE NEW REQUIRED SPEED	CONTOURING SPEED CAN BE SCALED UP OR DOWN BY PLAYING BACK A RECORDED SIGNAL AT AN APPROPRIATE SPEED OTHER THAN THE RECORDED ONE
SIZE SCALING	POSSIBLE ON MORE EXPENSIVE COPIERS	EASY TO IMPLEMENT BECAUSE OF AVAILABLE COMPUTER POWER	EASY TO IMPLEMENT; REQUIRES SCALING OF THE RADIAL AXIS ONLY
ACCURACY	DEPENDS ON THE ACCURACY OF THE SERVO CONTROLLER	RESOLUTION KNOWN AND HOMOGENEOUS WITHIN THE WORK SPACE	RADIAL RESOLUTION, CONSTANT; ANGULAR RESOLUTION, NOT HOMOGENEOUS WITHIN THE WORK SPACE; ACCURACY WITH RESPECT TO WORST CASE RESOLUTION EXPRESSED
WORK AREA	RECTANGULAR OR SQUARE, RESULTING IN BETTER UTILIZATION OF THE MACHINE SPACE	RECTANGULAR OR SQUARE; RESULTING IN BETTER UTILIZATION OF THE MACHINE SPACE	CIRCULAR; GENERALLY SMALLER THAN CARTESIAN COORDINATE BASED MACHINES
POWER UTILIZATION OF THE DRIVE MOTION	LOW FACTOR OF SAFETY ON TORQUE IS USED DUE TO PRESENCE OF FEEDBACK LOOP	LOW FACTOR OF SAFETY ON TORQUE IS USED DUE TO PRESENCE OF FEEDBACK TORQUE	REASONABLE FACTOR OF SAFETY ON TORQUE HAS TO BE IMPOSED; ALTERNATELY A METHOD CAN BE USED TO ACCURATELY GAGE THE TORQUE REQUIRED FOR A PARTICULAR OPERATION
REFERENCE POSITION	BOTH AXES LOCATION FOR THE REFERENCE POINT ARE FLOATING	BOTH AXES LOCATION FOR THE REFERENCE POINT ARE FLOATING	THE ANGULAR LOCATION OF THE REFERENCE POINT IS FLOATING, THE RADIAL REFERENCE HAS TO BE SET AT THE SAME LOCATION USED ON THE DIGITIZER
COST	MEDIUM COST	HIGH COST	LOW COST

CHAPTER 4

CONTOUR LOCATION FOR MINIMUM CONTOURING ERRORS ON THE POLAR MACHINE

4.1 Introduction

The digitizer signals received by the polar NC machine causes the axes-drives to move and trace a curve which approximates the digitized contour. The rate of incoming signals determines the contouring speed. If this rate is slowed down such that the response time of the axes-drives (that is to say, the time required to execute a signal) became comparatively negligible, the traced curve would be composed of linear segments along the radial axis joined by short circular arcs using the machine pole as a center. Such a contouring process is termed quasi-static. Figure 4.1 shows a contour and a curve approximating it produced by a point tool, $R=0$. Referring to the figure, there is a discrepancy between the contour and the approximating curve produced under quasi-static conditions. This discrepancy is indicative of the contouring accuracy.

This chapter will show that the accuracy of the contouring process in the polar contouring system depends upon the relative location between the contour pole and the machine pole. A method for increasing the contouring accuracy will be also presented.

4.2 Contouring error criterion

The absolute value of the maximum deviation between the machine generated contour and the reference contour can be used as an error criterion.

For NC machines, the deviation error is generally limited to one resolution. In the case of the proposed NC machine also the deviation error is limited to one resolution. However, due to the increase of the angular resolution with radial displacement, the deviation error is given as:

$$\epsilon_d = \begin{cases} \Delta R & \text{for } r \leq \frac{\Delta R}{\Delta \theta} \\ \Delta A & \text{for } r > \frac{\Delta R}{\Delta \theta} \end{cases} \quad 4.1$$

where ΔA is the angular resolution.

Another way of expressing the contouring error is to use the sum of the absolute values of the areas bounded by the contour and its approximation curve. This error is indicated in Figure 4.1 by the hatched areas. The error area criterion is more stringent than the one based on the deviation error. This can be typically portrayed as shown in Figure 4.1 where a small deviation error, sustained over a long length of the contour, results in a large area error. The area error criterion will be used in this thesis as the basis for estimating the contouring errors. Figure 4.2 is a

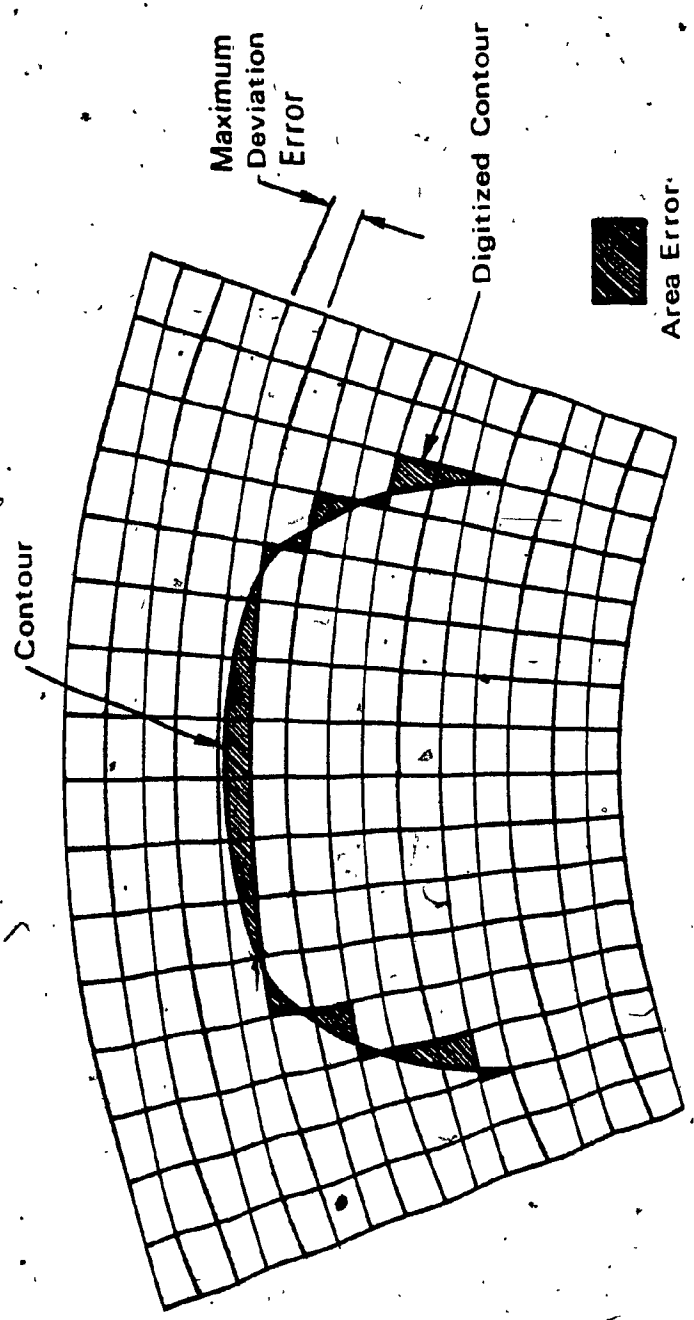


Figure 4.1: Error Criteria in the Contouring Operation.

magnification of one part of Figure 4.1 with some salient geometric parameters indicated. Referring to Figure 4.2, the total area error is given by:

$$\epsilon_a = \sum_{i=1}^n a^{(i)} \quad 4.2$$

where n is the number of the angular steps required to represent the contour.

The individual area errors $a^{(i)}$ for a contour $r=r\{\theta\}$ can be calculated from Figure 4.2 as follows:

$$a^{(i)} = \frac{1}{2} \left\{ \left| \int_{\theta^{(i)}}^{\nu^{(i)}} [r\{\theta\}]^2 d\theta - [r^{(i)}]^2 (\nu^{(i)} - \theta^{(i)}) \right| + \right. \\ \left. \left| \int_{\nu^{(i)}}^{\theta^{(i+1)}} [r\{\theta\}]^2 d\theta - [r^{(i)}]^2 (\theta^{(i+1)} - \nu^{(i)}) \right| \right\} \quad i = 1, 2, \dots, n \quad 4.3$$

where,

$$\theta^{(i)} = \theta^{(0)} + (i-1) \Delta\theta$$

$$r^{(i)} = r^{(i-1)} + k \Delta R$$

$$k = \text{integer} \left[\frac{r\{\theta^{(i+1)}\} - r^{(i-1)}}{\Delta R} \right]$$

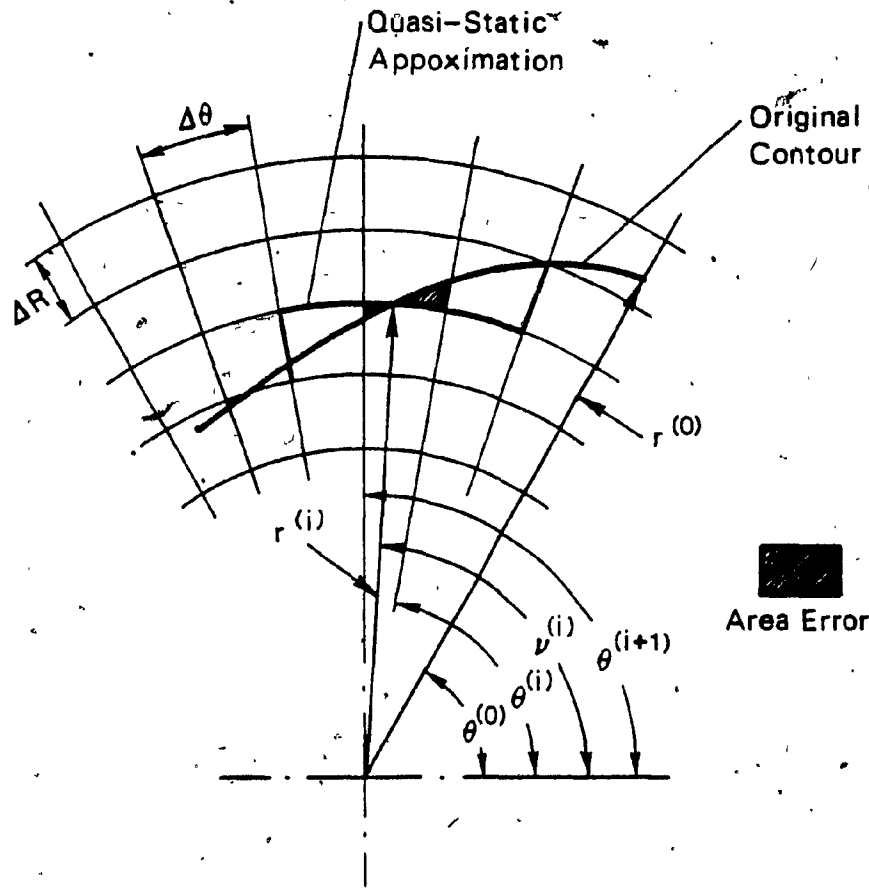


Figure 4.2: Salient Geometric Parameters for the Area Error Calculation.

$$v^{(i)} = \begin{cases} \theta^{(i)} & \text{for } \theta^{(i)} < \theta = \theta \{r^{(i)}\} < \theta^{(i+1)} \\ \theta^{(i+1)} & \text{for } \theta = \theta \{r^{(i)}\} > \theta^{(i+1)} \end{cases}$$

and,

$$I = \begin{cases} 0 & \text{for } v^{(i)} = \theta^{(i+1)} \\ 1 & \text{for } \theta^{(i)} < v^{(i)} < \theta^{(i+1)} \end{cases}$$

$r(0)$ and $\theta(0)$ are the first radial and angular grid lines intersected by the contour. Equation 4.3 and consequently Equation 4.2 are very difficult to evaluate analytically, and thus numerical evaluation has to be employed.

4.3 Factors affecting the area error

Perhaps the easiest method to reduce the area error and contouring errors in general, is to reduce the machine resolution. However, beyond a certain limit, the cost of reducing the resolution escalates faster than the benefit of error reduction. A further ill-effect of this reduction would be to reduce the maximum contouring speed that can be attained.

A close examination of the equation for the area error shows that this error depends upon the contour representation with respect to the machine pole, or in other words, on

the location of the contour within the work area. For the same resolution sizes, a reduction in the area error could be achieved by a careful selection of contour location.

4.4 An optimization problem for area error minimization

The evaluation of the exact path of the approximating contour is, in normal operation, a dynamic problem where factors such as resisting forces, inertias, and contouring speed would be involved. For the purpose of finding the optimal location of the contour for minimum reproduction error, the assumption of quasi-static operation is justified due to the following reasons:

a) Such a condition results in the maximum deviation of the approximating curve from the original contour and thus results in an upper bound for error.

b) A contour location that would minimize the error for quasi-static operation would also entail minimizing the error for conditions of normal operation. This point can be further explained with the aid of Figure 4.3. The figure shows four curves: (A) the original contour, (B) an approximating curve that would be produced under quasi-static conditions, and two dynamic curves (C) and (D) that would be produced in normal operation. The underdamped oscillatory trace (C) represents the case of a predominantly inertial load, and the overdamped trace (D) represents an application where large dissipative forces, such as in metal grinding, are involved. The area error bound by trace (C)

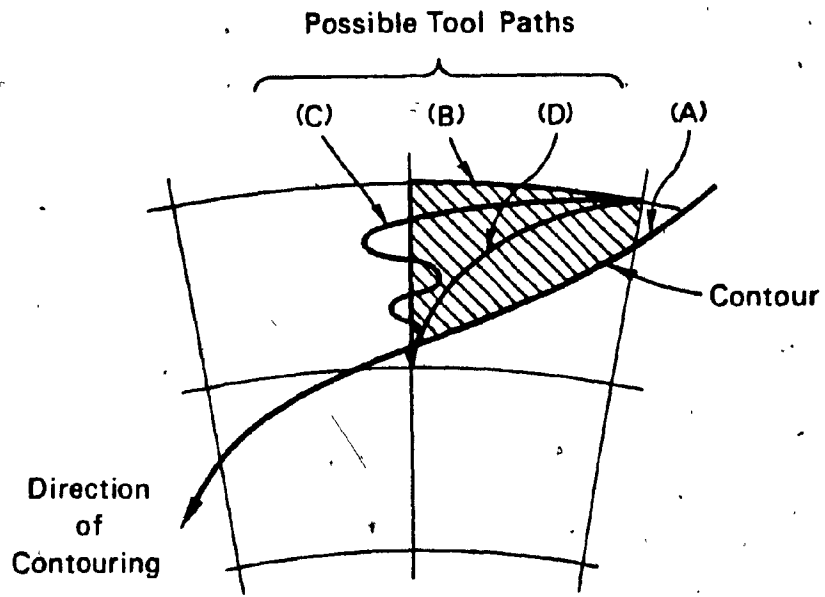


Figure 4.3: Different Tool Paths When Tracking a Contour.

and the original contour can be shown to be equal for all practical purposes to the area error for the quasi-static case. The area error for trace (D), however, is smaller than that for the quasi-static case. This discussion can be carried further to include other stepping situations.

As outlined previously, the area error varies with the location of the contour and can be calculated from Equation 4.3. Due to the complexity and discontinuous nature of the area error expression, analytic methods cannot be used to locate the contour within the work area for minimum error. Hence, numerical optimization techniques have to be employed. For the problem of minimizing the area error, the normal approach would be to use the area error expression from Equation 4.2 as an objective function. The most efficient and commonly used optimization techniques belong to either of the following two categories [31]: direct search techniques and gradient search techniques. Although gradient techniques are the more efficient of the two schemes, they require the derivative of the function with respect to the optimization parameters. For the area error minimization, such a derivative cannot be evaluated. Hence, the less efficient direct search techniques have to be used. For this problem, the use of direct search techniques requires large computer time, (several thousands of central processor seconds for one run using a CDC CYBER 835) due to the time required to evaluate the area error and the large number of function evaluations required. Furthermore,

the problem becomes unmanageable in cases where a narrow ridge is encountered in the objective function and the number of function evaluations required to yield a solution become prohibitively large.

4.5 Selection of an alternate objective function

Another approach to deal with this optimization problem is to find an alternative objective function that is faster to evaluate and at the same time quantitatively duplicates the relationship of the area error function with respect to the machine pole. That is to say, the extrema of the alternative objective function would coincide in location with those of the area error function. In the search for an alternate objective function, one approach that would result in a reduction of the area error, is to reduce the resolution of the polar machine. This approach in effect increases the number of radial and angular steps representing the contour. It is possible, however, to alter the number of radial and angular steps representing the contour by simply changing the location of the contour pole with respect to the machine pole.

To study the relationship between the number of steps and the area error, an algorithm is formulated to alter the location of a contour and to calculate the area error, and the radial and angular steps representing the contour. A straight line path is chosen as a study case. The reasons for this choice are three-folds: first, the calculation of

the area error for a straight line is much simpler than that for any other contour, a factor of paramount importance due to the large number of evaluations required to study the desired relationship; secondly, a straight line template can be accurately and easily machined for digitization and testing on the prototype template digitizer; and lastly, any contour could be approximated by a number of straight line segments, an approach which is practical in dealing with a general curve. Proper choice of the line segments representing the contour can result in an advantage of simplicity which would outweigh the disadvantages of resultant error due to the approximation. This piecewise linear approximation is used later in this chapter.

The number of radial and angular steps representing a straight line are combined together to form two functions which are formulated as follows:

Consider a straight line of length L which is divided into n number of small segments of length ℓ , thus

$$L = \sum_{i=1}^n \ell^{(i)}$$

4.4

Let $N_R^{(i)}$ and $N_\theta^{(i)}$ be the number of radial and angular steps registered in tracing the i th segment. Then, the first function F_{sum} is formulated as:

$$F_{\text{sum}} = \begin{cases} \sum_{i=1}^n \left| N_R^{(i)} + N_{\Theta}^{(i)} \right| & \text{for } N_R^{(i)} < N_{\Theta}^{(i)} \\ \sum_{i=1}^n \left| N_R^{(i)} + N_{\Theta}^{(i)} \frac{K}{R_m} \right| & \text{for } N_R^{(i)} > N_{\Theta}^{(i)} \end{cases} \quad 4.5$$

where K is the ratio of the radial to angular step size, $\Delta R/\Delta \theta$, and has the dimension of length, and R_m is the radial displacement of the mid-point of the line.

This function needs to be maximized in order to increase the number of steps representing the contour.

The second function is formulated with the objective to prevent the dominance of either the radial or angular steps over the other, and is given by:

$$F_{\text{dif}} = \begin{cases} \sum_{i=1}^n \left| N_R^{(i)} - N_{\Theta}^{(i)} \right| & \text{for } N_R^{(i)} < N_{\Theta}^{(i)} \\ \sum_{i=1}^n \left| N_R^{(i)} - N_{\Theta}^{(i)} \frac{K}{R_m} \right| & \text{for } N_R^{(i)} > N_{\Theta}^{(i)} \end{cases} \quad 4.6$$

Minimizing F_{dif} causes the number of steps taken by both

axes-drives to be close to each other.

When a straight line passes through the machine pole, and the pole lies at either end or beyond the length of the line, no angular steps would be required to represent the line, and the magnitudes of the two functions reach an extreme value:

$$F_{\text{sum}} = F_{\text{dif}} = L/\Delta R \quad 4.7$$

When the machine pole lies somewhere on the line, in between its two ends, the two function values from Equation 4.5 and Equation 4.6 respectively become:

$$F_{\text{sum}} = L/\Delta R + 2\pi/\Delta\theta \quad 4.8$$

$$F_{\text{dif}} = L/\Delta R - 2\pi/\Delta\theta \quad 4.9$$

Figure 4.4.b and Figure 4.5.b show plots of F_{sum} and F_{dif} versus the angular orientation of a straight line for different minimum radii R_{min} . The plots have been normalized with respect to the values F_{sum} and F_{dif} obtained when the line forms an equilateral triangle with respect to the machine pole and has a height equal to 7.62 cm. (3 inches). Plots of the actual area error for the straight line calculated based on Equation 4.2 and normalized in a manner similar to that described above are shown in Figures 4.4.a and 4.5.a for comparison purposes. In the plot of the area error, it should be noted that at γ equals zero and π radians the area error is zero. However, for a small perturbation in γ about zero or π radians the area error

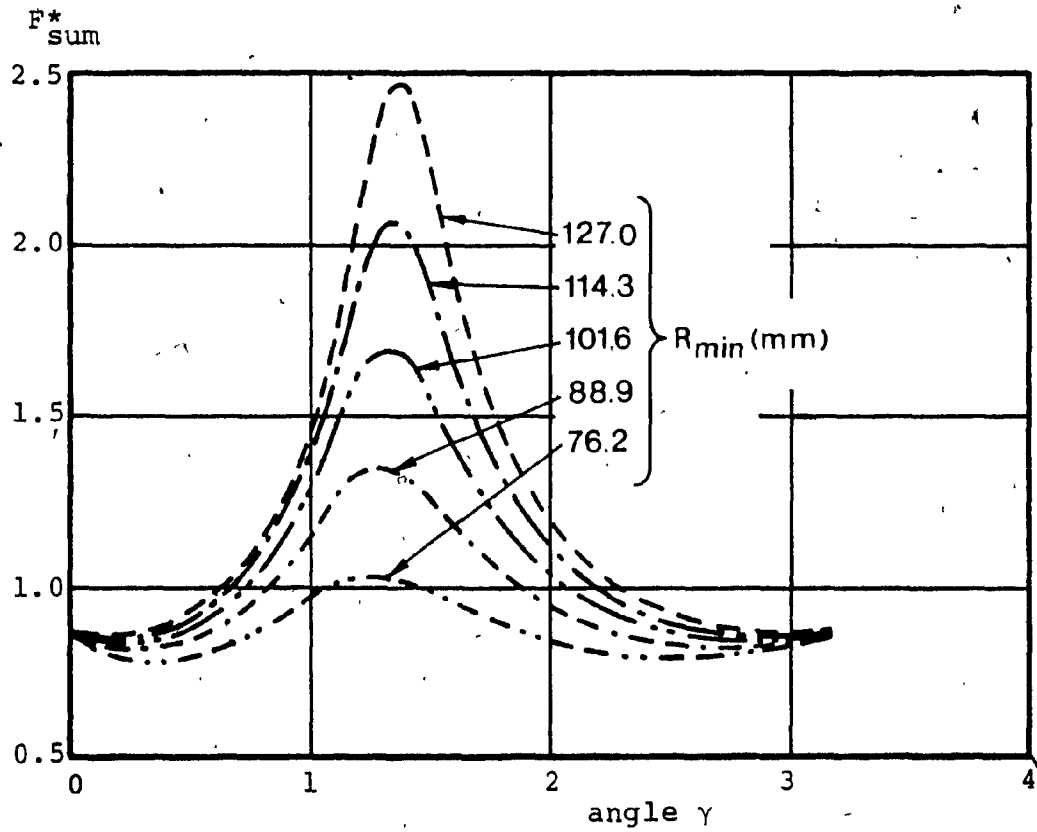
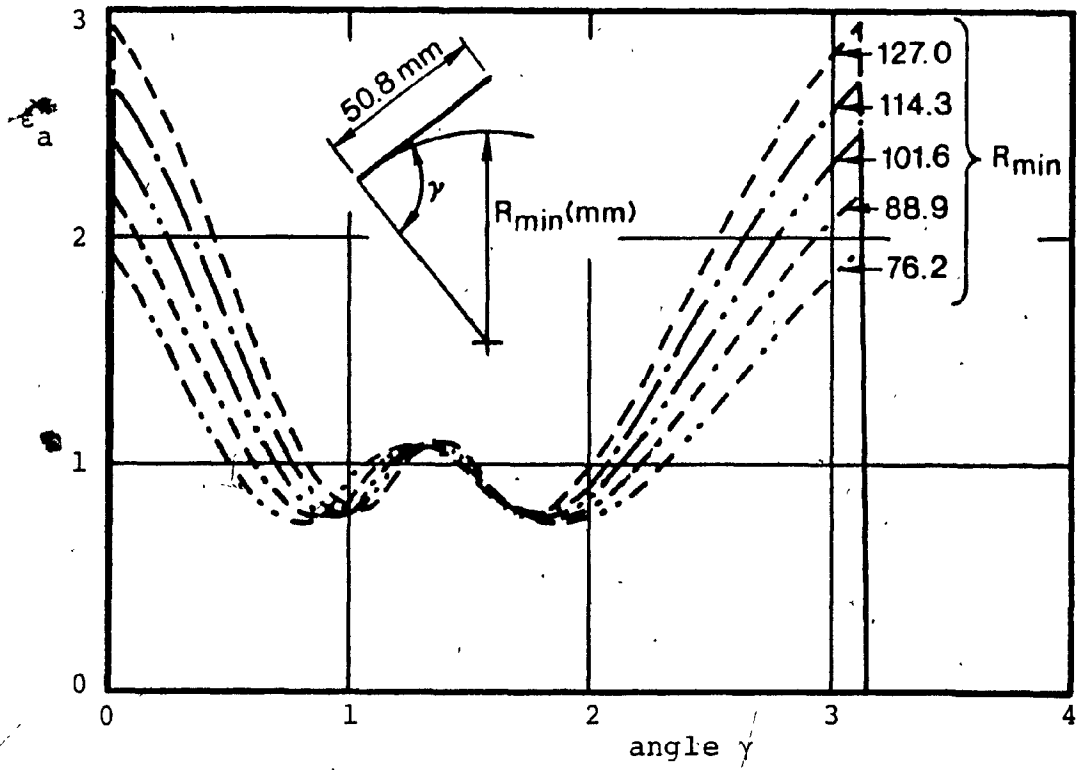


Figure 4.4: Normalized F^*_{sum} and ϵ_a Versus γ .

reaches a maximum value. The method used for calculating the two functions and the area error, as well as the algorithm implementing the method are given in Appendix (E).

Figure 4.4 shows that the F_{sum} function does not duplicate the relationship of the area error, although both have their maxima at approximately 1.3 radians. The F_{sum} function also exhibits two regions of minima on either side of its maxima, similar to the area error function. The location of the two minima, however, do not coincide in location with those of the area error function.

The behavior of F_{dif} as portrayed in Figure 4.5 is similar to that of the area error. However, comparing the minima for different values of R_{min} , there is a considerable spread in the function value F_{dif} in contrast to the area error. Also the value of the function F_{dif} at the minima, decreases with increasing R_{min} , and exhibits a reverse trend to that of the area error. Because of these factors, other types of objective functions which are combinations of F_{sum} and F_{dif} were examined for their effectiveness in emulating the area error plots.

Two such functions that are combinations of F_{sum} and F_{dif} are:

$$F_1 = F_{\text{dif}}/F_{\text{sum}} \quad 4.10$$

$$F_2 = F_{\text{dif}} + 1/F_{\text{sum}} \quad 4.11$$

Experimentation with both functions showed that the function in Equation 4.11 becomes progressively insensitive

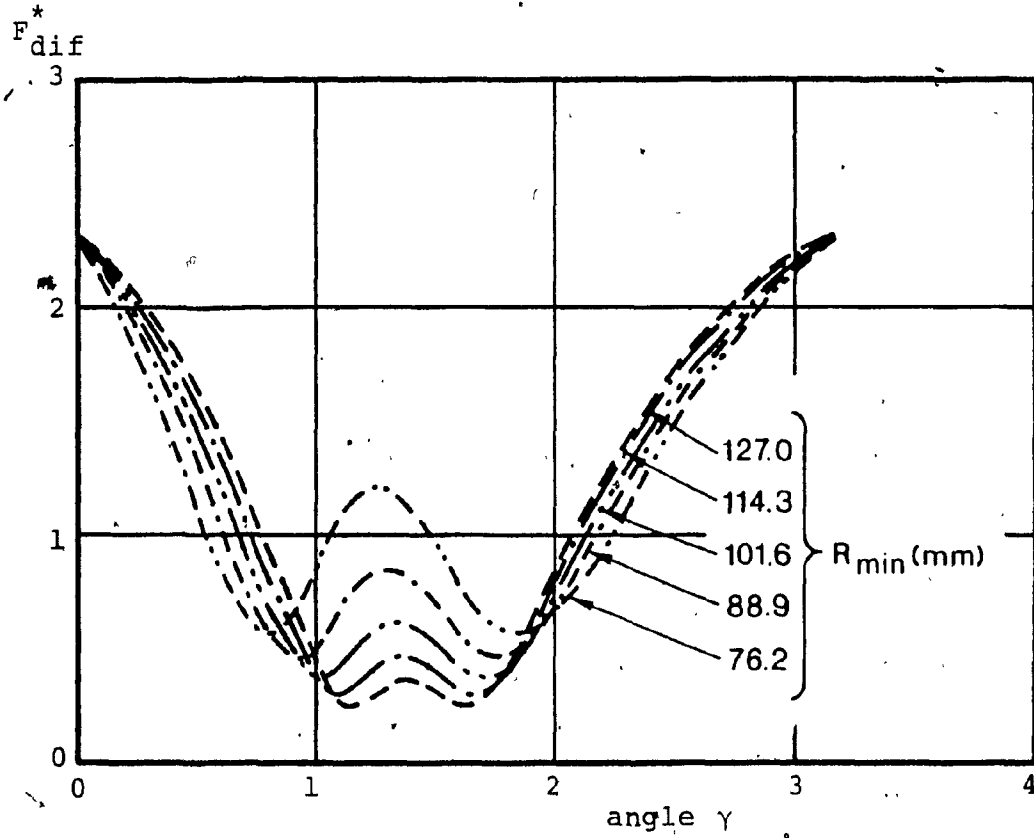
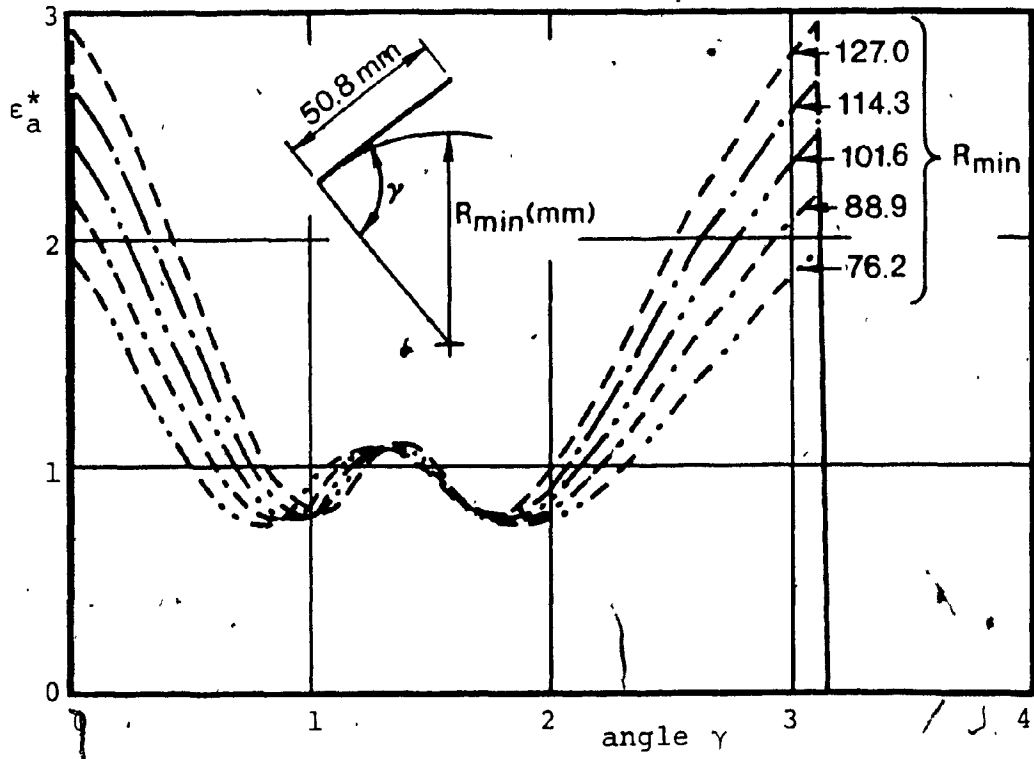


Figure 4.5: Normalized F_{dif}^* and ϵ_a^* Versus γ .

as F_{sum} increases and F_{dif} becomes dominant. The function in Equation 4.10 was found suitable and hence is chosen as the objective function for optimally locating the contour pole with respect to the machine pole.

Figure 4.6 shows a plot of this objective function corresponding to the functions F_{sum} and F_{dif} of Figure 4.4 and Figure 4.5 respectively. Again, here, the area error is provided for comparison. Figure 4.6 shows that the objective function F_1 behaves very similarly to the area error, and has its maxima and minima coinciding in location with those of the area error, and thus can be used as an objective function to predict the optimal location for minimum error.

It should be mentioned here that the factor K/R_m is introduced in F_{sum} and F_{dif} as a penalty factor. Figure 4.7.a shows the effect of this penalty factor on the function F_1 in contouring a line segment. The line segment under consideration is shown in Figure 4.7.b with some salient geometric parameters indicated. Referring to Figure 4.7.b, the ratio of the number of angular to radial steps is given by:

$$\frac{N_{\theta}}{N_R} = \cos^{-1} \left[\frac{(c^*)^2 - 1 + 2(r^*)^2 + 2r^*c^*}{2r^*c^* + 2(r^*)^2} \right] \frac{K}{c^*L} \quad 4.12$$

where c^* is a nondimensional parameter,
and r^* is the nondimensional radial displacement.

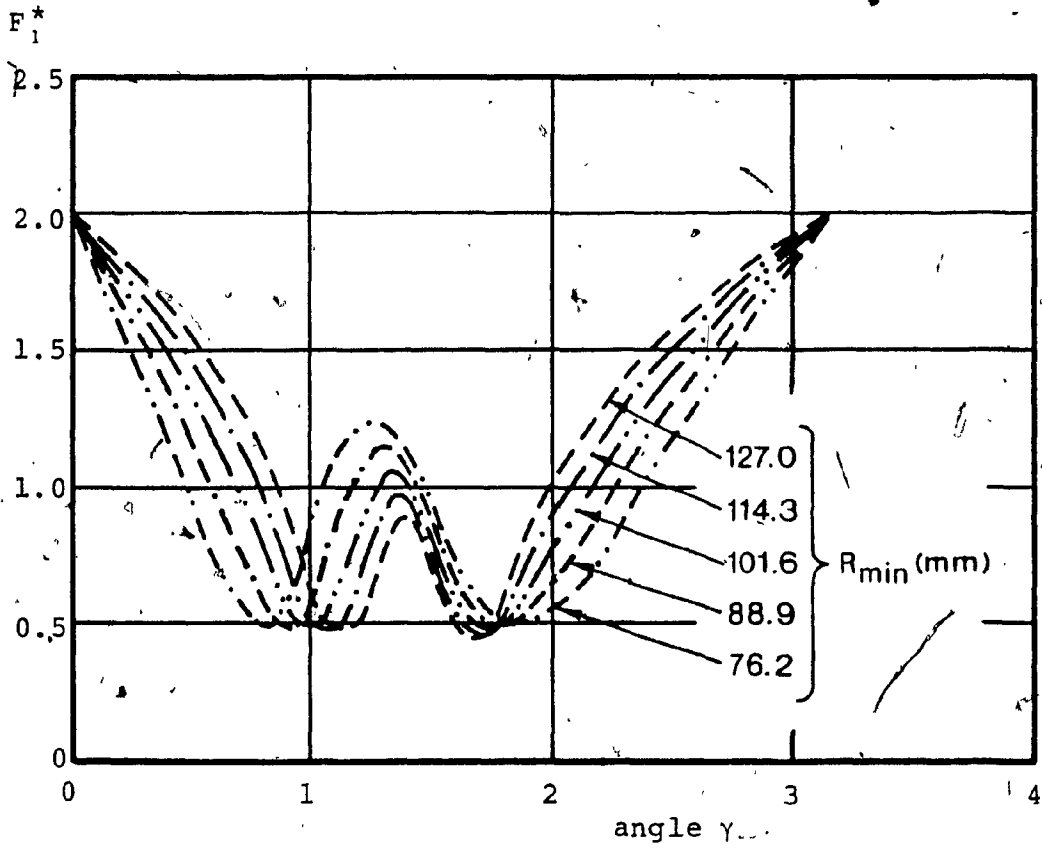
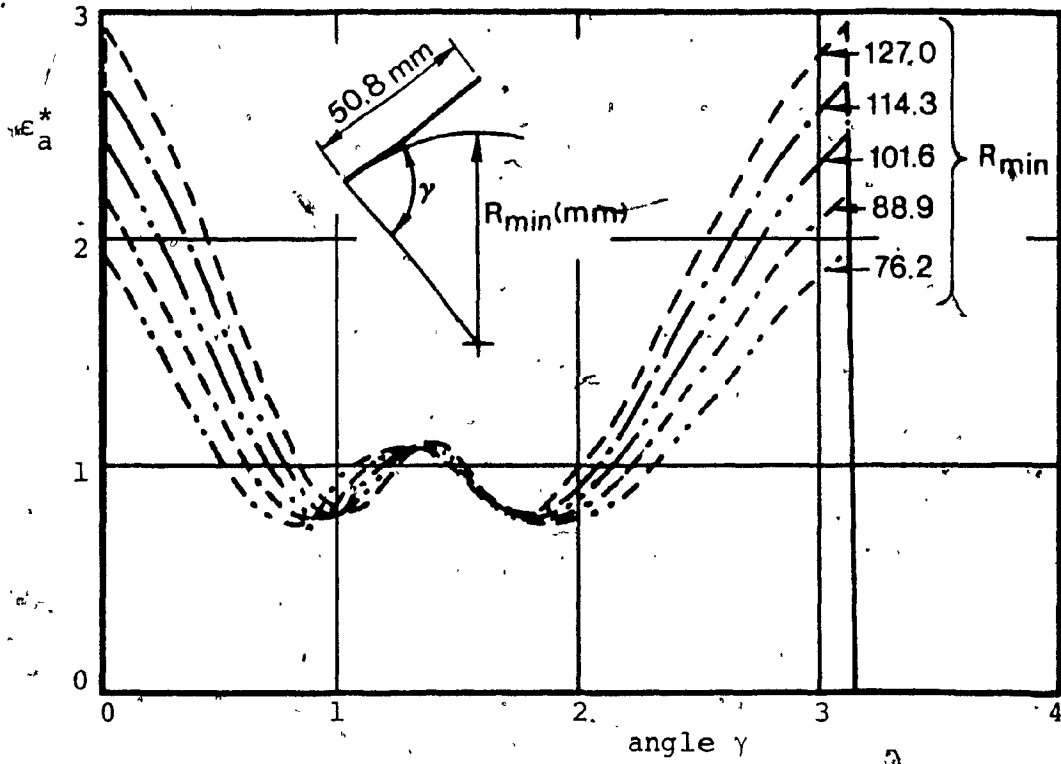


Figure 4.6: Normalized Objective Function F_1 Versus γ .

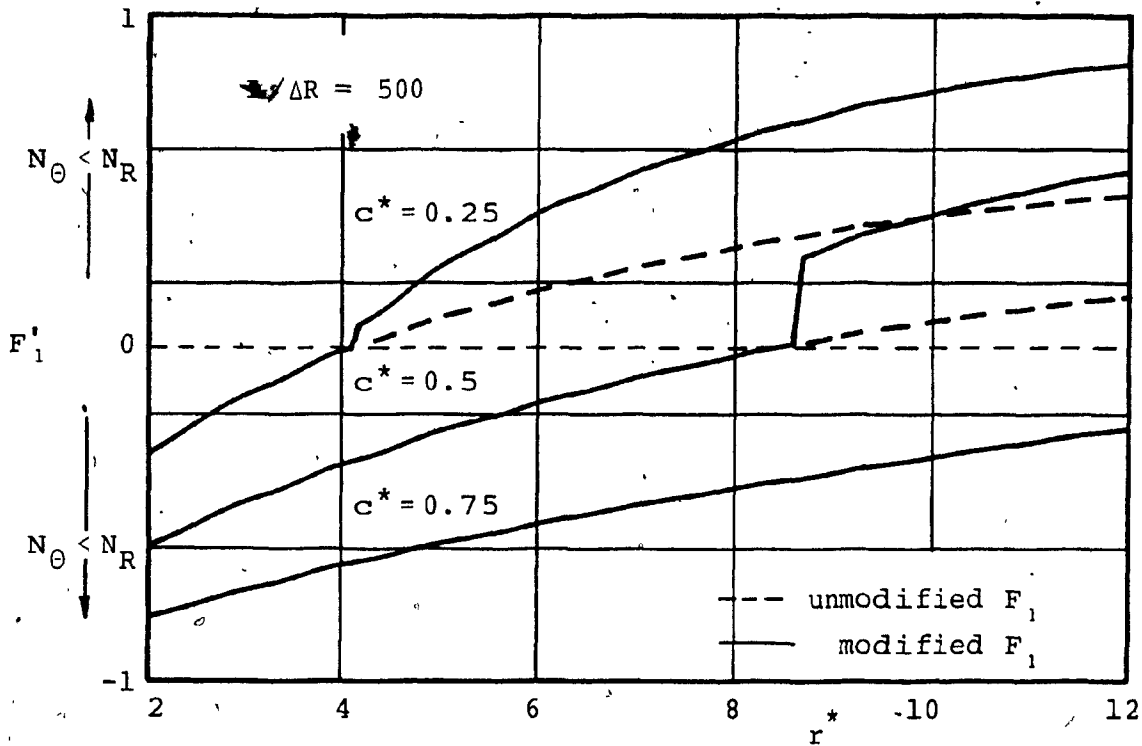
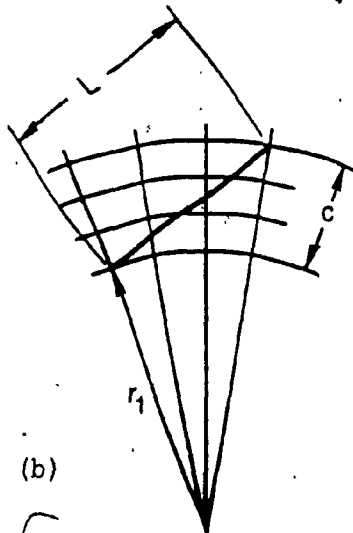


Figure 4.7.a



(b)

Figure 4.7: Effect of the Penalty Factor K/R_m on the Objective Factor F_j .

F'_j is the sign-ed value of F_j .

The parameter c^* is indicative of the inclination of the line on the radial axis. At $c^*=1$, the line segment is collinear with the axis. The plots in Figure 4.7.a show that below $N_\theta/N_R=1$ and as c^* tends towards unity, the slope of the function F_1 decreases rapidly, especially at large radial displacements. For small radial displacements, the slope increases slightly in the region very close to $c^*=1$. The solid lines on the curves show the objective function F_1 including the effect of using the above-mentioned penalty factor. The dashed lines show the trend in F_1 if the penalty factor was not used. With reference to the figure the penalty factor steepens the plots in the region where it operates. This action causes the function F_1 to react faster to small changes in the position of the line within this region. The parameters r^* and c^* are functions of the relative location between the contour pole and the machine pole, $(C,/\beta)$.

4.6 Experimental verification of the objective function F_1

In order to verify the calculated objective function and to evaluate the performance of the template digitizer, a template of a straight line has been manufactured and was digitized on the prototype template digitizer. The data were collected as described in Appendix [D], using a hybrid computer, for five different pole locations of the template contour. Substituting the experimental data in Equations 4.5, 4.6, and 4.10, the objective function for the

five locations is calculated. These experimental results are shown in Figure 4.8 together with the theoretically calculated objective function.

The plot shows that, for such a line at the given radial displacement, only one minimum exists and is at an angular orientation of 1.35 radians (77,3 deg.). The figure also shows correspondance between the theoretical and experimental results.

The good correlation between the experimental and theoretical results also provides implicit verification of the performance of the template digitizer.

4.7 Formulation of the optimization problem

The evaluation of the function F_1 at every iterative step in the optimization requires the calculation of the number of radial and angular steps representing the contour segments. For contours that has equations characterizing their geometry, the function F_1 can be simplified by substituting;

$$N_R = \int dr/\Delta R \quad 4.13$$

$$N_\theta = \int d\theta/\Delta\theta \quad 4.14$$

into Equation 4.10.

In general, if a contour is represented by a piecewise linear approximation, such that the line segments join successively all the stationary points on the contour, at the least, then the objective function F_1 calculated by

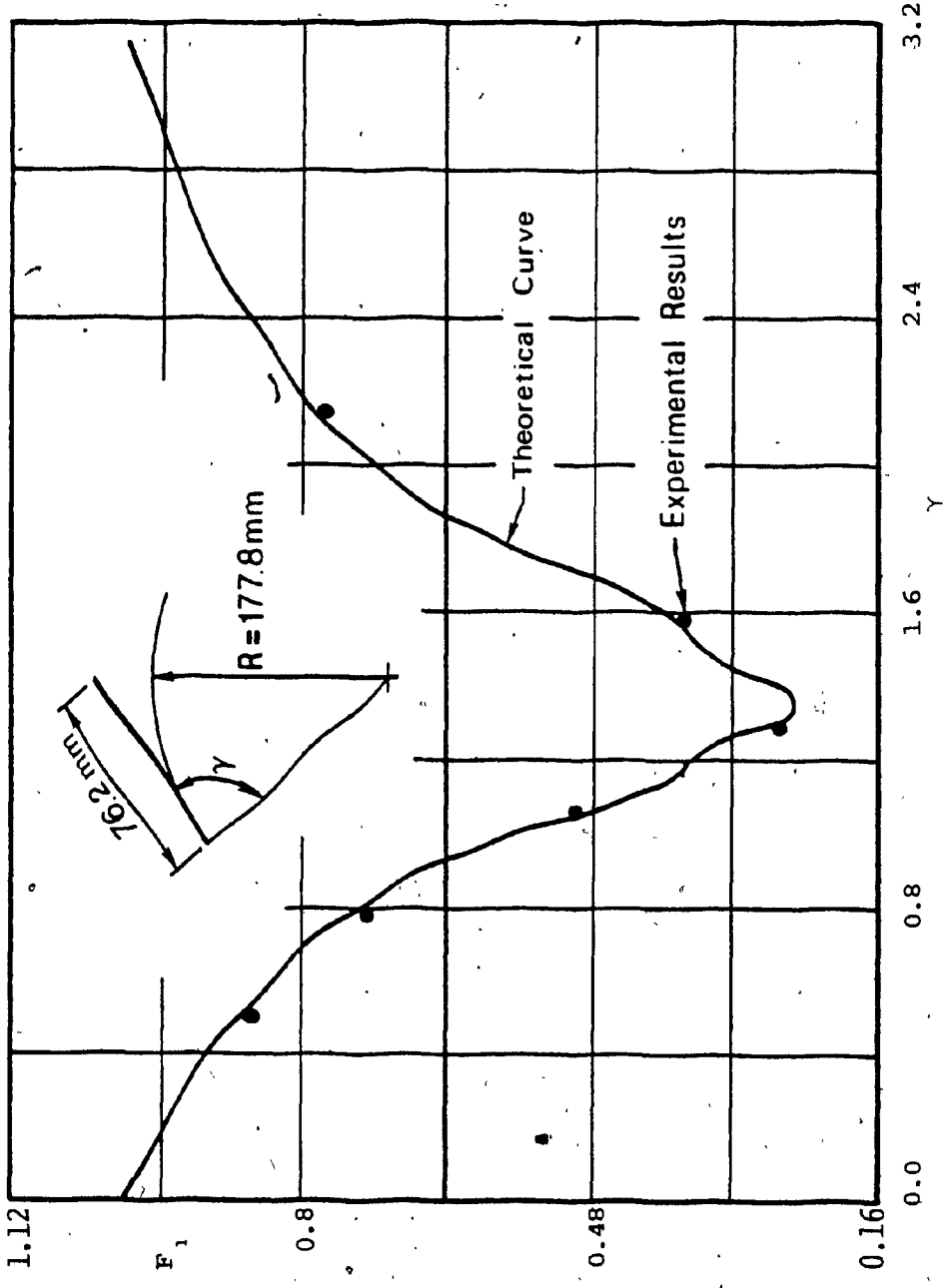


Figure 4.8: Theoretical and Experimental Results of the Objective Function F_1 for a Straight Line.

combining Equations 4.10, 4.13, and 4.14 reduces to:

$$F_1 = \begin{cases} \frac{\sum_{i=1}^n \left| \frac{|dr|}{\Delta R} - \frac{|d\theta|}{\Delta \theta} \right|}{\sum_{i=1}^n \left\{ \frac{|dr|}{\Delta R} + \frac{|d\theta|}{\Delta \theta} \right\}} & \text{for } \frac{|dr|}{\Delta R} < \frac{|d\theta|}{\Delta \theta} \\ \frac{\sum_{i=1}^n \left| \frac{|dr|}{\Delta R} - \frac{|d\theta|}{\Delta \theta} \frac{K}{R_m} \right|}{\sum_{i=1}^n \left\{ \frac{|dr|}{\Delta R} + \frac{|d\theta|}{\Delta \theta} \frac{K}{R_m} \right\}} & \text{for } \frac{|dr|}{\Delta R} > \frac{|d\theta|}{\Delta \theta} \end{cases} \quad 4.15$$

where n is the number of line segments representing the contour,

and

$$\frac{dr}{d\theta} = - \frac{b[\cos\theta + m \sin\theta]}{[\sin\theta - m \cos\theta]^2} \quad 4.16$$

calculated from the equation of a straight line in polar coordinates:

$$r = b/[\sin\theta - m \cos\theta] \quad 4.17$$

where b is the intercept of the line in the Y-axis,

and m is the slope of the line.

The optimization problem for locating the contour with respect to the machine pole can be mathematically represented as:

minimize F_1 (Equation 4.15)

subject to;

a) Work area constraint of the template digitizer or NC machine and given by:

$$7.62 \text{ cm. (3 inch)} < r < 33.02 \text{ cm. (13 inch)}$$

$$0 < \theta < 2.8 \text{ (in radians)}$$

b) A constraint that would not allow the placement of the machine pole inside a closed contour due to geometrical limits imposed by the construction of the template digitizer.

4.8 Optimization algorithm

An optimization routine having as objective function F_1 of Equation 4.15 was constructed. The routine is based on the direct search algorithm proposed by Hooke and Jeeves. The algorithm is composed of two sections, an exploratory move section, and a pattern move section. In the exploratory move, the objective function is evaluated at equal and orthogonal vectors that originate in all directions from a base point. The resultant vector that cause an improvement in the objective function value is then calculated from these vectors. If no improvement is found, the algorithm scales down the orthogonal vectors, and the exploratory process restarted. In the pattern move, the algorithm transports the base point along the resultant

vector and beyond its length. A detailed description of this algorithm can be found in Reference [31] (pp.69).

4.9 Case study results on the suitability of the objective function in predicting the location for minimum area error

In order to evaluate the effectiveness of using the above mentioned objective function, a number of contours were selected and their positions within the polar coordinate grid was optimized to give minimum area error. To verify how closely the objective function F_1 simulate the trends of the area error, another computer program was constructed to digitize the contours and the actual area error was calculated. Listings of both algorithms are given in Appendix [E]. Three curves are chosen as test contours. These curves represent open, closed, and sharply undulating types, and are as follows:

1) The Witch of Agnesi given by:

$$y = 8a^3/[x^2 + 4a^2] \quad 4.18$$

2) The Limacon of Pascal given by:

$$r = b + 2a \cos\theta \quad 4.19$$

3) The Serpentine curve given by:

$$y = abx/[a^2 + x^2] \quad 4.20$$

Figures 4.9, 4.10, and 4.11 show these curves as well as their topographical contours of the objective function.

(cm)
76

• Location of Minimum Area Error

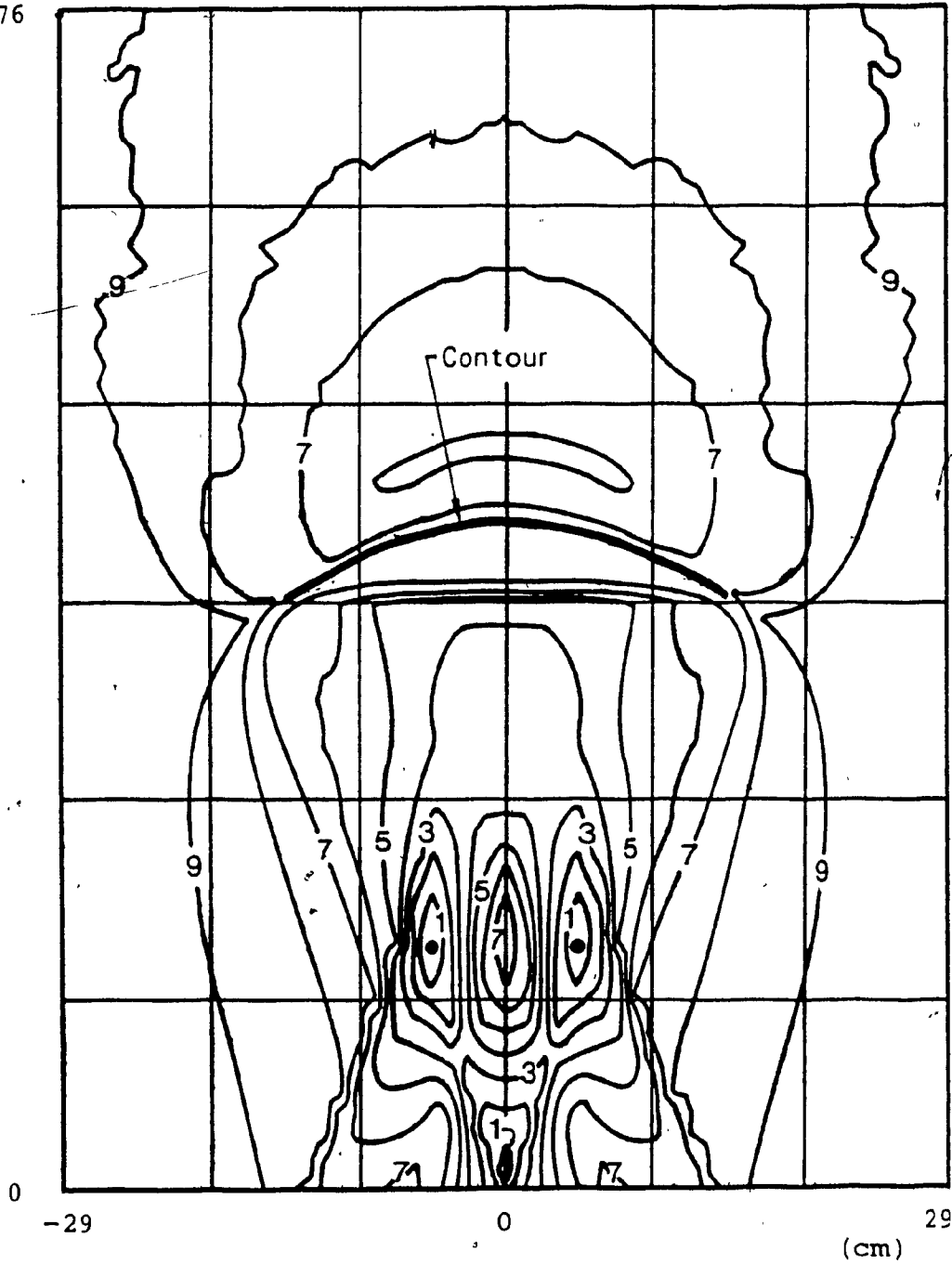


Figure 4.9: Topographical Plots of the Objective Function F_1 for the Witch of Agnesi Contour.

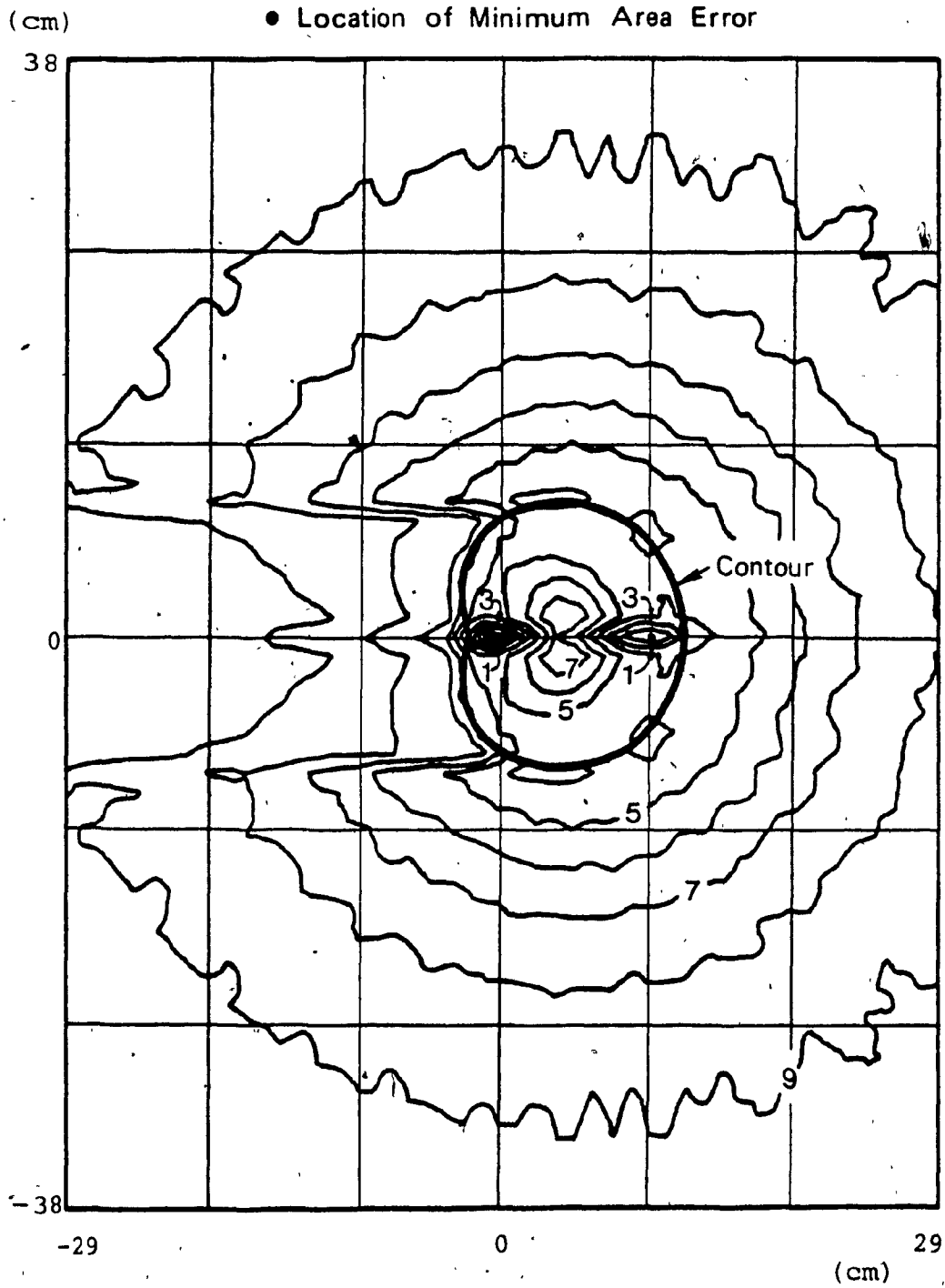


Figure 4.10: Topographical Plots of the Objective Function F_1 for the Limacon of Pascal Contour.

The topographical contours in these figures represent machine pole locations where the values of the objective functions are equal. The topographical contours numbered from 1 to 9, with higher numbers indicating larger objective function F_1 value. The topographical contours are not part of the optimization procedure and are introduced here to give a visual image of the behavior of the objective function, and hence of the area error. The procedure consisted of running the optimization routine with the objective function (Equation 4.15) and finding the location of the pole for minimum area error. The algorithm that calculates the exact area error (Equation 4.2) was then used to evaluate the error for a number of randomly selected locations within the neighborhood of the optimally located pole position based on the objective function F_1 . The locations of the pole for the minimum area error found using the randomly selected locations are also shown on the topographical plots.

The test contours parameters, as well as numerical results of the study are tabulated in Table 4.1.

For the "Witch of Agnesi" and the "Serpentine" curves the optimization routine was able to identify the location of the pole for minimum error accurately, as can be seen from Figures 4.9 and 4.11. For the "Limacon of Pascal" the optimization routine identified a point very close to that of the actual minimum area error. The percentage difference in area error between the identified and the actual locations

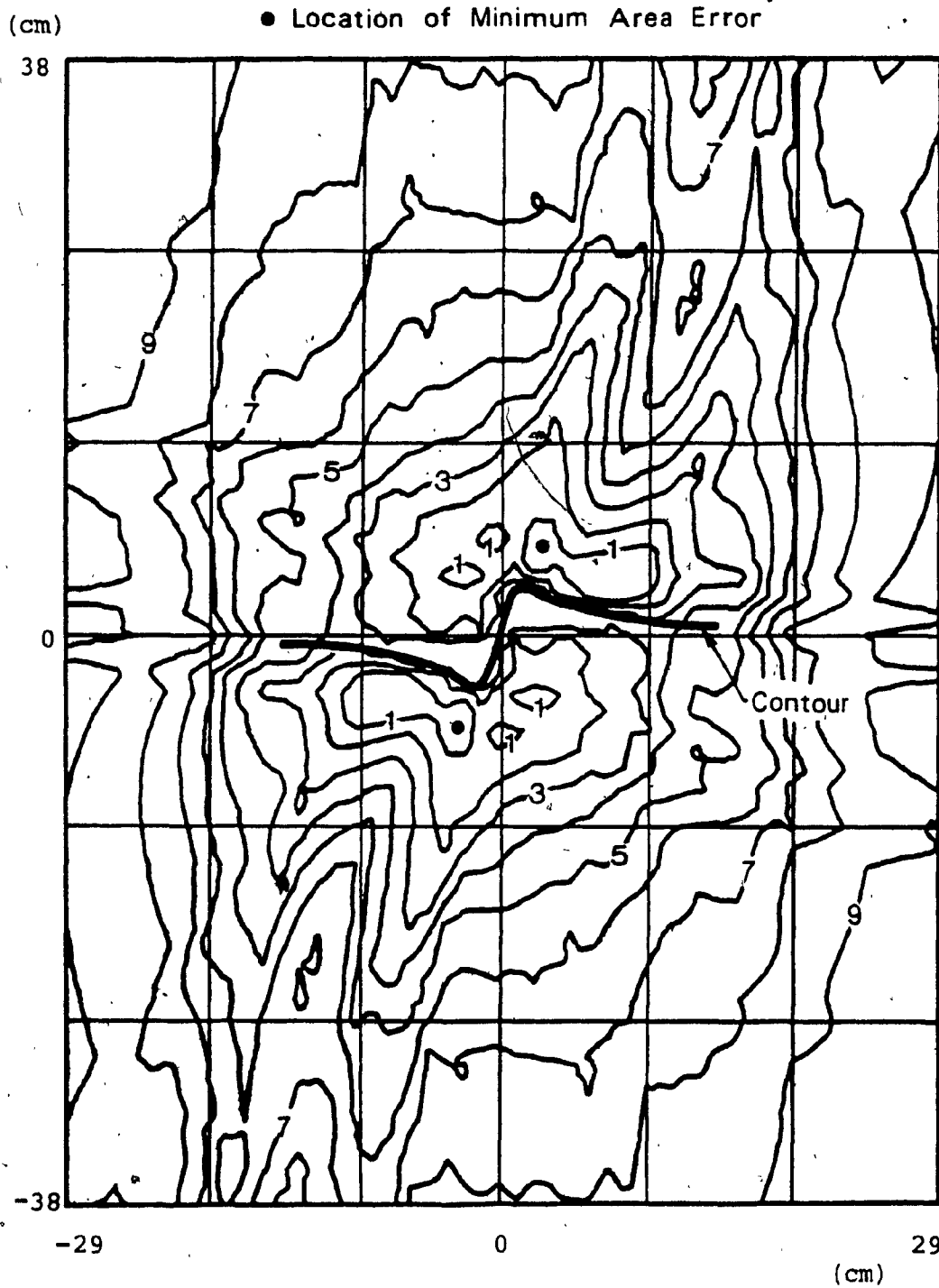


Figure 4.11: Topographical Plots of the Objective Function F_1 for the Serpentine Contour.

Table 4.1: Test Contour Parameters and Results of Optimization for Area Error Minimization

Test Contour Parameter Results	Witch of Agnesi	Limacon of Pascal	Serpentine
Mathematical representation	$y = 8a^3/(x^2 + 4a^2)$	$r_1 = b + a \cos \theta_1$	$y = abx/(a^2 + x^2)$
Contour constants	$a = 21.59 \text{ cm} (8.5 \text{ inch})$	$a = 5.08 \text{ cm} (2 \text{ inch})$ $b = 7.62 \text{ cm} (3 \text{ inch})$	$a = 1.27 \text{ cm} (0.5 \text{ inch})$ $b = 7.62 \text{ cm} (3 \text{ inch})$
Optimal location of machine pole for F_1 junction	$C = 15.46 \text{ cm} (6.09 \text{ inch})$ $\beta = 1.236 \text{ radians, or } = 1.905 \text{ radians}$	$C = 0.86 \text{ cm} (0.34 \text{ inch})$ $\beta = 2\pi \text{ radians}$	$C = 5.37 \text{ cm} (2.11 \text{ inch})$ $\beta = 1.105 \text{ radians, or } = 4.247 \text{ radians}$
Area error value	$\epsilon_a = 2.59 \text{ sq.mm}$ $(0.409 \times 10^{-2} \text{ sq.inch})$	$\epsilon_a = 4.05 \text{ sq.mm}$ $(0.628 \times 10^{-2} \text{ sq.inch})$	$\epsilon_a = 4.563 \text{ sq.mm}$ $(0.707 \times 10^{-2} \text{ sq.inch})$
Optimal location of machine pole for area error	same location as for F_1 function	$C = 1.27 \text{ cm} (0.5 \text{ inch})$ $\beta = 2\pi \text{ radians}$	same location as for F_1 function
Area error value	same as for optimal location of F_1 function	$\epsilon_a = 4.01 \text{ sq.mm}$ $(0.6216 \times 10^{-2} \text{ sq.inch})$	same as for optimal location F_1 function
Percentage difference in area error value	0%	0.97%	0%

in this particular case is 0.96 %.

4.10 Summary

In this chapter it was shown that for evaluating the performance of the contouring process, an area error criterion is more stringent than the deviation error. It was also shown that the area error is a function of the relative position of the contour pole from the machine pole. Thus by varying the location of the contour pole, the area error can be minimized. The calculation of the area error is lengthy and cumbersome, and using it as an objective function for optimization proves impractical.

An alternate objective function is formulated based upon maximizing the ratio of F_{dif} , defined as the difference between the number of radial and angular steps representing the contour, to F_{sum} , defined as the sum of the radial and angular steps representing the contour. It is shown in this chapter that the alternate objective function duplicates the trends of the area error, and is easy to use. The alternate objective function is incorporated in an optimization routine to locate the contour pole for minimum area error. Test results show that the optimization algorithm is able to accurately identify the minimum area location.

This chapter deals exclusively with the case of a point tool. And although it is difficult to formulate analytically the objective function in cases where the tool has a finite diameter, reason suggests that the technique

presented in this chapter is equally applicable to these cases. This is because the formulated area error minimization method is based on the number of radial and angular steps representing the contour and is independent of the tool diameter.

CHAPTER 5

**DYNAMIC ANALYSIS
OF THE POLAR NC MACHINE**

5.1 Introduction

The NC machine operates in an open loop control scheme as has been described earlier. This scheme has the advantage of reduced complexity of the NC controller. Open loop control, however, does not have the capability of detecting the failure of an axis-drive to respond to a command (loss of synchronism) and compensating for the failure. The loss of synchronism would occur if the torque imposed by the load exceed the torque capacity of the drive.

The upper limit of the torque that can be imposed on a stepping motor without loss of synchronism decreases as the rate of incoming step signals increases. The torque as well as the rate of step signals of each of the radial and angular axes stepping motors depend on the contour as well as such operating conditions as machining forces and contouring speed. Changes in the torque required and torque available from the axes-drives as the machining conditions change should be thoroughly understood. This knowledge would be used to identify the operating limits of the NC machine for a given set of machining conditions beyond which synchronism failure may occur.

The study of the torque changes in the NC machine axes-drives is a dynamics problem that deals with the

dynamics of motion along the contour and not with the dynamics of a single step. In this study it is assumed that the signals generated by the digitizer have been properly processed to insure constant contouring speed as has been discussed in Chapter 2. The kinematics of the arm and carriage mechanisms is studied with a tool moving at a constant speed and producing a contour according to the signals received from the digitizer. The instantaneous velocity and acceleration of each axis are calculated and used in the dynamic analysis in order to determine the torque required from the stepping motors. The velocity of each axis is further used to determine the limiting torque available from the corresponding stepping motor.

5.2 Kinematic analysis of the NC machine arm and carriage mechanism

Figure 5.1 shows a vector representation of the prototype NC machine. The figure shows the machine pole (O) displaced from the contour pole (O_1) by a vector (C, β) and a tool of radius R_r touching the required contour $r_1 = r_1(\theta_1)$ at a point (P).

With reference to the figure, for machining operations requiring no tool offset (i.e. $R_r = 0$) like plasma or flame cutting, the tool centre coincides with (P) and moves along the contour. This case of no tool offset represents the simplest configuration of the vector diagram and will be studied first.

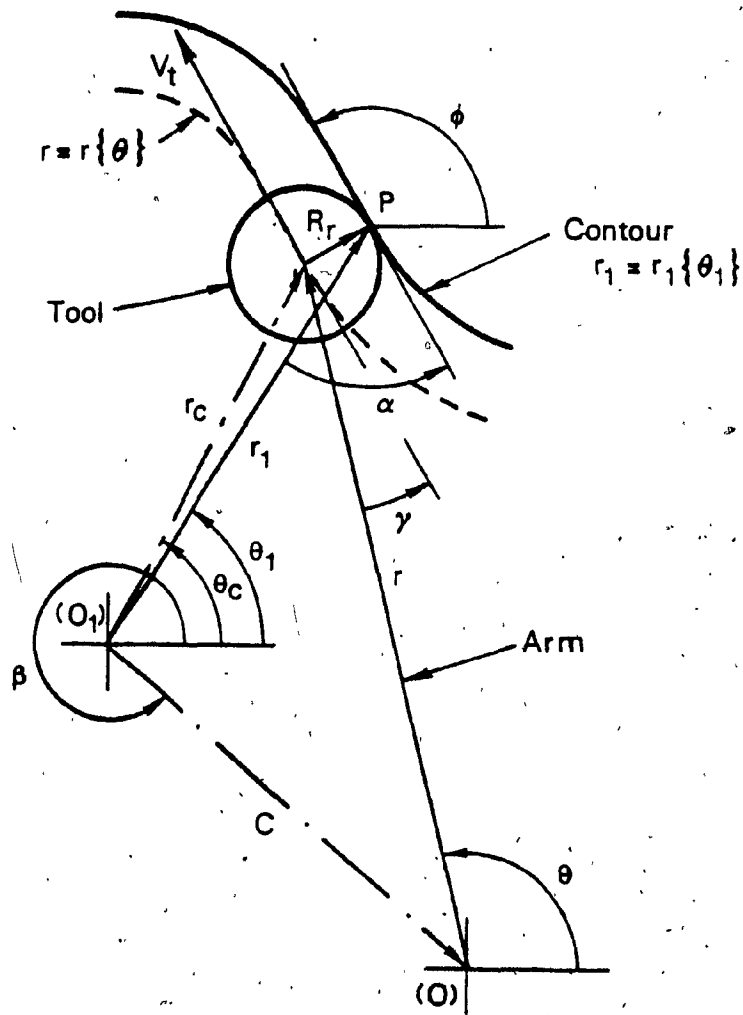


Figure 5.1: Vector Representation of the Polar System in Contouring.

5.2.1 Case 1: Tool with no offset (zero radius)

With reference to Figure 5.1, for the case of no tool offset, the vector r_1, θ_1 coincide with (r, θ) . Hence, the velocity vector of the centre of the tool and the carriage can be expressed with respect to the machine pole (O) by:

$$V_t e^{j\phi} = \dot{r} e^{j\theta} + j r \dot{\theta} e^{j\theta} \quad 5.1$$

Resolving the velocity equation in the radial and tangential directions give:

$$\dot{r} = V_t \cos \gamma \quad 5.2$$

$$\dot{\theta} = (V_t \sin \gamma) / r \quad 5.3$$

where,

$$\gamma = \cos^{-1} \left[\frac{\Lambda_1 \Lambda_3}{r^2 \Lambda_2 - r \Lambda_1 \Lambda_4} \right] \quad 5.4$$

$$\Lambda_1 = \left[r_C - C \cos(\theta_C - \beta) \right] \frac{dr_C}{d\theta_C} + r_C C \sin(\theta_C - \beta)$$

$$\Lambda_2 = C^2 + 2r C \cos(\theta - \beta) + r^2$$

$$\Lambda_3 = r + C \cos(\theta - \beta)$$

$$\Lambda_4 = C \sin(\theta - \beta)$$

The acceleration of point (P) is obtained by differentiating Equation 5.1 with respect to time as follows:

$$\begin{aligned}
 a_c &= a_t e^{j\phi} + j v_t \dot{\phi} e^{j\phi} \\
 &= \ddot{r} e^{j\theta} + 2j \dot{r} \dot{\theta} e^{j\theta} + j r \ddot{\theta} e^{j\theta} - r(\dot{\theta})^2 e^{j\theta} \quad 5.5
 \end{aligned}$$

Since it is desired to maintain a constant contouring speed along the contour, it follows that the acceleration a_c of point (P) tangential to the contour is identically zero.

Resolving Equation 5.5 to its components along the arm and normal to it, yields:

$$\begin{aligned}
 a_{cr} &= v_t \dot{\phi} \sin\gamma \\
 &= \ddot{r} - r(\dot{\theta})^2 \quad 5.6
 \end{aligned}$$

$$\begin{aligned}
 a_{cn} &= v_t \dot{\phi} \cos\gamma \\
 &= r \ddot{\theta} + 2\dot{r} \dot{\theta} \quad 5.7
 \end{aligned}$$

In Equation 5.6 the term $r(\dot{\theta})^2$ is the centripetal acceleration of the carriage and its direction is always towards the pole. The term $2\dot{r}\dot{\theta}$ of Equation 5.7 is the Coriolis acceleration and has a direction normal to the arm in the sense of the angular velocity or opposing it for cases of positive or negative radial velocities respectively.

The time rate of change of the velocity vector direction $\dot{\phi}$ is given by:

$$\dot{\phi} = v_t / \rho \quad 5.8$$

where ρ is the radius of curvature at point (P),

and is calculated as shown in Equation 3.4.

5.2.2 Case 2: Tool with finite radius

In contouring applications where a tool of finite radius is used, as in grinding and milling operations, the tool offsets the centre of the carriage from the required contour by a distance equal to its radius. Let the loci of the tool centre be designated $r=r(\theta)$. With reference to Figure 5.1, for a point (P) on the contour $r_1\{\theta_1\}$, given r_1 or θ_1 , r and θ can be solved for implicitly from the following equations:

$$\begin{aligned} r &= \left[r_c^2 + C^2 - 2r_c C \cos(\theta_c - \beta) \right]^{\frac{1}{2}} \\ r_c &= \left[r_1^2 + R_r^2 - 2r_1 R_r \sin\alpha \right]^{\frac{1}{2}} \\ \theta_c &= \theta - \sin^{-1} \left[\frac{C}{r_c} \sin(\theta - \beta) \right] \end{aligned} \quad 5.9$$

The kinematic relations for this case can now be formulated by substituting for r , r_c , θ_c and $dr_c/d\theta$ from Equation 5.9 into the kinematic relationship for the case of no tool offset. The derivative $dr_c/d\theta_c$ is given as follows:

$$\frac{dr_c}{d\theta_c} = \frac{\Lambda_5 \Lambda_6}{1 - \Lambda_5 \Lambda_7} \quad 5.10$$

where,

$$\Lambda_5 = \left[r_1 \frac{dr_1}{d\theta_1} - \frac{dr_1}{d\theta_1} R_r \sin\alpha + R_r r_1 \cos\alpha \frac{d\alpha}{d\theta_1} \right] / r_c$$

$$\Lambda_6 = \left[r_c r_1 - r_c R_r \sin\alpha \right] / \left[r_c r_1 - r_c R_r \sin\alpha + R_r r_c \sin\alpha \frac{d\alpha}{d\theta_1} \right]$$

$$\Lambda_7 = R_r \cos\alpha / \left[r_c r_1 - r_c R_r \sin\alpha + R_r r_c \sin\alpha \frac{d\alpha}{d\theta_1} \right]$$

and,

$$\frac{d\alpha}{d\theta_1} = \left[r_1 \frac{d^2 r_1}{d(\theta_1)^2} - \left(\frac{dr_1}{d\theta_1} \right)^2 \right] / \left[r_1^2 + \left(\frac{dr_1}{d\theta_1} \right)^2 \right]$$

5.3 Dynamic analysis of the polar NC machine

The focus here is on the calculation of the dynamic forces that must be overcome by the stepping motors. All components of the NC machine will be considered as rigid bodies.

- a) The swinging arm,
- b) The worm and worm-gear reducer,
- c) The carriage, and
- d) The power screw and nut assembly.

Figure 5.2 shows pictorially the arm and carriage mechanisms of the polar NC machine with salient parameters indicated.

The free body diagram of these components and the forces acting on them are shown in Figure 5.3. In devel-

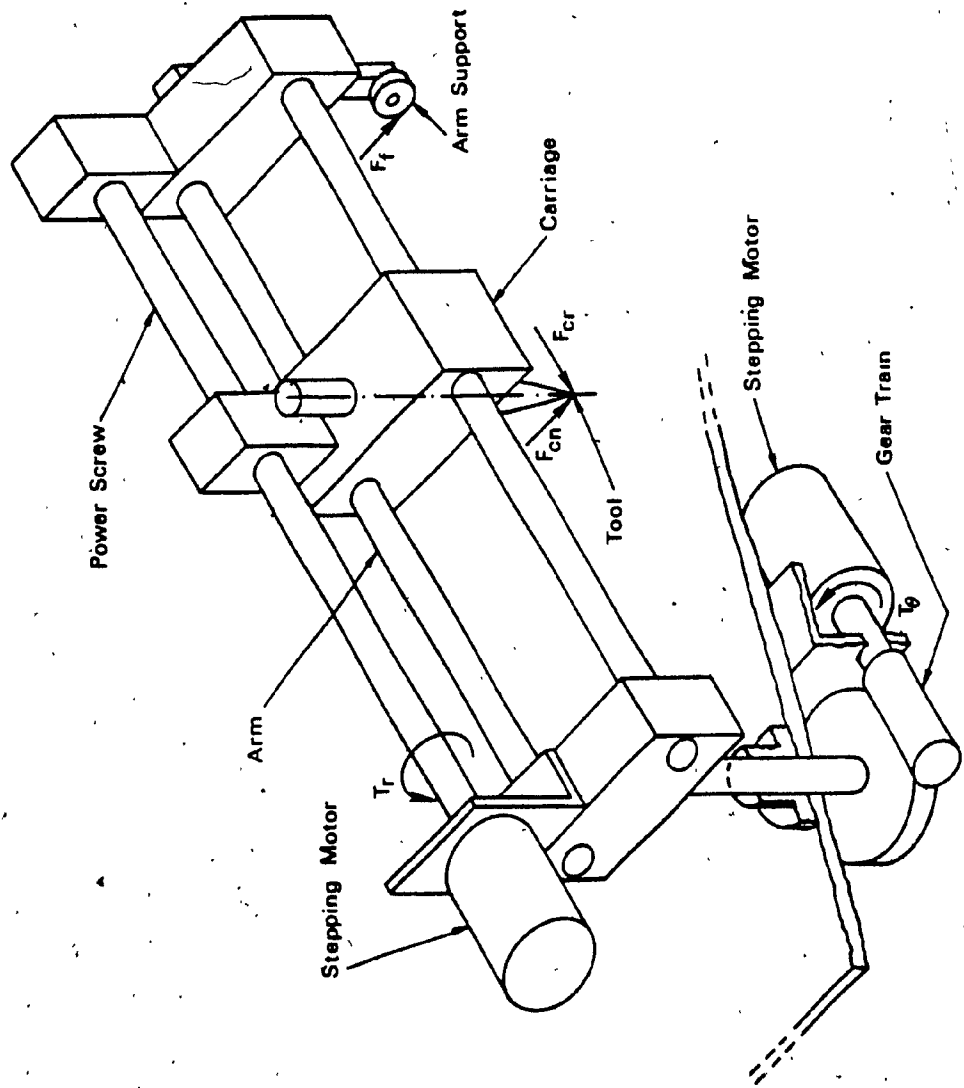


Figure 5.2: Pictorial Diagram of the NC Machine.

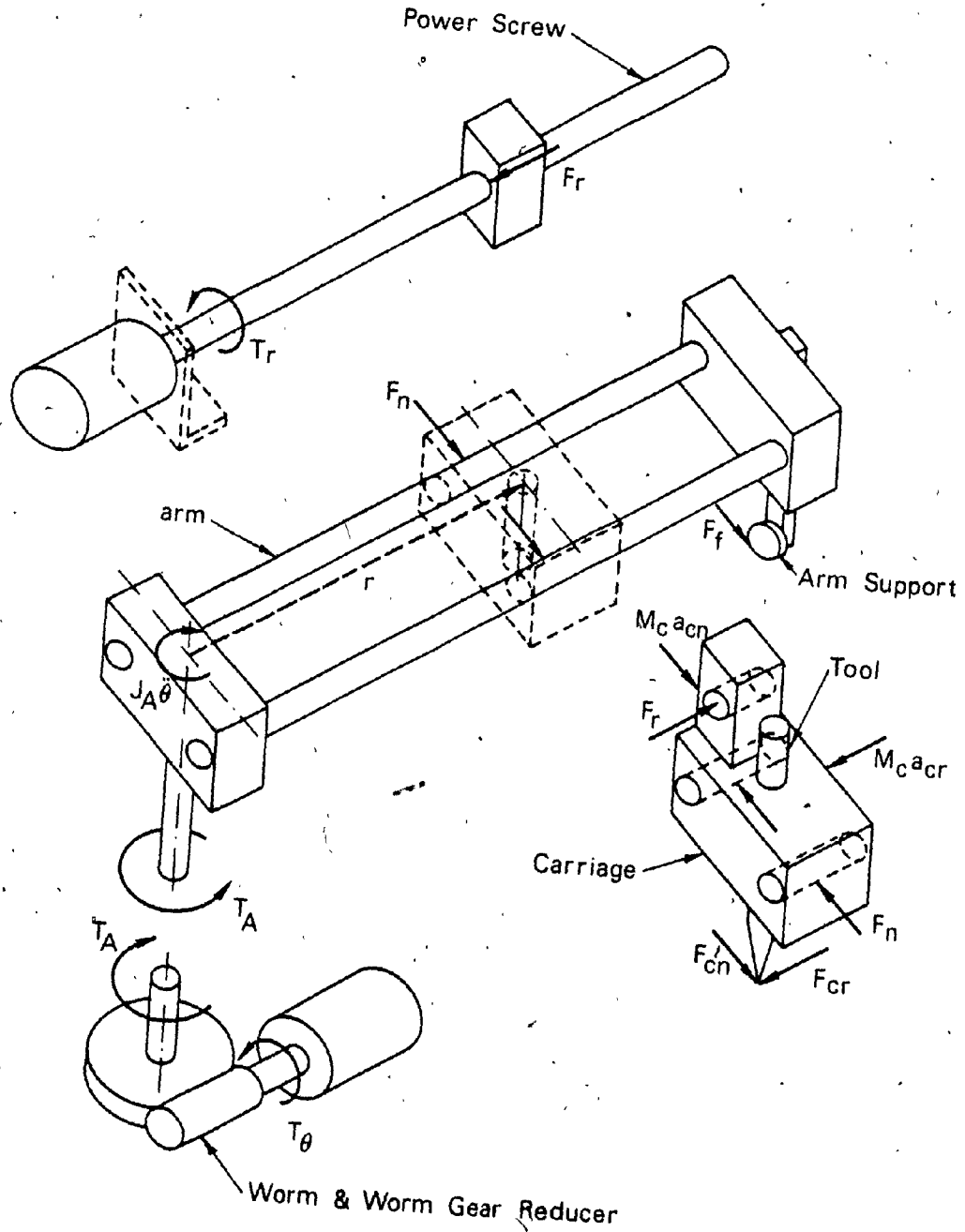


Figure 5.3: Free Body Diagram of the NC Machine.

oping the free body diagram, the mass moment of inertia of the worm-gear, the lead screw, and the radial axis stepping motor are lumped with that of the arm. Also, the mass moments of inertia of the power screw and the radial axis stepping motor are reflected to the mass of the carriage-nut assembly. The power screw and nut assembly is considered to be a transformer with friction losses only. Reaction forces to ground and machine body are not shown since they do not contribute to the torque equations. With reference to the free body diagram, the balance of forces and moments equations for the four components of the NC machine are as follows:

For the arm:

$$T_A = J'_A \ddot{\theta} + F_m r + F_f L_A \quad 5.11$$

where J'_A is the equivalent mass moment of inertia of the arm.

T_A is the sum of all the torques that act on the arm,

F_m is the force transmitted from the carriage normal to the arm,

and F_f is the friction force of the arm support.

For the worm and worm-gear reducer:

$$\begin{aligned}
 T_{\theta} &= K_1 T_A + J_M \frac{R_g}{R_w} \ddot{\theta} \\
 &= K_1 \left[J_A \ddot{\theta} + F_{cn} r + F_f L_A \right]
 \end{aligned}
 \tag{5.12}$$

where,

$$J_A = J'_A + \frac{J_M R_g}{R_w K_1}$$

where J_M is the mass moment of inertia of the angular axis motor and the worm combined,

K_1 is a factor that combines both the torque magnification due to the gearing, and the friction losses between the worm and worm-gear, and is given by Reference [32] (pp.545) as:

$$K_1 = \frac{R_w}{R_g} \frac{[\cos \zeta \sin \lambda + \mu_1 \cos \lambda]}{[\mu_1 \sin \lambda - \cos \zeta \cos \lambda]}$$

where R_w, R_g are the pitch radii of the worm and worm-gear respectively,

ζ is the pressure angle of the gear system,

λ is the lead angle of the worm-gear,

and μ_1 is the friction coefficient between the worm and the worm-gear.

For the carriage:

$$\left. \begin{aligned} F_r &= M'_C a_{cr} + F_{cr} \\ F_n &= M'_C a_{cn} + F_{cn} \end{aligned} \right\} \quad 5.13$$

where F_m, F_m is the sum of all the radial and normal, forces acting on the carriage respectively

For the power screw and nut assembly:

$$\begin{aligned} T_R &= J_M a_{cr} \frac{2\pi}{l} + K_2 F_r \\ &= K_2 [M'_C a_{cr} + F_{cr}] \end{aligned} \quad 5.14$$

where,

$$M'_C = M'_C + \frac{2\pi J_M}{l K_2}$$

K_2 is the torque to force transformation factor of the power screw and nut assembly. This factor also takes into account the friction losses. K_2 is given in Reference [33] (pp.3-42) by:

$$K_2 = R_s \frac{[1 + 2\pi R_s \mu_2 \sec \xi (1 - \sin \psi \sin \xi)^{\frac{1}{2}}]}{[2\pi R_s - l \mu_2 \sec \xi (1 - \sin \psi \sin \xi)^{\frac{1}{2}}]}$$

where R_s is the mean radius of the thread
 l is the lead,

μ_2 is the friction coefficient between the nut and power screw,
and ψ, ξ are the helix and thread angles respectively.

Combining Equations 5.11 to 5.14 yield the torques required from the angular and radial axes stepping motors as follows:

$$T_R = K_2 [M_C a_{cr} + F_{cr}] \quad 5.15$$

$$T_\theta = K_1 [J_A \ddot{\theta} + F_{cn} r + F_f L_A + M_C r a_{cn}] \quad 5.16$$

As the tool travels along the contour, the torque required from the stepping motors as given by Equations 5.15 and 5.16 varies. Each stepping motor has to be able to provide a torque at least equal to the maximum required torque.

5.4. Torque speed relationship of a stepping motor

As mentioned in Section 2.4, the wave energization scheme is used for driving both the radial and angular stepping motors. Although this scheme is not commonly used, the justification for using it here has been given earlier. Pull-out torque-speed characteristics of stepping motors operating with wave energization are not commonly available from the manufacturers. Pull-out torque curves (T_p versus steps/s) show for a given speed (steps/second), the limit torque at which missing of steps start to occur. Testing

the motors in order to obtain these characteristics is a lengthy and complicated procedure. A description of the procedure is given in Appendix [G]. Appendix [G] presents a derivation of the characteristics for the pull-out torque of a stepping motor operating with the wave energization scheme. The relation is given by:

$$T_P = \frac{1.17632 V K_T}{[R_a^2 + \omega^2 L_a^2]^{\frac{1}{2}}} - \frac{K_V \omega R_a K_T}{N_s (R_a^2 + \omega^2 L_a^2)} \quad 5.17$$

where K_T, K_V are the torque and voltage constants of the stepping motor respectively,
 R_a, L_a are the motor winding resistance and inductance respectively,
 V is the power supply voltage,
 and ω is the angular velocity of the motor (in electric radians/s).

The angular velocity of each of the stepping motors can be found from the respective axes velocity \dot{r} and $\dot{\theta}$ given in Equations 5.2 and 5.3 as follows:

$$\omega_R = 2\pi N_s k_R \dot{r} \quad 5.18$$

$$\omega_\theta = 2\pi N_s k_\theta \dot{\theta} \quad 5.19$$

Substituting Equations 5.18 and 5.19 in Equation 5.17 result in the pull-out torques T_{PR} and $T_{P\theta}$ for the radial and angular axes as follows:

$$T_{PR} = \frac{1.17632 V K_T}{[R_a^2 + \omega_R^2 L_a^2]^{\frac{1}{2}}} - \frac{K_V \omega_R R_a K_T}{N_s (R_a^2 + \omega_R^2 L_a^2)} \quad 5.20$$

$$T_{P\theta} = \frac{1.17632 V K_T}{[R_a^2 + \omega_\theta^2 L_a^2]^{\frac{1}{2}}} - \frac{K_V \omega_\theta R_a K_T}{N_s (R_a^2 + \omega_\theta^2 L_a^2)} \quad 5.21$$

5.5 Effect of the contouring speed, load, and contour on the axes-drives torque

A parameter called "torque ratio", and defined as the quotient of the torque required from an axis-drive to the pull-out torque available from the respective drive, is used as a measure of the success or failure of a contouring operation. A torque ratio larger than unity means that the torque required from a stepping motor exceeds that which it is able to deliver, and hence missing of steps.

Equations 5.15 and 5.16 show that the torques required from the two axes-drives are function of the load as well as on the kinematic relations for the axes. Equations 5.1 to 5.10 show explicitly the dependence of these kinematic relations on the contouring speed as well as on the contour, and its location from the machine pole. Furthermore, the pull-out torque available from the axes-drives, and given by Equations 5.20 and 5.21, are also functions of these kinematic relations.

The load on the NC machine consists of the inertia of the tool and its accessories, and the force acting on the tool. This load varies from one application to another. For example in the case of metal removal by grinding, these loads are predominantly dissipative, while in the case of plasma or flame cutting it is predominantly inertial, where the cutting nozzle and associated metering instruments provide the added mass on the carriage.

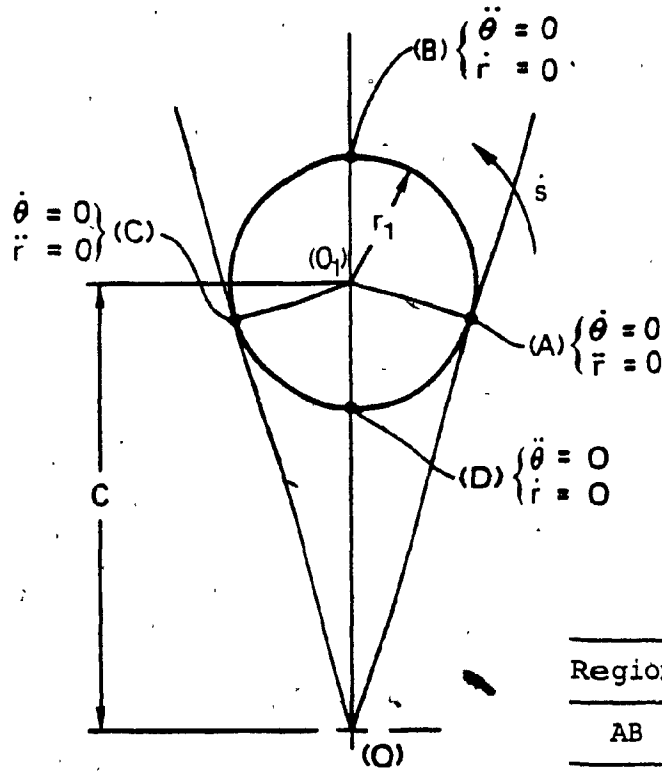
A computer algorithm implementing the dynamic analysis has been formulated in order to evaluate the effect of different loading conditions and contours on the torque ratio. Four curves shown in Figures 5.4 to 5.7 are used as test contours, these are:

- a) a circle,
- b) a Witch of Agnasi,
- c) a Limacon of Pascal, and
- d) a Serpentine curve.

These curves are chosen to cover cases of profiles having symmetric, open, and closed contours. A straight line, however, was not chosen as a test curve since its radius of curvature is at infinity, and with reference to Equations 5.6, 5.7, 5.8, 5.15, and 5.16 inertial load on the mechanism has no effect on the axes-drives when the radius of curvature is of infinite length.

Inertial as well as grinding operations are considered for the above-mentioned test contours in order to study the effect of the load, the contouring speed, and the contour on

$r_1 = \text{constant}$
 $= 5.08 \text{ (2 inch)}$
 $C = 17.78 \text{ cm (7 inch)}$
 $\beta = 3/4$



Region	\dot{r}	\ddot{r}	$\dot{\theta}$	$\ddot{\theta}$
AB	+	-	+	+
BC	-	-	+	-
CD	-	+	-	-
DA	+	+	-	+

Figure 5.4: Test Contour : Circle.

$$y = \frac{8a^3}{x^2 + 4a^2}$$

$$a = 21.59 \text{ cm (8.5 inch)}$$

$$C = 25.4 \text{ cm (10.0 inch)}$$

$$\beta = \pi/2$$

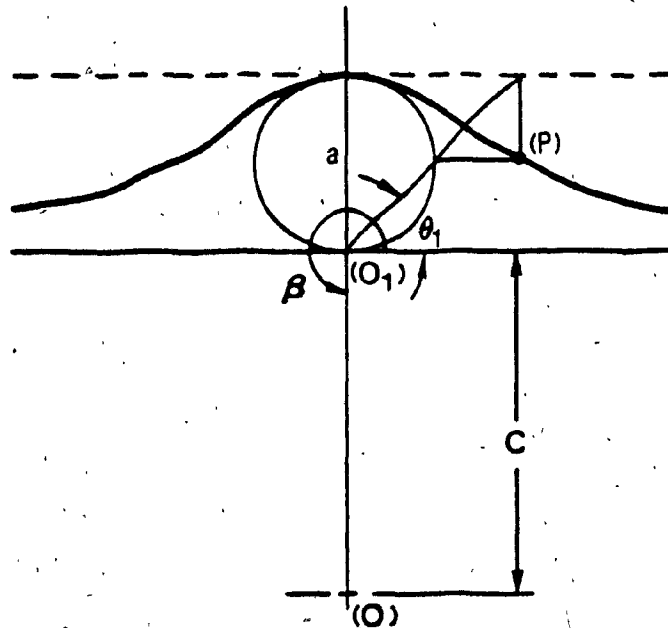


Figure 5.5: Test Contour : Witch of Agnesi.

$$r_1 = b + a \cos\theta_1$$

$a = 5.08 \text{ cm (2 inch)}$
 $b = 7.62 \text{ cm (3 inch)}$
 $c = 17.78 \text{ cm (7 inch)}$
 $\beta = 3./4$

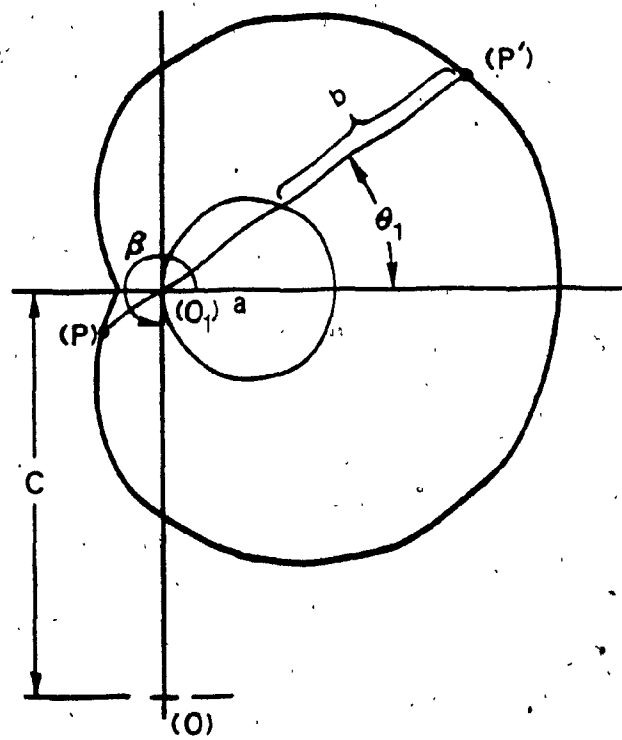


Figure 5.6: Test Contour : Limacon of Pascal.

$$y = \frac{abx}{a^2 + x^2}$$

$$a = 1.27 \text{ cm (0.5 inch)}$$

$$b = 7.62 \text{ cm (3 inch)}$$

$$c = 17.78 \text{ cm (7 inch)}$$

$$\beta = 3\pi/4$$

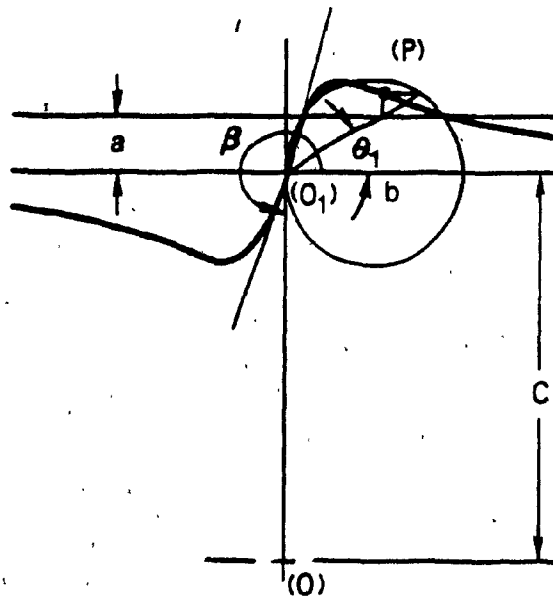


Figure 5.7: Test Contour : Serpentine.

the axes-drives torque. The system parameters and operating conditions are listed in Table 5.1.

5.5.1 Inertial load

For the case of inertial loads, Figures 5.8 to 5.15 show plots of the torque ratios versus the tool location on the contour for different values of mass on the carriage. Plots for two contouring speeds are also shown for each contour. The machine pole in each case is situated as shown in Figures 5.4 to 5.7. Plots for the circular contour will be analyzed first, the reason being that the contour is symmetric around all its axes and has a constant radius of curvature. Because of the aforementioned two features of the circular contour, it is possible to study the isolated effect of the machine load on the torque ratio. All observations concerning the torque ratio plots for the circular contour are common to all the other contours.

In Figure 5.4, the regions of positive and negative values of axes accelerations and velocities for the circular profile are identified and will be frequently referred to subsequently.

Case (a): Circular contour

The plots in Figures 5.8.a and 5.8.b for the circular contour show that for the radial axis, the torque ratios are symmetric about $\theta = \pi/2$. The reduction in the magnitude of the torque ratio while the tool is tracking the part of the

Table 5.1: System/Operating Parameter

System Parameters

Equivalent Mass of the Carriage	$M_C = 0.9 \text{ kg}$	0.061 slugs
Equivalent Inertia of the Arm	$J_A = 0.217 \text{ kg m}^2$	0.16 slug ft ²
Friction Torque due to Arm Support	$F_{fA} L_A = 0.127 \text{ Nm}$	0.094 lbf.ft
Worm Worm-Gear Factor	$K_1 = 2.78 \times 10^{-2}$	-
Power Screw Split Nut Factor	$K_2 = 2.25 \times 10^{-2} \text{ m}$	$7.38 \times 10^{-2} \text{ ft}$
Worm Worm-Gear Reduction	$k_\theta = 40:1$	-
Power Screw Split Nut Reduction	$k_R = 7.874 \text{ Rev/cm}$	20 Revs/in
Stepping Motor Power Supply	$V \pm 24 \text{ Volts}$	-
Stepping Motor Voltage Constant	$K_V = 0.068 \frac{\text{Volts/winding}}{\text{rad/s}}$	-
Stepping Motor Torque Constant	$K_T = 0.0759 \text{ Nm}$	0.056 lbf ft/amp
Number of Teeth on Stepping Motor Rotter	$N_S = 50$	-
Resistance of Stepping Motor Coil and Drive Circuit	$R_a = 6.5 \Omega$	-
Inductance of Stepping Motor Coil	$L_a = 6.3 \times 10^{-4} \text{ Henry}$	-
Maximum Contouring Speed	$\hat{V}_t = 1.746 \text{ cm/s}$	3.438 ft/min

Operating Parameters

Inertial Load:

Inertial Load Added to the Mass
of the Carriage

$M_C = 14.6 \text{ kg}$
 29.2 kg
 43.8 kg

1 slug
2 slugs
3 slugs

Contouring Speed

$V_t = 0.51 \text{ cm/s}$
 1.51 cm/s

1 ft/min
3 ft/min

Grinding Application

Grinding Tool Peripheral Speed

$V_{\text{tool}} = 16.62 \text{ m/s}$

54.5 ft/s

Width of cut

$w = 0.635 \text{ cm}$

0.25 inch

Grinding Wheel-Workpiece Force
Factor

$k_C = 6.46 \times 10^7 \text{ KN/m}^2$

$1.35 \times 10^9 \text{ lbf/ft}^2$

Normal to Tangential Grinding
Force Ratio

$C_1 = 1.66$

Depth of Cut

$d = 0.254 \times 10^{-2} \text{ mm}$
 $0.508 \times 10^{-2} \text{ mm}$

0.001 in
0.002 in

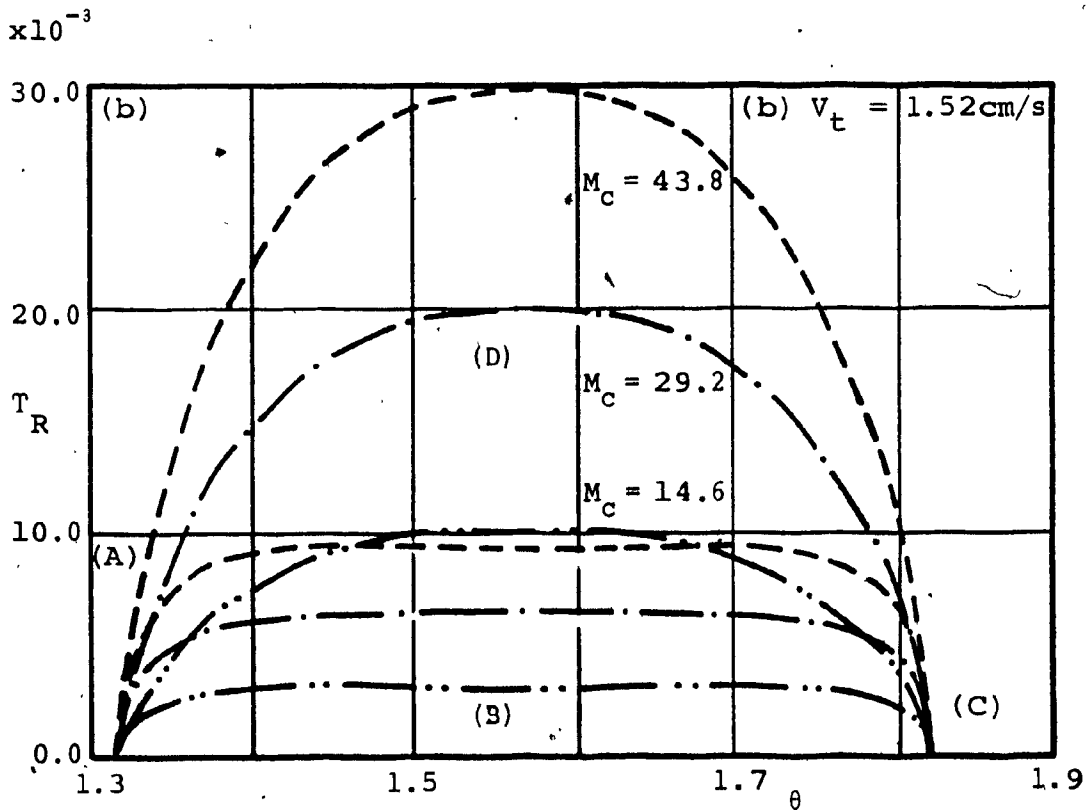
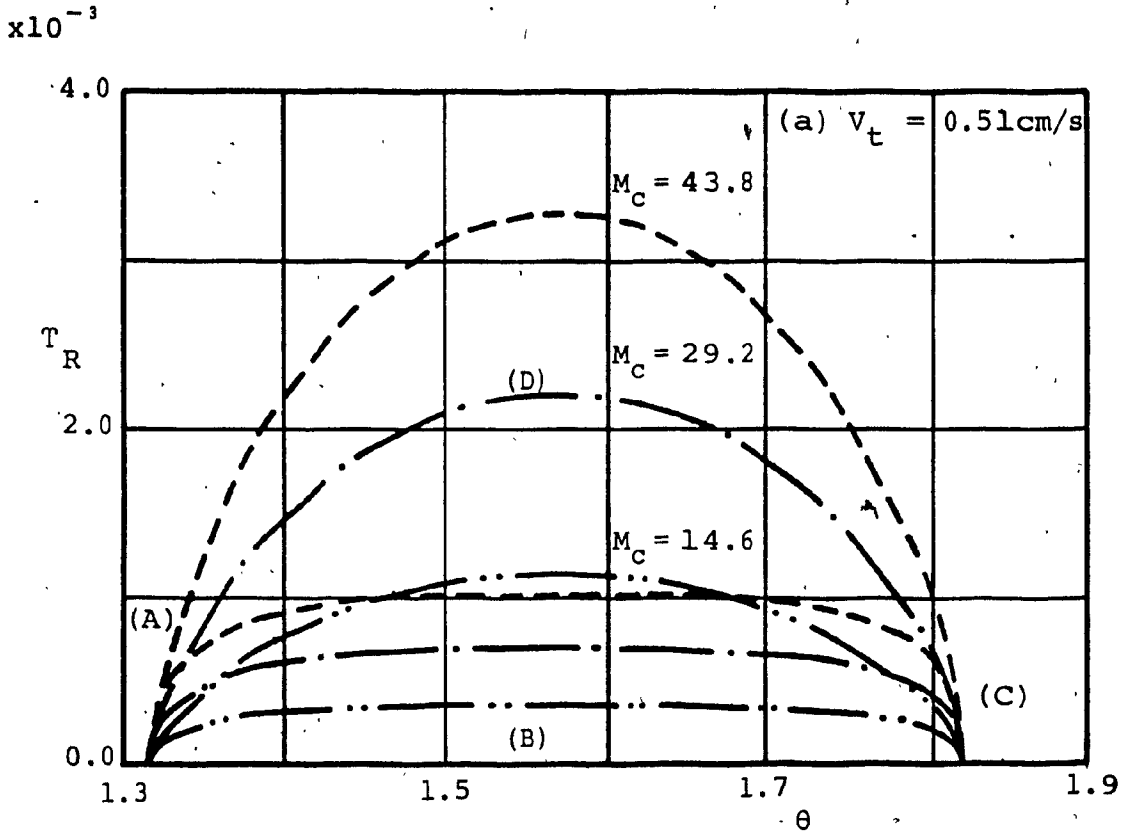


Figure 5.8: Radial Axis Torque Ratio Plots for Circular Contour (Inertial Load). M_c is in kgs.

circle furthest away from the machine pole, ABC, is due to the fact that the inertial force due to the radial acceleration and the centrifugal force are in the same direction as the force due to radial axis stepping motor and thus reduces the torque demanded of the motor (refer to the part ABC of the circle in Figure 5.4). For the part CDA of the circle, the force due to the radial acceleration and the centrifugal force oppose each other, and depending on their magnitudes, they may either reduce or increase the torque demand from the radial axis motor.

At the two extreme positions of the arm, at $\theta = 1.32$ and $\theta = 1.82$ radians, the radial axis torque is zero, since $\ddot{r} = 0$ and $\dot{\theta} = 0$ at the positions indicated A and C as shown in Figure 5.4.

The plots also show that the torque ratio increase with either the increase of the contouring speed or the mass on the carriage.

The plots of the torque ratio for the angular axis, shown in Figure 5.9.a and 5.9.b exhibit similar characteristics of an increase in the peak value of the torque ratio for the increase of either the contouring speed or the mass on the carriage. The lack of symmetry about $\theta = \pi/2$ is attributed to the change in the direction of the Coriolis acceleration due to the change in the direction of the radial velocity in the four segments of the circle. Furthermore, in both figures the torque ratio plots are biased away in the torque ratio axis by a constant amount. This shift is

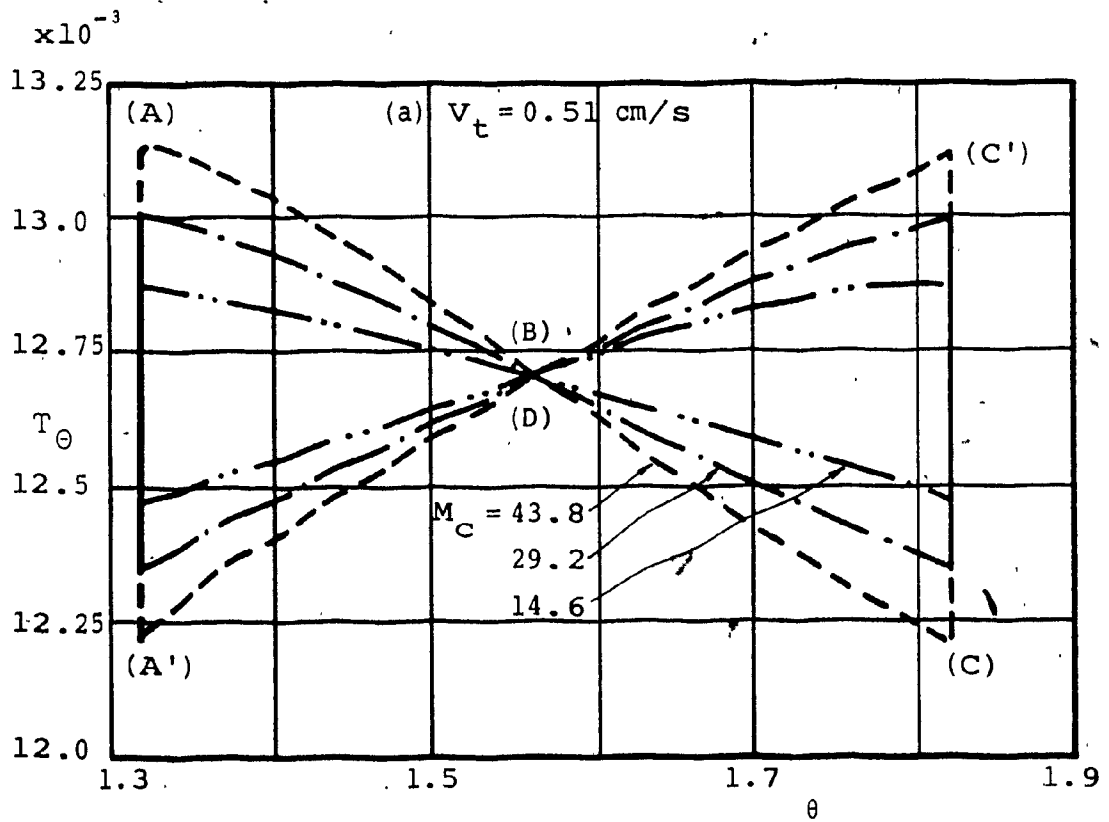
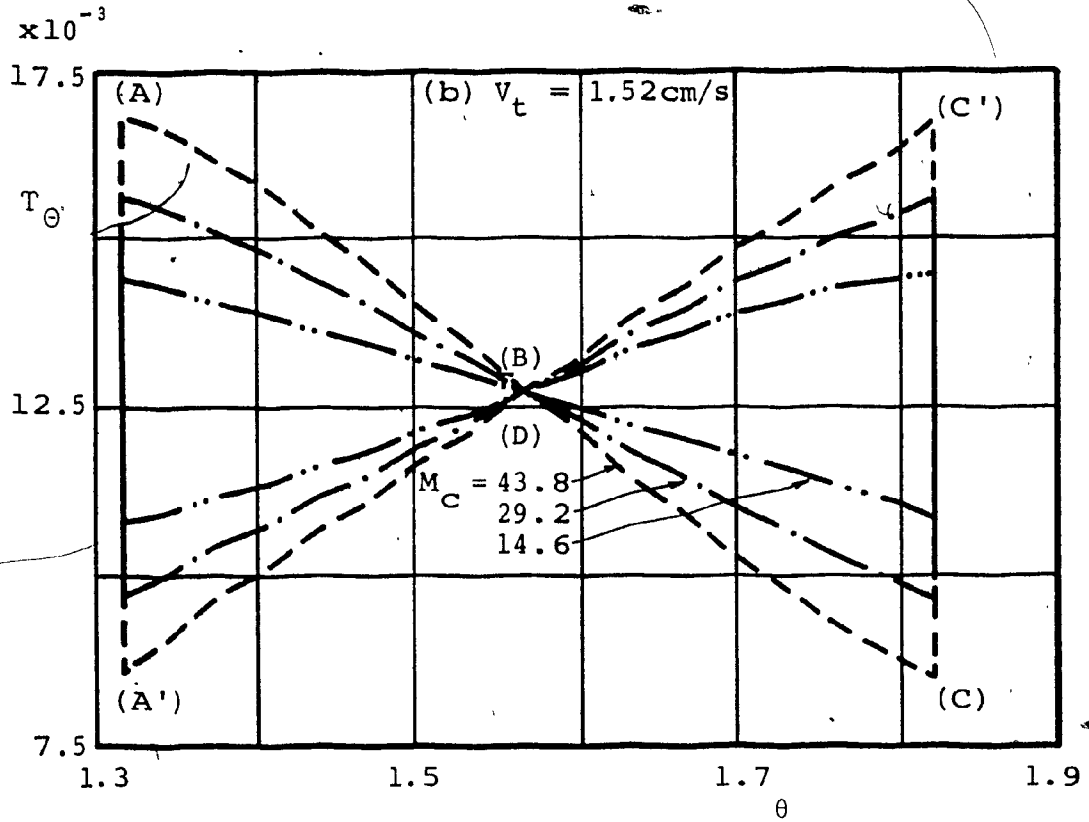


Figure 5.9: Angular Axis Torque Ratio Plots for Circular Contour (Inertial Load). M_C is in kgs.

due to the friction torque resulting from the arm support and is comparable to the inertial torque at low speeds. This bias causes the torque ratio for the angular axis to decrease for the circular parts BC and DA and increase for the parts AB and CD with the increase of either the contouring speed or the mass on the carriage. The "node" seen on the plots at $\theta = \pi/2$ occurs due to zero inertial torque at that point. This is due to vanishing transverse acceleration of the carriage at that point resulting from zero values for the radial velocity and angular acceleration. For both low and high contouring speeds, the magnitude of the torque ratio is the same at the location of the node. The sudden change in the magnitude of the torque ratios at the extreme positions of the arm results due to the Coulomb friction force of the arm support when the arm changes direction of motion.

Case (b): Witch of Agnesi contour

The torque ratio plots for the Witch of Agnesi in Figures 5.10 and 5.11 are symmetric about $\theta = \pi/2$ for the radial axis, but are asymmetric for the angular axis. This asymmetry is due to the change in the direction of the Coriolis acceleration. The vanishing effect of the inertial torque on the angular axis can be seen at $\theta = \pi/2$ in Figure 5.11, and results in a node at which all plots for different masses on the carriage pass. The magnitude of the torque ratio at the node corresponds to the friction torque

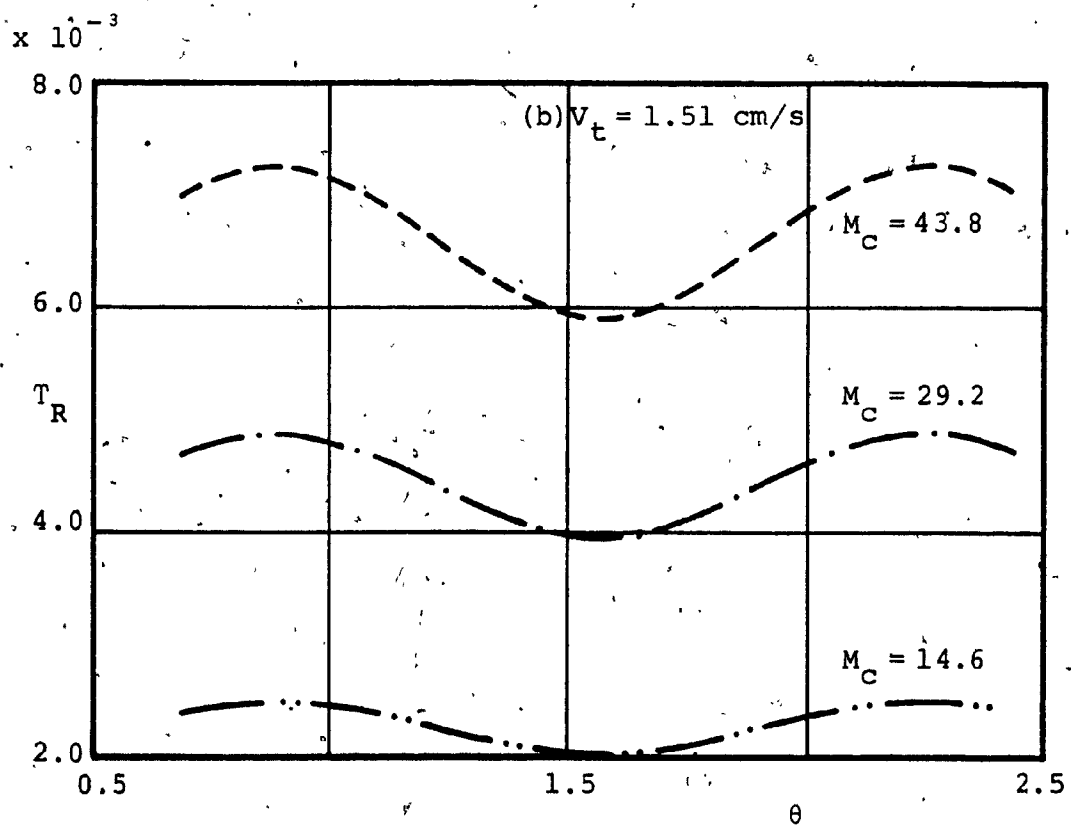
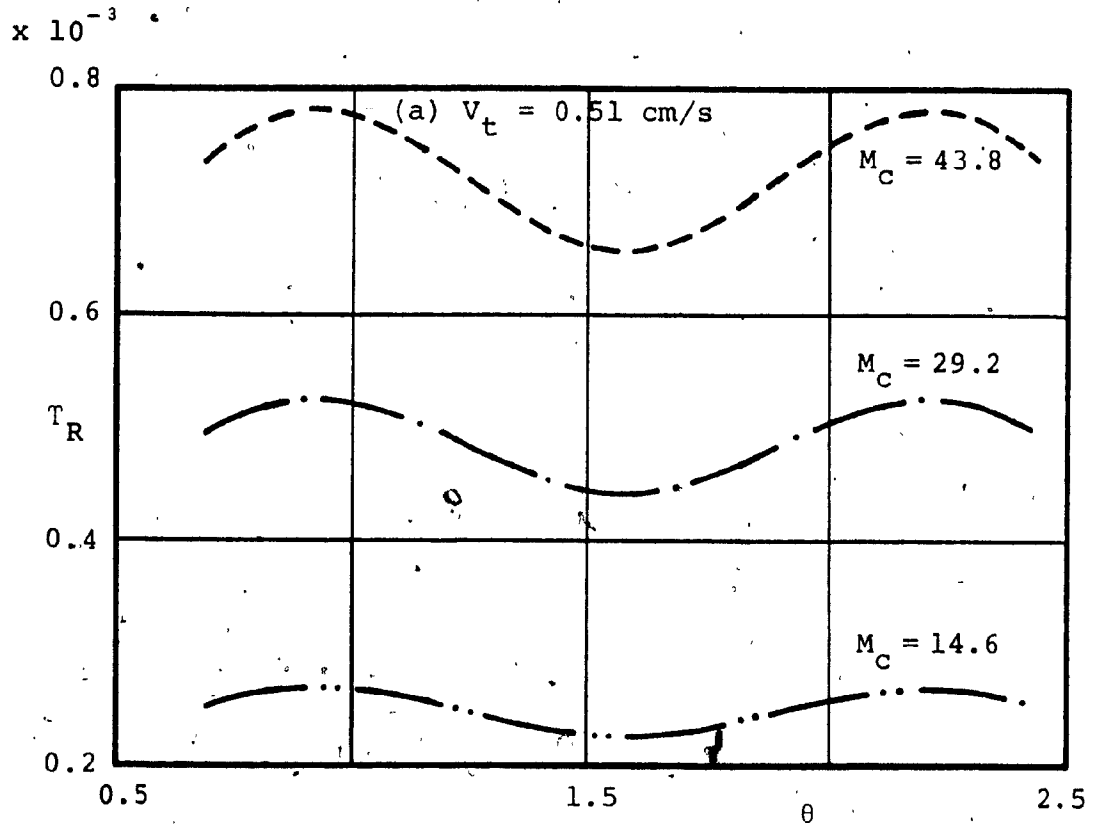


Figure 5.10: Radial Axis Torque Ratio Plots for Witch of Agnesi Contour (Inertial Load). M_C is in kgs.

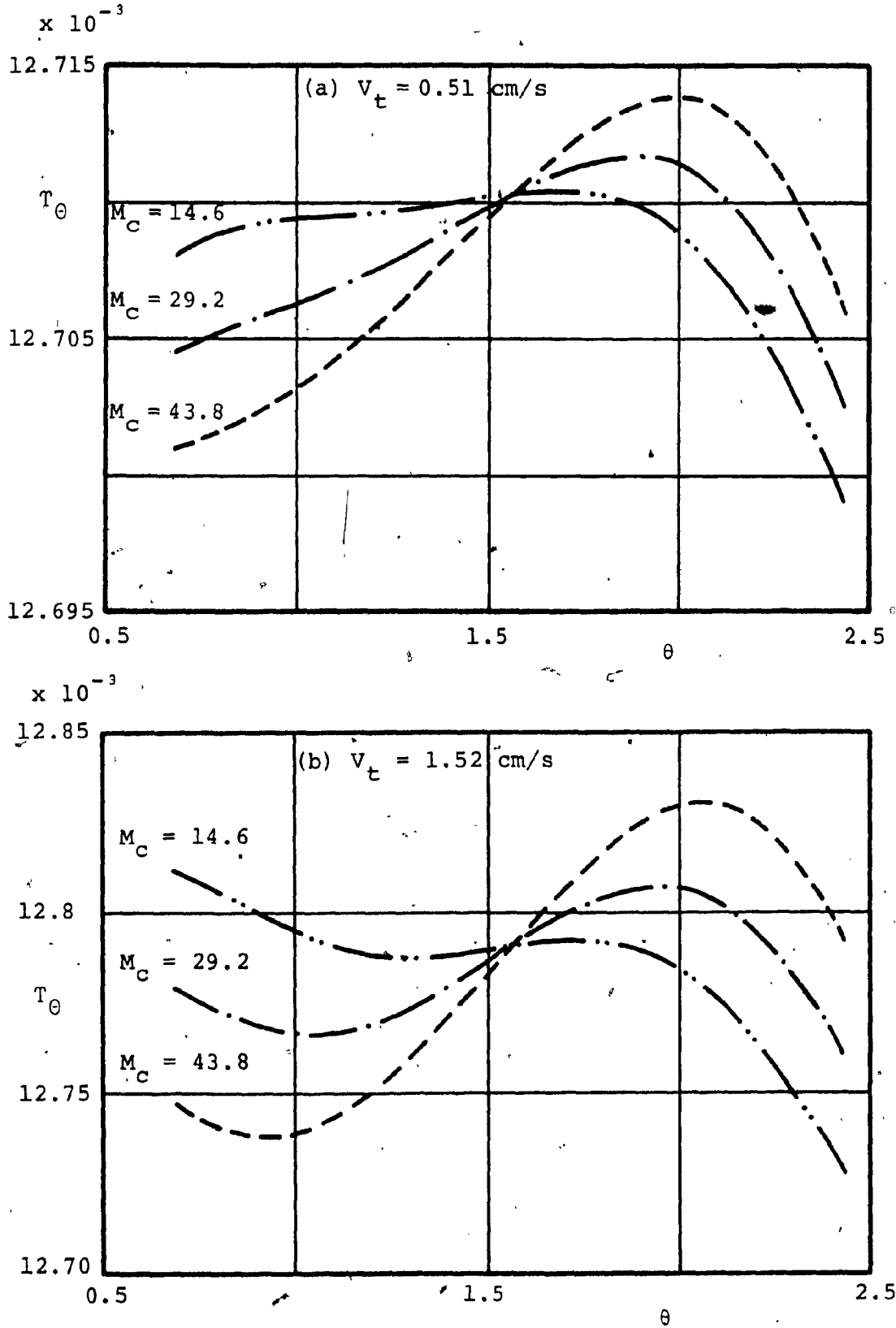


Figure 5.11: Angular Axis Torque Ratio Plots for Witch of Agnesi Contour (Inertial Load). M_C is in kgs.

of the arm support.

The torque ratios for this contour are smooth due to the slow and gradual change of both γ and the radius of curvature along the contour. Since the arm did not change direction while the tool is tracking the contour, there is no sudden jump in the torque ratios that would result due to the Coulomb friction in the arm support.

Case (c): Limacon of Pascal contour

In the case of the Limacon of Pascal, the plots shown in Figures 5.12 and 5.13 are similar to those of the circular contour. Both the radial and angular axes plots, however, show some small jumps between $\theta = 1.67$ and $\theta = 1.72$ radians due to the change in radial acceleration which results from the indentation in the curve at $\theta_1 = \pi$ (refer to Figure 5.6). The angular axis plots show the same disturbances at the above mentioned angles, the disturbances here however, are more accented by the Coulomb effect of the support friction force. The plots here are slightly lopsided and shifted from $\theta = \pi/2$ as a result of the relative location between the machine pole and the contour pole as can be seen in Figure 5.6.

Case (d): Serpentine contour

For the Serpentine profile, the torque ratios experience a sharp change in magnitudes at approximately $\theta = 1.5$ and $\theta = 1.66$ radians as can be seen from the plots in

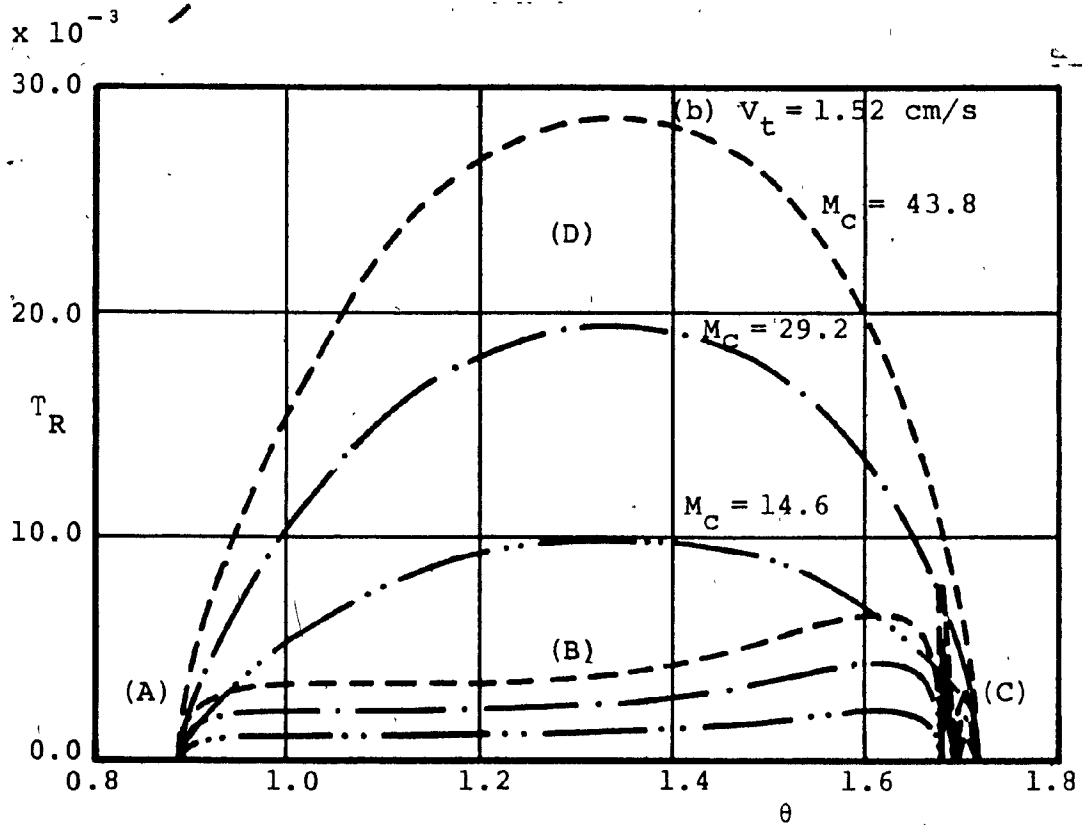
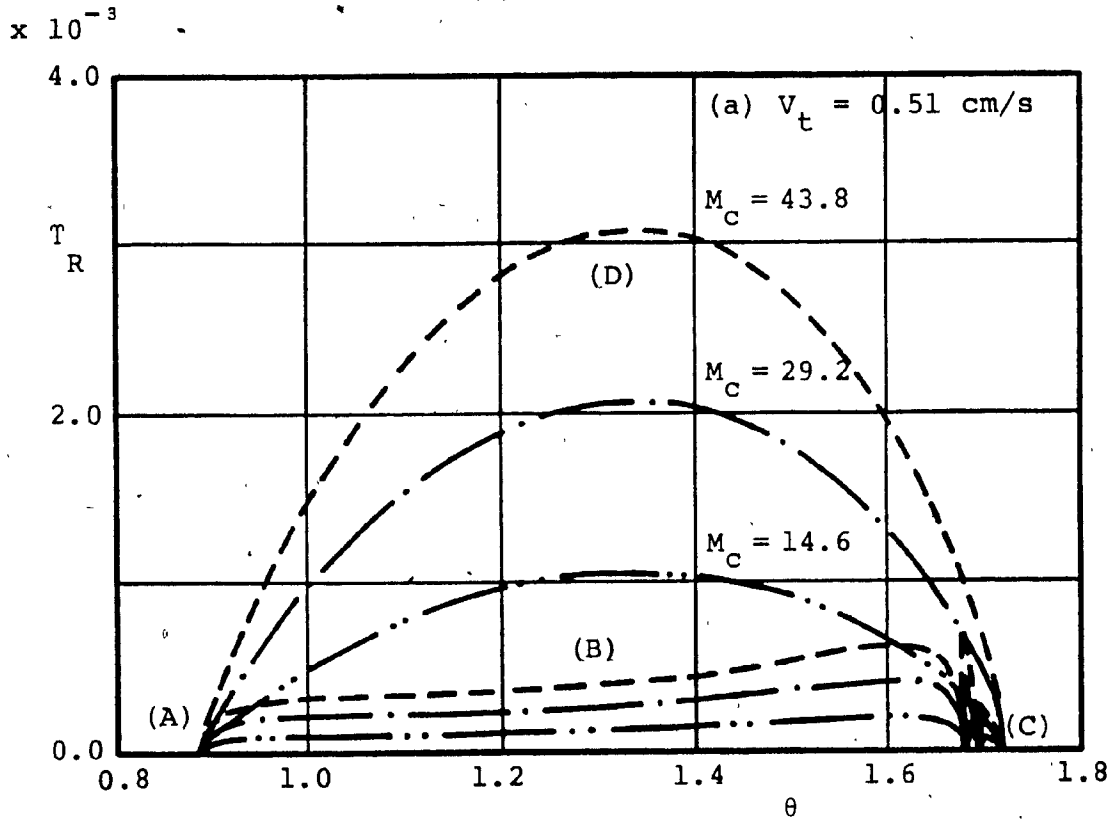


Figure 5.12: Radial Axis Torque Ratio Plots for Limacon of Pascal Contour (Inertial Load). M_C is in kgs.

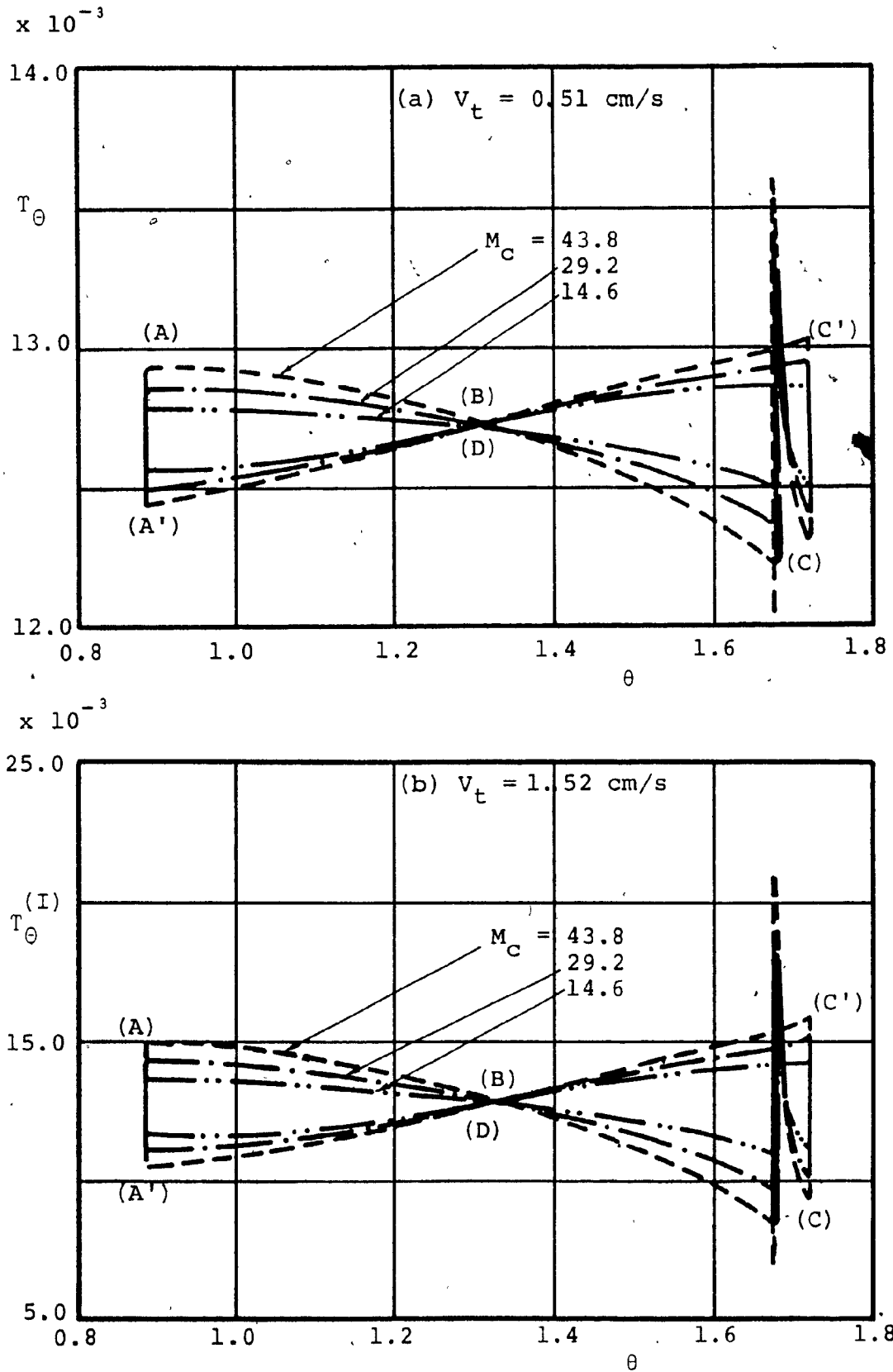


Figure 5.13: Angular Axis Torque Ratio Plots for Limacon of Pascal Contour (Inertial Load). M_C is in kgs.

Figures 5.14 and 5.15. The sharp change results when the tool leaves the smooth part of the curve and starts tracking that part of the curve that has an asymptote inclined at approximately 1.4 radians to the contour axis. The transition between one part of the curve to the other is fast, that is to say, the change in γ and in the radius of curvature is fast, and causes a sharp increase in the magnitude of both the radial and angular accelerations, and hence the required torque.

The torque ratios for both axes increase with either the increase in contouring speed or mass on the carriage. The increase due to the mass on the carriage, however, is not apparent from the plots in Figures 5.14 and 5.15 since all the curves for the different cases coincide.

The torque ratio plots, in Figures 5.15.a and 5.15.b, for the angular axis show that for the major portion of the contour the torque ratio is more or less the same. The torque ratio at each of the two spikes (at $\theta=1.5$ and $\theta=1.66$ radians) changes magnitude from above the nominal value to below it, when the motor decelerates the arm and carriage rapidly. This is caused by the decrease of the angular acceleration when the tool is tracking the asymptote.

5.5.2 Grinding application

For the case of a grinding application the magnitude and direction of the cutting force F_c and α_c respectively are given in References [34] and [35] by:

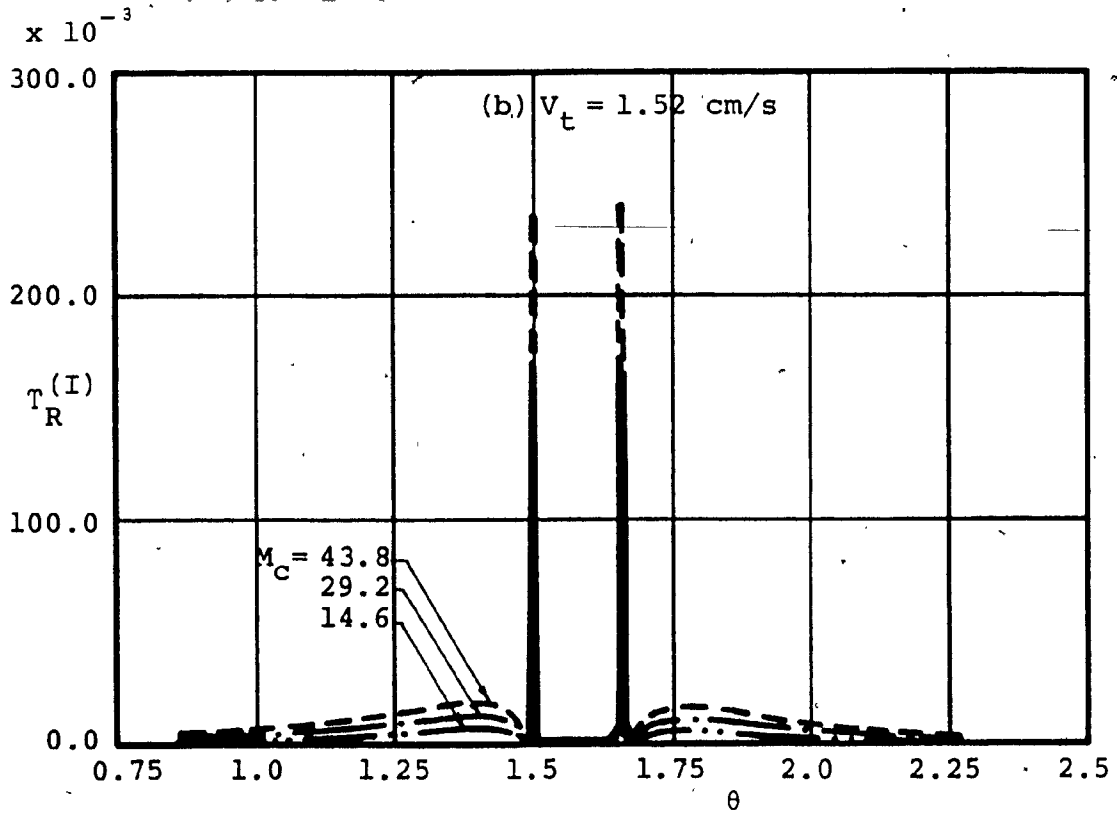
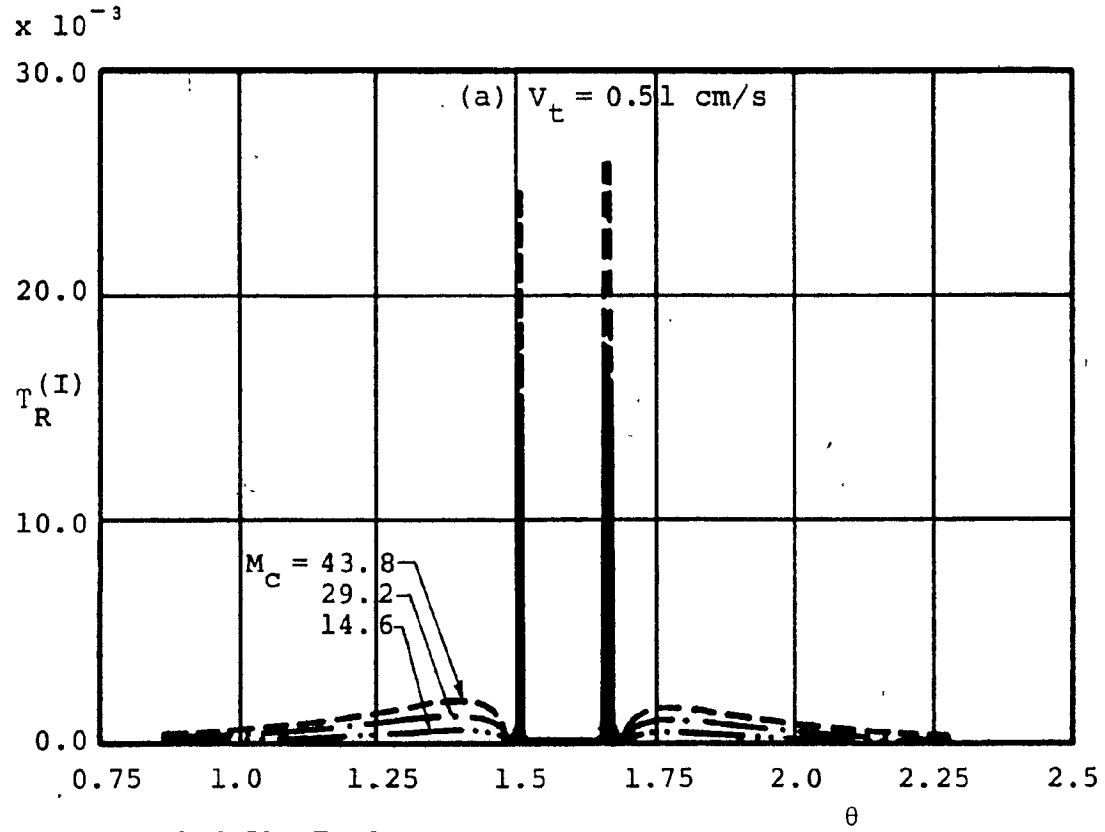


Figure 5.14: Radial Axis Torque Ratio Plots for Serpentine Contour (Inertial Load). M_C is in kgs.

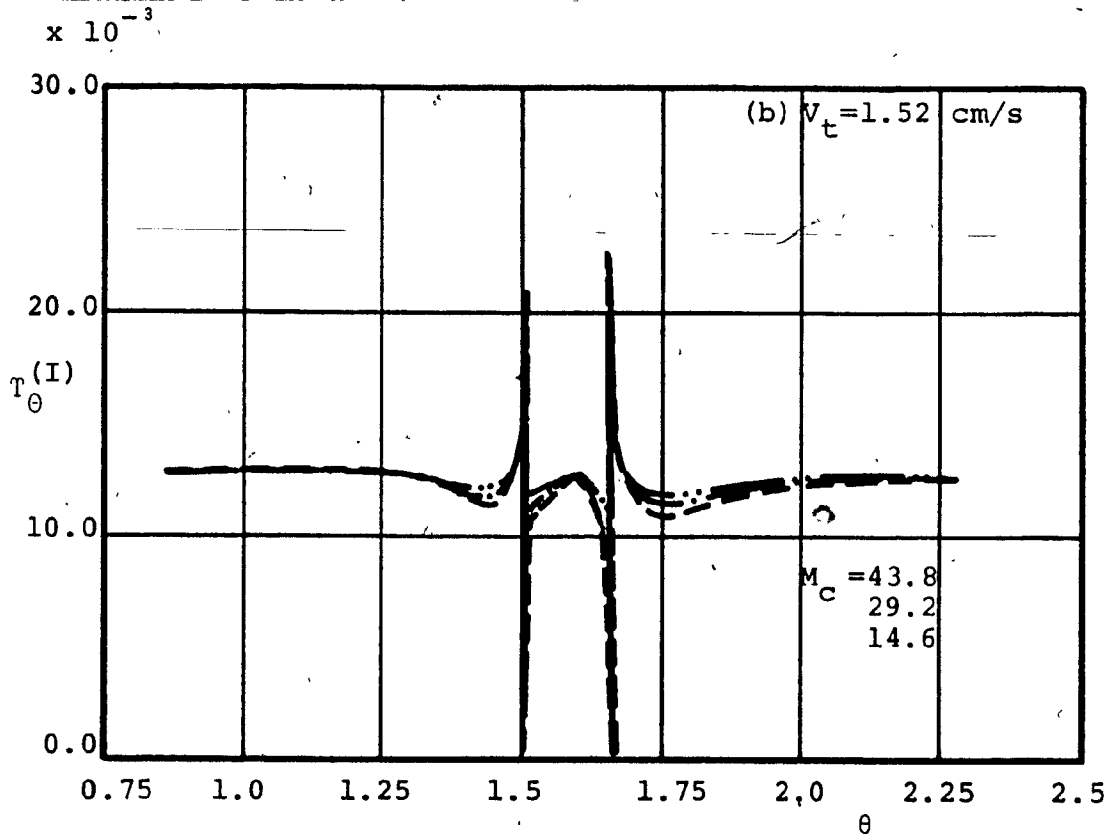
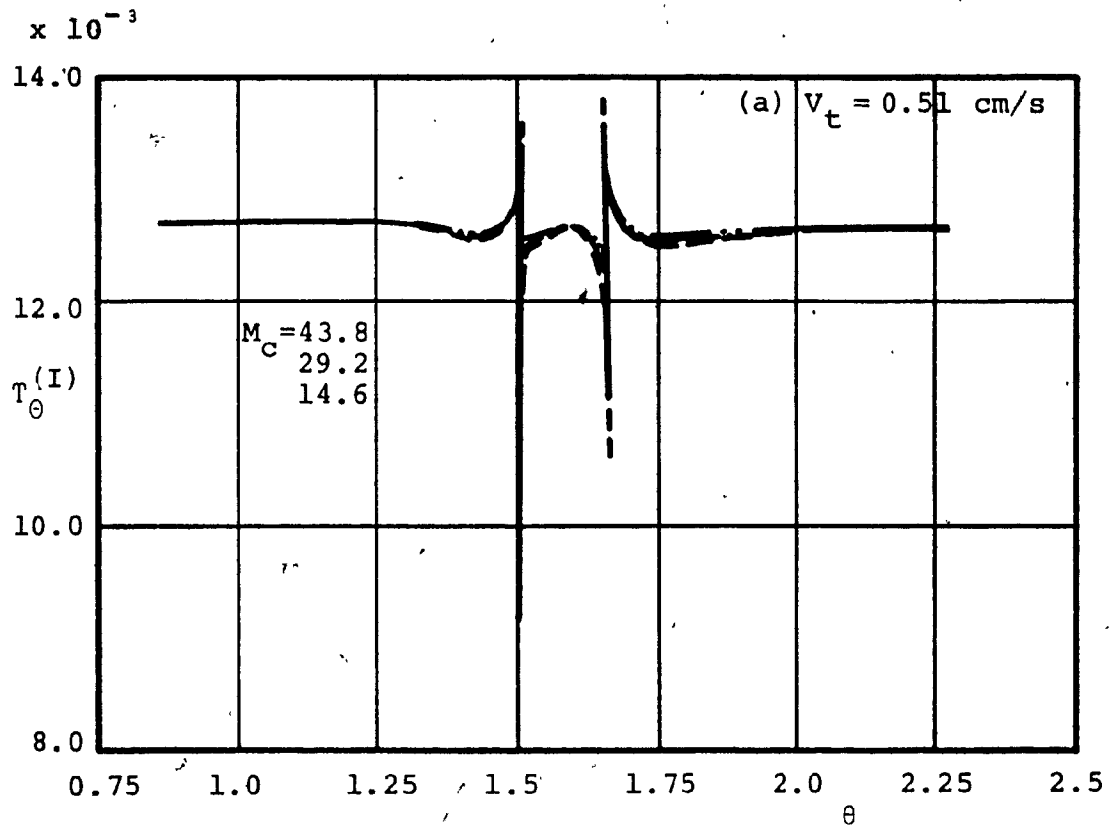


Figure 5.15: Angular Axis Torque Ratio Plots for Serpentine Contour (Inertial Load). M_c is in kgs.

$$F_c = K_c V_t \quad 5.22$$

$$\alpha_c = \tan^{-1} (c_1) \quad 5.23$$

$$K_c = k_c [1 + c_1^2]^{\frac{1}{2}} \frac{dw}{V_{\text{tool}}}$$

where α_c is the angle of inclination of the cutting force to the surface,
 c_1 is the ratio of the normal to tangential forces to the surface,
 k_c is a constant that depends on the materials of the workpiece and the grinding wheel,
 d is the depth of cut,
 w is the width of cut,
and V_{tool} is the peripheral velocity of the grinding wheel.

The ratio c_1 varies between 1.5 and 3 [34] (pp. 548), with larger values corresponding to larger depth of cut and higher grinding wheel peripheral velocity.

The plots for the torque ratios while grinding the four contours are shown in Figures 5.16 to 5.19. In each figure, the torque ratios are plotted for different feed rates.

Case (a): Circular contour

Figure 5.16.a shows that for a circular contour, the

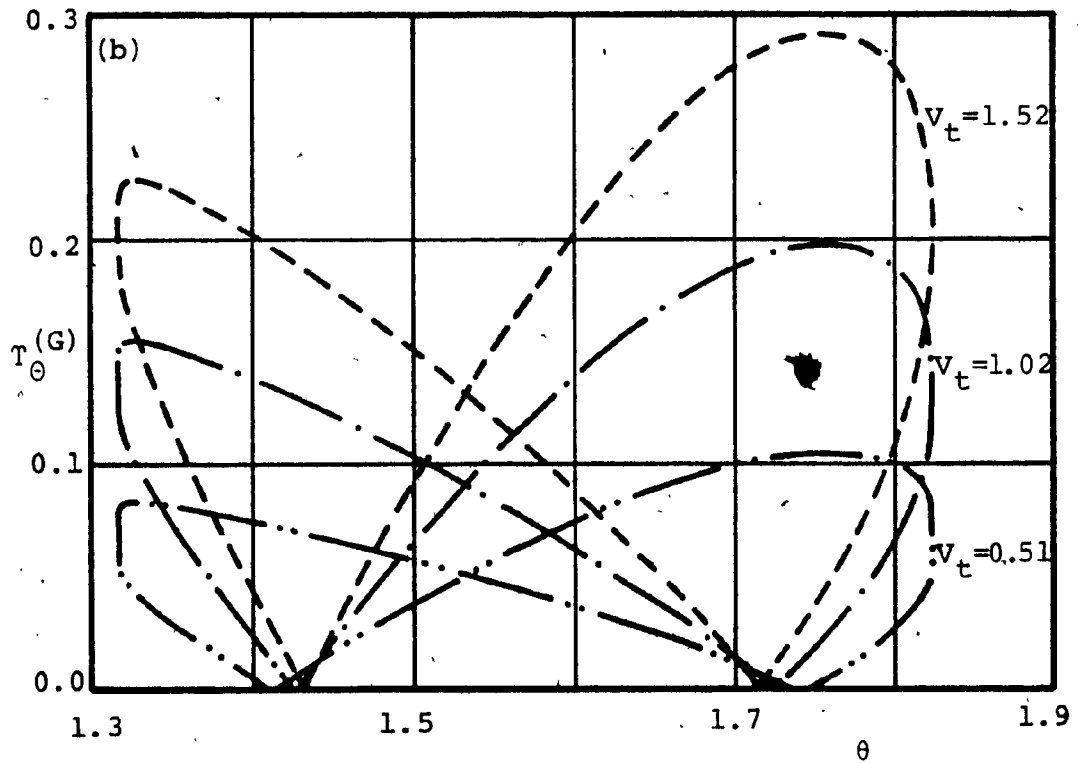
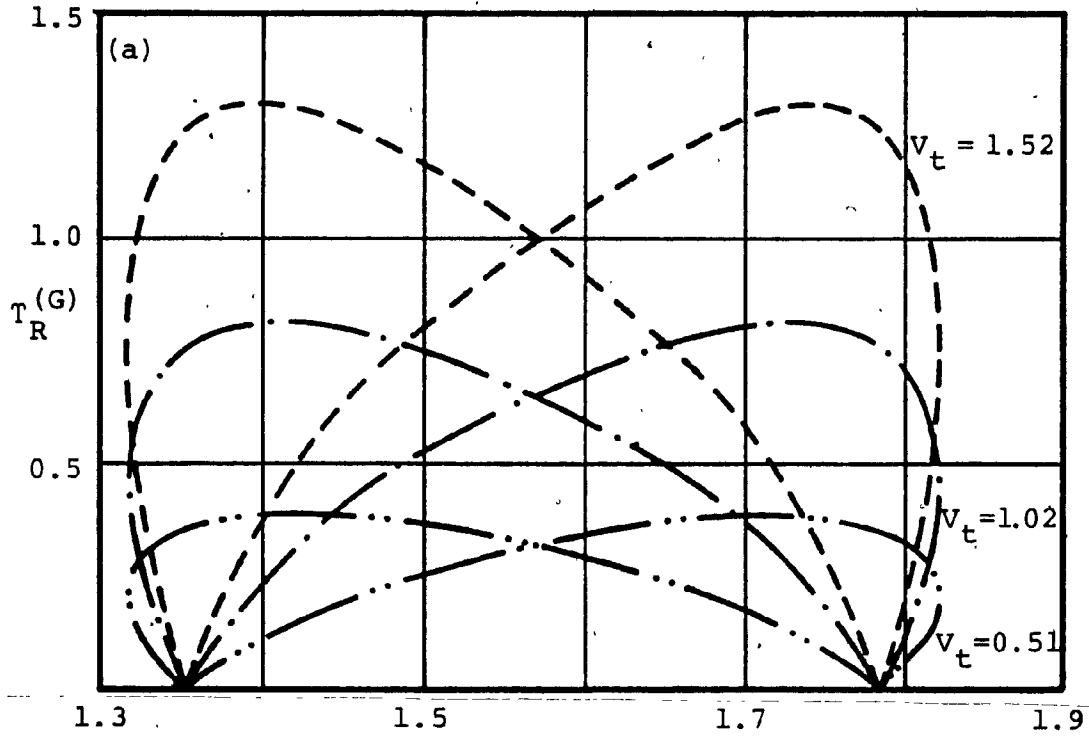


Figure 5.16: Torque Ratio Plots for the Circular Contour. (Grinding Application). v_t is in cm/s.

torque ratio in the radial axis have no symmetry similar to the case of the inertial load. This is due to the dominance of the cutting force over the inertial force acting on the mechanism, and due to the inclination α_c of this force on the tangent to the contour. The locations where the torque ratios are equal to zero are shifted from the maximum swing angles of the arm at $\theta=1.327$ and $\theta=1.824$ as can be seen from the figure. This shift which does not occur in the case of inertial application, Figures 5.8.a and 5.8.b, results due to the inclination α_c of the cutting force on the contour tangent. For a contouring speed of 1.52 cm/s (3 ft/min) the torque ratio exceeds unity and indicates that for the machine settings corresponding to this plot, the contouring operation will fail.

For the angular axis plots in Figure 5.16.b, the torque resulting from the cutting force dominates over both the inertial and friction torques. The friction torque however, can still be seen at $\theta=1.327$ and $\theta=1.824$ radians as a small jump in the torque ratio values.

The positions where the angular axis torque ratio is equal to zero, shift along the θ -axis with the change in the contouring speed as can be observed around $\theta=1.46$ and $\theta=1.67$ radians in Figure 5.16.b. This occurs at the points of equilibrium between the inertial force and the sum of the cutting and frictional forces.

The plots in Figure 5.16 also show that the maxima of the radial axis torque ratio and the minima of the angular

axis torque ratio, and vice-versa, occur at almost the same angular locations. At these locations, the dominant cutting force is either aligned with the arm (for maximum radial torque ratio) or is perpendicular to it (for maximum angular torque ratio).

Case (b): Witch of Agnesi contour

For the Witch of Agnesi contour, Figure 5.17.a shows that for the radial axis plots, the torque ratios are asymmetric about $\theta = \pi/2$ (unlike the case of the inertial load in Figure 5.11). This is due to the inclination α_c of the cutting force to the contour tangent. For a contouring speed of 1.52 cm/s (3 ft/min), the torque ratio exceeds unity, thus indicating contouring failure. The absence of the node (refer to the case of an inertial load) is also attributed to the dominance of the cutting force over the inertial and friction forces and due to its inclination to the contour surface.

The plots in Figure 5.17 show that the peak value of the torque ratio in one axis occurs at the same location where the minimum value of the torque ratio for the other axis occurs.

Case (c): Limacon of Pascal contour

The Limacon of Pascal plots in Figure 5.18 bear no resemblance to those of the inertial application in Figures 5.12 and 5.13. The plots of the angular axis show

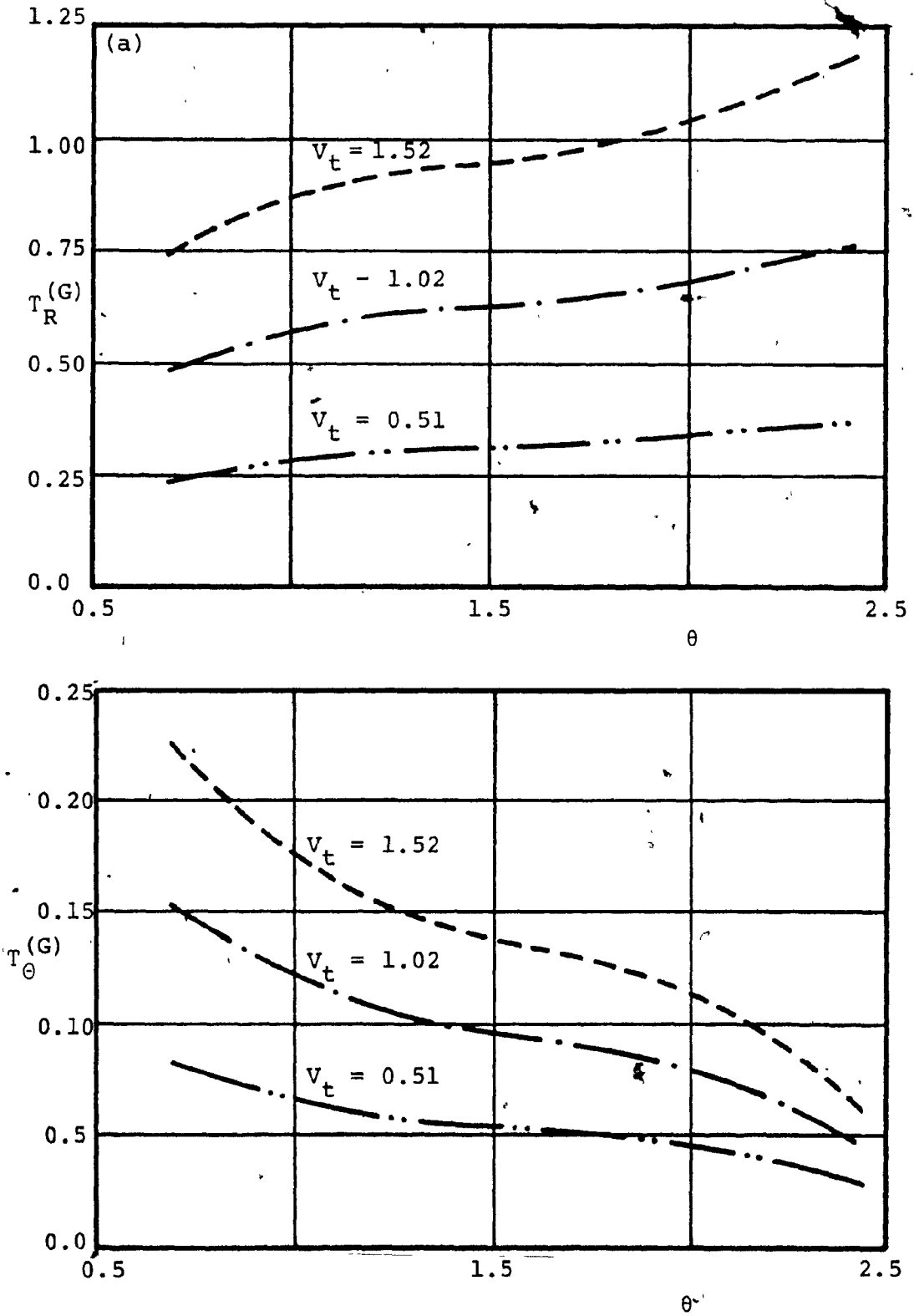


Figure 5.17: Torque Ratio Plots for the Witch of Agnesi. (Grinding Application). V_t is in cm/s.

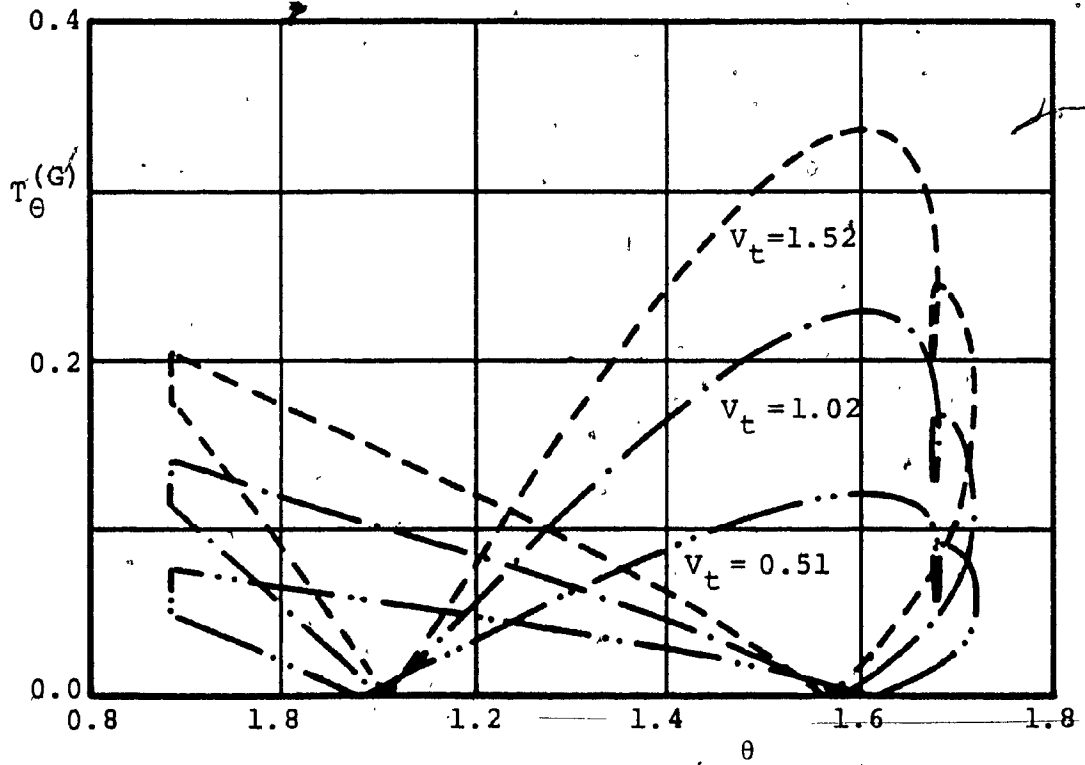
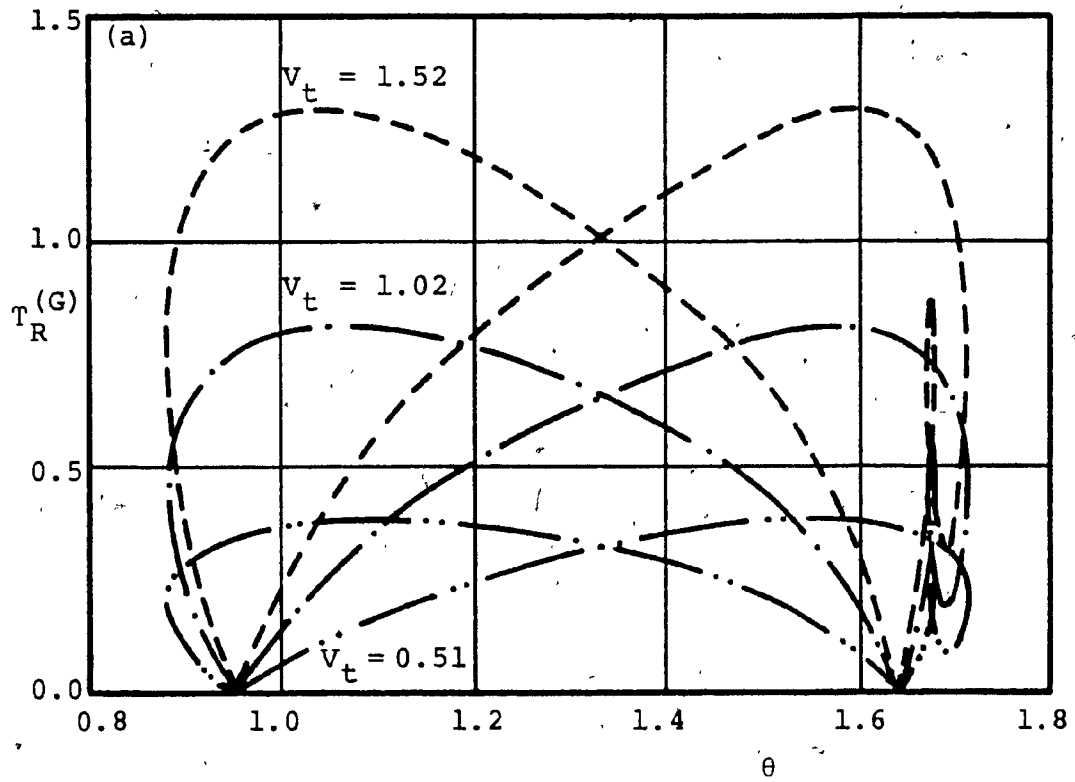


Figure 5.18: Torque Ratio Plots for Limaçon of Pascal. (Grinding Application). v_t is in cm/s.

the effect of the Coulomb friction at $\theta=0.88$, $\theta=1.67$, and $\theta=1.72$. Also the positions where the torque ratio is equal to zero, change with the change in contouring speed. The effect of the indentation in the contour is apparent in both plots between $\theta=1.67$ and $\theta=1.72$.

Similar to the previous two cases, the torque ratio plots show that the peaks on one axis coincide in location with that of the minimum values on the other axis.

Case (d): Serpentine contour

Figure 5.19 show the torque ratio plots for the Serpentine curve. Both plots for the radial and angular axes show large jump in the magnitudes of the torque ratio at $\theta=1.5$ and $\theta=1.66$ radians. These jumps occur at the same angular orientation as in the case of the inertial load.

For this contour also, the peaks of the torque ratio on one axis coincide in location with that of the minimum values on the other axis.

5.6 Effect of relative location between the contour pole and the machine pole on the torque ratios

In the study outlined in Section 5.5 the results are presented for several contours with the contour pole located at a particular point with respect to the machine pole. The radial and angular kinematic relations, and consequently the axes torques, have been shown to depend upon the contour as well as the relative location between the contour pole and

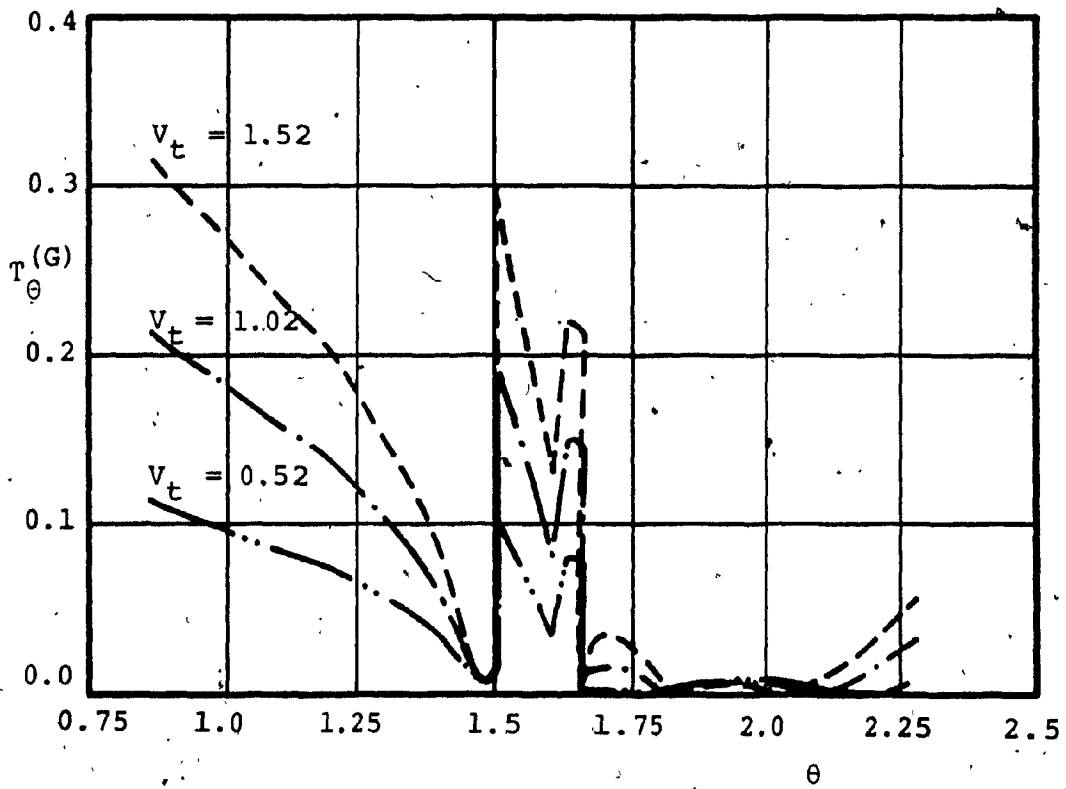
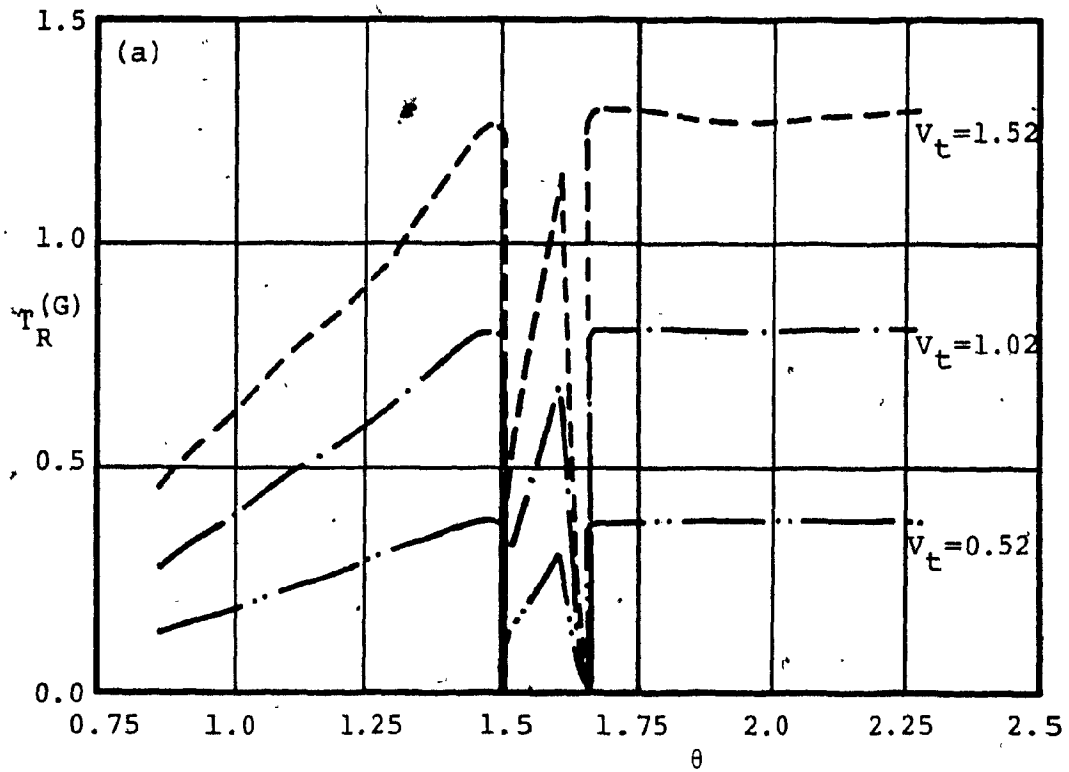


Figure 5.19: Torque Ratio Plots for Serpentine. (Grinding Application). v_t is in cm/s.

the machine pole as evident from Equations 5.2 to 5.10. Hence it is necessary to study the effect of the relative location between the contour pole and the machine pole on the torque ratios. For this purpose, the analysis was carried out for both the inertial load and the grinding operation with the machine pole located at a point where the contouring error is minimum. It should be noted that this location for each contour is the same as that found in the study in Chapter 5. This study is conducted only for the Witch of Agnesi, the Limacon of Pascal, and the Serpentine contours.

5.6.1 Inertial load

Figures 5.20 to 5.22 show the results for the case of inertial load.

For the Witch of Agnesi contour, Figure 5.20, the radial axis plots show some resemblance to those of Figure 5.10.b. The magnitude of the torque ratio, however, is lower. The angular axis plots show that the torque ratio decreases with the increase of mass on the carriage. The relative position of the contour pole with respect to the machine pole is such that the torque due to the carriage acceleration in the transverse direction, a_t , decreases with the increase in the mass on the carriage.

The plots in Figure 5.21 show that for the Limacon of Pascal, the torque ratios are considerably larger with the machine pole at the minimum area error location than those

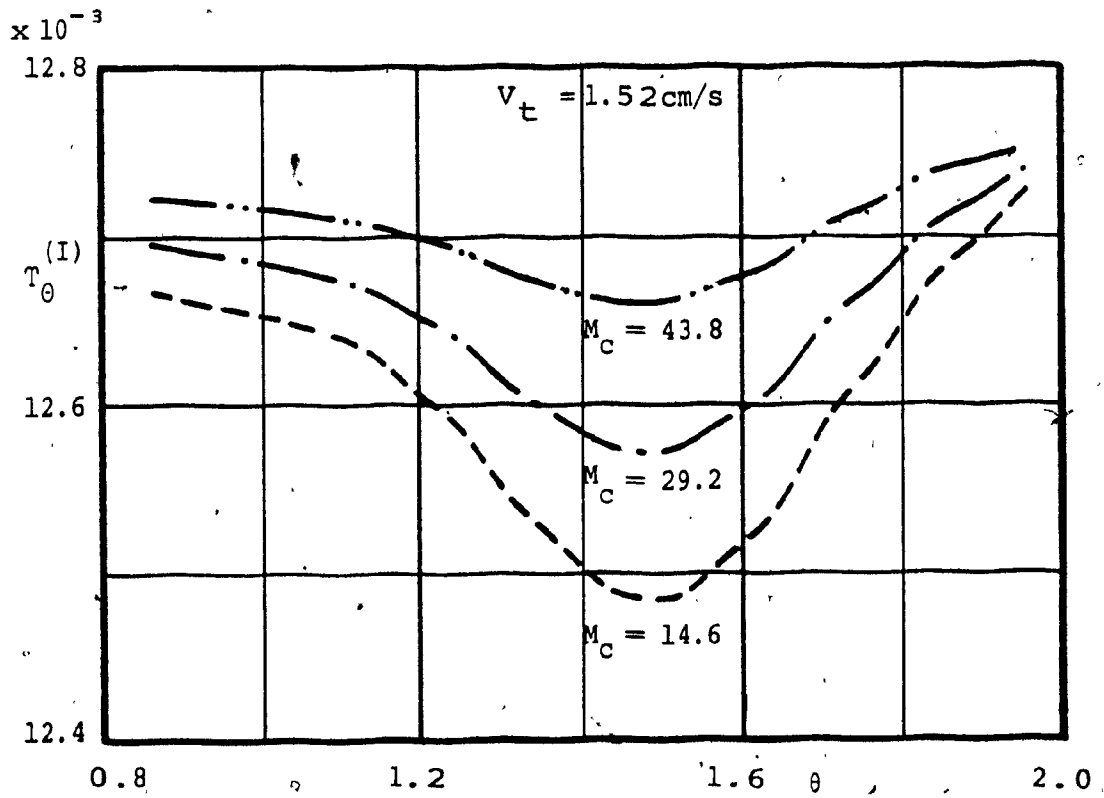
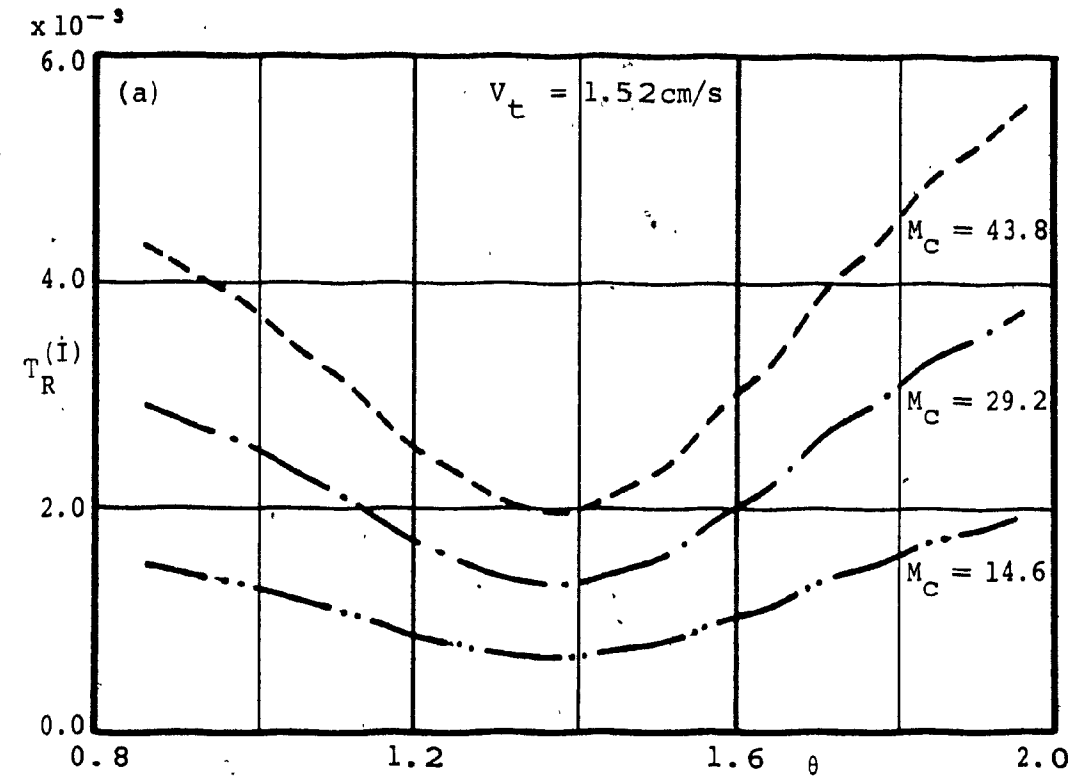


Figure 5.20: Torque Ratio Plots for Machine Pole at the Location of Minimum Area Error: Witch of Agnesi Contour (Inertial Load). M_C is in kgs.

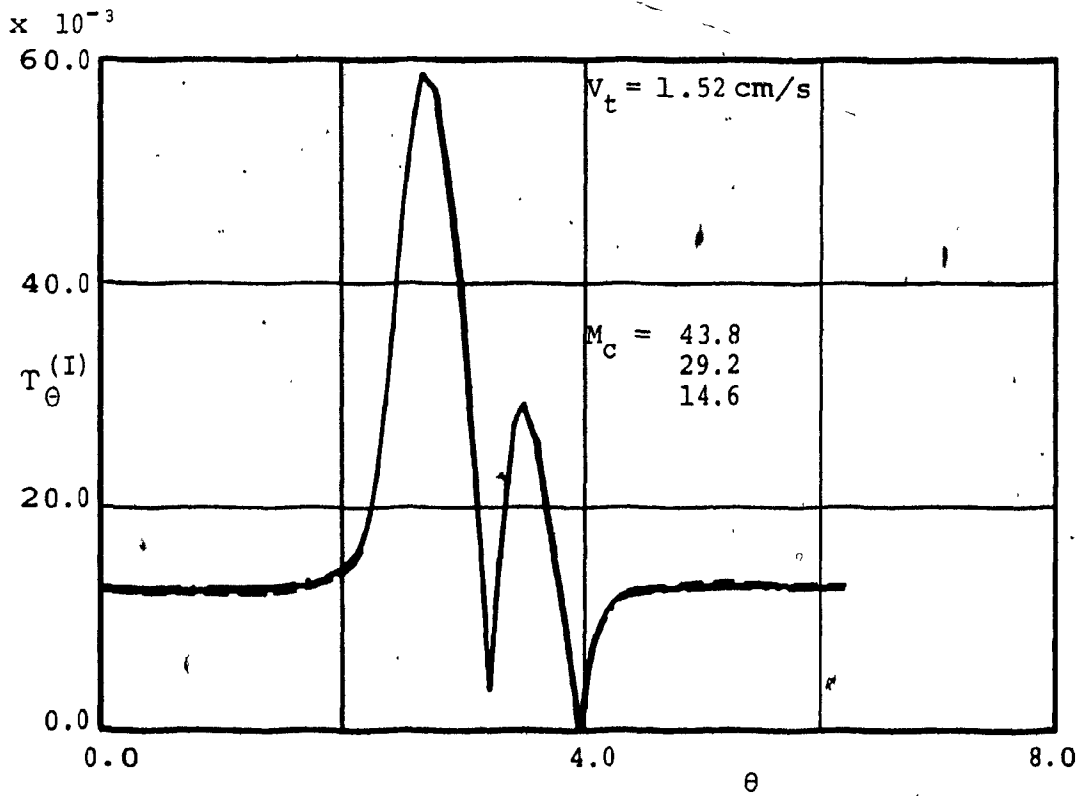
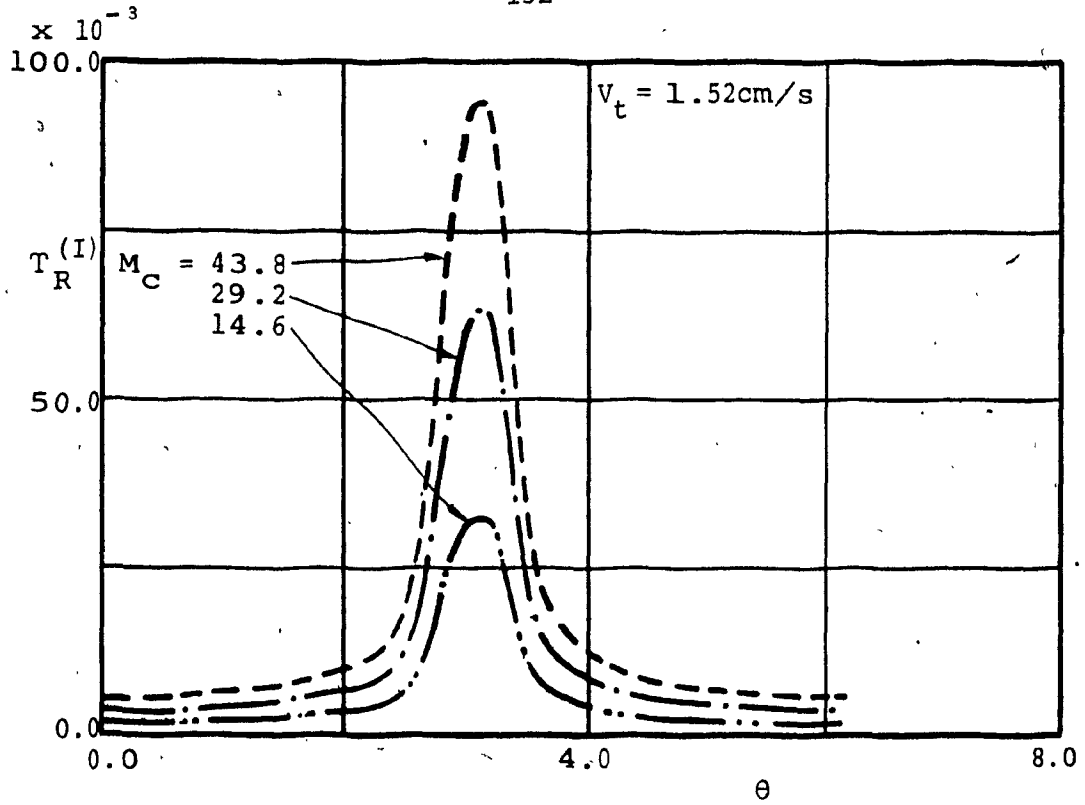


Figure 5.21: Torque Ratio Plots for Machine Pole at the Location of Minimum Area Error: Limacon of Pascal Contour (Inertial Load). M_C is in kgs.

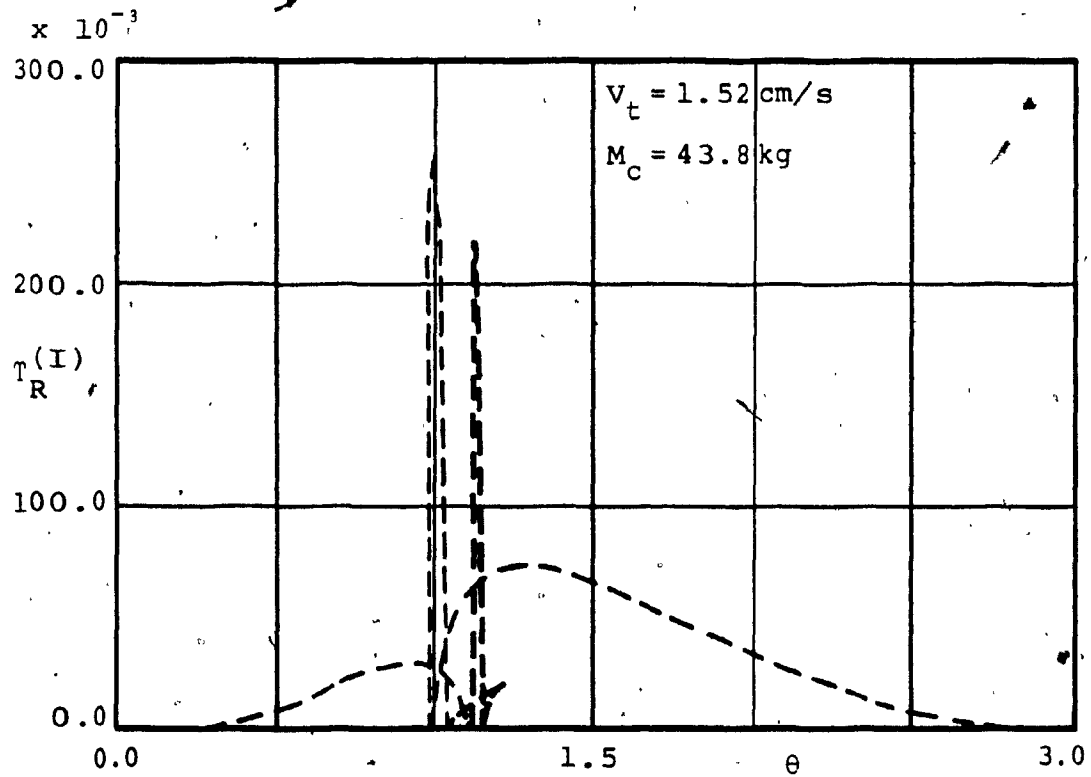
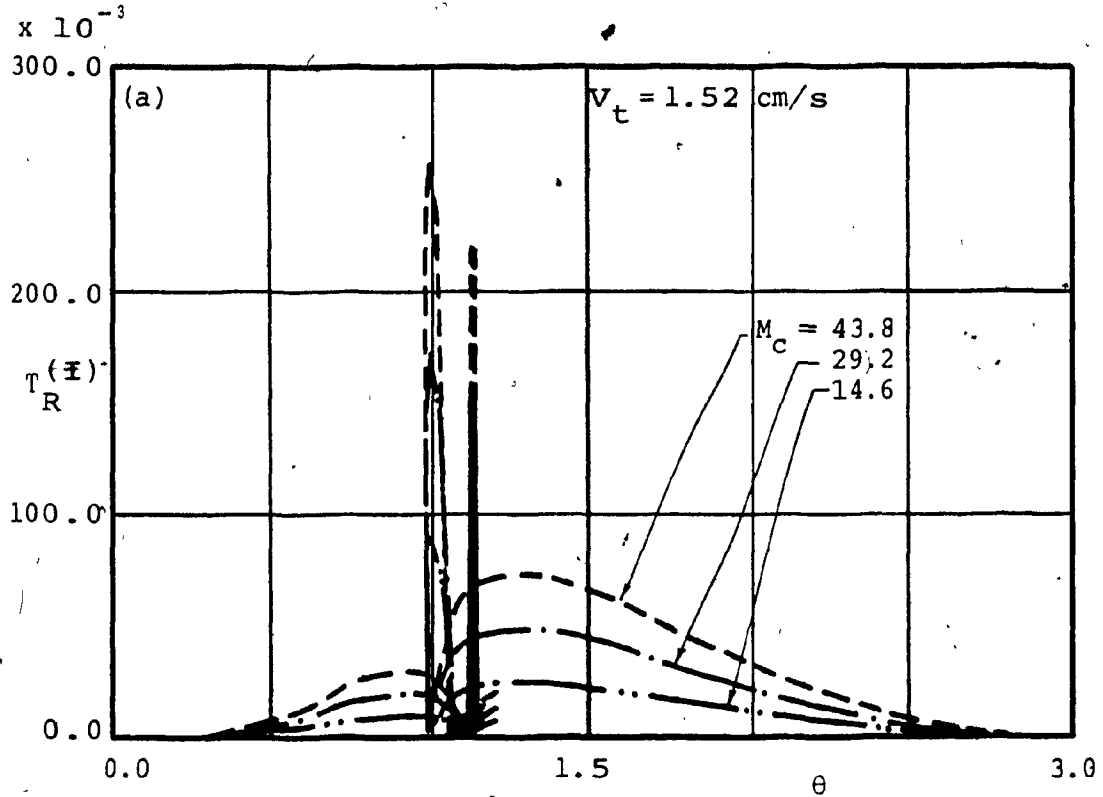


Figure 5.22: Torque Ratio Plots for Machine Pole at the Location of Minimum Area Error: Serpentine Contour (Inertial Load). M_C is in kgs.

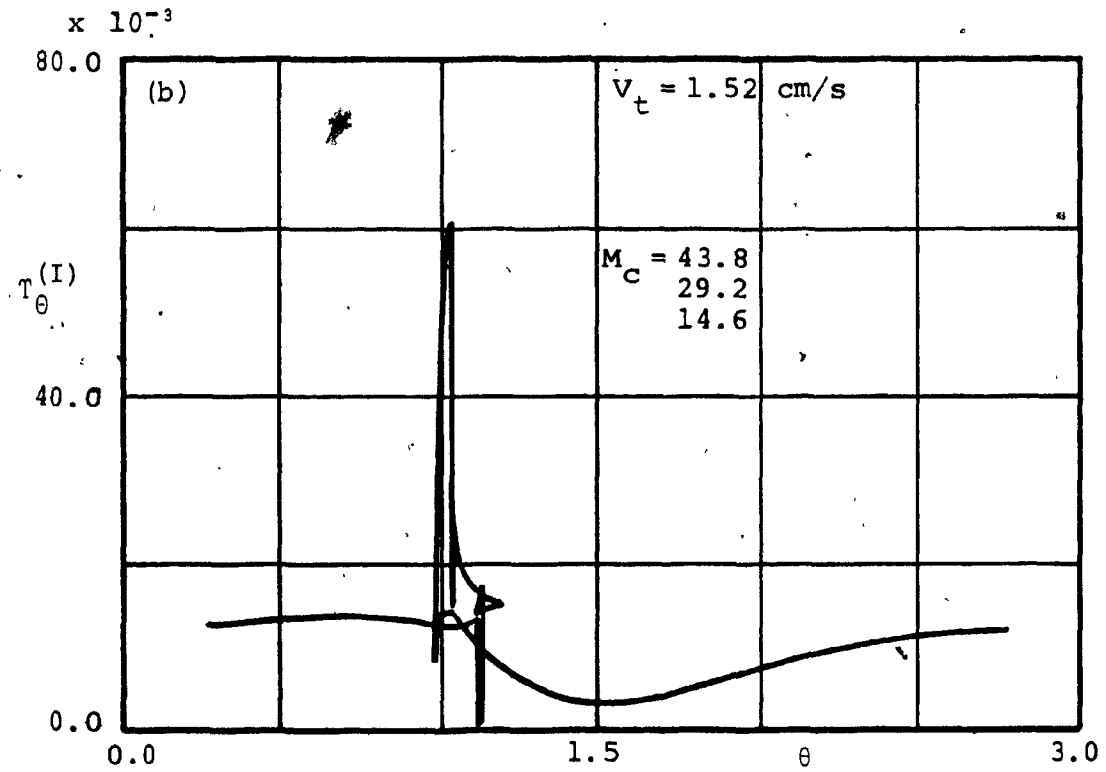


Figure 5.22: Torque Ratio Plots for Machine Pole at the Location of Minimum Area Error: Serpentine Contour (Inertial Load). M_c is in kgs.

in Figures 5.12.b and 5.12.d. The machine pole in this case is located within the contour and hence the angular orientation in Figure 5.21 extend from $\theta=0$ to $\theta=2\pi$. Furthermore, the shape of the plots bears no resemblance to those in the previous study.

The Serpentine contour plots in Figure 5.22 show that the radial axis torque ratio does not seem to be affected by the change in mass on the carriage. However, the angular axis torque ratio is considerably larger than that in Figure 5.15.b.

5.6.2 Grinding application

For the case of a grinding application the torque ratio plots are shown in Figures 5.23 to 5.25 for the three contours.

For the Witch of Agnesi contour, Figure 5.23, locating the machine pole at the position of minimum area error causes the maximum value of the radial axis torque ratio not to exceed unity for the contouring speed of 1.52 cm/s (3 ft/min), contrary to the earlier case presented in Figure 5.17.a. The maximum value of the angular axis torque ratio, however, has a larger value than that of the previous case (Figure 5.17.b).

The torque ratio plots in Figure 5.24 for the Limacon of Pascal contour show that the magnitude of the maximum radial axis torque ratio remains essentially unchanged from those in the previous case shown in Figure 5.18.a. However,

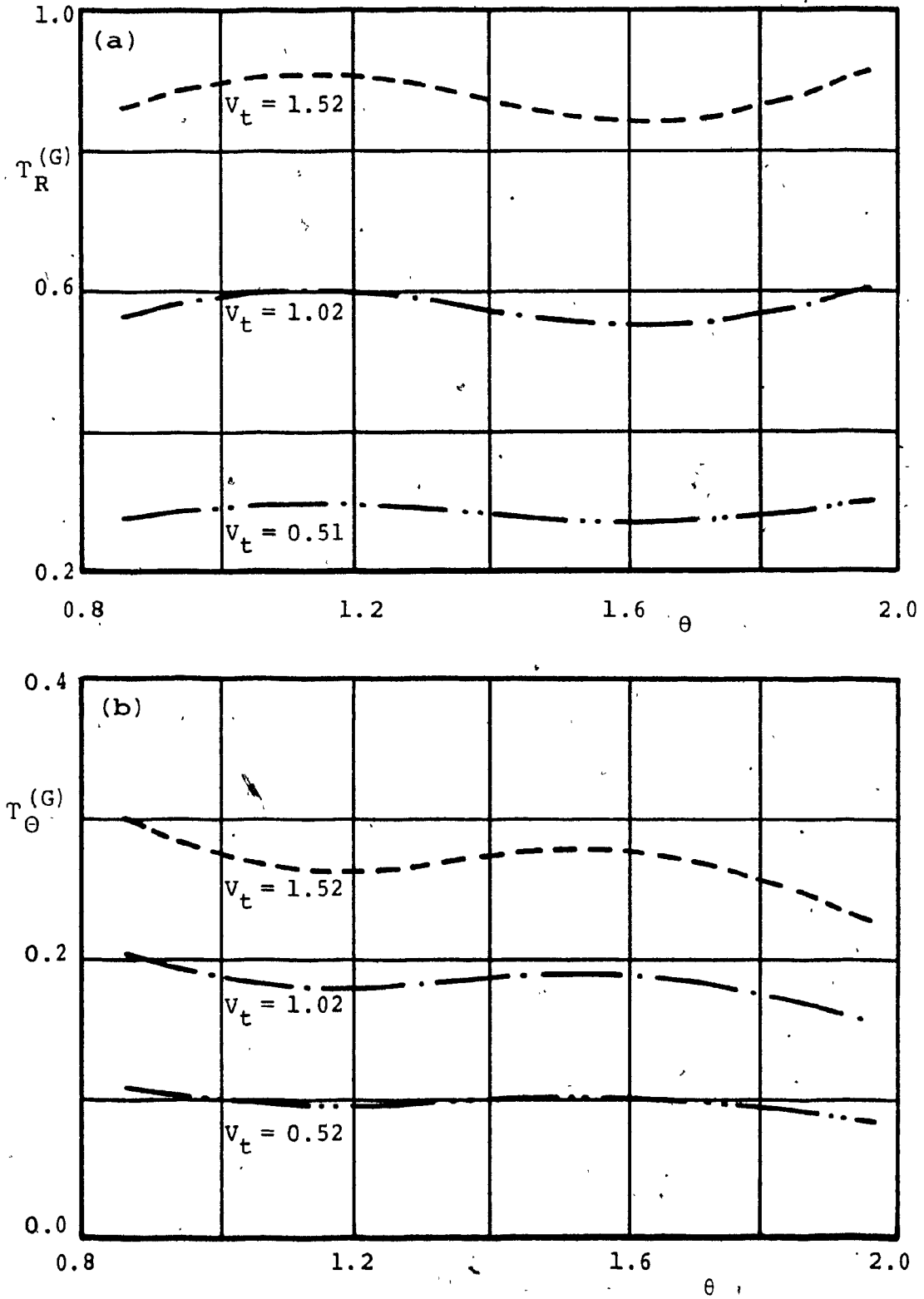


Figure 5.23: Torque Ratio Plots for Machine Pole at the Location of Minimum Area Error: Witch of Agnesi Contour (Grinding Application). V_t is in cm/s.

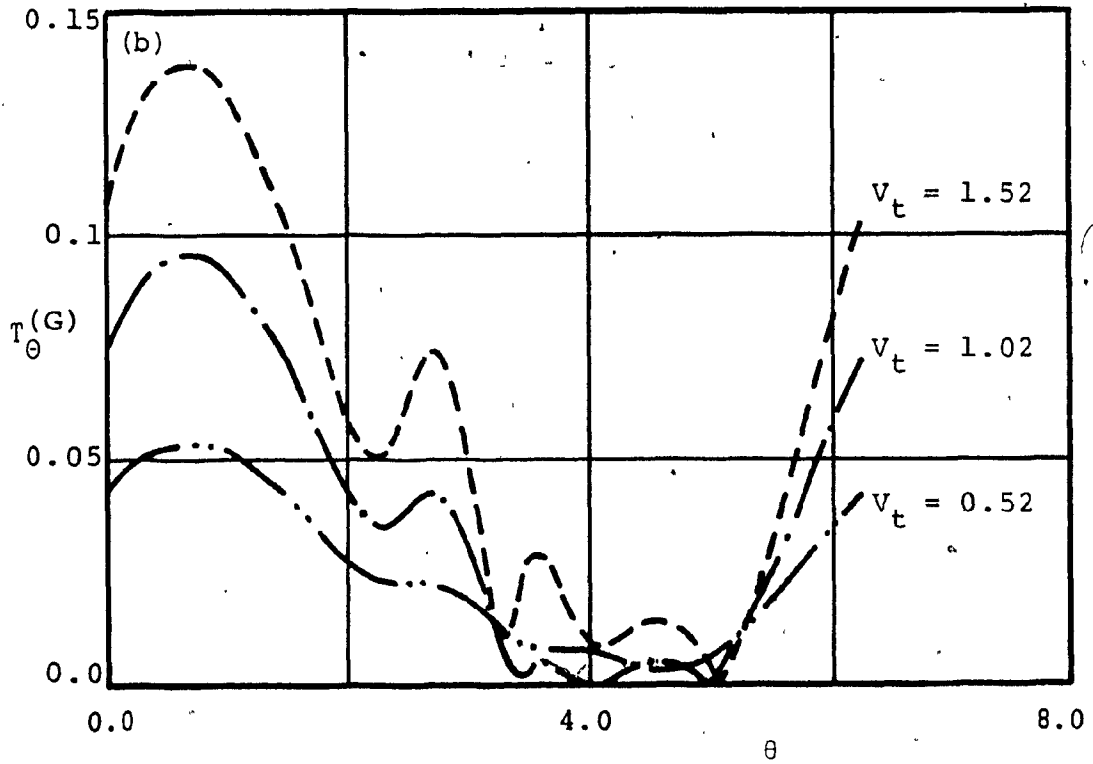
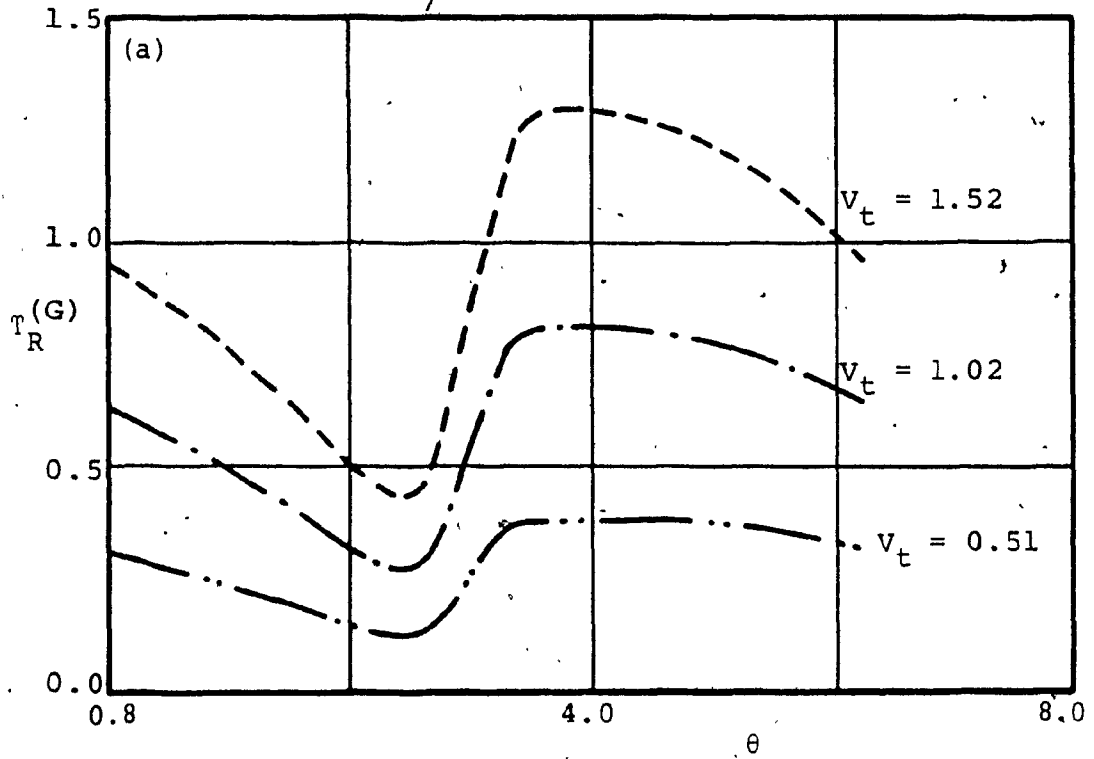


Figure 5.24: Torque Ratio Plots for Machine Pole at the Location of Minimum Area Error: Limacon of Pascal Contour (Grinding Application). v_t is in cm/s.

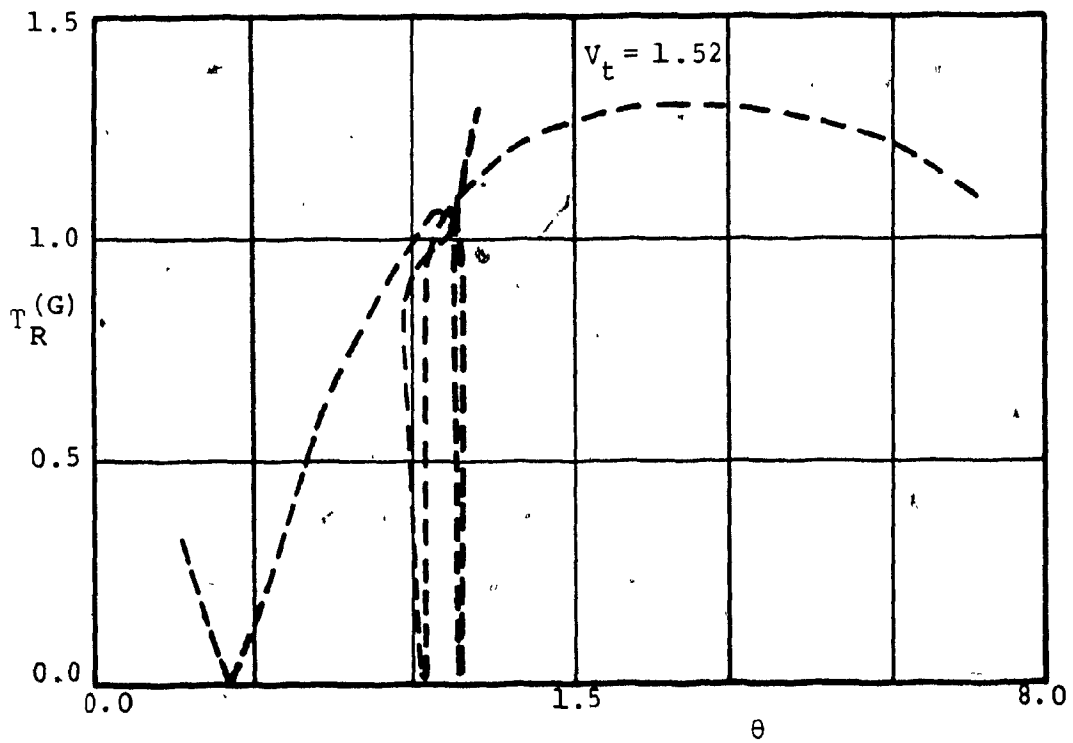
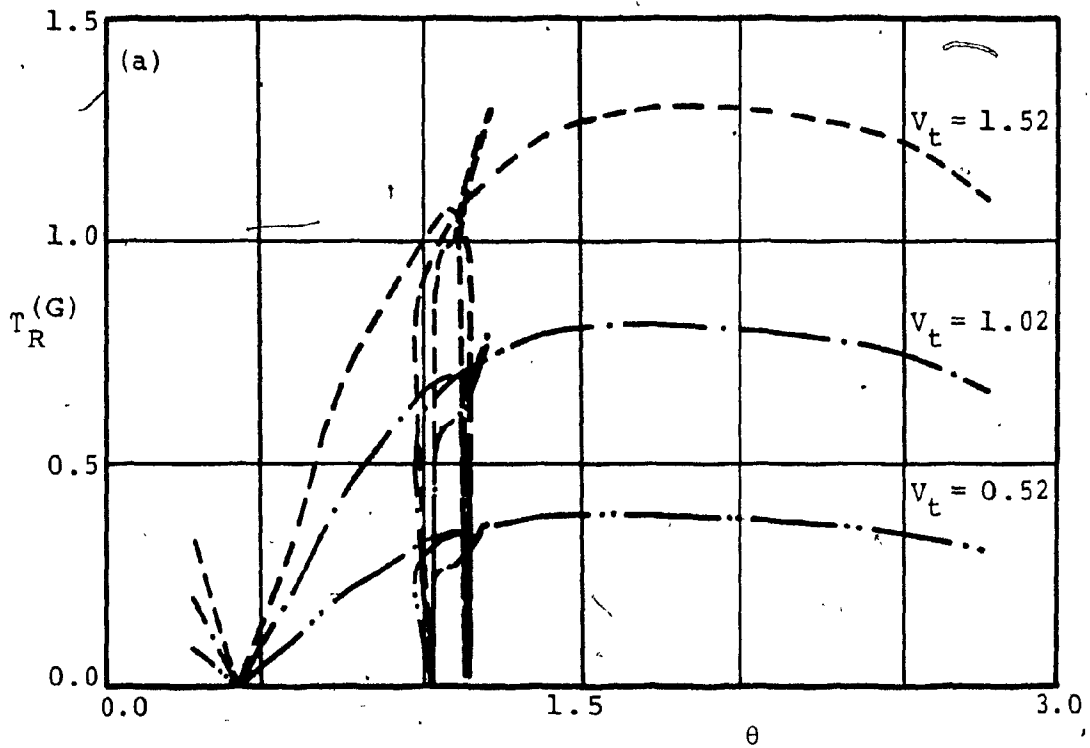


Figure 5.25: Torque Ratio Plots for Machine Pole at the Location of Minimum Area Error: Serpentine Contour (Grinding Application). V_t is in cm/s.

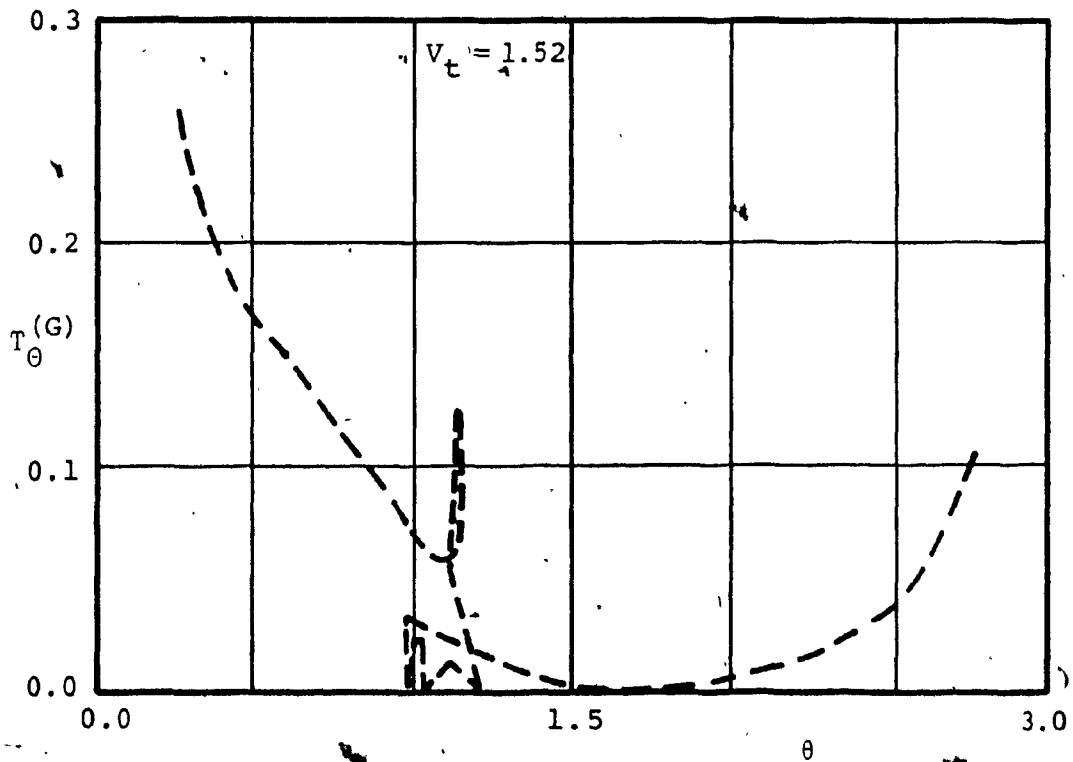
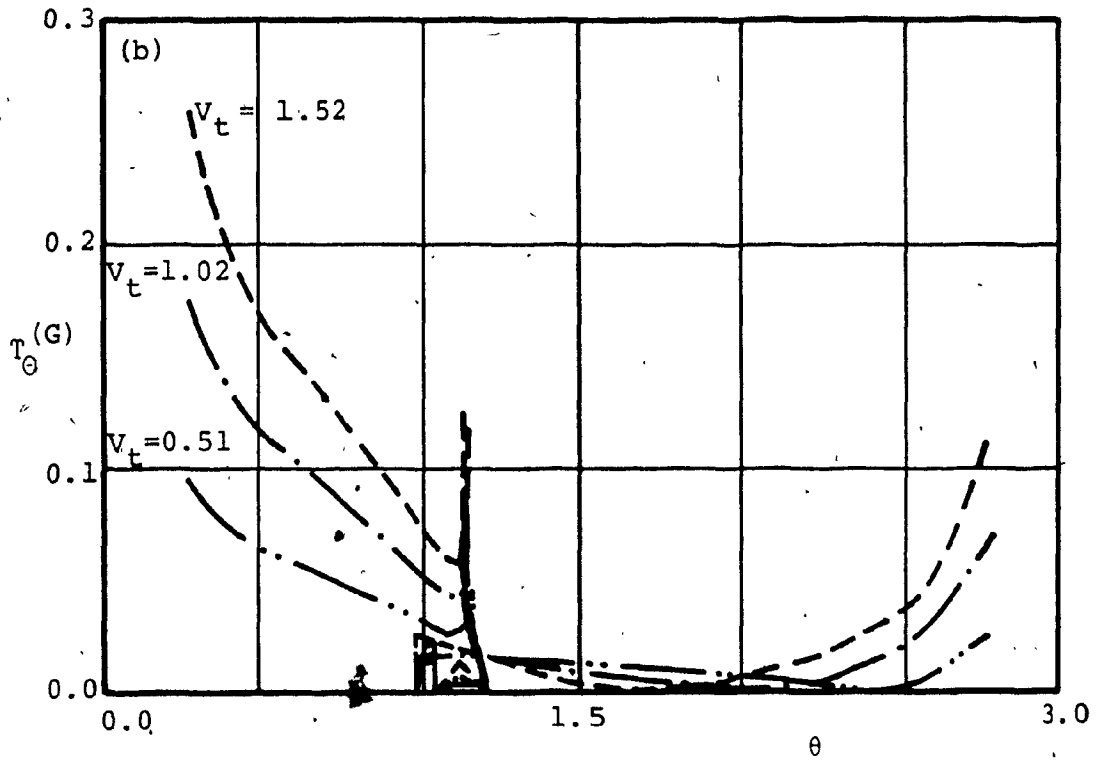


Figure 5.25: Torque Ratio Plots for Machine Pole at the Location of Minimum Area Error: Serpentine Contour (Grinding Application). v_t is in cm/s.

the maximum value of the angular axis torque ratio decreased by approximately 50% in comparison to the torque ratio in Figure 5.18.b. By comparing Figures 5.24.b and 5.18.b, it can be seen that the angular axis plots do not exhibit the sudden jump in the torque ratio resulting from the Coulomb friction. This is due to the fact that the machine pole is located within the contour, which causes the angular axis to move only in one direction.

The plots for the Serpentine contour in Figure 5.25 show that at the new machine pole location, the radial axis torque ratio is comparable to that of the previous pole location (Figure 5.19.a). The angular axis torque ratio, however, is marginally lower than that of the previous case shown in Figure 5.19.b.

5.7 Summary

This chapter deals with the dynamics of the polar NC machine. The kinematic analysis shows that the velocities of the arm and the carriage at any point on the contour are functions of the contouring speed V_t and the inclination of the contour tangent to the arm γ . The acceleration of the arm and the carriage are also functions of V_t and γ , however, are inversely proportional to the radius of curvature ρ of the contour at the operating point. The role of γ in the kinematic relationships is to proportion the total velocity and acceleration over the two machine axes.

In the dynamic analysis presented in this chapter, it

is assumed that the components involved are rigid. The analysis results in relationships for the torque required from the radial and angular axes-drives of the NC machine for inertial and grinding type loads.

The stepping motors used in the prototype NC machine are energized using the wave energization scheme. Wave energization results in a finer resolution and less resonance during operation than the other energization schemes. The pull-out torque-speed relationship for stepping motors operating with the wave energization scheme is derived in this chapter.

The quotient of the torque required from an axis-drive to the pull-out torque available from that drive is defined as the torque ratio. This ratio determines the success or failure of a contouring operation. A ratio larger than unity indicates more torque required from the axis-drive than the torque available from that drive, hence contouring failure.

The effects of the nature of the contour, the type and the magnitude of the load on the NC machine, the contouring speed, and the relative location between the contour pole and the machine pole on the torque ratios are also studied in this chapter. The study shows that in general, an increase in the contouring speed or the magnitude of the machining load causes an increase in the torque ratio. Furthermore, sharply undulating contours result in a higher torque ratio than smooth contours. The loads in a grinding

application have more effect on the torque ratio of both axes than inertial loads. The effect of the contour radius of curvature on the torque ratios is more apparent in an inertial type application than in the grinding application (Refer to the cases of the Serpentine contour).

In the case of a grinding application, ~~peak~~ values of the torque ratio in one axis coincide in location with the minima of the torque ratio in the other axis.

The relative location between the contour pole and the machine pole was shown to affect the magnitudes of the torque ratios.

CHAPTER 6

ANALYTICAL

STUDY FOR PARAMETRIC VARIATION
AND OPTIMUM LOADING OF THE NC MACHINE

6.1 Introduction

In Chapter 5, the effects of the type of load and its magnitude, the contouring speed, the type of contour, as well as the relative location between the contour pole and the machine pole on the torque ratios have been studied. In this chapter, an analytical study is carried out to evaluate the isolated effect of each of the above parameters on the magnitude of the torque ratios. The effect of these parameters on the location of the maximum value of the torque along the contour is also studied. The study in Chapter 5 also showed that the magnitude of the maximum axes torques change with the change in the relative location between the contour pole and the machine pole. Based on this fact, an objective function for optimization is then formulated which, when minimized, results in a location for the contour pole where the peak load on the axes drives is minimum. The results of the parametric study are then utilized to selectively increase the machine settings (i.e. contouring speed and loads), so as to utilize the mechanism to its full capacity.

Throughout this chapter, a " $\hat{\cdot}$ " will be used to indicate the maximum values of torque and torque ratio along a

contour. Furthermore, the superscripts (I) and (G) will be used to indicate inertial and grinding cases respectively.

6.2 Effect of inertial load

6.2.1 Variable inertial loads with constant contouring speed

For the case of pure inertial load there is no force acting on the tool. However, extra mass is added and is lumped with that of the carriage. The torque ratios are hence given by:

$$T_R^{(I)} = M_C \frac{a_{cr} K_2}{T_{PR}} \quad 6.1$$

$$T_\theta^{(I)} = \frac{(J_A \ddot{\theta} + F_f L_A) K_1}{T_{P\theta}} + M_C \frac{a_{cn} r_i K_1}{T_{P\theta}} \quad 6.2$$

Equations 6.1 and 6.2 show that the torque ratios are directly proportional to the mass on the carriage.

The radial axis torque ratio plots for the inertial case shown in Chapter 5 verifies this proportionality. As an example the Limacon of Pascal plots in Figure 5.11.b show that at $\theta = \pi/2$, the torque ratio is linearly proportional to the mass on the carriage.

For the angular axis, the results in Chapter 5 do not readily show the proportionality as per Equation 6.2. This is due to the intercept in the torque ratio axis.

(Equation 6.2) given by the first term in the R.H.S.

6.2.2 Constant inertial load with variable contouring speeds

Isolating the contouring speed in Equations 6.1 and 6.2 yields:

$$T_R^{(I)} = \frac{\Lambda_8 V_t^2 + \Lambda_9 V_t^4}{[\Lambda_{10}^2 + \Lambda_{11}^2 V_t^2]^{\frac{1}{2}} - \Lambda_{12} V_t} \quad 6.3$$

$$T_\theta^{(I)} = \frac{\Lambda_{14} + \Lambda_{15} V_t^2 + \Lambda_{16} V_t^4}{[\Lambda_{10}^2 + \Lambda_{17}^2 V_t^2]^{\frac{1}{2}} - \Lambda_{18} V_t} \quad 6.4$$

where,

$$\Lambda_8 = [M_c K_2 R_a^2 \sin \gamma] / \rho$$

$$\Lambda_9 = \Lambda_8 [2\pi N_s k_R L_a \cos \gamma]^2 / R_a^2$$

$$\Lambda_{10} = 1.17632 V K_T R_a$$

$$\Lambda_{11} = \Lambda_{10} [2\pi N_s k_R L_a \cos \gamma] / R_a$$

$$\Lambda_{12} = K_V 2\pi R_a K_T k_R \cos \gamma$$

$$\Lambda_{13} = [\Lambda_{10}^2 + \Lambda_{11}^2 V_t^2]^{\frac{1}{2}} - \Lambda_{12} V_t$$

$$\Lambda_{14} = R_a^2 F_f L_a K_1$$

$$\Lambda_{15} = R_a^2 K_1 \left[J_A \left(\frac{\cos \gamma}{r \rho} - \frac{\sin 2\gamma}{r^2} \right) + M_c \frac{r \cos \gamma}{\rho} \right] +$$

$$K_1 \left[(F_f L_a 2\pi N_s k_\theta L_a \sin \gamma) / r \right]$$

$$\Lambda_{16} = K_1 \left[J_A \left(\frac{\cos \gamma}{r \rho} - \frac{\sin 2\gamma}{r^2} \right) + M_C \frac{r \cos \gamma}{\rho} \right] x$$

$$\left[(2N_s k_\theta L_a \sin \gamma) / r \right]$$

$$\Lambda_{17} = \Lambda_{10} (2\pi N_s k_\theta L_a \sin \gamma) / (R_a r)$$

$$\Lambda_{18} = (K_y R_a K_T 2\pi k_\theta \sin \gamma) / r$$

$$\Lambda_{19} = [\Lambda_{10}^2 + \Lambda_{17}^2 V_t^2]^{\frac{1}{2}} - \Lambda_{18} V_t$$

Equations 6.3 and 6.4 show that the torque ratio for both axes is a quartic polynomial in the contouring speed, V_t .

Differentiating Equations 6.3 and 6.4 partially with respect to the contouring speed gives the sensitivities $\Gamma_R^{(I)}$ and $\Gamma_\theta^{(I)}$ as:

$$\Gamma_R^{(I)} = \frac{\partial T_R}{\partial V_t} = \left[2 \Lambda_{13} V_t + 4 \Lambda_{15} V_t^3 - T_R \left(\frac{\partial \Lambda_{13}}{\partial V_t} \right) \right] / \Lambda_{13} \quad 6.5$$

$$\Gamma_\theta^{(I)} = \frac{\partial T_\theta}{\partial V_t} = \left[2 \Lambda_{15} V_t + 4 \Lambda_{16} V_t^3 - T_\theta \left(\frac{\partial \Lambda_{15}}{\partial V_t} \right) \right] / \Lambda_{15} \quad 6.6$$

where;

$$\frac{\partial \Lambda_{13}}{\partial V_t} = [\Lambda_{10}^2 + \Lambda_{11}^2 V_t^2]^{-\frac{1}{2}} \Lambda_{10}^2 V_t - \Lambda_{12}$$

$$\frac{\partial \Lambda_{19}}{\partial V_t} = [\Lambda_{10}^2 + \Lambda_{17}^2 V_t^2]^{-\frac{1}{2}} \Lambda_{17}^2 V_t - \Lambda_{18}$$

Figures 6.1 and 6.2 show plots of the sensitivity parameters $\Gamma_R^{(I)}$ and $\Gamma_\theta^{(I)}$ respectively. The plots are obtained for values of $\gamma = \pi/4$, $r = 7.62$ cm. (3 inch) and $\rho = 2.54$ cm. (1 inch). The plots indicate that both torque ratios increase monotonically and rapidly with the increase in contouring speed. For example, consider the torque ratio plots for the circular contour. At $\gamma = \pi/4$ the value of $\theta = 1.77$, and occurs on the lower part of the circle, CDA in Figure 5.4. For the radial axis referring to, Figure 5.8, at $\theta = 1.77$ on the path CDA the torque ratio increases by approximately 10 times for an increase of 3 times in the contouring speed.

For the angular axis, Figure 5.9, at $\theta = 1.77$ on the path CDA, the torque ratio increases by approximately 23% for an increase of 200% in the contouring speed. However, at the same angular location on the path ABC of the circle, Figure 5.9 shows a decrease in the torque ratio with an increase in the contouring speed. This is due to the fact that part of the inertial force acting on the carriage resulting from the Coriolis acceleration, helps the angular axis stepping motor to overcome the frictional force of the arm support and the inertial force resulting from the

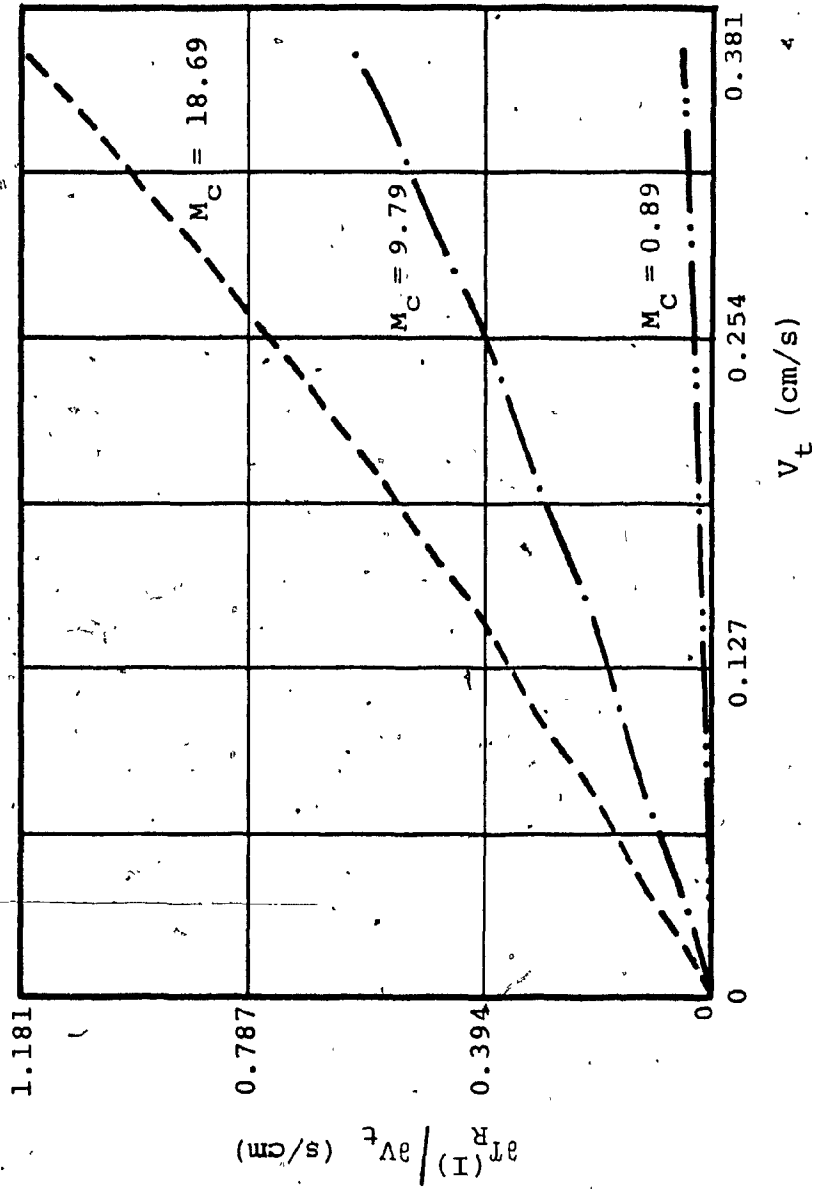


Figure 6.1: Sensitivity Parameter $\Gamma_{\theta}^{(I)}$ versus V_t .

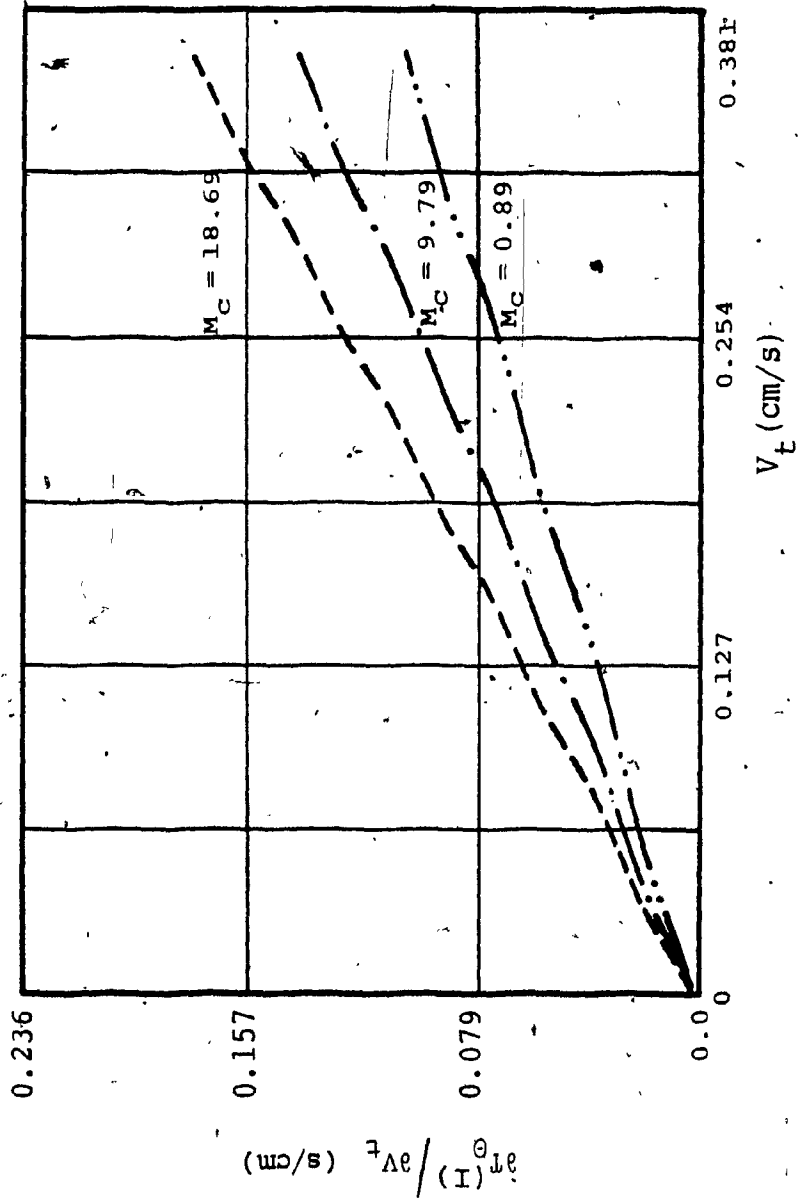


Figure 6.2: Sensitivity Parameter $\Gamma_{\theta}^{(I)}$ Versus V_t .

angular acceleration of the arm.

6.3 Effect of dissipative load (Grinding application)

6.3.1 Variable dissipative loads with constant contouring speed

For the case of the grinding application, the cutting force given by Equations 5.22 and 5.23 can be incorporated in the torque ratio relationships in Equations 5.15 and 5.16. The factor K_c which determines the magnitude of the cutting force can be isolated out to give:

$$T_R^{(G)} = \frac{M_c a_{cr} K_2}{T_{PR}} + K_c \frac{K_2 V_t \cos(\gamma - \alpha_c)}{T_{PR}} \quad 6.7$$

$$T_\theta^{(G)} = \frac{(J_A \ddot{\theta} + M_c r a_{cn} + F_f L_A) K_1}{T_{P\theta}} + K_c \frac{K_1 V_t r \sin(\gamma - \alpha_c)}{T_{P\theta}} \quad 6.8$$

In grinding applications, the machining force dominates over the inertial and the frictional forces. Thus with reference to Equations 6.7 and 6.8, the first two terms in the right hand side of both equations can be neglected. Then, both equations become linearly proportional to the machining force. This proportionality can be readily seen in the torque ratio plots for the four test contours, Figures 5.16 to 5.19.

6.3.2 Constant dissipative load with variable contouring speeds

Rewriting Equations 6.7 and 6.3 so that the contouring speed can be isolated, yields:

$$\Gamma_R^{(G)} = \frac{[\Lambda_{10} V_t + \Lambda_8 V_t^2 + \Lambda_{21} V_t^3 + \Lambda_9 V_t^4]}{[\Lambda_{10}^2 + \Lambda_{11}^2 V_t^2]^{\frac{1}{2}} - \Lambda_{12} V_t} \quad 6.9$$

$$\Gamma_\Theta^{(G)} = \frac{[\Lambda_{14} + \Lambda_{22} V_t + \Lambda_{15} V_t^2 + \Lambda_{23} V_t^3 + \Lambda_{16} V_t^4]}{[\Lambda_{10}^2 + \Lambda_{17}^2 V_t^2]^{\frac{1}{2}} - \Lambda_{18} V_t} \quad 6.10$$

where,

$$\Lambda_{20} = R_a^2 K_C K_2 \cos(\gamma - \alpha_C)$$

$$\Lambda_{21} = K_C K_2 [2\pi N_s k_R L_a \cos\gamma]^2 \cos(\gamma - \alpha_C)$$

$$\Lambda_{22} = R_a^2 K_1 K_C r \sin(\gamma - \alpha_C)$$

$$\Lambda_{23} = \Lambda_{22} [2\pi N_s k_R L_a \cos\gamma]^2 / R_a^2$$

Equations 6.9 and 6.10 show that the torque ratios in this case are also represented by a quartic polynomial in the contouring speed, V_t . The sensitivities, $\Gamma_R^{(G)}$ and $\Gamma_\Theta^{(G)}$ are calculated by taking the partial derivatives of Equations 6.9 and 6.10 with respect to V_t , and are given by:

$$\Gamma_R^{(G)} = \frac{\partial T_R}{\partial V_t} = \left[\Lambda_{20} + 2\Lambda_8 V_t + 3\Lambda_{21} V_t^2 + 4\Lambda_9 V_t^3 - \right. \\ \left. T_R (\partial \Lambda_{13} / \partial V_t) \right] / \Lambda_{13} \quad 6.11$$

$$\Gamma_{\theta}^{(G)} = \frac{\partial T_{\theta}}{\partial V_t} = [\Lambda_{22} + 2\Lambda_{15}V_t + 3\Lambda_{23}V_t^3 + 4\Lambda_{16}V_t^3 - T_{\theta}(\partial\Lambda_{19}/\partial V_t)]/\Lambda_{19} \quad 6.12$$

Figures 6.3 and 6.4 show plots of Equations 6.11 and 6.12 respectively, for $\gamma = \pi/4$, $r = 7.62$ cm. (3 inch), and $\rho = 2.54$ cm. (1 inch). The plots indicate that, in this case, the torque ratios increase almost linearly and at a very slow rate with the increase in the contouring speed. experimentation with different values of γ , as well as all the angular axis torque ratio plots in Chapter 5, indicate that the above mentioned trend is true for all values of γ .

6.4 Effect of changes in the parameters on the location of the maximum torques and torque ratios along the contour

In this study the location of the maximum torque and torque ratios along the contour is given in terms of the angle γ . The angle γ is useful as a parameter for solving the equation set, 5.4, 5.9, and 5.10 in Chapter 5 in order to obtain θ .

Substituting Equations 5.6, 5.7, and 5.8 in Equations 5.15 and 5.16 yields the torque expressions for both axes as:

$$T_R = M_C K_2 V_t^2 \frac{\sin \gamma}{\rho} + K_C K_2 V_t \cos(\gamma - \alpha_C) \quad 6.13$$

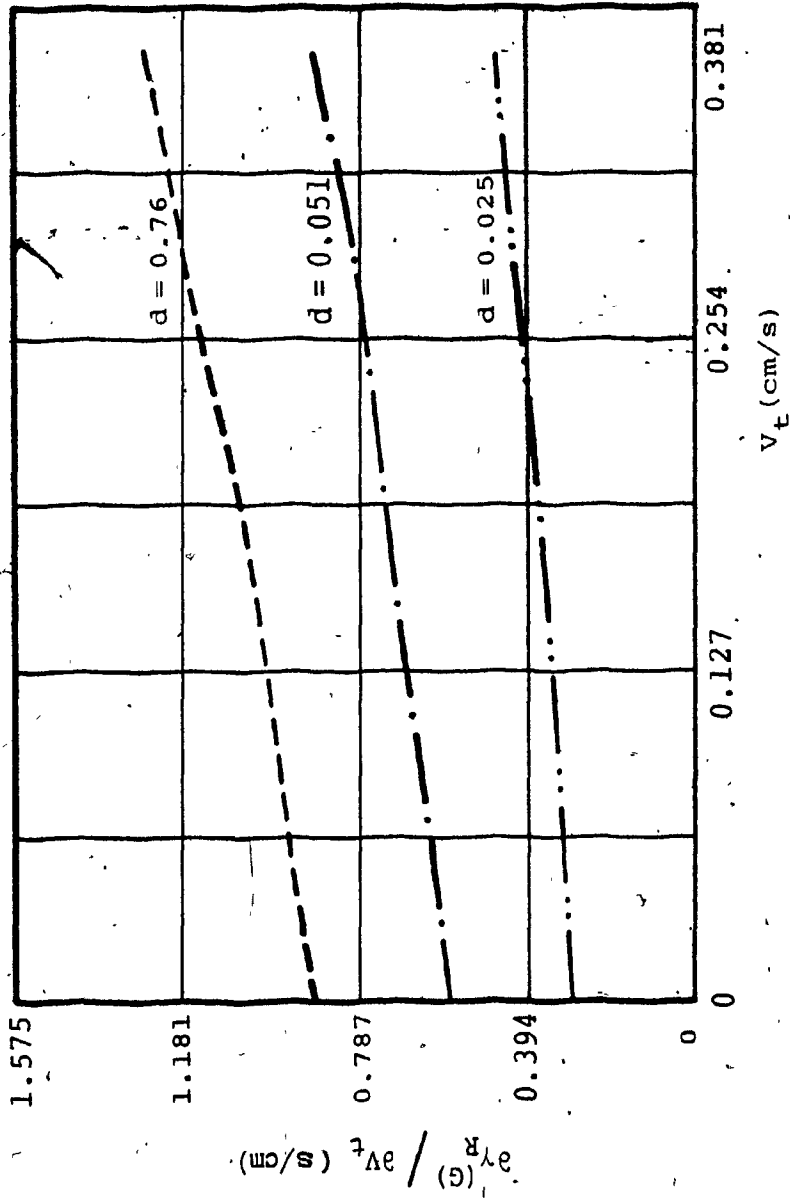


Figure 6.3: Sensitivity Parameter $\Gamma_R^{(G)}$ Versus V_t :

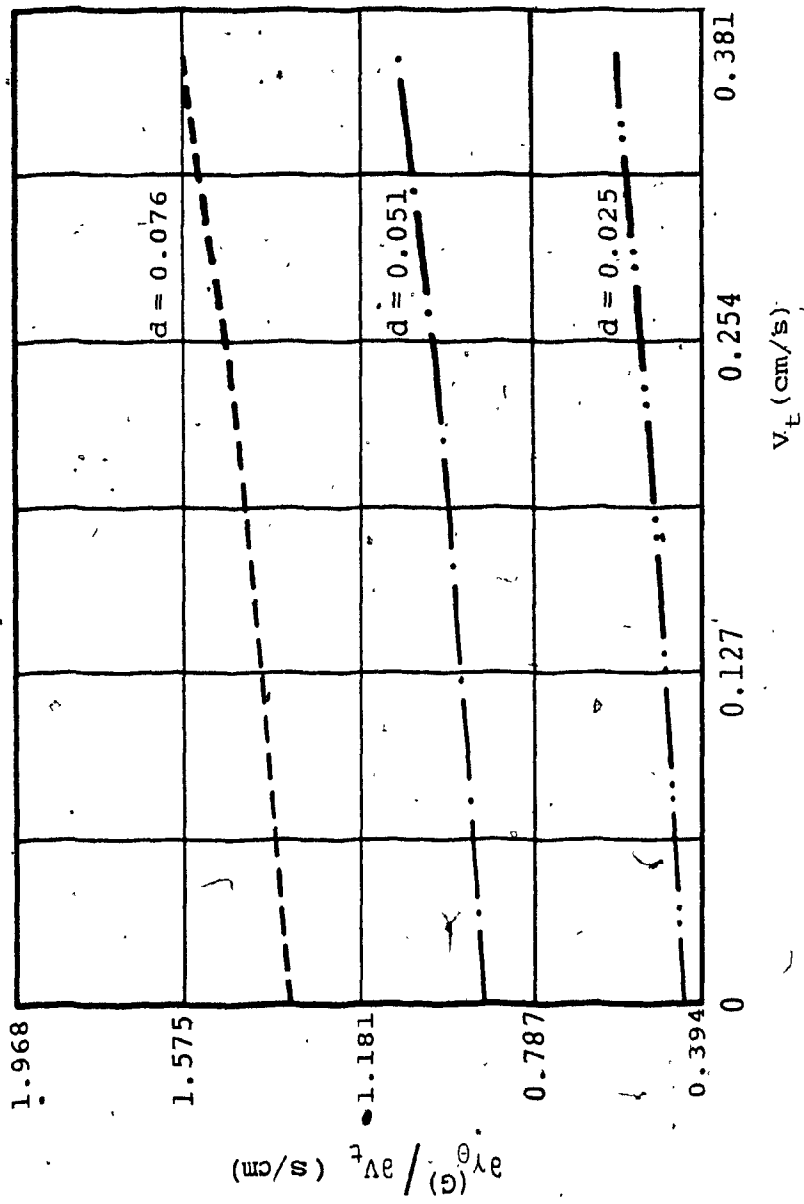


Figure 6.4: Sensitivity Parameter Γ_θ (G) versus V_t .

$$T_{\theta} = \frac{K_1 V_t^2}{\rho} \cos \gamma \left[M_C r + J_A / r \right] - \frac{2K_1 V_t^2}{r^2} \sin \gamma \cos \gamma + K_1 F_f L_A + K_C K_1 V_t \sin(\gamma - \alpha_C) \quad 6.14$$

6.4.1 Inertial load

In the case of inertial loads, the machining force components given by the last term in Equations 6.13 and 6.14 are identically zero. In order to find the location along the contour, of the maximum radial axis torque, Equation 6.13 is differentiated partially with respect to γ and the derivative is equated to zero. The result of this operation shows that the value of $\gamma_R^{(I)}$ for maximum torque in the radial axis is a constant and equal to $\pi/2$. That is to say, the maximum radial axis torque, and hence its maximum torque ratio, occur always at the same location θ on the contour irrespective of the changes in any of the parameters. This conclusion can be verified from the torque ratio plots of the radial axis for the case of inertial load shown in Sections 5.5.1 and 5.6.1.

For the angular axis, differentiating Equation 6.14 partially with respect to γ and equating the result to zero yields a quadratic equation in $\sin \gamma$. Solving for the value of $\gamma_{\theta}^{(I)}$ that gives the maximum angular axis torque, yields:

$$\gamma_{\theta}^{(I)} = \sin^{-1} \left\{ \frac{\left[\Lambda_{24} - (\Lambda_{24}^2 + 0.5\rho^2)^{1/2} \right]}{\rho} \right\} \quad \frac{3\pi}{2} < \gamma < 2\pi \quad 6.15$$

$$\Lambda_{24} = [M_C r^3 + J_A r] / 8$$

Equation 6.15 shows that $\gamma_R^{(I)}$ changes with the change in the inertial load M_C . The contouring speed, however, has no effect on the location of the maximum torque along the contour. In order to find the sensitivity of $\gamma_\theta^{(I)}$ to changes in M_C , Equation 6.15 can be differentiated with respect to M_C and gives:

$$\frac{\partial \gamma_\theta^{(I)}}{\partial M_C} = \left\{ [\Lambda_{24}^2 + 0.5\rho^2]^{\frac{1}{2}} - \Lambda_{24}^2 \right\} r^3 / \Lambda_{25}$$

$$\Lambda_{25} = 8 \left\{ [\Lambda_{24}^2 + 0.5\rho^2]^{\frac{1}{2}} [-2\Lambda_{24}^2 + 2\Lambda_{24}(\Lambda_{24}^2 + 0.5\rho^2)^{\frac{1}{2}} + 0.5\rho^2] \right\}^{\frac{1}{2}} \quad 6.16$$

The radius of curvature, ρ in Equation 6.16 can be expressed as [30]:

$$\frac{d\gamma}{d\theta} = \frac{ds/d\theta}{\rho} \quad 6.17$$

Equation 6.17 shows that in general the sensitivity of γ with respect to θ is inversely proportional to ρ and is directly proportional to $ds/d\theta$. The derivative $d\gamma/d\theta$ is a function of the inclination γ of the tangent on the radial vector, and has a value of zero for cases of $\gamma = \pi/2$ or $\gamma = 3\pi/2$, and a value of infinity for cases of $\gamma = 0$ or $\gamma = 2\pi$.

Solving Equations 6.16 and 6.17, for the angular axis,

the rate of change in angular location of the maximum torque on the contour, due to a change in the magnitude of the mass on the carriage is given by:

$$\frac{\partial \theta_{\theta}^{(I)}}{\partial M_c} = \frac{\left\{ \left[\Lambda_{24}^2 + 0.5 \rho^2 \right]^{\frac{1}{2}} - \Lambda_{24}^2 \right\} r^3 \rho}{\Lambda_{25} (ds/d\theta - \rho)} \quad 6.18$$

Figure 6.5 shows plots of $d\theta/dM_c$ versus ρ for different values of the mass on the carriage. The plots are obtained for typical values of the prototype parameters, given in Table 5.1, and for $r=20.32$ cm. (8 inch) and $ds/d\theta=2.54$ cm/rad (1 inch/rad). With reference to Figure 6.5, for all values of the mass on the carriage, $d\theta/dM_c$ approaches zero for either small or large values of ρ . This indicates that for small or large values of ρ , the maximum torque will occur at the same angular location on the contour irrespective of the magnitude of the mass on the carriage. This conclusion can be confirmed from the results shown in Figures 5.13.a and 5.13.b at $\theta=1.67$ radians when the mechanism is tracking the indentation in the Limacon of Pascal, and in Figures 5.15.a and 5.15.b at $\theta=1.5$ and $\theta=1.66$ when the mechanism is negotiating the tight curve at both ends of the asymptote of the Serpentine curve.

For values of ρ in a narrow region around $\rho=27$ cm, the value of $d\theta_{\theta}^{(I)}/dM_c$ deviates from zero depending upon the magnitude of M_c . This region occurs when the term $ds/d\theta - \rho$ in the denominator has a magnitude in the neighborhood of

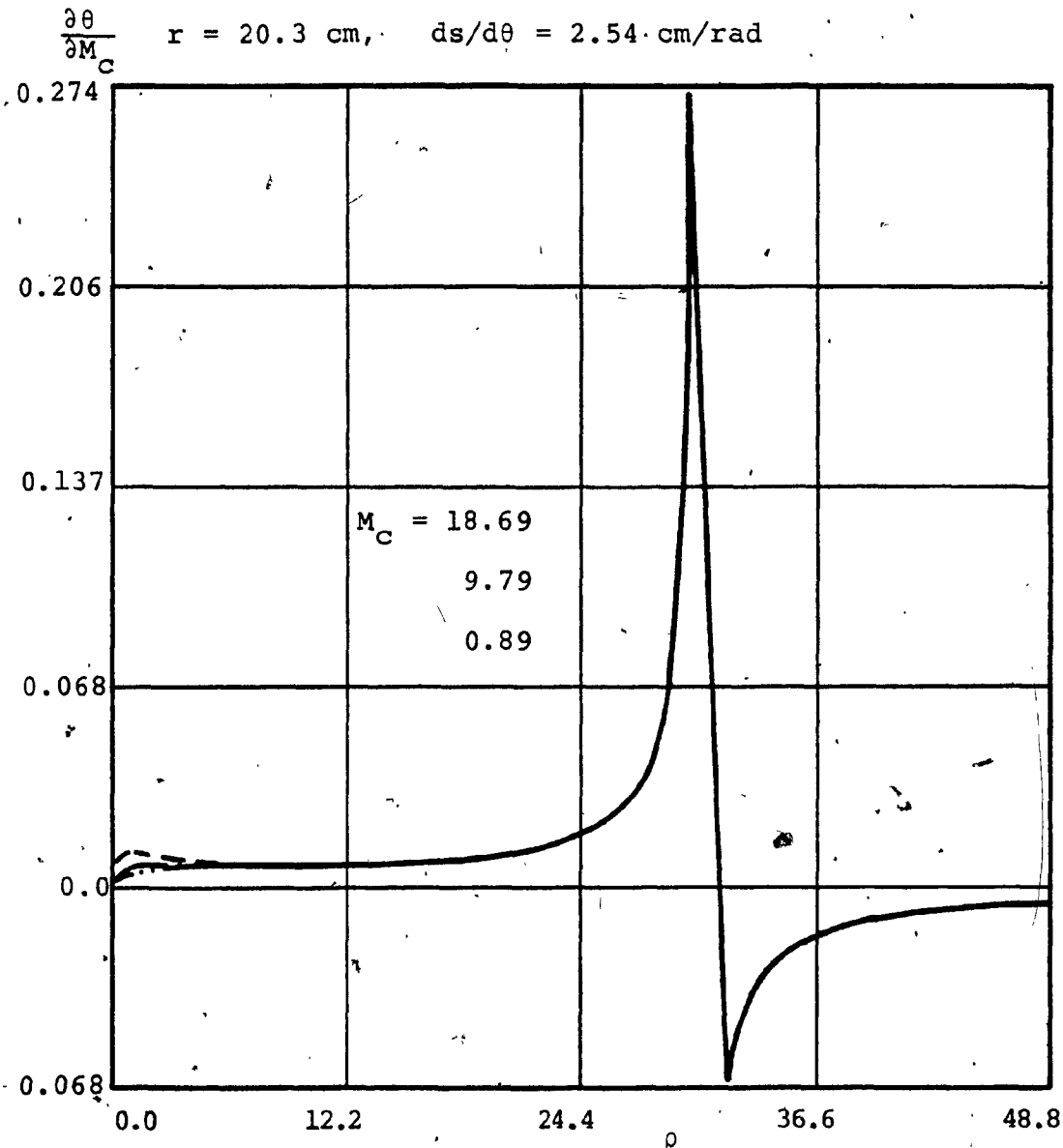


Figure 6.5: $d\theta/dM_C$ Versus ρ for the Maximum Angular Axis Torque for an Inertial Load.

zero. However with reference to Equation 6.17, this condition occurs when changes in γ are negligible due to changes in θ , and results in a wide region in which the magnitude of the torque changes marginally. The change in magnitude of $d\theta_{\theta}^{(I)} / dM_c$ indicates that the maximum torque shifts its location along the contour within this region of ρ values, as the magnitude of the mass on the carriage changes. This shift can be seen in the case of the Witch of Agnesi contour (Figure 5.11 a and 5.11.b) because of its radius of curvature falls within this region. The magnitude of the change, however, is small.

6.4.2 Grinding application

For the case of a grinding application, the second term in Equation 6.14 is insignificant in comparison with the torque due to the dissipative force and can be ignored. The location on the contour at which the maximum torque for the two axes occurs, is found by differentiating Equations 6.13 and 6.14 partially with respect to γ and equating the result to zero. Thus:

$$\gamma_R^{(G)} = \tan^{-1} \left[\frac{M_c V_t}{\rho K_c \cos \alpha_c} + \tan \alpha_c \right] \quad 6.19$$

$$\gamma_{\theta}^{(G)} = \cot^{-1} \left[\frac{V_t \cdot [M_c r + J_A / r]}{\rho K_c \cos \alpha_c} + \tan \alpha_c \right] \quad 6.20$$

To find the sensitivity of $\gamma^{(G)}$ and $\gamma_{\theta}^{(G)}$ to changes in

the contouring speed and the machining factor K_c . Equations 6.19 and 6.20 are differentiated partially with respect to V_t and K_c . The results of this operation gives:

For V_t :

$$\frac{\partial \gamma_R^{(G)}}{\partial V_t} = \frac{M_c \rho K_c \cos \alpha_c}{(M_c V_t)^2 + 2\rho K_c M_c V_t \sin \alpha_c + (\rho K_c)^2} \quad 6.21$$

$$\frac{\partial \gamma_\theta^{(G)}}{\partial V_t} = -\rho K_c \left[M_c r + J_A / r \right] \cos \alpha_c / \Lambda_{26}$$

$$\Lambda_{26} = \left[V_t (M_c r + J_A / r) \right]^2 - 2\rho K_c V_t (M_c r + J_A / r) \sin \alpha_c + (\rho K_c)^2 \quad 6.22$$

For K_c :

$$\frac{\partial \gamma_R^{(G)}}{\partial K_c} = - \frac{M_c V_t \rho \cos \alpha_c}{(M_c V_t)^2 + 2\rho K_c M_c V_t \sin \alpha_c + (\rho K_c)^2} \quad 6.23$$

$$\frac{\partial \gamma_\theta^{(G)}}{\partial K_c} = V_t \rho \left[M_c r + J_A / r \right] \cos \alpha_c / \Lambda_{26} \quad 6.24$$

Combining Equation 6.17 with each of Equations 6.21 to 6.24, gives a set of equations that relate the rate of change of the maximum torque location on the contour to the change in V_t and K_c . These are:

For V_t :

$$\frac{\partial \theta_R^{(G)}}{\partial V_t} = \frac{M_C \rho^2 K_C \cos \alpha_C}{[(M_C V_t)^2 + 2\rho K_C M_C V_t \sin \alpha_C + (\rho K_C)^2][ds/d\theta - \rho]} \quad 6.25$$

$$\frac{\partial \theta_\theta^{(G)}}{\partial V_t} = - \frac{\rho^2 K_C [M_C r + J_A/r]}{\Lambda_{26} [ds/d\theta - \rho]} \quad 6.26$$

For K_C :

$$\frac{\partial \theta_R^{(G)}}{\partial K_C} = - \frac{M_C V_t \rho^2 \cos \alpha_C}{[(M_C V_t)^2 + 2\rho K_C M_C V_t \sin \alpha_C + (\rho K_C)^2][ds/d\theta - \rho]} \quad 6.27$$

$$\frac{\partial \theta_\theta^{(G)}}{\partial K_C} = - \frac{V_t \rho^2 [M_C r + J_A/r]}{\Lambda_{26} [ds/d\theta - \rho]} \quad 6.28$$

In Equations 6.25 and 6.26 the denominator is a quadratic polynomial in V_t . The constant term $(\rho K_C)^2$ in the polynomial contains the grinding force factor and is typically much larger in comparison to all the other terms in general grinding applications (an approximate ratio of one million in the grinding case under consideration). Consequently changes in the contouring speed do not affect the location where the maximum torque occurs on the contour. This conclusion is confirmed from all the torque ratio plots for the grinding application, shown in Chapter 5. The effect of the term $ds/d\theta - \rho$ in this case is similar to that in the case of the inertial load discussed above, with the exception that the region in which $d\theta_R^{(G)}/dV_t$ and $d\theta_\theta^{(G)}/dV_t$ change is very narrow.

Equation 6.27 and 6.28 shows that the change in location of the maximum torque along the contour is inversely proportional to the square of the machining force factor K_C for both the radial and angular axes. Since typical values of the force factor K_C in grinding applications are large, it can be seen from Equations 6.19 and 6.20 that only marginal change in the location of the maximum torque along the contour will occur.

6.5 Highlights of the analytical parametric study

The above study shows the following:

6.5.1 Inertial load

- The radial and angular axes torque ratios vary linearly with the change in magnitude of the mass on the carriage.
- The radial axis torque ratio vary as a quartic polynomial in V_t and always increases as V_t increases.
- The angular axis torque ratio vary as a quartic polynomial in V_t . It may increase or decrease depending upon the magnitude and direction of motion of the carriage.
- The location on the contour where the maximum radial axis torque, and hence the radial axis torque ratio, occurs does not change with the change in the value of the mass on the carriage, or the contouring speed.
- For the angular axis, the location on the contour where

the maximum torque, and hence its torque ratio, varies with the change in the magnitude of the mass on the carriage. The contouring speed V_t has no effect on this location.

6.5.2 Grinding application

- The radial and angular torque ratios vary linearly with the variations in the machining force factor K_C .
- The radial and angular torque ratios vary as a quartic polynomial in the contouring speed. The variation, however, approaches a linear relationship.
- The location on the contour where the maximum torque, and hence torque ratio, does not change with either the change of the contouring speed or the mass on the carriage.

6.6 Optimum loading of the polar NC machine

In the previous chapter it was shown that a change in the relative location of the contour pole from the machine pole results in a change in the shape and magnitude of the torque ratio plots. This feature is used here to find a location for the contour pole that would give a minimum value for the total torque on both axes for a given machining operation. The minimization process in effect increases the load carrying capacity of the NC machine. After carrying out the minimization process, the load imposed on the machine can be increased further up to the limit when either

of the torque ratios have a value of unity.

6.6.1 Total torque required on both axes in contouring operation

The torque required by the two axes during a machining operation is given by:

$$T_T = T_R + T_G \quad 6.29$$

where T_T is the total torque of the two axes. This total torque varies as the tool travels along the contour. It is important to know its exact characteristics, and change in magnitude for parameter variations. Figures 6.6 to 6.19 show plots of the sum of torques T_T versus angular location on the contour.

For an inertial load

The figures are organized as follows:

Figures 6.6 to 6.9 are for the case of the contour poles located as shown in Figures 5.4 to 5.7.

Figures 6.10 to 6.12 are for the case of the contour pole location coinciding with that of minimum area error given in Chapter 5. The plots are given for one contouring speed of 1.52 cm/s (3 ft/min).

From the figures, it can be seen that for all the test contours and for the two cases of contour pole locations, the maximum total torque occur at exactly the same location on the contour irrespective of the contouring speed or the

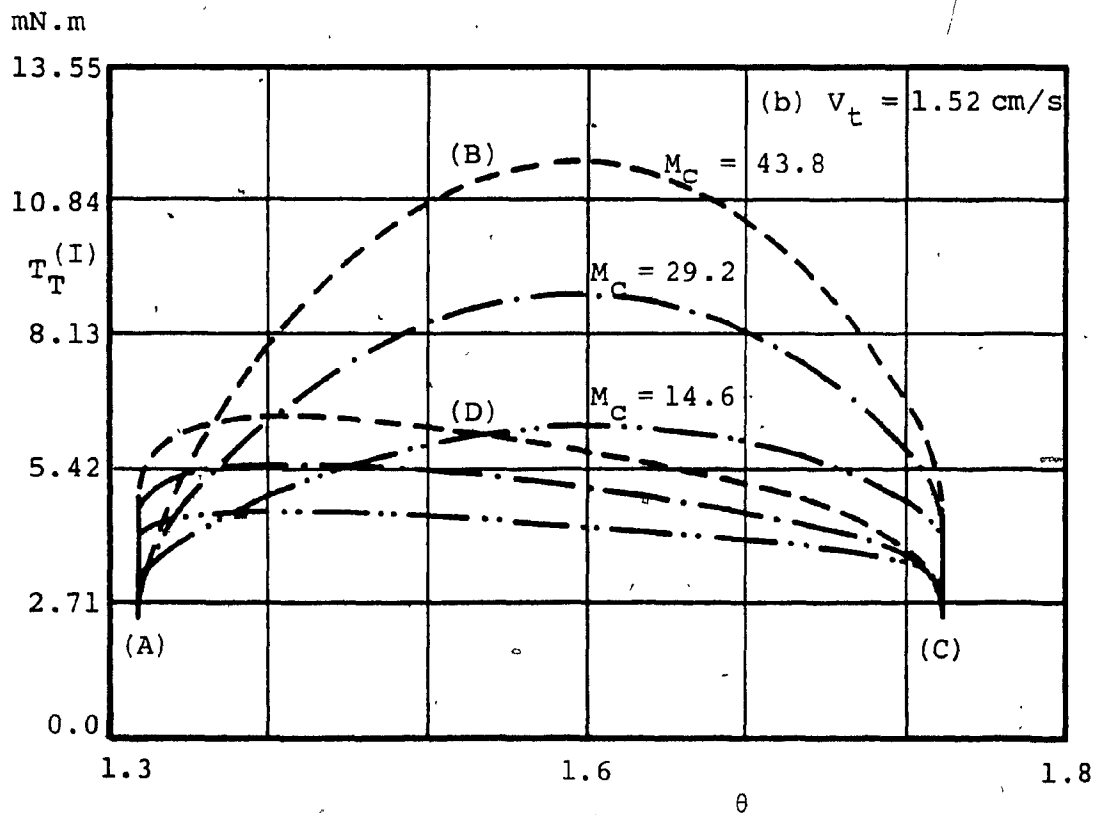
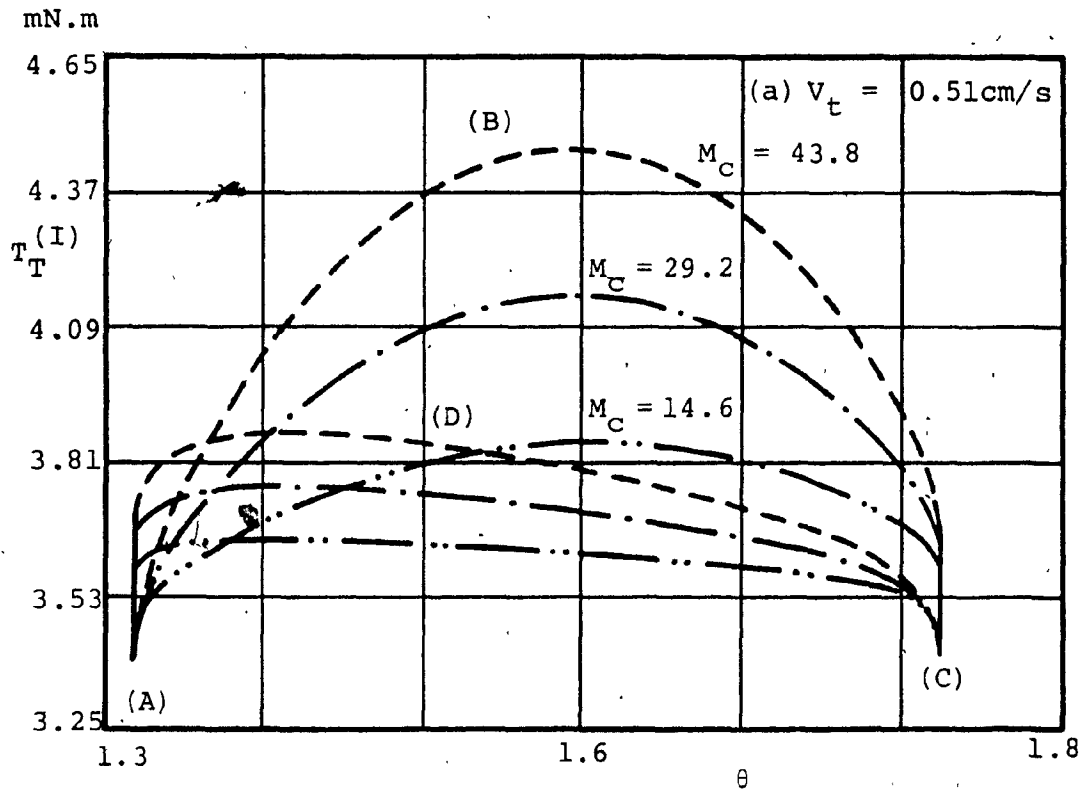


Figure 6.6: Sum of Torques Versus Angular Location for the Circular Contour (Inertial Load). M_C is in kgs.

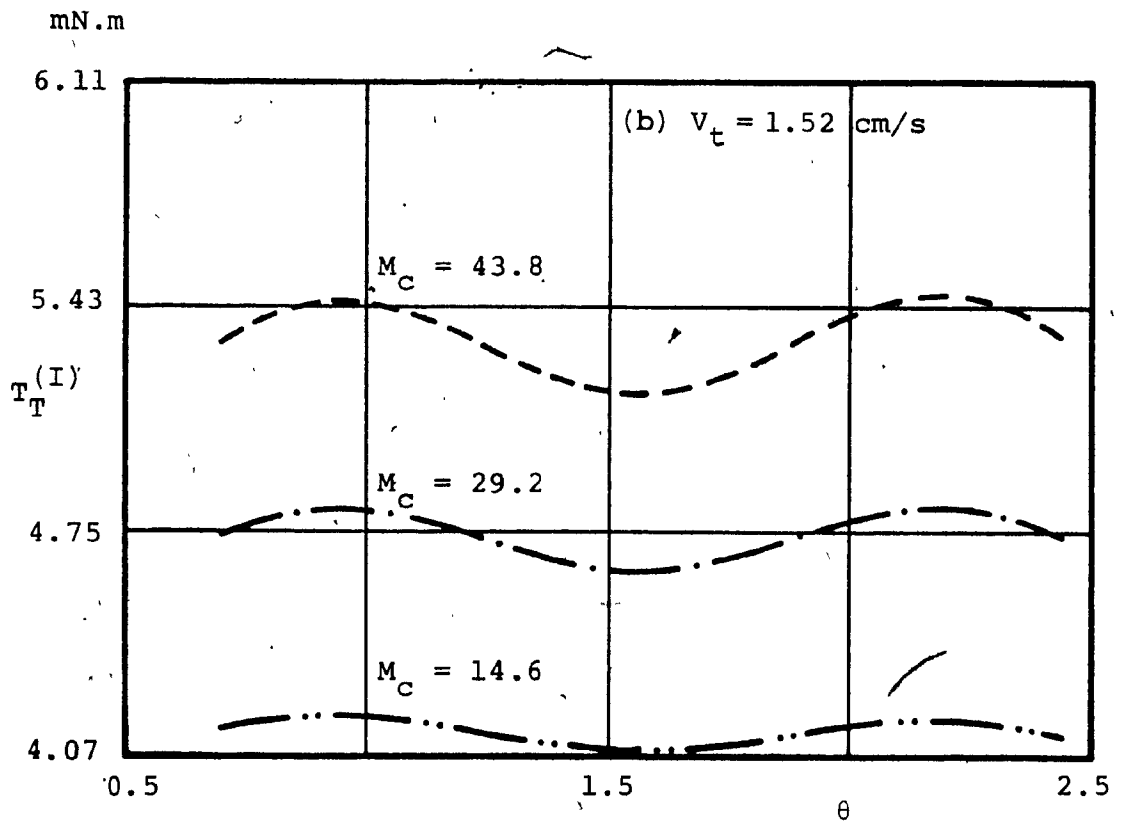
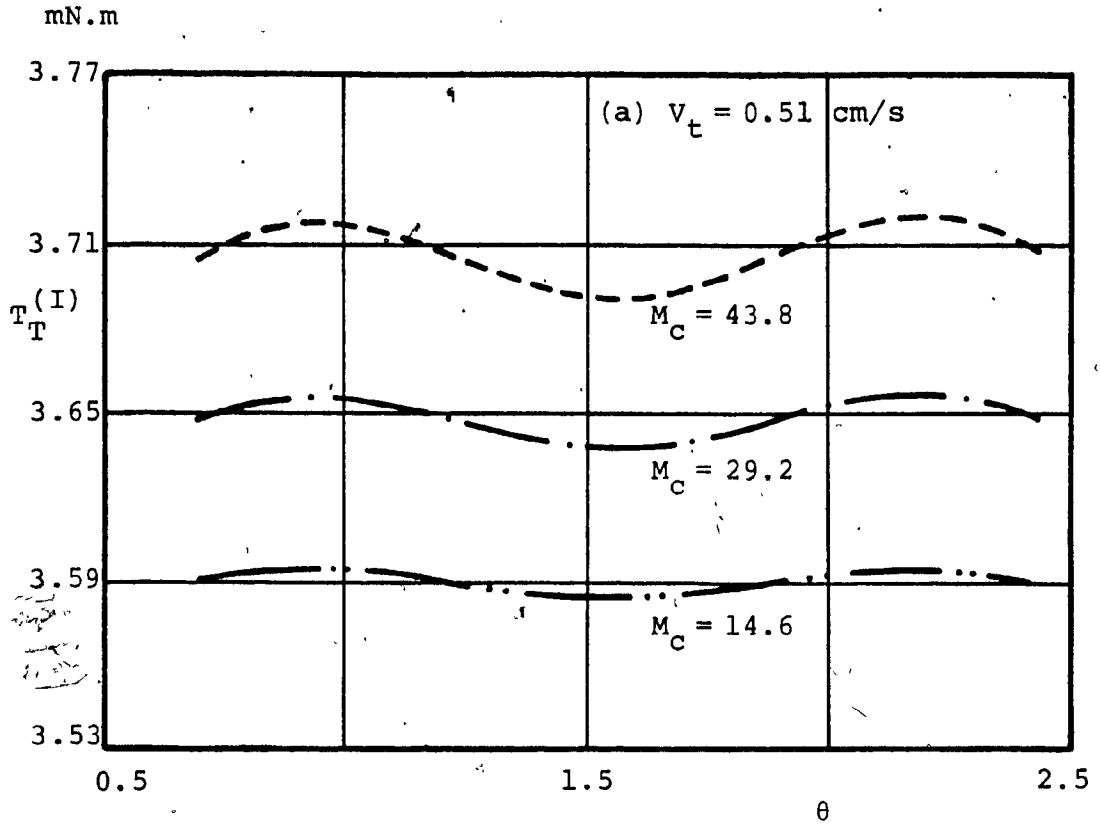


Figure 6.7: Sum of Torque Versus Angular Location for the Witch of Agnesi Contour (Inertial Load). M_C is in kgs.

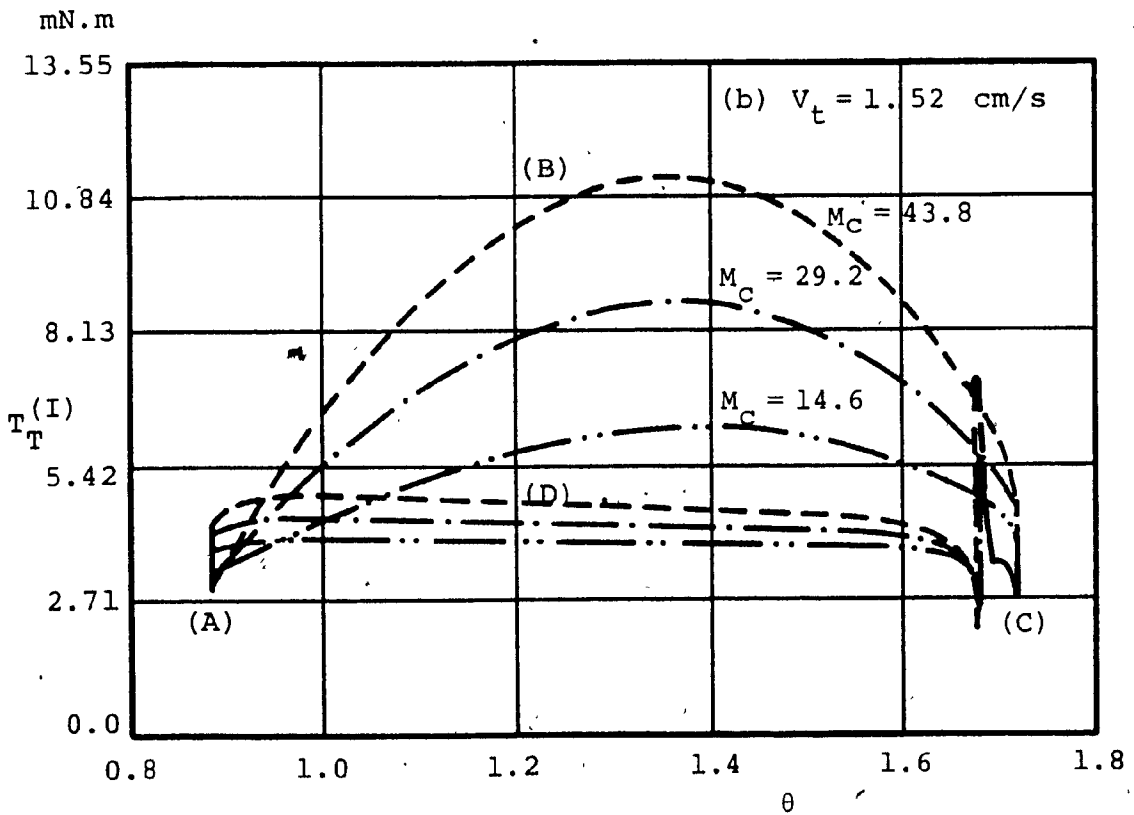
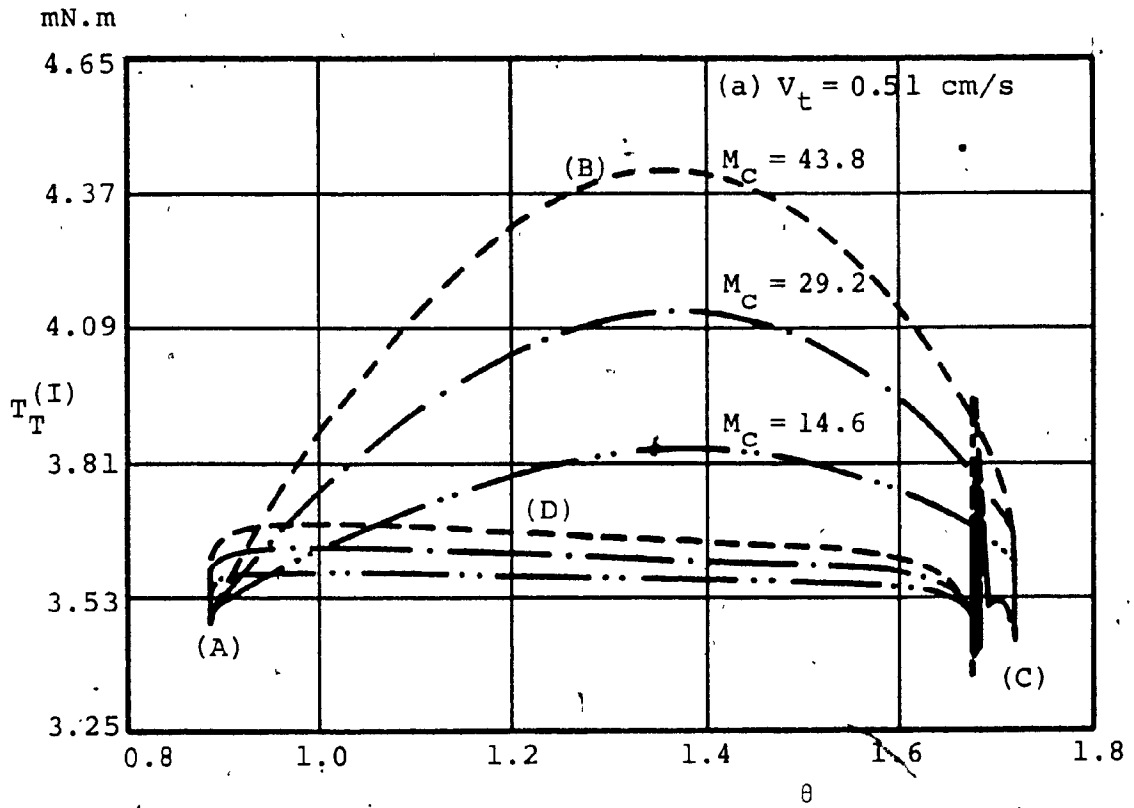


Figure 6.8: Sum of Torque Versus Angular Location for the Limacon of Pascal Contour (Inertial Load). M_C is in kgs.

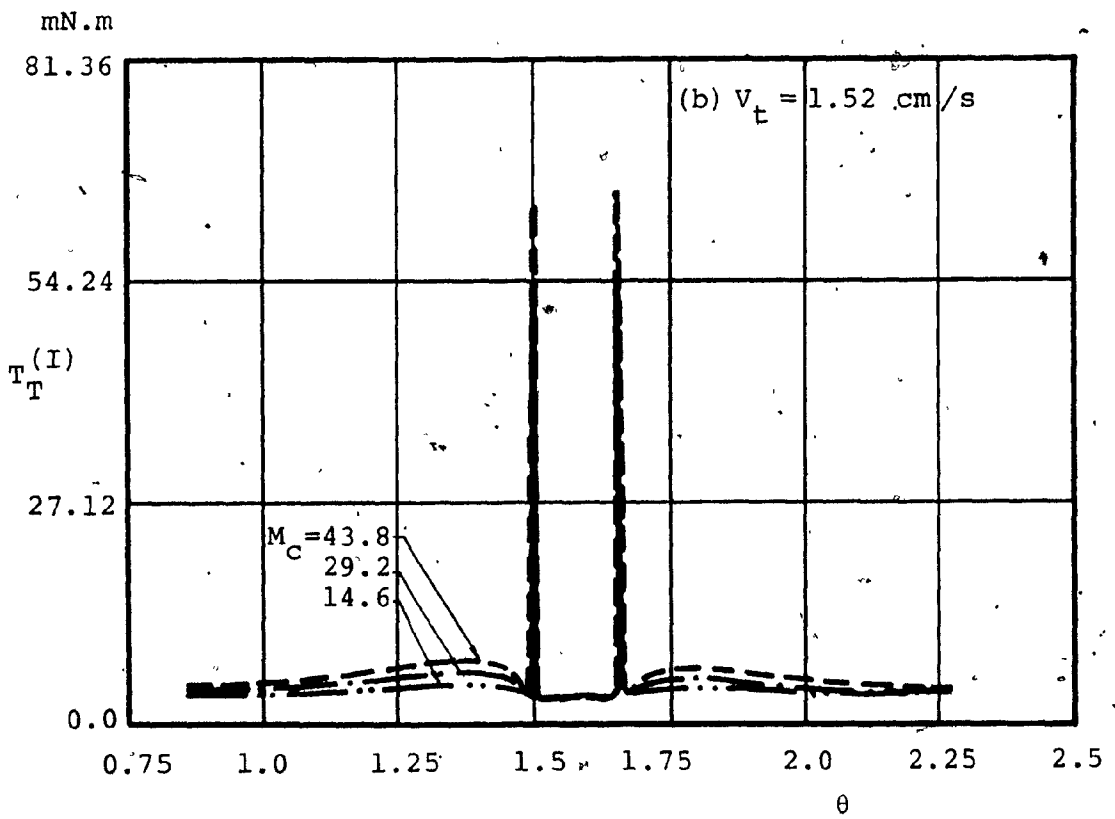
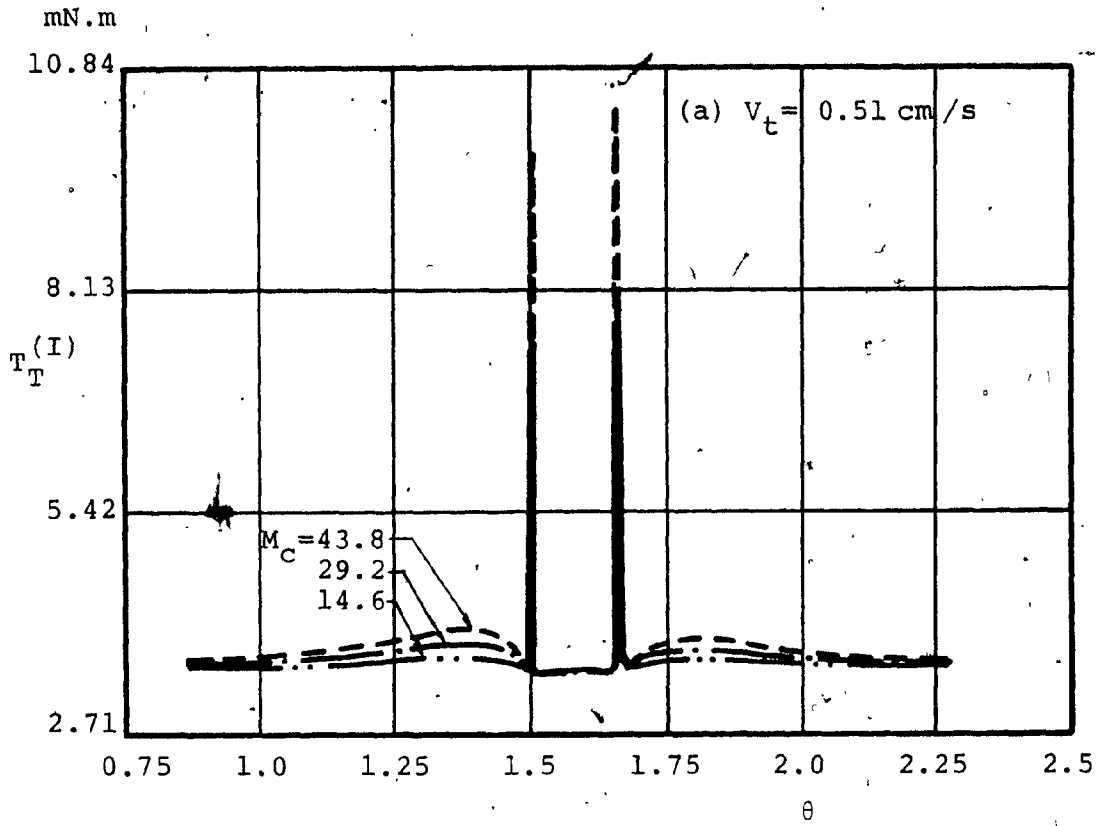


Figure 6.9: Sum of Torque Versus Angular Location for the Serpentine Contour (Inertial Load). M_C is in kgs.

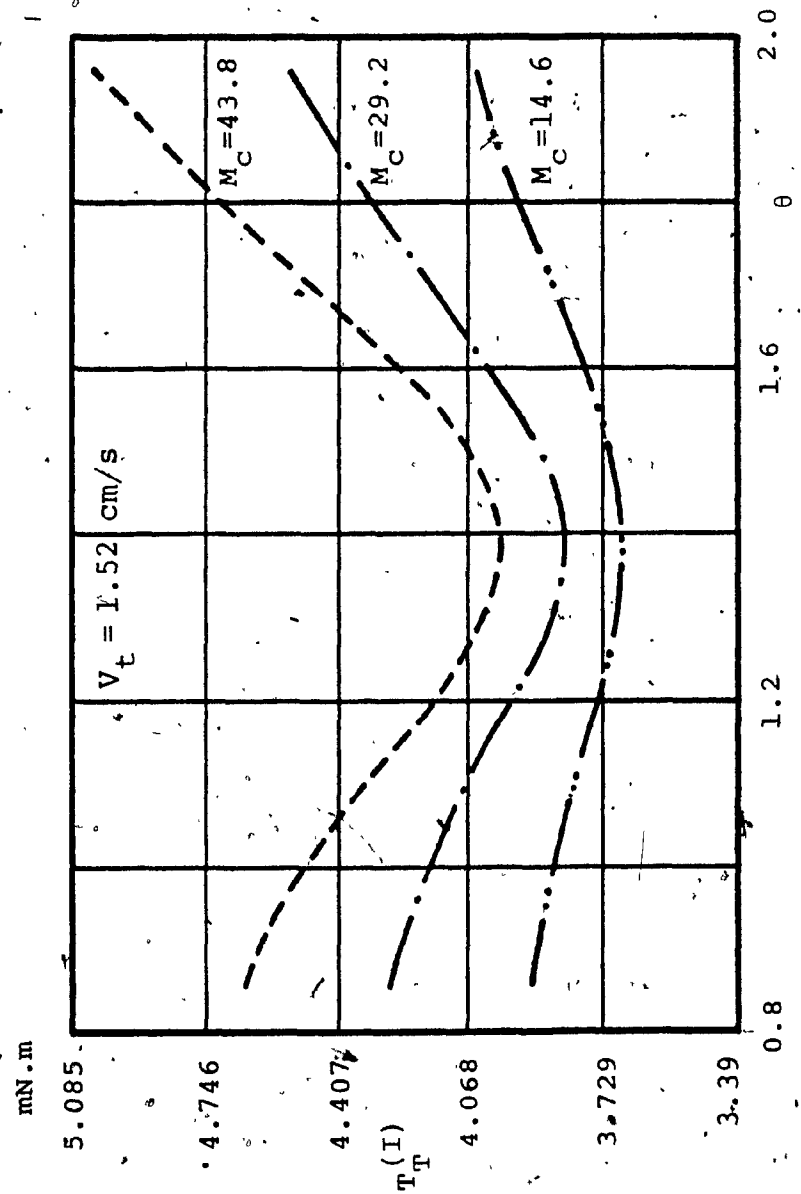


Figure 6.10: Sum of Torque Versus Angular Location for the Witch of Agnesi Contour, Pole at Location of Minimum Area Error (Inertial Load). M_C is in kgs.

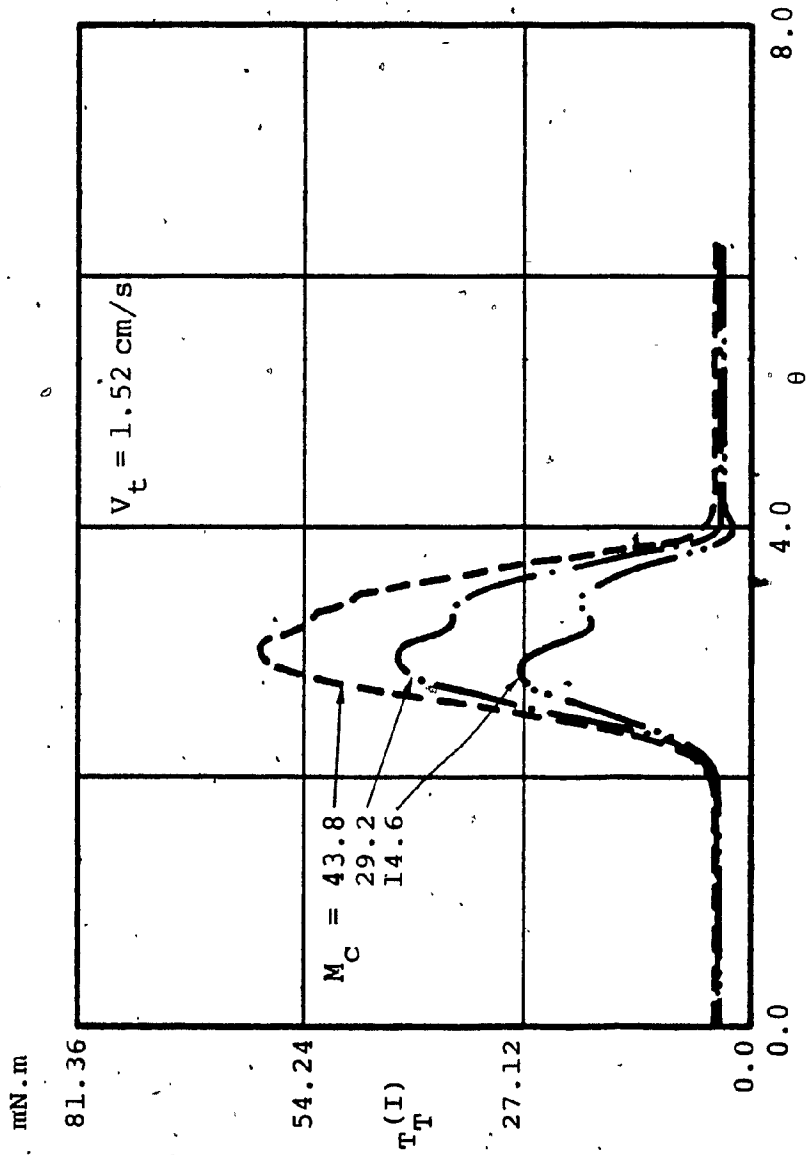


Figure 6.11: Sum of Torque Versus Angular Location for the Limacon of Pascal-Contour, Pole at the Location of Minimum Area Error (Inertial Load). M_C is in kgs.

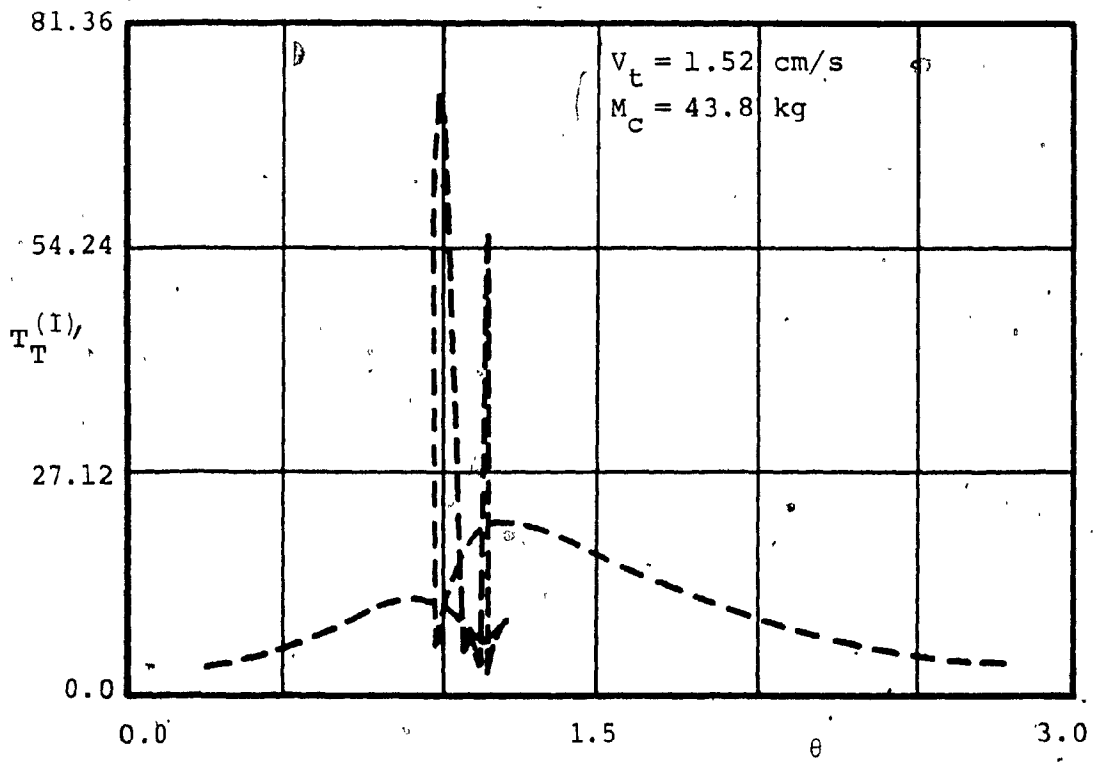
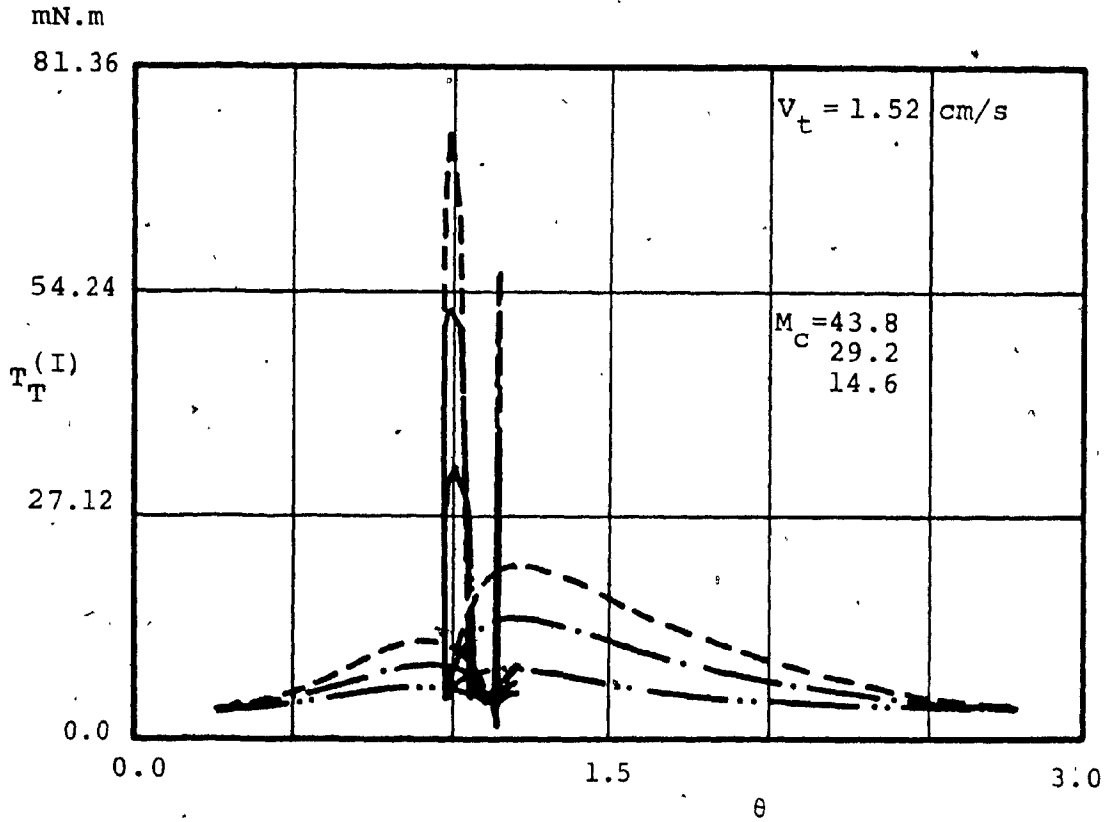


Figure 6.12: Sum of Torque Versus Angular Location for the Serpentine-Contour, Pole at the Location for Minimum Area Error (Inertial Load). M_c is in kgs.

mass on the carriage. This group of figures also show that the magnitude of the total torque changes with the change in the contour pole location. For example, the total torque for the Limacon of Pascal changes from $T_T = 1.15$ N.cm (0.85 lbf.ft) to $T_T = 6.1$ N.cm (3.24 oz.in) for a change of contour pole location from that shown in Figure 5.6 to that of minimum area error respectively.

For a grinding application

The figures are organized as follows:

Figures 6.13 to 6.16 are for cases of the contour pole location as shown in Figures 5.4 to 5.7.

Figures 6.17 to 6.19 are for the cases of the contour pole location

The plots in Figures 6.13 to 6.19 show that for all the test contours, the total torque increases linearly with the increase in the contouring speed. Test results (not presented) show that T_T also varies linearly with variation in the machining force factor K_C . Furthermore, the location of the maximum total torque along the contour does not change with the change in contouring speed or with K_C .

The plots also show that the change in contour pole location results in a change of the magnitude of the maximum total torque.

6.6.2 Formulation of the optimization problem

The objective here is to find the location of the

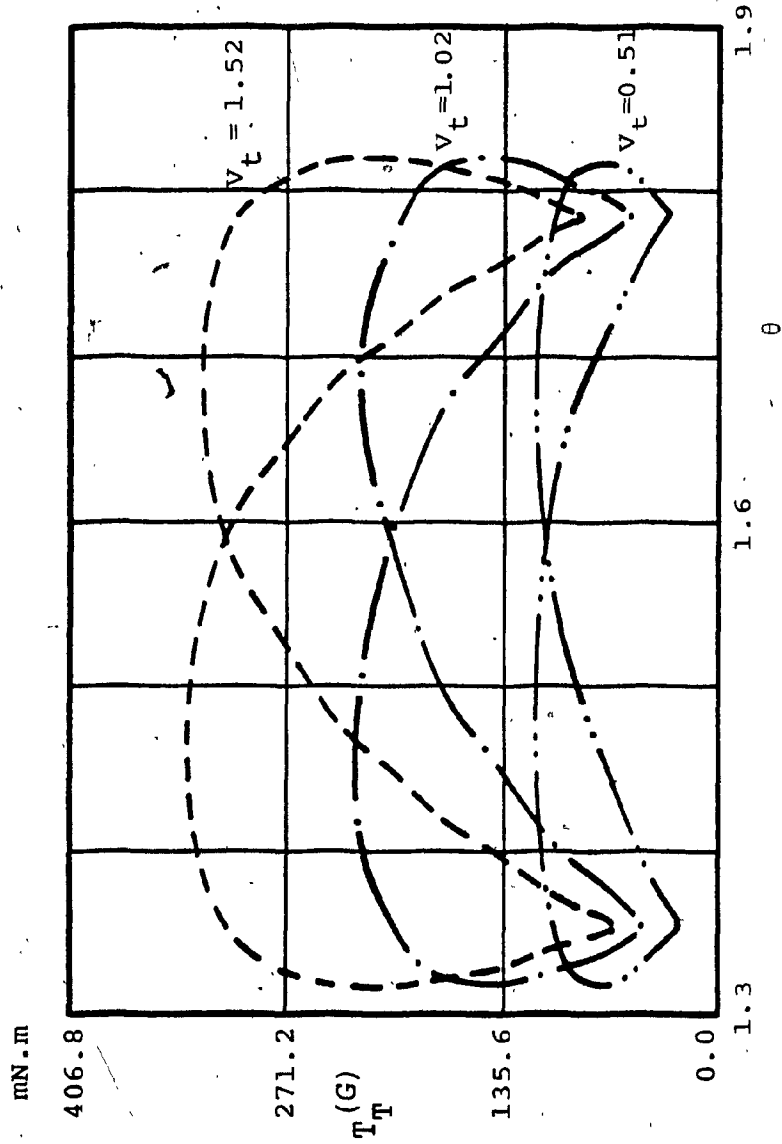


Figure 6.13: Sum of Torque Versus Angular Location for the Circular Contour (Grinding Application). V_t is in cm/s.

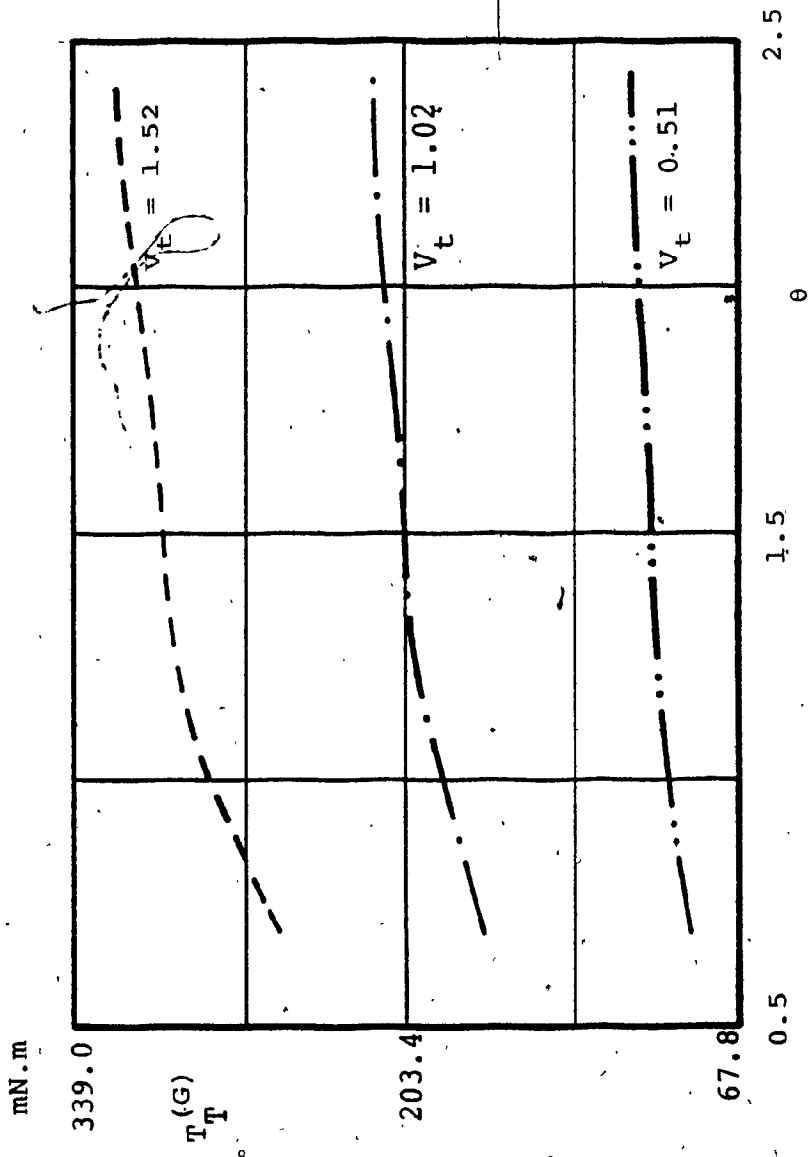


Figure 6.14: Sum of Torque Versus Angular Location for the Witch of Agnesi Contour (Grinding Application). V_t is in cm/s.

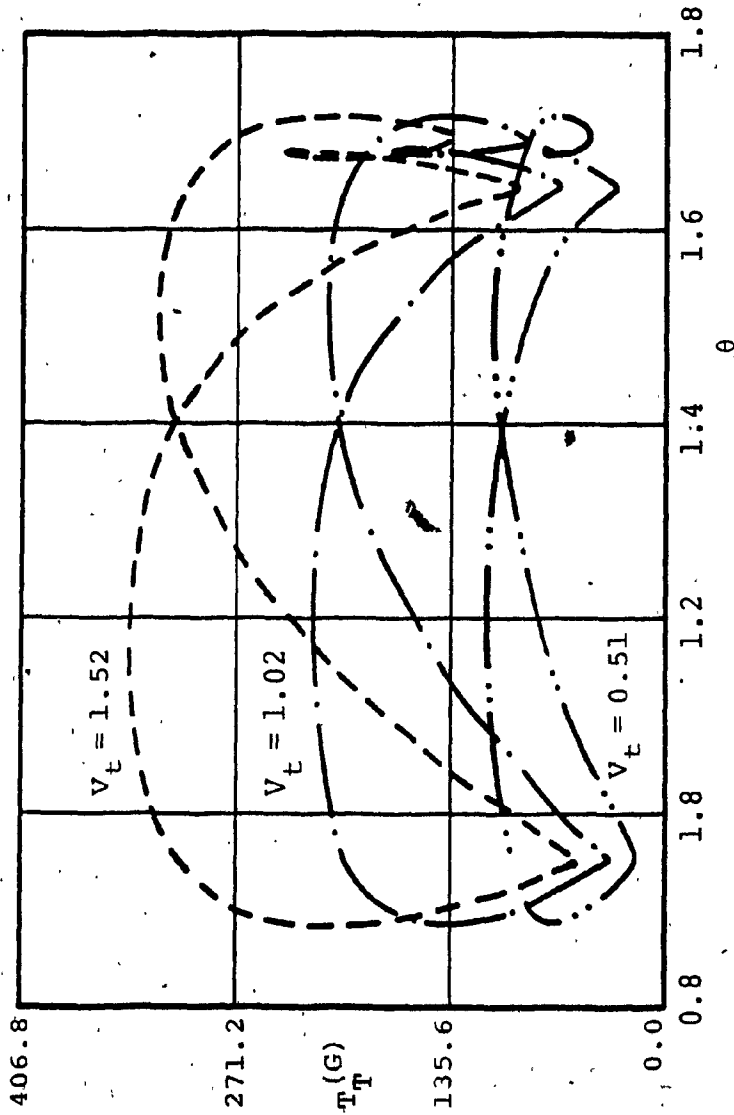


Figure 6.15: Sum of Torque Versus Angular Location for the Limacon of Pascal Contour (Grinding Application). V_t is in cm/s.

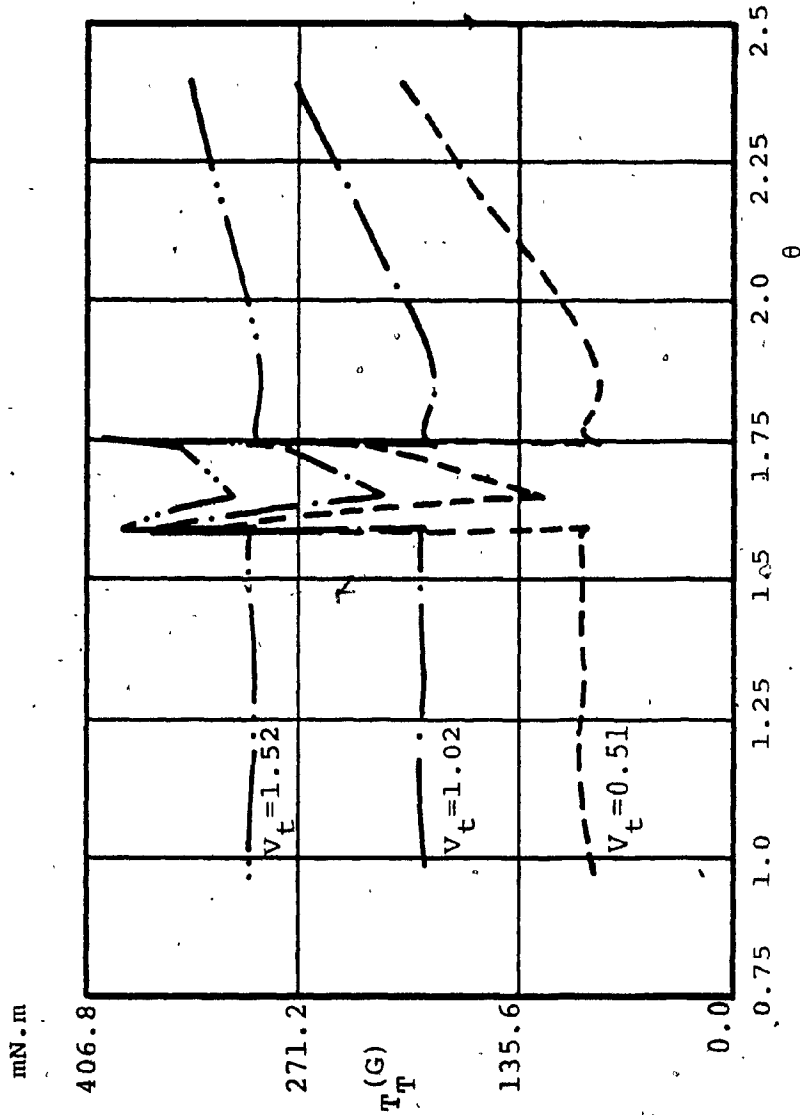


Figure 6.16: Sum of Torque Versus Angular Location for the Serpentine Contour (Grinding Application). V_t is in cm/s.

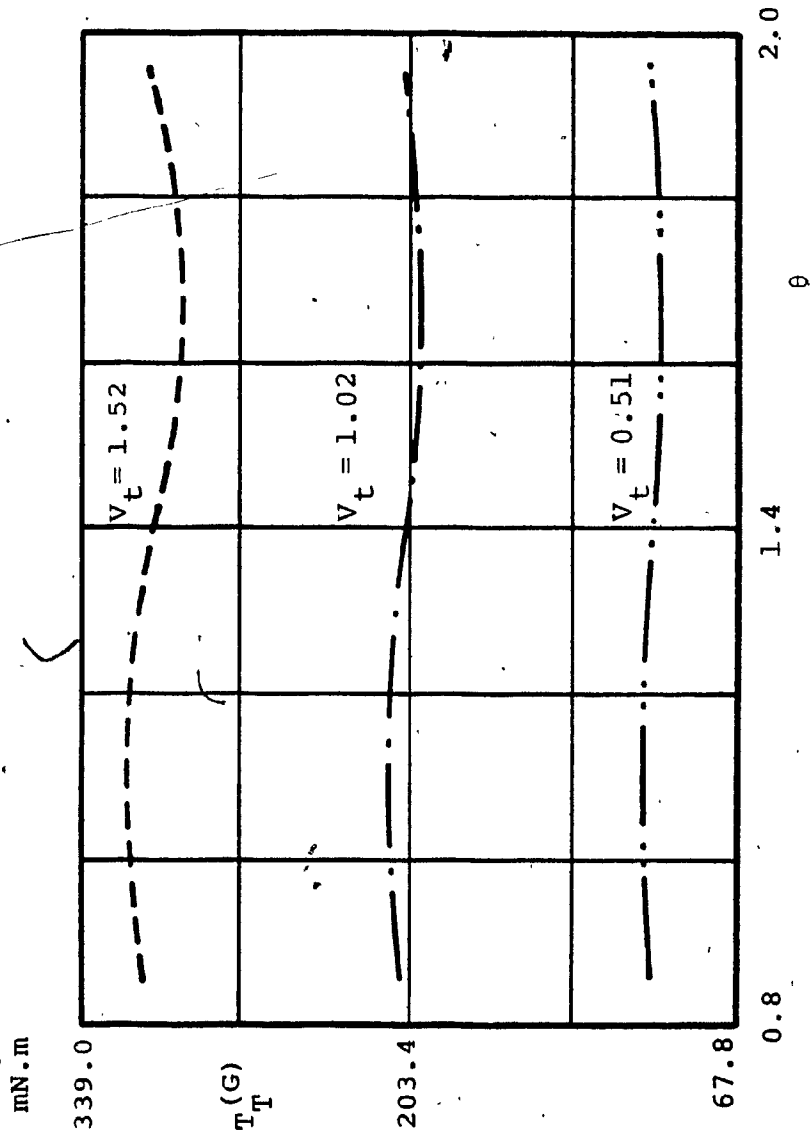


Figure 6.17: Sum of Torque Versus Angular Location for the Witch of Agnesi Contour, Pole at Location of Minimum Area Error (Grinding Application). V_t is in cm/s.

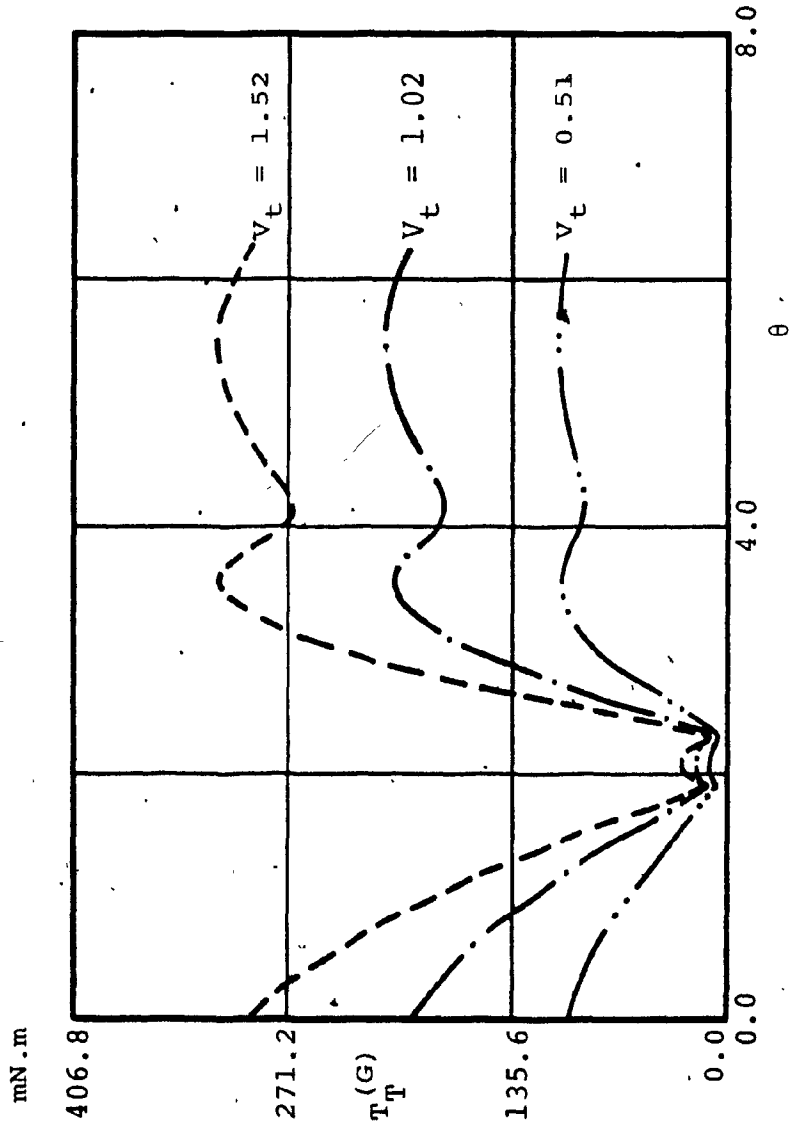


Figure 6.18: Sum of Torque Versus Angular Location for the Limacon of Pascal Contour, Pole at the Location of Minimum Area Error (Grinding Application). V_t is in cm/s.

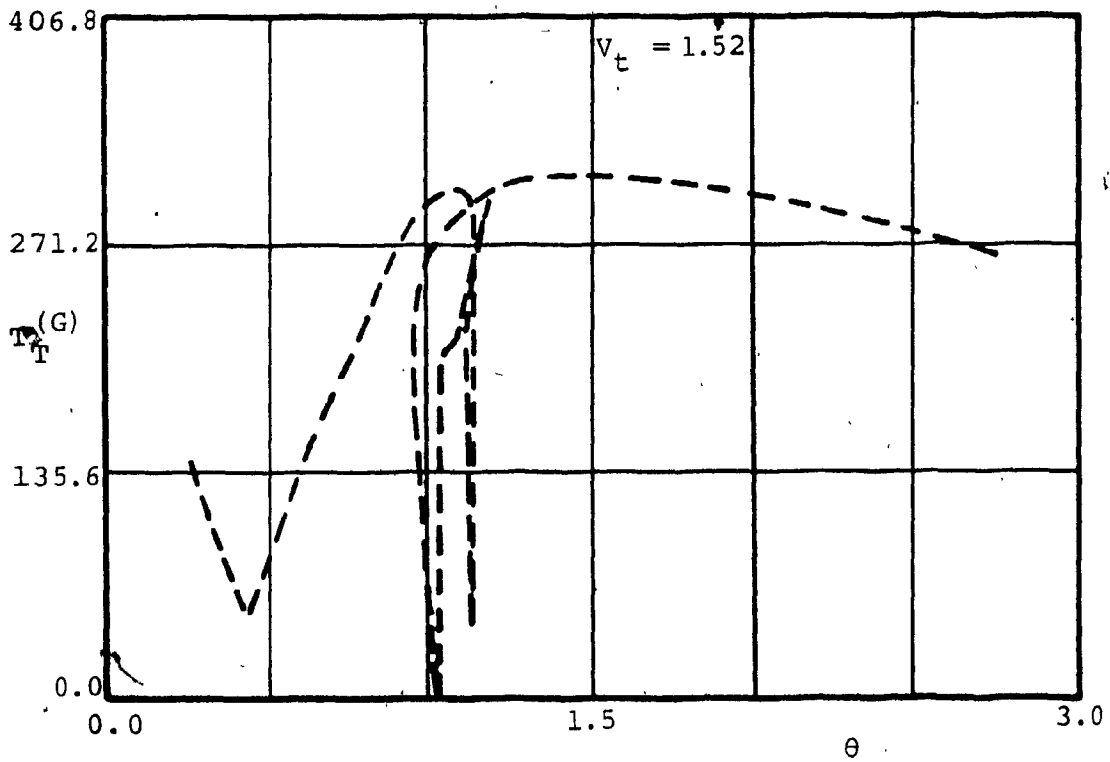
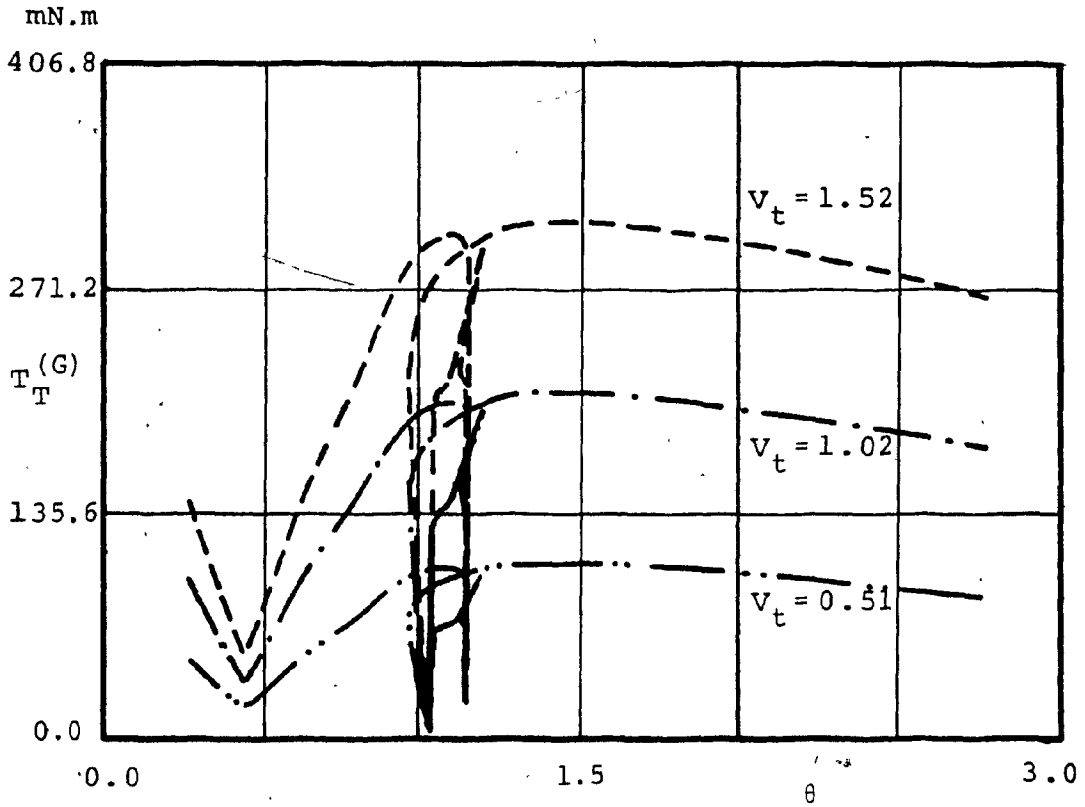


Figure 6.19: Sum of Torque Versus Angular Location for the Serpentine Contour, Pole at the Location for Minimum Area Error (Grinding Application). v_t is in cm/s.

contour pole (C, β) for a given contour, that will give a minimum value for the maximum total torque. Normalizing the value of axes torques by the available torque from the respective stepping motors, the objective function for minimization can be formulated as:

$$T_T = T_R + T_\theta \quad \text{maximum along the contour} \quad 6.30$$

In order that both stepping motors carry equal shares of the load, the objective function in Equation 6.30 can be modified and the optimization problem can be stated as follows:

Minimize;

$$\frac{T_T}{|1 - |(T_R - T_\theta)||} \quad 6.31$$

Subject to;

a) Work area constraint of the NC machine and is given by:

$$7.62 \text{ cm. (3 inch)} < r < 33.02 \text{ cm. (13 inch)}$$

$$0 < \theta < 2.8 \text{ (in radians)}$$

b) A constraint that would not allow the placement of the machine pole inside a closed contour due to geometrical limits imposed by the construction of the NC machine.

The Hooke and Jeeves optimization technique used earlier, and described in Chapter 4 is also used here. Upon convergence of the optimization, the program returns the maximum values of torque ratios found along the contour.

During the optimization process no constraint is

imposed on the magnitude of the radial and angular torque ratios and their values can exceed unity. Eliminating this constraint was found to speed up the optimization process dramatically. The torque ratio values returned by the optimization routine are subsequently scaled to unity by modifying the load on the mechanism or the contouring speed. Equations 6.1 to 6.12 are used to carry out the scaling. Changing the load on the NC machine or the contouring speed was shown, earlier in this chapter, to have no effect on the location where the maximum torques occur. The scaling procedure in effect increases the load carrying capacity of the NC machine.

6.6.3 Results of loading optimization for four test contours

The algorithm is tested on the four test curves used earlier namely, a) a circle, b) a Witch of Agnesi, c) a Limacon of Pascal, and d) a Serpentine curve.

Results for two inertial loads of 43.77 kg (3 slug) and 145.9 kg (10 slug) are given in Table 6.1. The results show that the magnitude of the inertial load has no bearing on the pole location for optimal loading, and an extremely large mass can be accommodated before the mechanism is overloaded. However, the contouring speed can be increased only up to 1.74 cm/s (3.44 ft/min). This is due to the fact that the mechanism is geared towards dissipative type applications and the axes drives reach their maximum stepping

Table 6.1: Results of Optimization for Loading Conditions (Inertial Load)

For contouring speed of 1.53 cm/s (3ft/min), and		Circle	Witch of Agnesi	Limacon of Pascal	Serpentine	
Initial mass on kg carriage (slug)	43.77 (3.0)	145.9 (10.0)	43.77 (3.0)	145.9 (10.0)	43.77 (3.0)	145.9 (10.0)
Initial machine r cm (in)	53.8 (21.213)	0.0 (0.0)	0.0 (0.0)	53.8 (21.213)	17.8 (7.0)	-
pole location: θ rad	3.927	0.0	0.0	3.927	4.712	-
Results from the optimization program,						
Optimum machine r cm (in)	0.0 (0.0)	299.2 (117.8)	4.06 (1.6)	21.6 (8.5)	-	-
pole location: θ rad	0.0	3.528	0.588	4.242	-	-
Objective function	0.0136	0.0126	0.0127	0.0136	0.0146	0.0145
Maximum torque T_R	0.0132	0.0126	0.0126	0.0133	0.0139	0.0144
ratios: T_Θ	4.2×10^{-4}	4.9×10^{-5}	1.2×10^{-3}	1.2×10^{-3}	4.2×10^{-3}	4.2×10^{-3}
To achieve maximum allowable torque ratios, $T_R = 1$ or $T_\Theta = 1$, set M_C or V_t to:						
Maximum mass on kg carriage (slug)	3316.2 (227.3)	3473.9 (238.1)	3291.5 (225.6)	3148.5 (215.8)	-	-
Maximum contouring speed (fpm)	1.75 (3.4375)	1.75 (3.4375)	1.75 (3.4375)	1.75 (3.4375)	1.75 (3.4375)	-

rate before the contouring speed is high enough to cause large inertial torques.

For dissipative type loads the grinding application is again used as an example. Results for loads corresponding to depth of cuts of 0.254 mm (0.01 inch) and 0.508 mm (0.02 inch) are shown in Table 6.2. Here also the magnitude of the load has no effect on the position of the contour pole for optimal loading. For the contours (a), (b), and (d) above, the results show that with a contouring speed of 1.016 cm/s (2 ft/min) the depth of cut can be increased beyond 0.508 mm (0.02 inch), while for the Limacon of Pascal a depth of cut of 0.457 mm (0.018 inch) cannot be exceeded. The table also shows that for the smaller load the contouring speed for all four contours can be increased to 1.74 cm/s (3.44 ft/min), which corresponds to the maximum stepping rate of the axes drives. For the larger load the contouring speed can be increased for contours (a), (b), and (d) but must be decreased for contour (c).

Table 6.2: Results of Optimization for Loading Conditions (Grinding Application)

	Circle	Witch of Agnesi	Limacon of Pascal	Serpentine			
For contouring speed of 1.02 cm/s (2ft/min), and							
Initial depth of cut	mm (in)	0.254 (0.01)	0.508 (0.02)	0.254 (0.01)	0.508 (0.02)	0.254 (0.01)	0.508 (0.02)
Initial machine pole location:	r cm (in)	53.8 (21.2)	0.0 (0.0)	0.0 (0.0)	53.8 (21.2)	17.8 (7.0)	-
	θ rad	3.927	0.0	0.0	3.927	4.712	-
Results from the optimization program,							
Optimum machine pole location:	r cm (in)	0.0 (0.0)	38.91 (15.32)	0.0 (0.0)	0.747 (0.294)	0.0 (0.0)	-
	θ rad	0.0	1.971	0.0	2.642	0.0	-
Objective function		0.454	0.894	0.217	0.421	0.550	1.088
Maximum torque ratios	T_R	0.274	0.042	0.198	0.383	0.075	0.121
	T_θ	0.426	0.823	0.186	0.376	0.543	1.086
To achieve maximum allowable torque ratios, $T_R = 1$ or $T_\theta = 1$, set d or V_t to:							
Depth of cut	d mm (in)	0.58 (0.023)	1.346 (0.053)	0.5 (0.019)	0.541 (0.0213)	-	-
Maximum contouring speed V_t	cm/s (fpm)	1.75 (3.437)	1.18 (2.33)	1.75 (3.437)	0.94 (1.86)	1.05 (2.06)	1.02 (2.0)

CHAPTER 7
GRAPHICAL PROCEDURE
FOR EVALUATING THE LOAD AND
THE LOAD CARRYING CAPACITY OF THE NC MACHINE

7.1 Introduction

In a practical environment, where production constraints such as shorter machining time and optimal machine load are considered, it is desirable to utilize the machinery to its full capability. With an open loop controller used on the NC machine, it is necessary to know the magnitude and type of the machining load, as well as the capability of the machine in order to avoid overloading the NC machine.

In a controlled and automated environment where computer capability is available, the analyses presented in Chapters 4, 5, and 6, may be used to prevent overloading the NC machine. In cases where decisions concerning the operating parameters have to be made on a machine shop floor, or in the absence of computer capability, a simple method to determine the load imposed by the machining operation and the load carrying capacity of the NC machine would prove helpful.

In this chapter, a graphical procedure is outlined for ease of evaluation of the load and the maximum load carrying capacity of the NC machine. The procedure is essentially a graphical solution of the torque equations, Equations 6.13

and 6.14, of the two axes. The graphical solution is presented in the form of composite plots of the torques versus the different contour and the operating parameters.

To use the graphical procedure, a user must know the minimum radius of curvature of the contour being tracked, and the relative location between the radial displacement of the point of minimum radius of curvature from the machine pole. Using this information, together with the information on the desired operating parameters, the maximum torque imposed by the machining operation on both axes and the respective stepping motors pull-out torque can be found.

7.2 Description and organization of the composite graphs

7.2.1 Inertial load

For the radial axis:

The maximum radial axis torque for the case of an inertial load was shown in Chapter 6 to occur at $\gamma_R^{(I)} = \pi/2$. Substituting for γ in Equation 6.13 and setting the force factor K_C to zero yields:

$$\hat{T}_R^{(I)} = M_C \tau_1 \quad 7.1$$

$$\tau_1 = K_2 V_t^2 / \rho$$

The torque available from the stepping motor is found by substituting $\gamma_R^{(I)} = \pi/2$ in Equation 5.20. Figure 7.1 shows

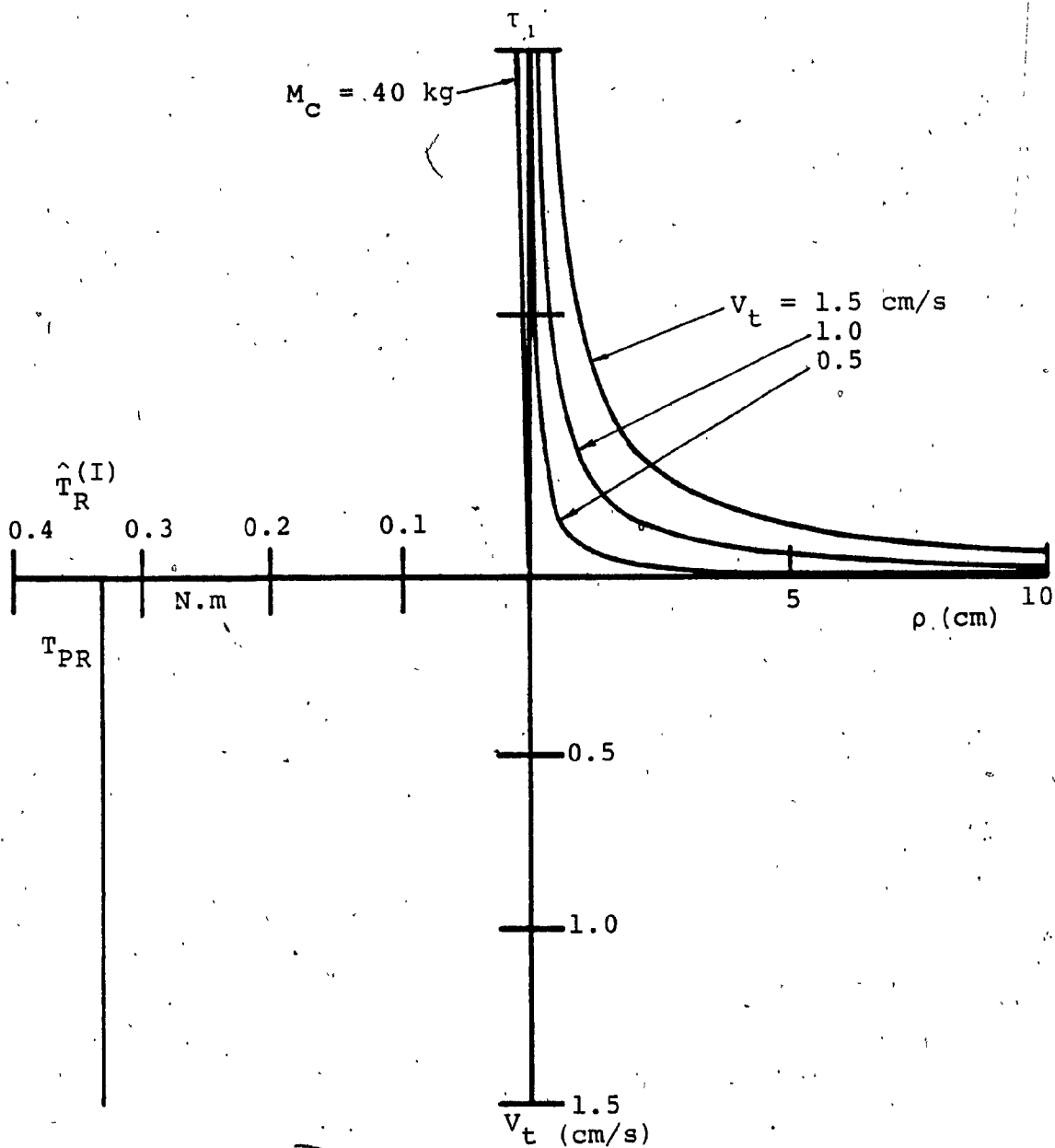


Figure 7.1: Torque Required and Available from the Radial Axis-Drive (Inertial Load).

the composite graph used to solve for $\hat{T}_R^{(I)}$, and for the torque available from the stepping motor T_{PR} . This graph is set up as follows:

- Quadrant I: τ_1 versus ρ for different V_t .
- Quadrant II: $\hat{T}_R^{(I)}$ versus τ_2 for different M_c .
- Quadrant III: T_{PR} versus V_t .

For the angular axis

The angle γ at which the maximum angular axis torque occurs is given by Equation 6.15. This value $\gamma_\theta^{(I)}$ is substituted in Equation 6.14 so as to obtain the maximum torque on the angular axis. The constant torque of the arm support, given by $K_{C f A} L$, is transferred with a negative sign to the stepping motor pull-out torque equation. Furthermore, the force factor K_C is set to zero. Thus:

$$\hat{T}_\theta^{(I)} = 2K_1 V_t^2 \tau_4 \quad 7.2$$

where;

$$\tau_4 = \left[5\tau_3 - \sqrt{\tau_3^2 + 0.5} \right] \times \left[0.5 - 2\tau_3^2 + 2\tau_3 \sqrt{\tau_3^2 + 0.5} \right]^{1/2}$$

$$\tau_3 = \tau_2 / \rho$$

$$\tau_2 = \Lambda_{24} = \left[M_c r^3 + J_A r \right] / 8$$

The torque available from the angular axis stepping motor is found by substituting for $\gamma_R^{(I)}$ in Equation 5.21.

Figures 7.2 and 7.3 are used to solve for $\hat{T}_\theta^{(I)}$ and $T_{PR}^{(I)}$. The figures are organized as follows:

Figure 7.2:

Quadrant I: τ_2 versus r for different M_C .

Quadrant II: τ_3 versus τ_2 for different ρ .

Quadrant III: τ_4 versus τ_3 for different r .

Quadrant IV: $\hat{T}_\theta^{(I)}$ versus τ_4 for different V_t .

Figure 7.3:

Quadrant I: τ_5 versus τ_3 for different r_C .

$$\tau_5 = \sin \gamma_\theta^{(I)} / r$$

$$= \frac{\tau_3 - [\tau_3^2 + 0.5]^{\frac{1}{2}}}{r}$$

Quadrant II: $T_{P\theta}$ versus τ_5 for different V_t .

7.2.2 Grinding application

The maximum torque for the radial and angular drives occurs at angles $\gamma_R^{(G)}$ and $\gamma_\theta^{(G)}$ given by Equations 6.19 and 6.20, respectively. Substituting these values in Equations 6.13 and 6.14, respectively, results in the maximum torques required from the axes drives while tracking a contour.

For the radial axis

The maximum torque is given by:

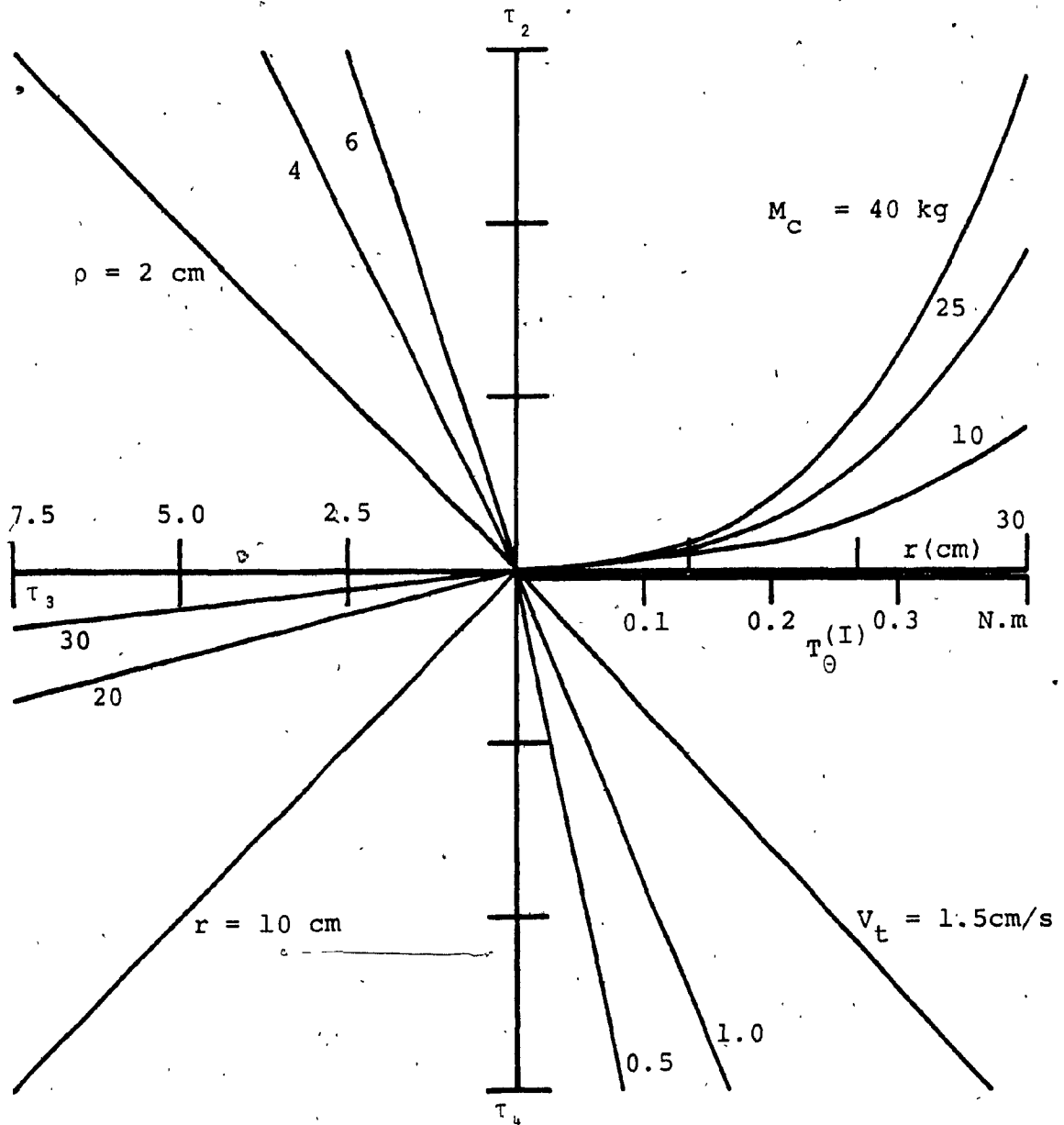


Figure 7.2: Torque Required and Available from Angular Axis-Drive (Inertial Load). Part 1 of 2.

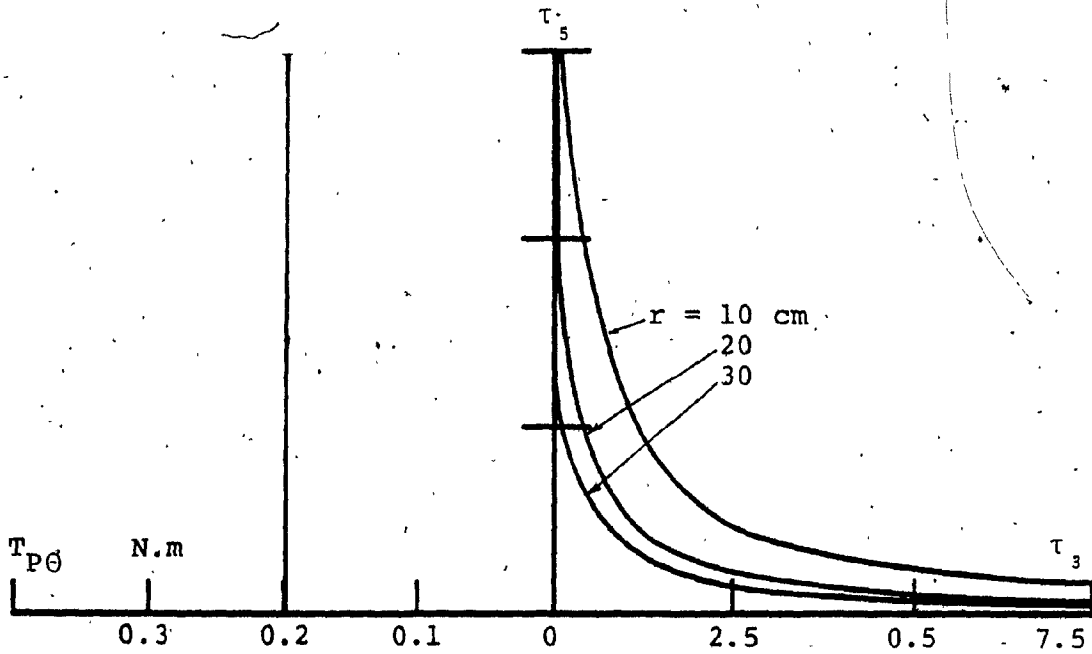


Figure 7.3: Torque Required and Available from the Angular Axis-Drive (Inertial Load). Part 2 of 2.

$$\hat{T}_R^{(G)} = V_t \tau_9$$

7.3

where;

$$\tau_9 = K_C \tau_8$$

$$\tau_8 = K_2 \left[M_C \tau_7 \sin \gamma + \cos(\gamma - \alpha_C) \right]$$

$$\tau_7 = V_t \tau_6$$

$$\tau_6 = 1 / (K_C \rho)$$

The pull-out torque of the radial axis stepping motor is found by substituting $\gamma_R^{(G)}$ from Equation 5.19 into Equation 5.20.

The graphs to solve for the maximum torque required from the radial axis-drive, and the pull-out torque of the stepping motor are organized in Figures 7.4 and 7.5 as follows:

Figure 7.4:

- Quadrant I: τ_6 versus ρ for different K_C .
- Quadrant II: τ_7 versus τ_6 for different V_t .
- Quadrant III: τ_8 versus τ_7 for different α_C .
- Quadrant IV: τ_9 versus τ_8 for different K_C .

Figure 7.5

- Quadrant I: $\gamma_R^{(G)}$ versus τ_7 for different α_C .
- Quadrant II: T_{PR} versus $\gamma_R^{(G)}$ for different V_t .
- Quadrant III: $\hat{T}_R^{(G)}$ versus τ_9 for different V_t .

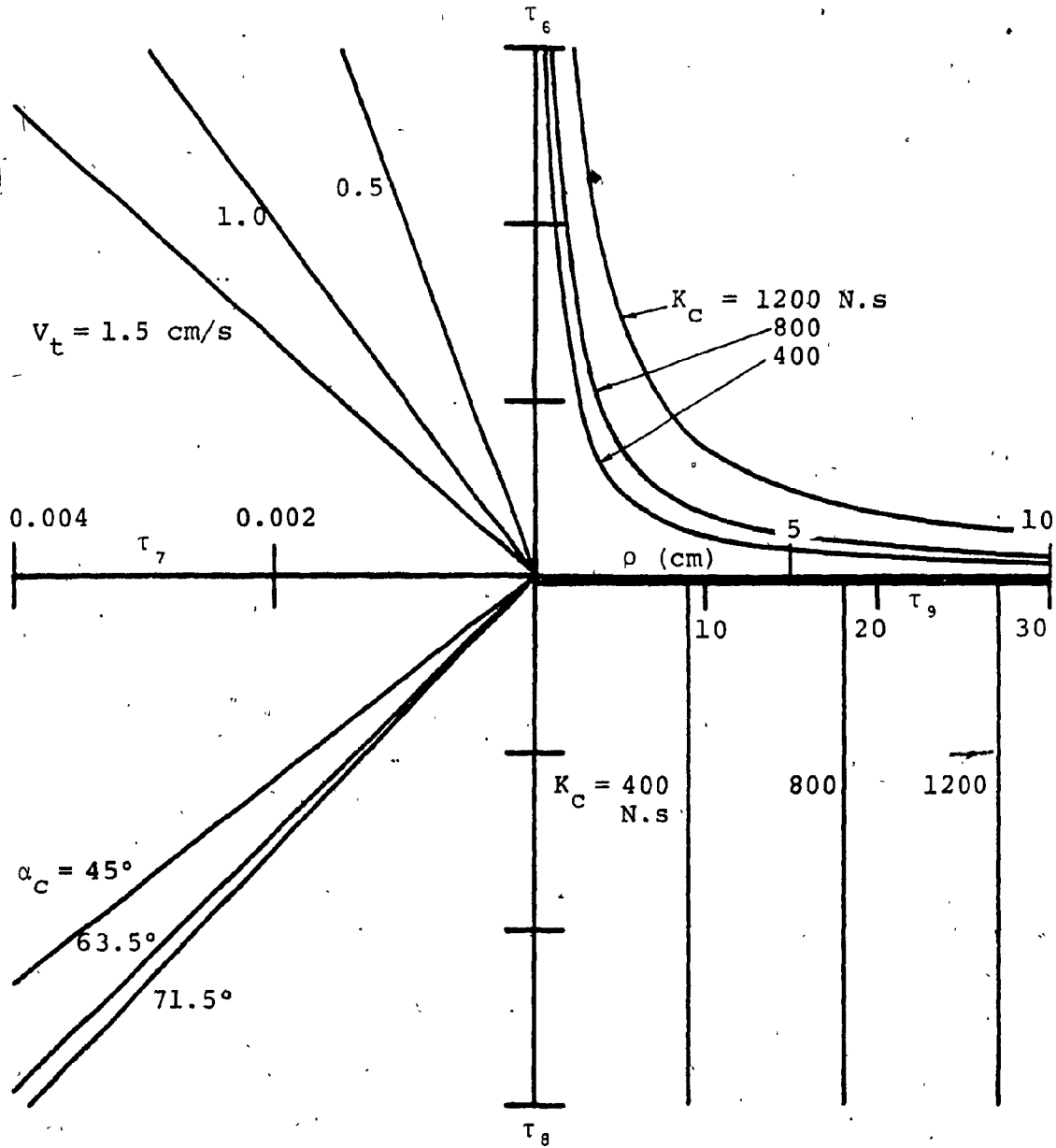


Figure 7.4: Torque Required and Available from the Radial Axis-Drive (Grinding Application). Part 1 of 2.

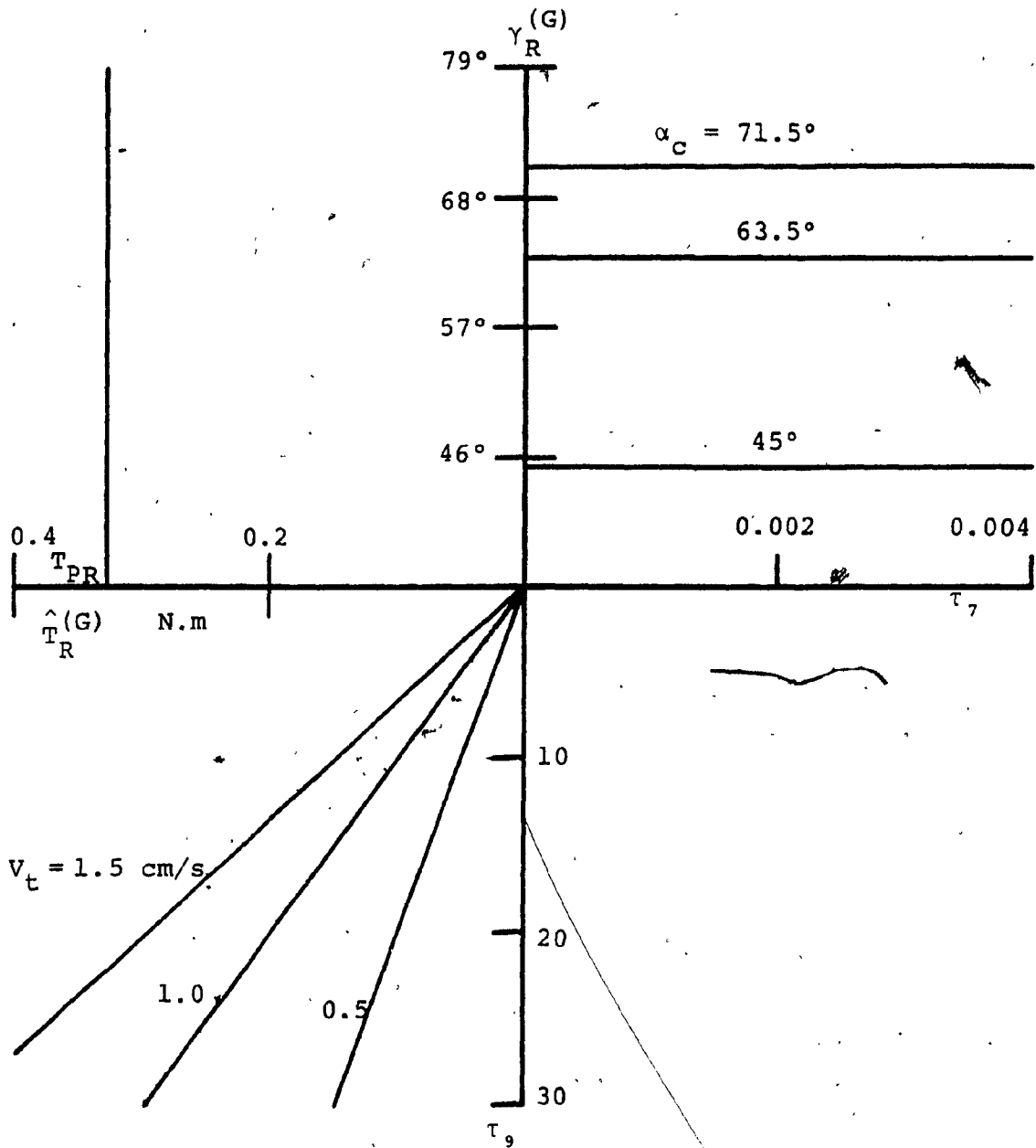


Figure 7.5: Torque Required and Available from the Radial Axis-Drive (Grinding Application). Part 2 of 2.

For the angular axis

The constant torque due to the friction force of the arm support in Equation 6.14 is transferred with a negative sign to the relation of the pull-out torque of the angular axis stepping motor. Furthermore, for a grinding application the second term of Equation 6.14 is negligible in comparison with the other two terms as mentioned previously.

The equation for the maximum torque acting on the angular axis is hence given by:

$$\hat{T}_{\theta}^{(G)} = v_t \tau_{12} \quad 7.4$$

where;

$$\tau_{12} = K_c K_1 \tau_{11}$$

$$\tau_{11} = \tau_{10} \cos \gamma + \sin(\gamma - \alpha_c)$$

$$\tau_{10} = \tau_6 \left[M_c r + J_A / r \right]$$

The pull-out torque of the angular axis stepping motor is found by substituting $\gamma_{\theta}^{(G)}$ from Equation 6.20 into Equation 5.21.

The graphs for this axis are organized in Figures 7.6 and 7.7 as follows:

Figure 7.6:

Quadrant I: τ_{10} versus τ_7 for different r .

Quadrant II: τ_{11} versus τ_{10} for different α_c .

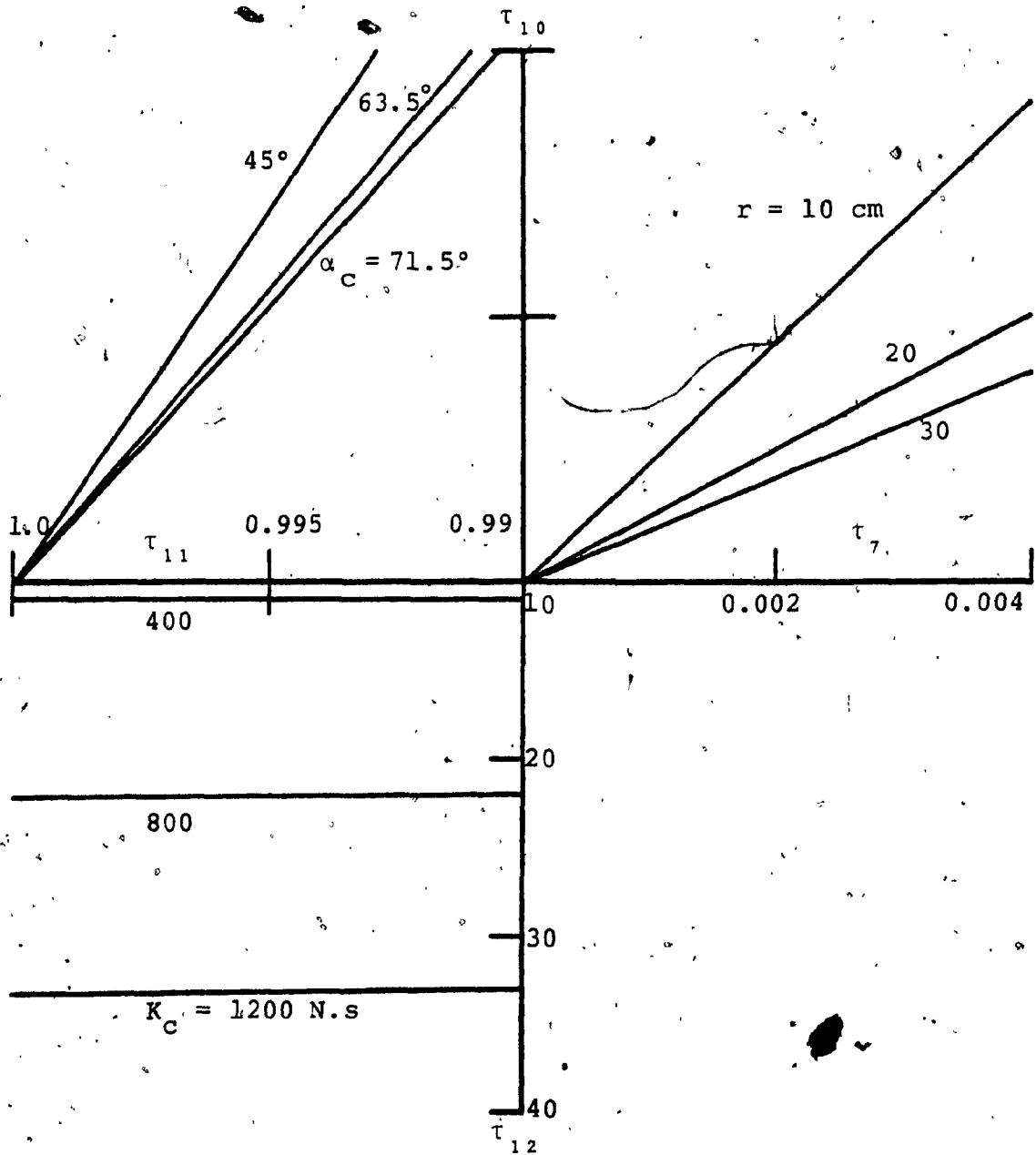


Figure 7.6: Torque Required and Available from the Angular Axis-Drive (Grinding Application). Part 1 of 2.

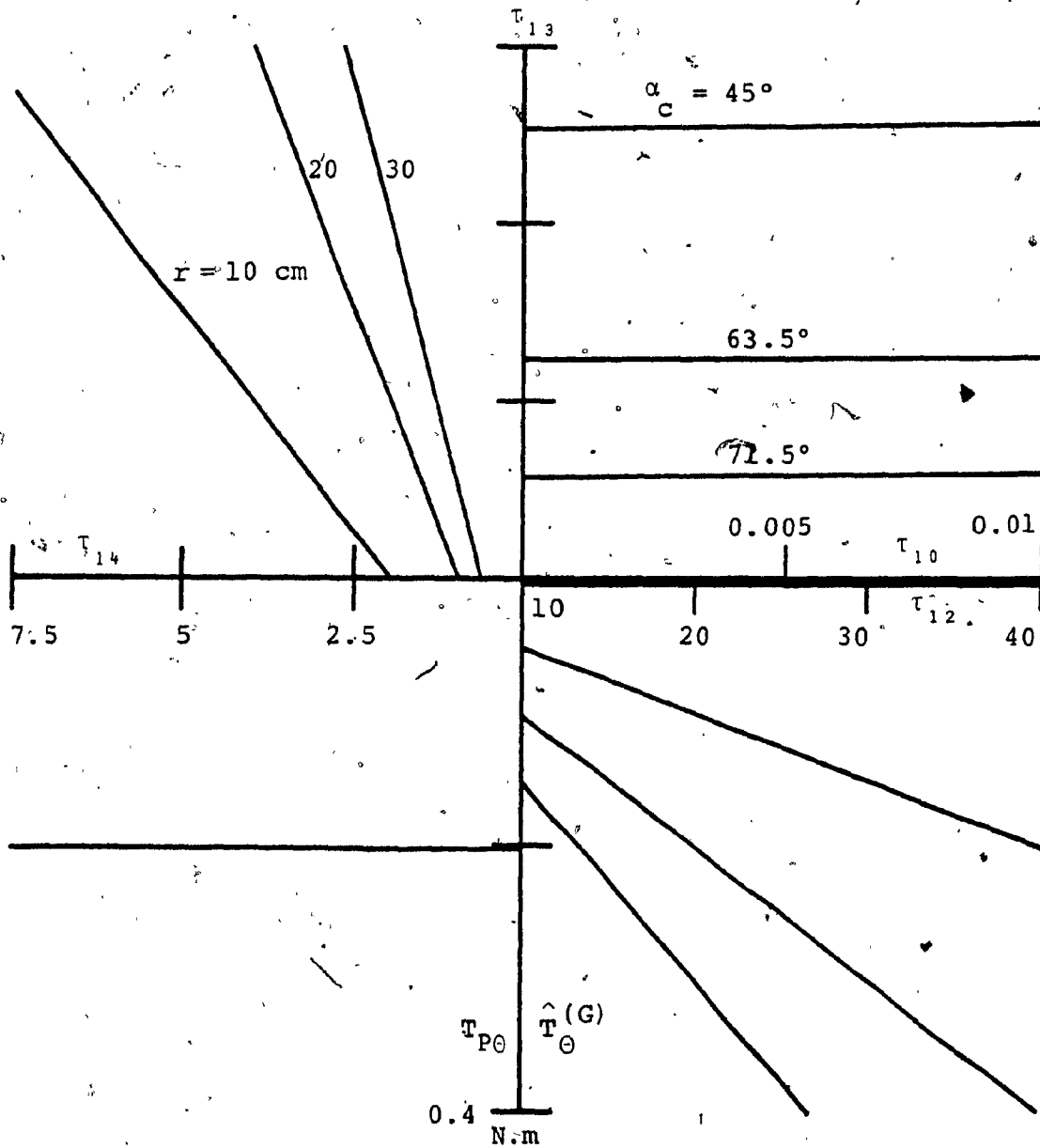


Figure 7.7: Torque Required and Available from the Angular Axis-Drive (Grinding Application). Part 2 of 2.

Quadrant III: τ_{12} versus τ_{11} for different K_C .

Figure 7.7:

Quadrant I: τ_{13} versus τ_{10} for different α_C .

$$\tau_{13} = \sin \gamma \theta^{(G)}$$

Quadrant II: τ_{14} versus τ_{13} for different r .

$$\tau_{14} = \tau_{13}/r$$

Quadrant III: $T_{P\theta}$ versus τ_{14} for different V_t

Quadrant IV: $\hat{T}_\theta^{(G)}$ versus τ_{12} for different V_t .

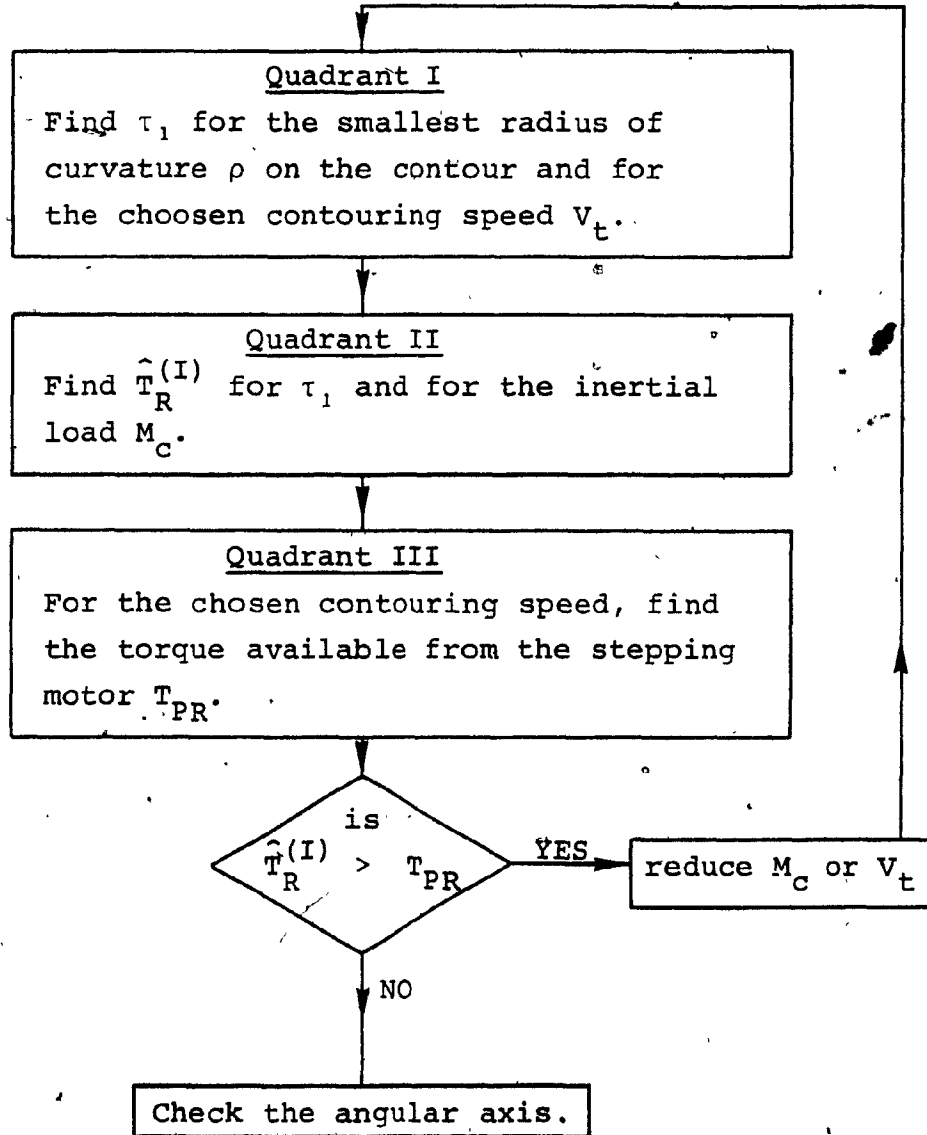
7.3 Description of the graphical procedure

The solution procedures for the load and the load carrying capacity of the NC machine axes are presented in flowchart form as follows.

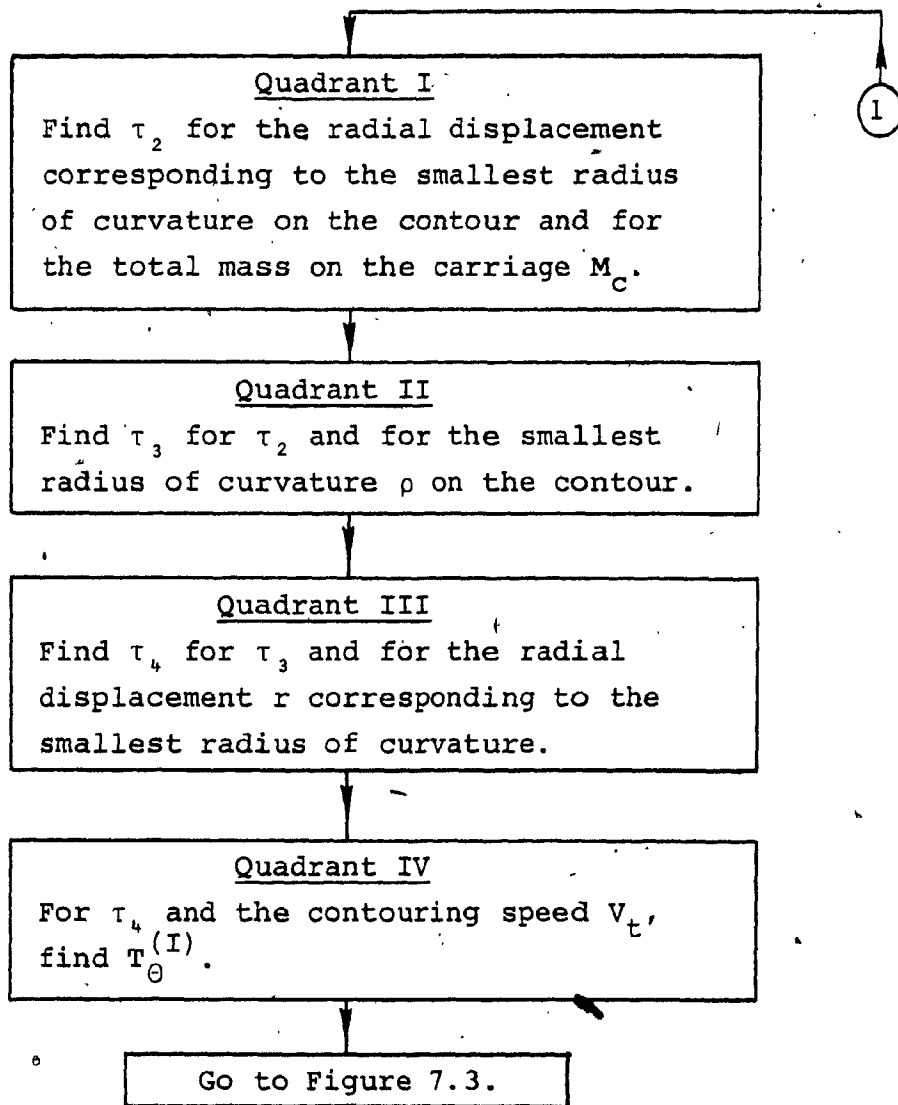
7.3.1 Inertial Load

For the radial axis

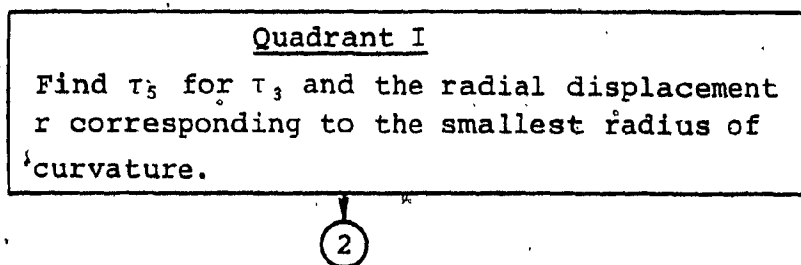
With reference to Figure 7.1

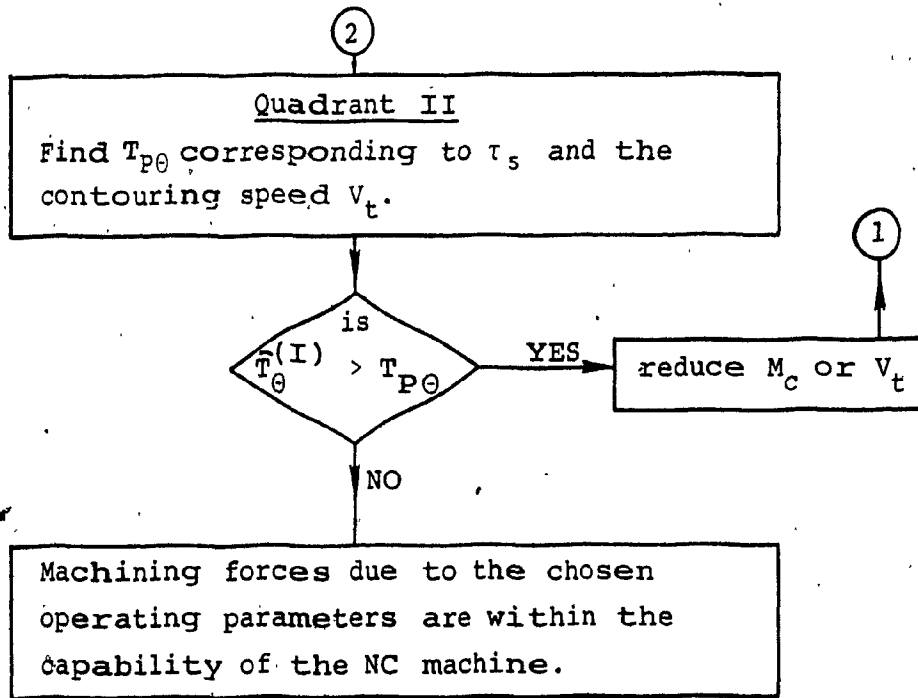


For the angular axis
With reference to Figure 7.2



With reference to Figure 7.3

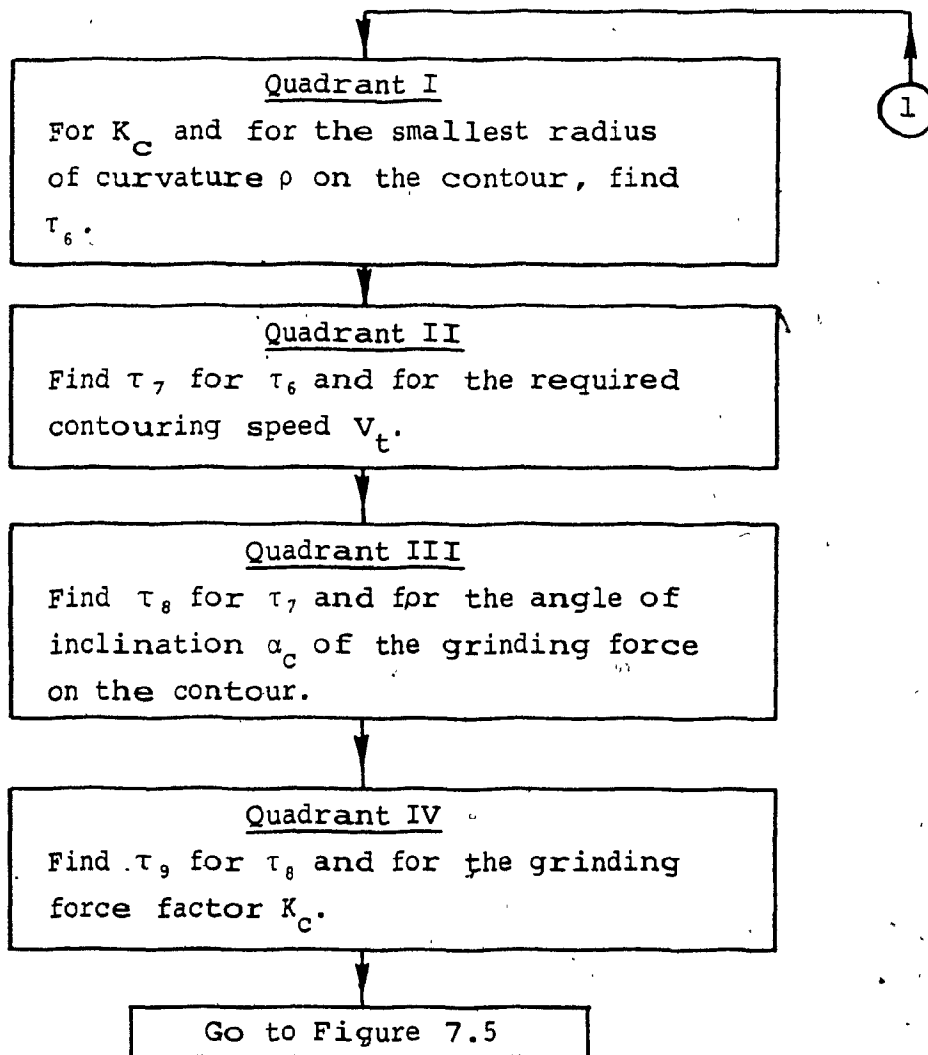




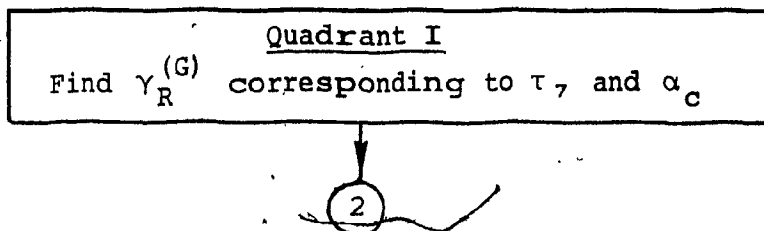
7.3.2 Grinding Application

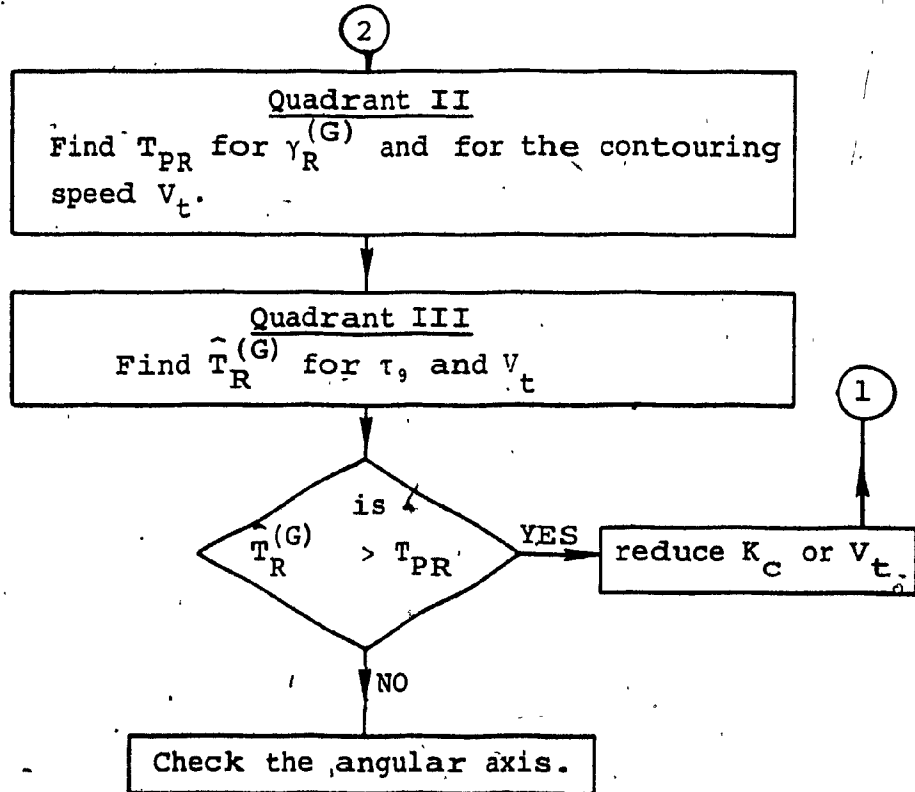
For the radial axis

With reference to Figure 7.4

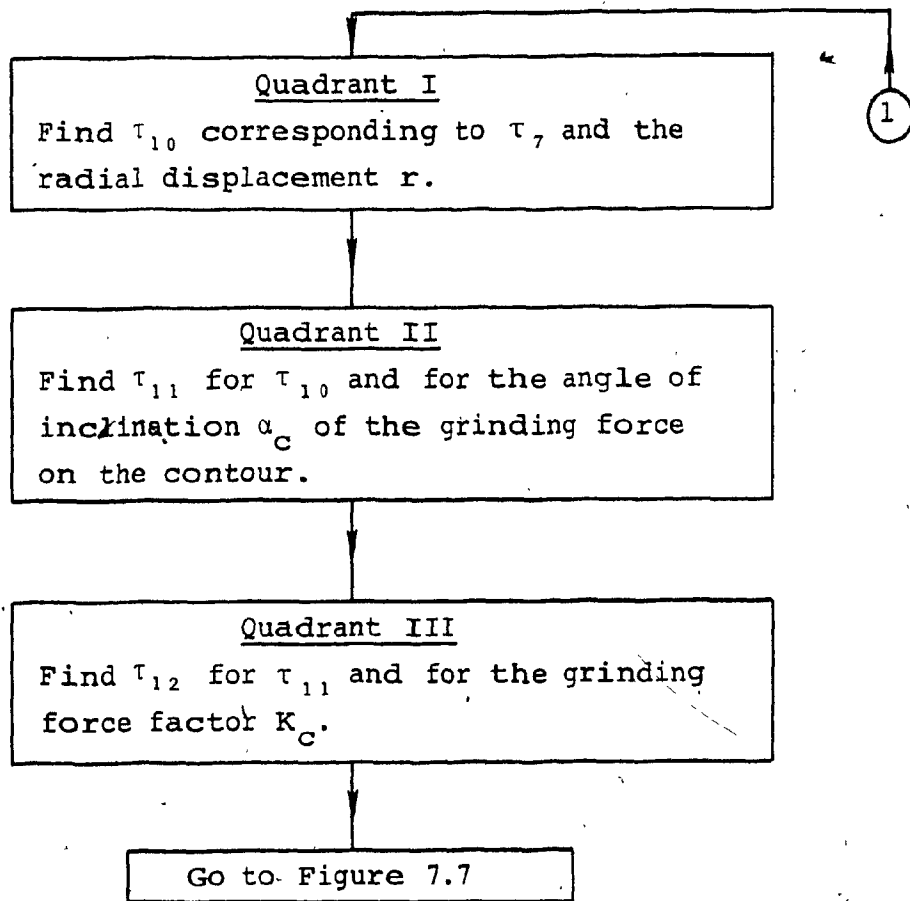


With reference to Figure 7.5

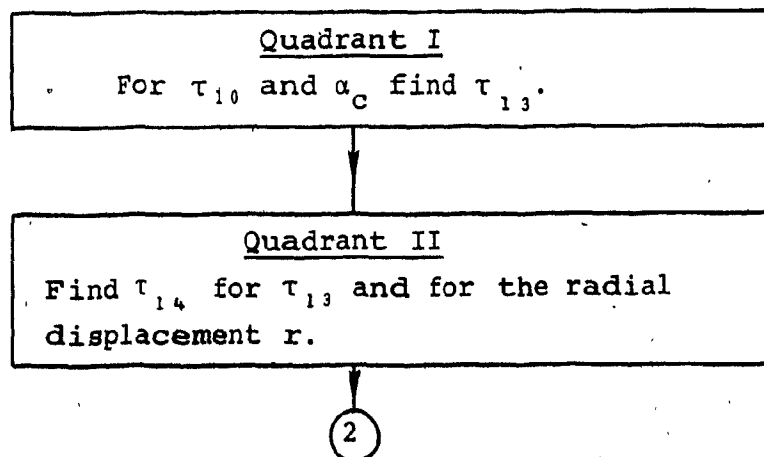




For the angular axis
With reference to Figure 7.6



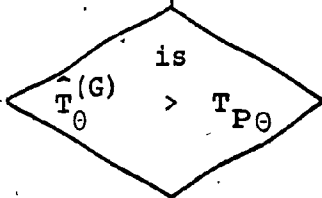
With reference to Figure 7.7



2

Quadrant III
Find $T_{P\theta}$ for τ_{14} and for the contouring speed V_t .

Quadrant IV
Find $\hat{T}_\theta(G)$ for τ_{12} and V_t .



YES

reduce K_c or V_t

1

Machining forces due to the chosen operating parameters are within the capability of the NC machine.

CHAPTER 8

CONCLUSION

AND RECOMMENDATION FOR FUTURE WORK

8.1 Conclusion and major highlights

This thesis presents the design, analysis and performance evaluation of a polar based contouring system. The system is composed of a digitizer and an NC machine. The digitizer can be either a template digitizer (TD) or a software digitizer (SD). The system can thus be operated as a TD/NC machine or a SD/NC machine.

The template digitizer uses a unique method of tracking a template. The tracking mechanism consists of two rollers powered by electric motors which are connected in such a way so as to produce a mechanical differential effect. The two rollers are preloaded against each other and together track a ribbon-like template which is positioned in between them. The rollers are mounted on a carriage which in turn is mounted on an arm. The arm swings around a pivot and represents the angular axis of the polar set. The position of the carriage on the arm represents the radial axis. Two encoders, mounted on the arm-pivot and on the carriage, supply data on the angular and radial position. Due to the roller-differential arrangement, nearly constant tracking speeds are possible. Two types of template intended for accurate and non-accurate contouring have been described.

The software digitizer is composed of two parts, a

digitizer algorithm and an output algorithm. The digitizer algorithm can run under BATCH mode on time-shared computers, and it generates the positional and time data required for contouring. The output algorithm is short and simple, and its function is to transfer the data generated by the digitizer algorithm to the output device. This algorithm require real-time computing. The accuracy of the tracking speed for the software digitizer depend upon the resolution of the real-time clock of the output computer. Typical resolutions for such clocks are within 10 to 30 sec. The control signals from either digitizer can be recorded on commercial stereo tape recorders for later use or may be supplied directly to the NC machine.

The NC machine is composed essentially of an arm and carriage arrangement similar to that of the template digitizer. The machine operates with an open loop controller. Stepping motors operating with a wave energization scheme are used to drive both the radial and angular axes.

Prototypes of both digitizers as well as of the NC machine have been built and tested. The configuration of the polar based contouring system offers a number of operational features as well as some advantages over commercially available copying or NC machines.

One of the important features of the system is that it can operate as a copier (TD/NC machine) or as an NC system (SD/NC machine). When operating as a copier, the contour

information is in the form of a physical template, and the template digitizer is used to translate the given template into numerical data. When a software digitizer is used, the system resembles the commercially available NC systems but with no on-board computer.

An important advantage of this system over a Cartesian-based system is the ease with which size scaling is achieved. For a polar-based system, scaling is accomplished solely by radial axis scaling. A simple method for carrying out the scaling has been described in Section 3.7. When the NC machine is operated with prerecorded digitizer data, speed scaling can be achieved by altering the play-back speed. Chapter 3 discusses and tabulates a number of other features and advantages of the proposed system over the commercially available systems.

The major drawback of the polar system is the dependence of the angular resolution on the radial displacement. The variation of the angular resolution necessitates optimal location of the contour with respect to the machine pole in order to reduce the errors due to the digitization of the contour. An area error criterion has been developed in Chapter 4 and has been shown to be more stringent than the traditionally used deviation error. It was also shown that the area error generated under quasi-static conditions is a conservative representation of the error generated during actual operation. It was also shown that the area error is a function of the relative

location of the contour pole from the machine pole. Thus by varying the location of the contour pole, the area error can be minimized. The calculation of the area error is lengthy and cumbersome, and using it as an objective function for optimization proves impractical. An alternate objective function has been developed and was shown to duplicate the behavior of the area error. This alternate function can be easily and rapidly calculated. Comparative tests carried out on three test contours show that the alternate objective function can be used to accurately determine the contour location for minimum area error.

A dynamic analysis of the NC machine has been presented. The analysis takes into account the contour being tracked and the diameter of the tool used on the NC machine. The analysis is used to calculate the torque required from the axes-drives during the contouring process. These torques have to be less than the pull-out torques available from the stepping motors powering the respective axes. The torque ratio is defined as the ratio of the torque required to the pull-out torque of the stepping motors.

The effect of the type and magnitude of the load and of the contouring speed and of the type of contour has been studied. In general, an increase in the magnitude of the load or of the tracking speed causes an increase in the torque ratio for all contours. Furthermore, it was shown that the torque required from an axis-drive, and

consequently the torque ratio, increases rapidly with the decrease of the radius of curvature of the contour. The study also showed that the magnitude of the load or of the contouring speed has no effect on the location, along the contour, of the maximum value of the sum of torques required from both axes.

During the course of the study it was observed that the change in the location of the contour causes a change in the torque ratio. This phenomenon is utilized as shown in Chapter 6, in an optimization routine to locate the contour relative to the machine pole such that the maximum value of the sum of the torque ratios is a minimum. Results of a parametric study, conducted in Chapter 6, are subsequently utilized in order to find the limiting machine setting beyond which failure would occur.

In Chapter 7, a procedure using composite graphs is provided for rapid calculation of the maximum torque required and available from the axes-drives in different contouring operations.

8.2 Recommendation for future work

The studies conducted in this thesis prove the feasibility of the polar-based, contouring system. They also point out to a number of desirable features inherent to the polar axis system, as well as others that result from the configuration of the system.

In order to advance the concept to a commercially

viable stage, further studies should be conducted. A dynamic analysis of the template digitizer mechanism should be carried-out in order to improve the design. Such a study would also prove helpful in eliminating or reducing the oscillations of the digitizer rollers that have been found to occur at the beginning of the tracking of a template.

The effect of size scaling on the contour pole location for minimum area error should also be investigated.

The dynamic analysis that has been conducted on the NC machine is geared towards estimating the load on the machine axes. The scope of the study should be expanded to include such areas as rigidity and vibration effects of the arm and carriage mechanism.

A control concept of modifying the timing of the original control data in order to compensate for positional errors at higher contouring speeds or loads should be studied. To perform such a modification, a dynamic model that includes the behaviour of the system within a step must be developed. Finally, to enhance the performance of the contouring system, a small on-board microcomputer may be employed to carry out the auxiliary functions that may be required during a machining operation. The interaction between these functions and the contouring process should be carefully coordinated.

The possibility of implementing the proposed concept in a 2½D and 3D contouring system should be considered.

REFERENCES

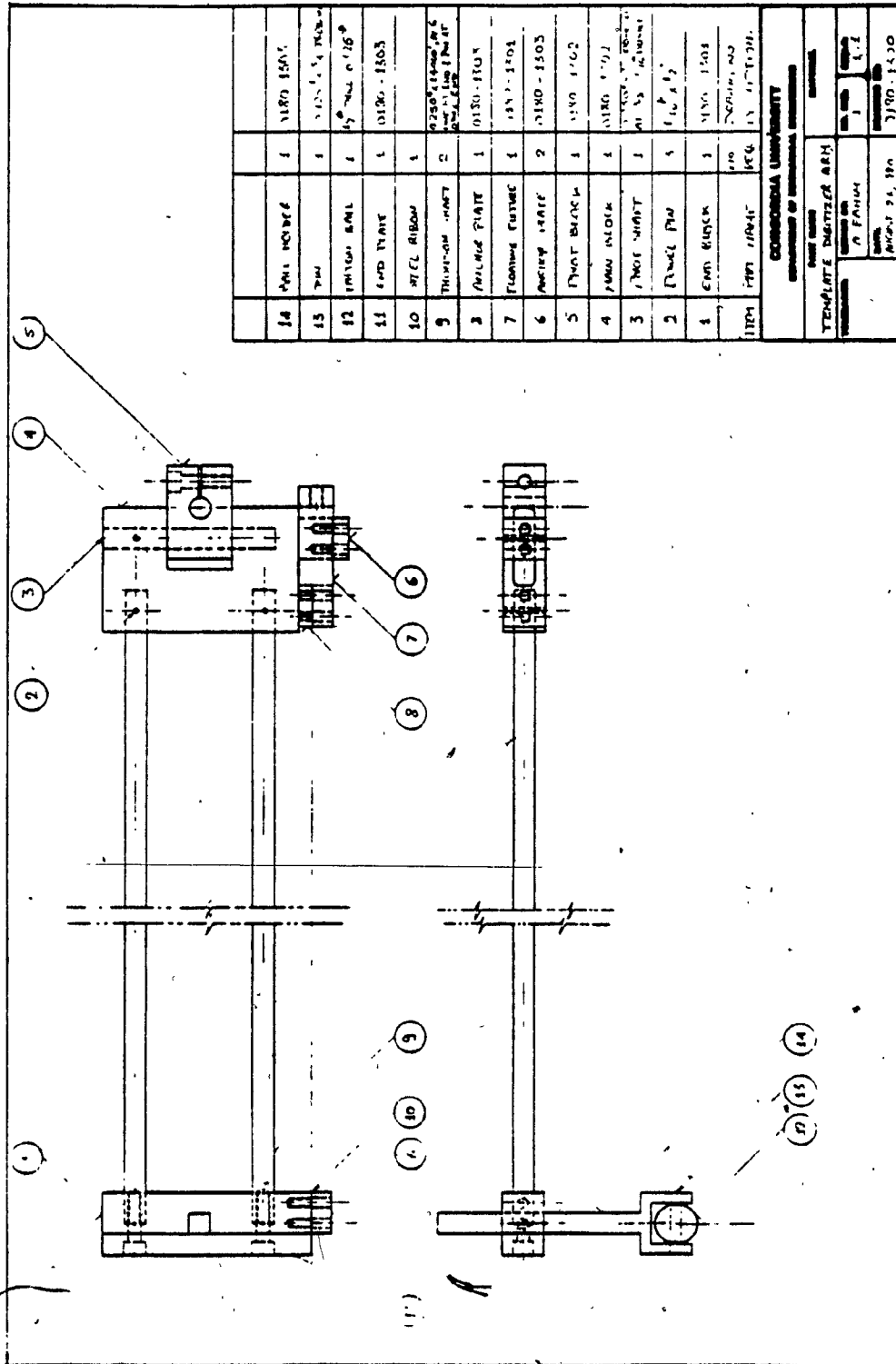
1. Chironis, N.P., "Mechanisms, Linkages, and Mechanical Controls", McGraw-Hill Book Company, first edition.
2. Svoboda, A., "Computing Mechanisms and Linkages", Dover Publications Inc.
3. Sankar, Seshadri, "Dynamic Accuracy and Stability of Machine-Tool Systems", Doctoral Theses, Mechanical Engineering Department, Concordia University, Montreal, Canada, 1973.
4. Anon, HEATH Shape Cutters MCD series description brochure. HEATH Engineering Company, Fort Collins, Colorado, U.S.A.
5. Anon, RETICON RO-64 self-scanned circular photodiode array technical information sheet, RETICON Corporation, Sunnyvale, California, U.S.A.
6. NECCHI "Profile Stitcher" Model: 1501-S
7. Mansour W M., and Pavlov D., "The Mechanism of Gyroscopic Tracking", Parts 1 and 2, ASME Transaction, J. Engng. Indust. 95, Series B, No 2, 1973, pp 430-444.
8. Mansour W., "Coupled Gyroscopic Mechanism for Centerless Gyrogrinders", Mechanisms and Machine Theory, 1976, Vol. 11, pp 201-212.
9. El-Chaer Carlos, and Mansour M. W., "Gyroscopic Centerless Grinders with Rotation of the Cam", Proceedings of the Third Brazilian Congress of

- Mechanical Engineering, Rio de Janeiro, Dec 1975, pp 587-600.
10. Osman M. O. M., Sankar S., and Dukkipati R. V., "Design Synthesis of a Gyrogrinder Using Direct Search Optimization", Mechanism and Machine Theory Vol.17, No.1, pp.33-45, 1982.
 11. Bezier P., "Numerical Control", (translated by FORREST A. R., and Pankhurst Anne F.), John Wiley and Sons, London, 1970.
 12. Pressman Roger S., and Williams John E., "Numerical Control and Computer Aided Manufacturing", John Wiley and Sons, 1977.
 13. McPherson D. (editor), "Advances in Computer Aided Manufacturing", North Holland Publishing Company, 1977.
 14. Devries M. A. (editor), "The Expanding World of NC", (Numerical Control Society), The Village Press 1972.
 15. Hatvary J. (editor), "Computer Languages for Numerical Control", North Holland Publishing Company, 1973.
 16. Leslie W. H. P. (editor). "Numerical Control Programing Languages", North Holland Publishing Company, 1970.
 17. Auslander David M., and Sagues Paul, "Microprocessors for Measurement and Controls", OSBORNE/McGraw-Hill, California, U.S.A., pp. 117, 1981.
 18. Burden Richard L., Fairs J. Douglas, and Reynolds Albert C., "Numerical Analysis" Prindle, Weber & Schmidt, Boston, U.S.A., 1981.

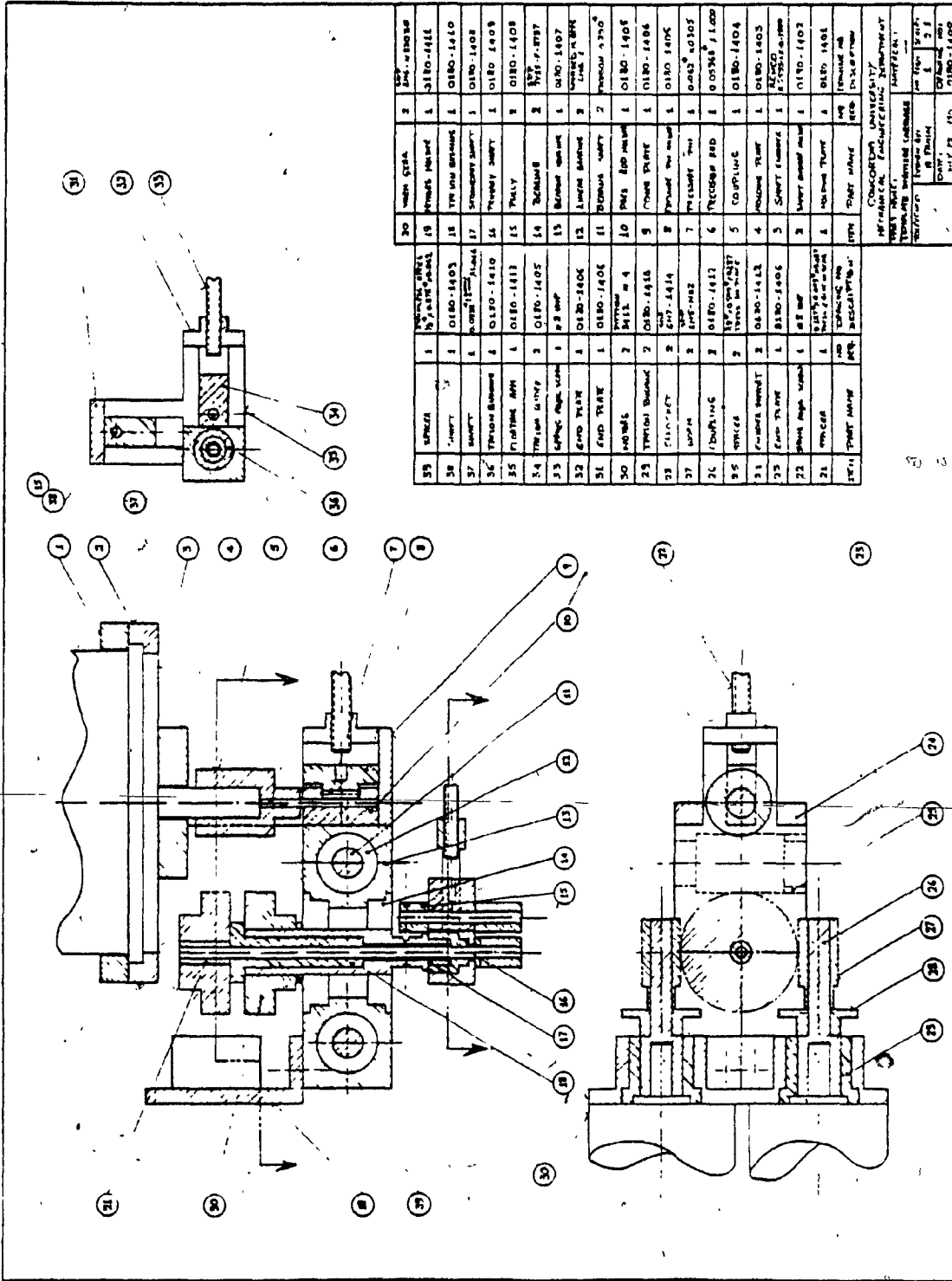
19. Carnahan Brice, Luther H. A., and Wilkes James O ,
"Applied Numerical Methods", John Wiley & Sons, New
York, pp.113, 1969.
20. Goode George & Associates, "TM 990, Introduction to
Microprocessors Hardware and Software", first edition,
Texas Instruments, 1979.
21. Anon, "TM 990/189 Microcomputer User's Guide", Texas
Instruments, 1979.
22. Kuo Benjamin C. (editor), "Theory and Applications of
Step Motors", West Publishing Company, New York, 1974.
23. Leenhouts Albert C., "Stepping Motors in Industrial
Control", technical paper No.80L-1, The Superior
Electric Company, Bristol, Connecticut, 1980.
24. Russel A. P. and Leenhouts Albert C., "An
Application-Oriented Approach to the Prediction of
Pull-out Torque/Speed Curve for Permanent Magnet
stepping Motors", The Superior Electric Company,
Bristol, Connecticut, 1980.
25. Singh G., Leenhouts Albert C., and Mosel E. F.,
"Electromagnet Resonance In Permanent-Magnet Step
Motors", technical paper, The Superior Electric
Company, Bristol, Connecticut, 1976.
26. Leenhouts Albert C., and Singh G., "An Active
Stabilization Technique for Open-Loop Permanent Magnet
Step Motor Drive Systems", technical paper, The
Superior Electric Company, Bristol, Connecticut, 1976.
27. Dinuzzo F. M., "Development of Programmed Sequences

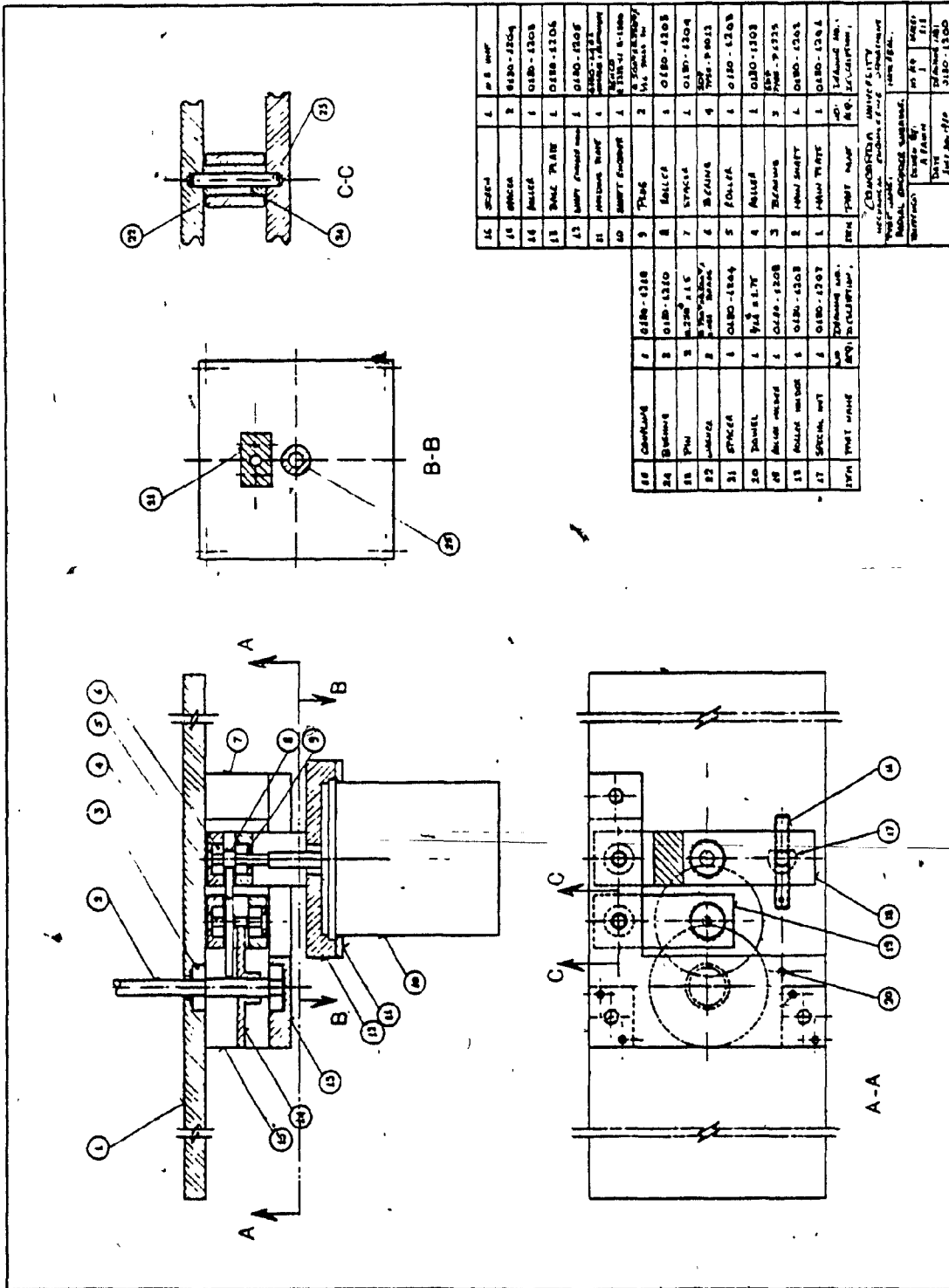
- for Stepping Motors", proc. of the jt. Automation Control Conference, V 1, San Fransisco, 1980.
28. Gauthier R., Meeker L. D., and Taft C. K., "Stepping Motors Dynamics and the Phase Plane", proc. of the jt. Automation Control Conference, V 1, San Fransisco, 1980.
 29. Oedel Richard H., "A Stepping Motor Behavior Model", MS Thesis, University of New Hampshire, September, 1977.
 30. Korn Granino A., and Korn Theresa M., "**Mathematical Handbook for Scientists and Engineers**", McGraw-Hill Book Company, Second Edition, 1968.
 31. Dixon L. C. W., "**Nonlinear Optimization**", Crane, Russak, and Company, Inc., New York, 1972.
 32. Shiglay Joseph E., "**Mechanical Engineering Design**", Mcgraw-Hill Book Company, Second Edition, 1972.
 33. Baumeister Theodore (editor), "**Standard Handbook For Mechanical Engineers**", Mcgraw-Hill Book Company, Seventh Edition, 1967.
 34. Arshinov V., Alekseev G, "**Metal Cutting Theory and Cutting Tool Design**", MIR Publishers, Moscow, 1976.
 35. Banerjee, J.K., "Some Aspects of Flat Surface Grinding With Intermittent Cross-Feed", Parts 1 & 2 , Journal of Engineering for Industry, Transactions of the ASME, Vol. 101, May 1979.

APPENDIX A
ASSEMBLY DRAWINGS OF
THE TEMPLATE DIGITIZER,
AND THE NC MACHINE



14	WAL NUTS	1	1180-1504
15	WAL	1	1180-1504
12	WAL NUT	1	1180-1504
11	END PLATE	1	0190-1505
10	WAL RIBBON	1	0250-1504, P.C. 1180-1504
9	THROAT WAFER	2	0250-1504, P.C. 1180-1504
8	WAL NUT	1	0130-1504
7	FLANGE WAFER	1	1180-1504
6	WAL NUT	2	0190-1505
5	WAL NUT	1	1180-1502
4	WAL NUT	1	1180-1502
3	WAL NUT	1	1180-1502
2	WAL NUT	1	1180-1502
1	END BLOCK	1	1180-1502
ITEM	QTY	UNIT	REF. NO.
CONSTRUCTION UNIVERSITY			
DEPARTMENT OF MECHANICAL ENGINEERING			
PART NAME: TEMPLATE MITERING ARM DRAWING NO: A-1 DATE: 11/20/15 SCALE: 1:1			

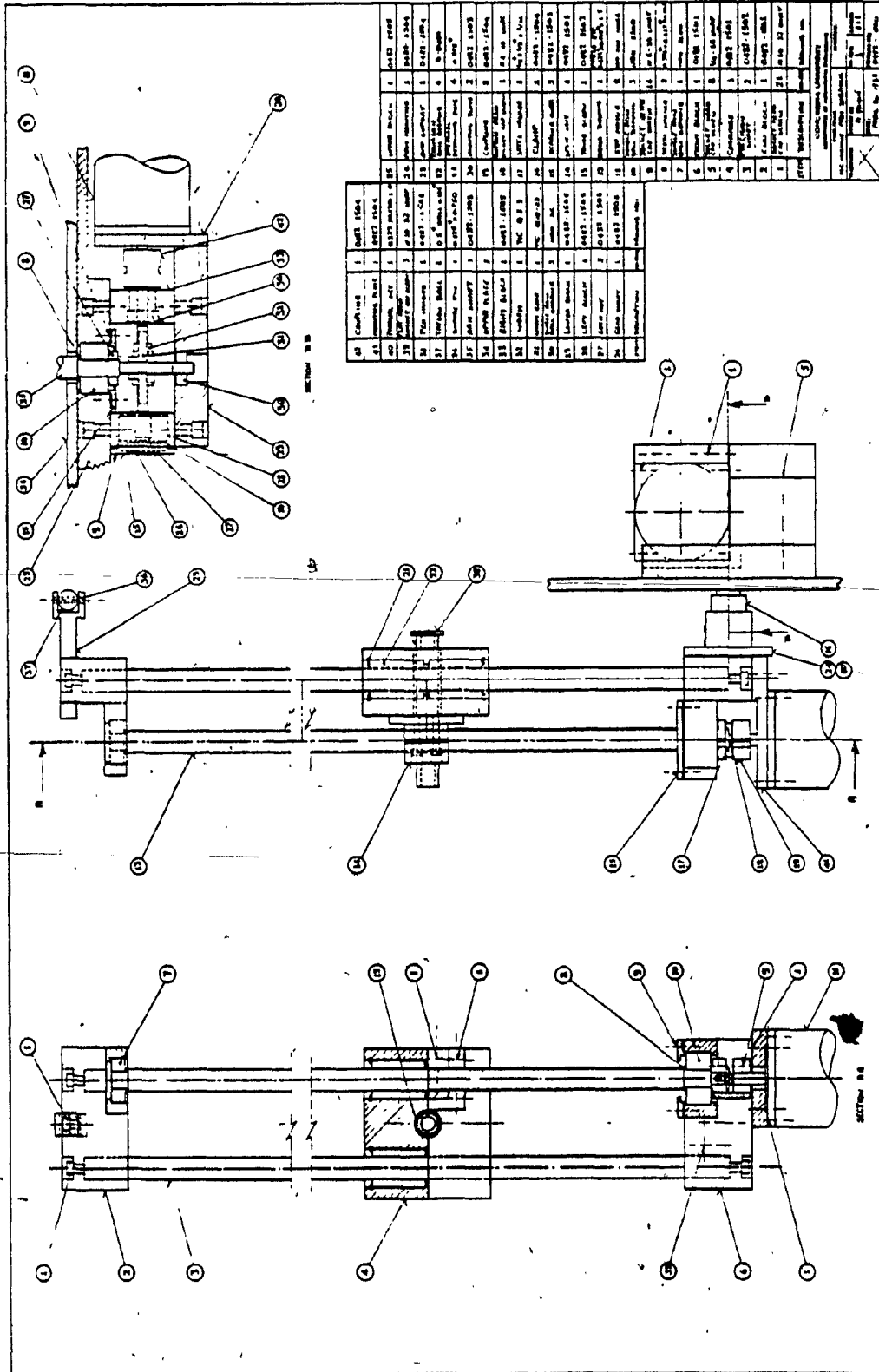




14	SPACER	1	SP 8	SP 8
15	SPACER	2	0180-1204	0180-1204
16	WASHER	1	0180-1208	0180-1208
17	WASHER	1	0180-1206	0180-1206
18	WASHER	1	0180-1208	0180-1208
19	WASHER	1	0180-1208	0180-1208
20	WASHER	1	0180-1208	0180-1208
21	WASHER	1	0180-1208	0180-1208
22	WASHER	1	0180-1208	0180-1208
23	WASHER	1	0180-1208	0180-1208
24	WASHER	1	0180-1208	0180-1208
25	WASHER	1	0180-1208	0180-1208
26	WASHER	1	0180-1208	0180-1208
27	WASHER	1	0180-1208	0180-1208
28	WASHER	1	0180-1208	0180-1208
29	WASHER	1	0180-1208	0180-1208
30	WASHER	1	0180-1208	0180-1208
31	WASHER	1	0180-1208	0180-1208

1	0180-1208	1	0180-1208
2	0180-1208	2	0180-1208
3	0180-1208	3	0180-1208
4	0180-1208	4	0180-1208
5	0180-1208	5	0180-1208
6	0180-1208	6	0180-1208
7	0180-1208	7	0180-1208
8	0180-1208	8	0180-1208
9	0180-1208	9	0180-1208
10	0180-1208	10	0180-1208
11	0180-1208	11	0180-1208
12	0180-1208	12	0180-1208
13	0180-1208	13	0180-1208
14	0180-1208	14	0180-1208
15	0180-1208	15	0180-1208
16	0180-1208	16	0180-1208
17	0180-1208	17	0180-1208
18	0180-1208	18	0180-1208
19	0180-1208	19	0180-1208
20	0180-1208	20	0180-1208
21	0180-1208	21	0180-1208
22	0180-1208	22	0180-1208
23	0180-1208	23	0180-1208
24	0180-1208	24	0180-1208
25	0180-1208	25	0180-1208
26	0180-1208	26	0180-1208
27	0180-1208	27	0180-1208
28	0180-1208	28	0180-1208
29	0180-1208	29	0180-1208
30	0180-1208	30	0180-1208
31	0180-1208	31	0180-1208

1	0180-1208	1	0180-1208
2	0180-1208	2	0180-1208
3	0180-1208	3	0180-1208
4	0180-1208	4	0180-1208
5	0180-1208	5	0180-1208
6	0180-1208	6	0180-1208
7	0180-1208	7	0180-1208
8	0180-1208	8	0180-1208
9	0180-1208	9	0180-1208
10	0180-1208	10	0180-1208
11	0180-1208	11	0180-1208
12	0180-1208	12	0180-1208
13	0180-1208	13	0180-1208
14	0180-1208	14	0180-1208
15	0180-1208	15	0180-1208
16	0180-1208	16	0180-1208
17	0180-1208	17	0180-1208
18	0180-1208	18	0180-1208
19	0180-1208	19	0180-1208
20	0180-1208	20	0180-1208
21	0180-1208	21	0180-1208
22	0180-1208	22	0180-1208
23	0180-1208	23	0180-1208
24	0180-1208	24	0180-1208
25	0180-1208	25	0180-1208
26	0180-1208	26	0180-1208
27	0180-1208	27	0180-1208
28	0180-1208	28	0180-1208
29	0180-1208	29	0180-1208
30	0180-1208	30	0180-1208
31	0180-1208	31	0180-1208



APPENDIX B

ELECTRIC DIFFERENTIAL MECHANISM

B.1 Introduction

A mechanical differential is a power transmission mechanism that is used to distribute power from one input shaft to two output shafts. This is done in such a way that the sum of the rotational speeds ω_{10} and ω_{20} of the two output shafts is equal to the rotational speed of ω_i of the input shaft, or a constant multiplier of that speed, that is to say

$$\omega_i = \omega_{10} + \omega_{20} \quad \text{B.1}$$

Furthermore the torque T_i of the input shaft is equally distributed to the two output shafts, thus:

$$T_i = T_{10} + T_{20} \quad \text{B.2}$$

where T_{10} , T_{20} are the torques of the two output shafts.

A mechanical differential is essentially composed of linkages and gears. In some cases, physical constraints do not permit the use of a mechanical differential. Also when a mechanical differential is to be used, and the output shafts have to be far apart, a large number of additional power transmission components have to be utilized to transmit power.

Two direct current (DC), permanent magnet (PM), electric motors connected in series were found to duplicate

the function of a differential mechanism. This arrangement will be referred to as an "electric differential mechanism". In applications where a mechanical differential is cumbersome, or impossible to use, an electric differential mechanism can be used. When an electric motor is utilized as the power source, the use of an electric differential mechanism would simplify the design considerably. A typical example of such a case is the driving mechanism of the roller arrangement on the prototype template digitizer. In this case the two output shafts have to be concentric, and electric motors have to be used as the power source.

B.2. Analysis of the electric differential mechanism

For a DC-PM motor operating below its magnetic saturation level, the voltage relation can be approximated by:

$$V_s = R_a i + L_a \frac{di}{dt} + K_v \omega \quad \text{B.3}$$

where V_s is the applied voltage,
 L_a, R_a are the motor winding inductance and resistance respectively,
 i is the current passing in the motor winding,
 K_v is the motor voltage constant,
and ω is the motor shaft rotational speed.

The relation between the torque generated by the motor and the windings current is given by:

$$T = K_T i \quad \text{B.4}$$

where T is the torque generated,
and K_T is the motor torque constant.

Figure B.1 shows a schematic diagram of the circuit of the electric differential mechanism. With reference to the figure, the equations of the circuit are derived as follows: Subscripts 1 and 2 refer to the first and second motor respectively.

$$V_s = V_1 + V_2 \quad \text{B.5}$$

$$T_t = T_1 + T_2 \quad \text{B.6}$$

$$i = i_1 + i_2 \quad \text{B.7}$$

where V_s is the power supply voltage,
 T_t is the total torque of the motors,
and i is the current passing through the motors.

For identical motors, the equations are given by:

$$V_1 = R_a i + L_a \frac{di}{dt} + K_v \omega_1 \quad \text{B.8}$$

$$T_1 = K_T i \quad \text{B.9}$$

$$V_2 = R_a i + L_a \frac{di}{dt} + K_v \omega_2 \quad \text{B.10}$$

$$T_2 = K_T i \quad \text{B.11}$$

Solving Equations B.5 to B.11 simultaneously give:

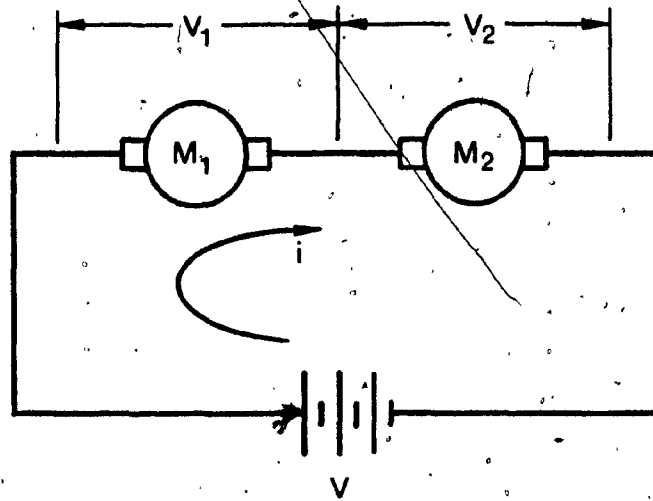


Figure B.1: Circuit Diagram of an Electric Differential Mechanism.

$$V_s = (2R_a)i + (2L_a) \frac{di}{dt} + K_v(\omega_1 + \omega_2) \quad \text{B.12}$$

$$T_1 = T_2 = T_t/2 \quad \text{B.13}$$

Equations B.12 and B.13 resembles those of an equivalent motor with the following parameters;

Winding resistance = $2R_a$

Winding inductance = $2L_a$

Voltage constant = K_v

Torque constant = $2K_T$

The equivalent motor has a rotational speed given by:

$$\omega_i = \omega_1 = \omega_2 \quad \text{B.14}$$

Equations B.13 and B.14 of the motor arrangement in Figure B.1 resembles those of the mechanical differential given by Equations B.2 and B.1 respectively.

B.3 Performance of the electric differential

The torques generated by the two motors in Figure B.1 are equated to the load torques on the motors as follows:

$$T_1 = T_{L1} + J \dot{\omega}_1 + T_F + B \omega_1 \quad \text{B.15}$$

$$T_2 = T_{L2} + J \dot{\omega}_2 + T_F + B \omega_2 \quad \text{B.16}$$

where T_{L1} , T_{L2} are the load torques on the two motors respectively,

J is the combined load and motor inertia,

T_F is the frictional torque of the motor,

and B is the motor damping.

Solving Equations B.15 and B.16 with Equations B.9, B.11, and B.12 simultaneously give:

At steady state $di/dt=0$, thus;

$$\left[\frac{K_V K_T + 2R_a + B}{K_V K_T} \right] \omega_1 + \omega_2 = \frac{V_s}{K_V} - \frac{2R_a (T_{L1} + T_F)}{K_V K_T} \quad \text{B.17}$$

$$\omega_1 + \left[\frac{K_V K_T + 2R_a + B}{K_V K_T} \right] \omega_2 = \frac{V_s}{K_V} - \frac{2R_a (T_{L2} + T_F)}{K_V K_T} \quad \text{B.18}$$

Equations B.17 and B.18 are solved simultaneously to evaluate the two output shafts speeds of the electric differential mechanism at different loading conditions.

The measured and calculated parameters of the PM-DC motors used to drive the template digitizer rollers are listed in Table B.1.

Figure B.2 shows the theoretical and the experimental torque-speed characteristics of the electric differential mechanism. The experimental results were obtained by loading both motors to their total torque setting such that they are operating at different speeds. The rotational speeds of the two motors as well as the sum of the speeds are indicated on the figure. The figure shows an excellent agreement between the theoretical and the experimental results.

B.4 Control scheme for the electric differential mechanism

The rollers (G) and (G') of the template digitizer are

Table B.1: Data of the Motors Used in the Electric Differential Mechanism

No Load Speed	=	804 rad/s	—
Stall Torque	=	35.79 mN.m	5.07 oz in
Friction Torque T_F	=	2.47 mN.m	0.35 oz in
Inertia J	=	4.66 gm cm ²	3.44x10 ⁻⁷ slug ft ²
Maximum Voltage V	=	24 V	—
Stall Current I	=	1.4 A	—
Voltage Constant K_V	=	0.0273 V/rad/s	—
Torque Constant K_T	=	27.32 mN.m/A	3.87 oz in/A
Coil Resistance R_a	=	17.15 Ω	—
Coil Inductance L_a	=	8.62 mH	—
No Load Current	=	0.113 A	—

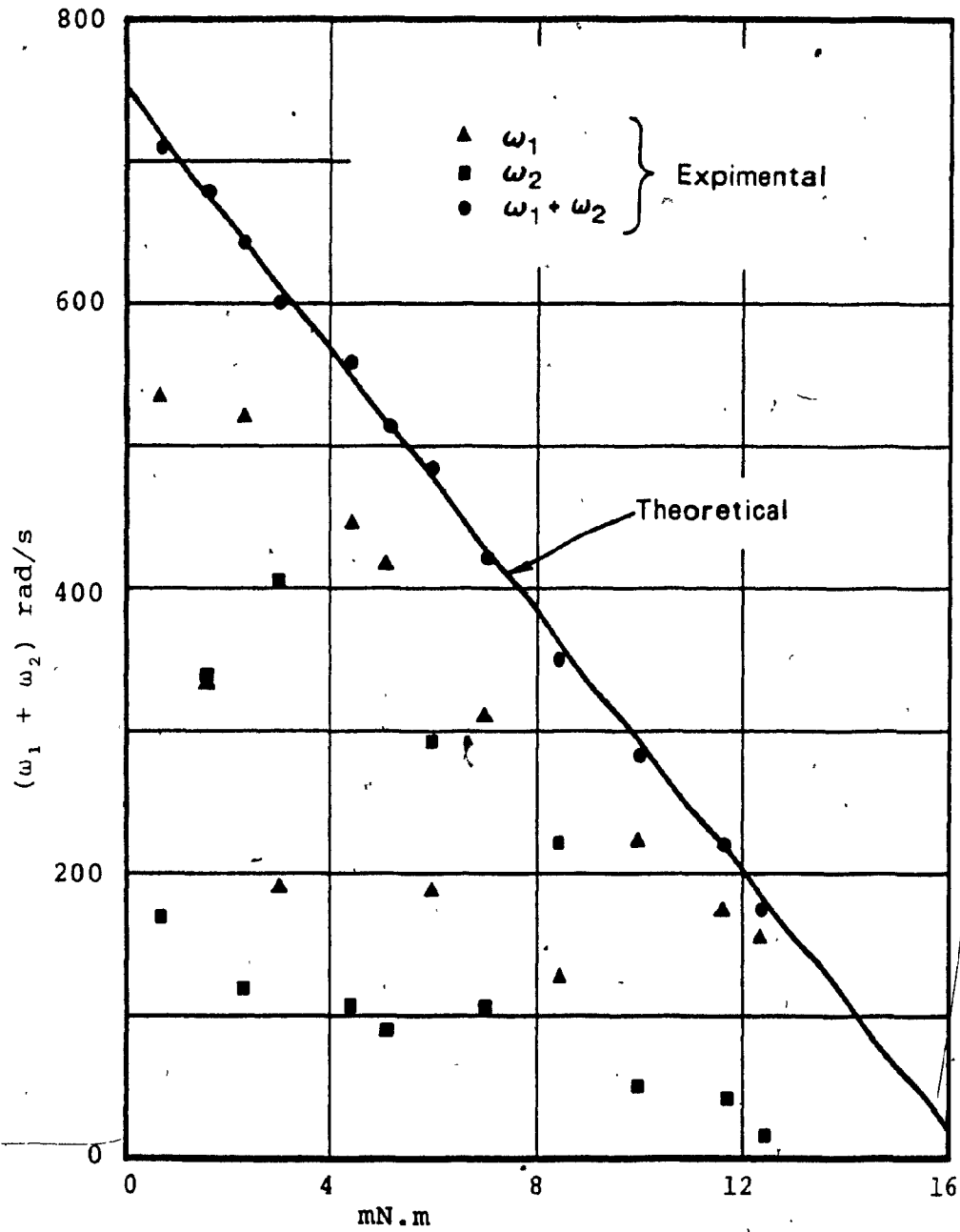


Figure B.2: Torque-Speed Characteristics of an Electric Differential Mechanism.

powered through the electric differential mechanism as described in Section 2.2. Furthermore, the analysis in Section 3.5 shows that in order to maintain a constant contouring speed, a controller utilizing speed feedback from roller (G) has to be used. The controller required to regulate the speed of (G) is complicated in design. This is because it has to be able to vary the speed of roller (G) from infinity to zero while the roller mechanism is tracking certain contours as shown in Figure 3.7.b at sections (1) and (2) respectively

For moderately undulating contours, such a control scheme can be implemented successfully by utilizing conventional feedback controllers, or phase lock loop controllers.

A much simpler control scheme to implement, would entail holding the sum of the two motors speeds constant. This can be implemented by utilizing speed feedback from both rollers. Alternatively, negative impedance circuits, with impedances matched to those of the equivalent motor shown in Section B.2, may be used. This control scheme result in small fluctuations in the contouring speed as shown in Section 3.4. The magnitude of the fluctuations is subject to the nature of the contour.

APPENDIX C

SOFTWARE

DIGITIZER ALGORITHMS

```
-----
C
C THIS PROGRAM KINEMATICALLY RESEMBLES THE INPUT PART
C OF THE POLAR TEMPLATE DIGITIZED SYSTEM.
C THE PROGRAM PRODUCES A FILE CONSISTING OF AXES
C INCREMENTATION VERSUS TIME.
C THE OUTPUT FILE CAN BE TRANSFERED ON MAGNETIC
C TAPE USING THE OUTPUT ROUTINE WHICH IS PROVIDED
C FOLLOWING THIS PROGRAM.
C
C-----
C
COMMON/CURVE/ RI, EPS, RR, BB, AA
COMMON/PAR/ PY, ROOT(4), WE(4), NN
COMMON/OPR/ FUN
DATA KKK/1/
DATA RI, EPS, RR, AA, BB/5.0, 70.0, 0.125, 2.0, 3.0/
DATA ROOT/2*0.3399810435849, 2*0.861136311594/
DATA WE/2*0.6521451548625, 2*0.3478548451374/, IK/1/, IL/1/
C-----
C ENTER CONTOURING SYSTEM RESOLUTIONS, RADIAL THEN ANGULAR
PRINT *, 'ENTER RADIAL THEN ANGULAR RESOLUTIONS'
READ *, DELR, DELTH
C-----
C ENTER NUMBER OF ITERATIONS BEYOND WHICH SEARCH OR THE
C ROOT IS INITIATED IN THE REVERSE DIRECTION
PRINT *, 'ENTER MAXIMUM ALLOWABLE NUMBER OF ITERATIONS'
READ *, NN
C-----
C ENTER OPERATING PARAMETERS:
C RI = CONTOUR POLE RADIAL DISPLACEMENT
C EPS = CONTOUR POLE ANGULAR DISPLACEMENT
C RR = TOOL RADIUS
PRINT *, 'ENTER CONTOUR POLE RADIAL AND ANGULAR DISPLACEMENTS'
READ *, RI, EPS
PRINT *, 'ENTER TOOL RADIUS'
READ *, RR
C-----
C ENTER CONTOUR PARAMETERS
PRINT *, 'ENTER CONTOUR PARAMETERS'
READ *, AA, BB
C IF MORE PARAMETERS ARE REQUIRED TO EXPRESS THE CONTOUR, ADD
C THEM TO THE COMMON BLOCK "CURVE".
C-----
ROOT(2) = -ROOT(2)
ROOT(4) = -ROOT(4)
PY = 2 * ASIN(1.0)
THE = 34.50471682
GAM = GAMM = 0.0
AL = 8.294224337
EPS = EPS * PY / 180.0
DELTH = DELTH * PY / 180.0
THE = THE * PY / 180.0
GAM = GAMM = GAM * PY / 180.0
ALL = INT(AL / DELR) * DELR
10 CONTINUE
T = TEMP
NM = NM + 1
GAMM = GAM
TT = TT + T
PRINT 1000, NM, T, LLL, KKK, THE, ALL, GAM, FUN, TT, AL
IF(GAM .GT. 2 * PY) GO TO 100
31 CONTINUE
THE = THE + IK * DELTH
GAM = GAMA(GAM, THE, AL, 0, N)
IF(N .LT. NN) GO TO 30
IK = -IK
THE = THE + IK * DELTH
GO TO 31
30 CONTINUE
SD = SR(GAMM, GAM)
T = TEMP = SD / VEL
810
```

```
M=ABS(ALL-AL)/DELR 820
IF(M .LT. 1) GO TO 10 830
TEMPAC=0.0 840
DO 20 I=1,M 850
41 CONTINUE 860
ALL=ALL+IL*DELR 870
GAM=GAMA(GAMM,THE,ALL,1,N) 880
IF(N .LT. NN) GO TO 40 890
IL=-IL 900
ALL=ALL+IL*DELR 910
GO TO 41 920
40 CONTINUE 930
SD=SR(GAMM,GAM) 940
GAMM=GAM 950
T=SD/VEL 960
TEMPAC=TEMPAC+T 970
NM=NM+1 980
TT=TT+T 990
PRINT 1000, NM, T, KKK, LLL, THE, ALL, GAM, FUN, TT 1000
20 CONTINUE 1010
TEMP=TEMP-TEMPAC 1020
GO TO 10 1030
100 CONTINUE 1040
1000 FORMAT(1X, I6, 2X, E18.10, 2X, 2(I1, 2X), 6(F10.6, 2X)) 1050
STOP 1060
END 1070
C 1080
C 1090
C 1100
FUNCTION GAMA(GAA,THE,AL,IFL1,N) 1110
C----- 1120
C 1130
C THIS ROUTINE ITERATIVELY FINDS THE ANGULAR AND RADIAL 1140
C DISPLACEMENTS OF A POINT ON THE CONTOUR WITH RESPECT 1150
C TO THE MACHINE POLE. 1160
C THE ROUTINE USES NEWTON RAPHSON UNMODIFIED ITERATIVE 1170
C METHOD TO SOLVE FOR THE ROOTS OF THE EQUATIONS 1180
C DESCRIBING THE SYSTEM 1190
C----- 1200
C 1210
C 1220
COMMON/CURVE/ RI, EPS, RR, BB, AA 1230
COMMON/PAR/ PY, ROOT(4), WE(4), NN 1240
COMMON/OPR/ FUN 1250
C----- 1260
C FOR THE FLAG "IFL" 1270
IFL=0 EXECUTE ANGULAR LOOP 1280
IFL=1 EXECUTE RADIAL LOOP 1290
C----- 1300
GMA=GAA 1310
DO 40 K=1,NN 1320
GAMA=GMA 1330
CALL EBUA(GAMA, FUN, DFUN, DDFUN) 1340
IF(ABS(DFUN) .LT. 1.0E+99) GO TO 10 1350
PHI=0 1360
GO TO 20 1370
10 CONTINUE 1380
IF(ABS(DFUN) .GE. 1.0E-99) GO TO 30 1390
PHI=PY/2.0 1400
GO TO 20 1410
30 CONTINUE 1420
PHI=PY/2.0-ATAN(DFUN/FUN) 1430
20 CONTINUE 1440
DPHI=(DFUN**2-FUN*DDFUN)/(DFUN**2+FUN**2) 1450
IF(IFL1.EQ. 1) GO TO 50 1460
SINE=SIN(THE-GAMA) 1470
F=RI*SIN(EPS-THE)-RR*Cos(THE-GAMA-PHI)-FUN*SINE 1480
DF=-RR*SIN(THE-GAMA-PHI)*(1+DPHI)-DFUN*SINE+FUN*Cos(THE-PHI) 1490
GO TO 60 1500
50 CONTINUE 1510
GOSPH=COS(PHI) 1520
SINPH=SIN(PHI) 1530
```



```
SUM=(GAMM+GAM)/2.0
AI=0.0
DO 10 I=1,4
X=SUM+DIF*ROOT(I)
CALL EQUA(X,FUN,DFUN,DDFUN)
AI=AI+WE(I)*FUN
10 CONTINUE
SR=ABS(DIF*AI)
RETURN
END
EO: ENCOUNTERED.
```

2260
2270
2280
2290
2300
2310
2320
2330
2340
2350

*				100
	OUTPUT PROGRAM FOR THE SOFTWARE DIGITIZER.			110
	PROGRAM IN TI-990/980 MICRO COMPUTER ASSEMBLER CODE			120
	DATA STORED AS FOLLOWS:			130
	BIT 0 = 1 TO ALLOW REAL TIME CLOCK OPERATION			140
	BITS 1 TO 14 CONTAIN THE TIME PERIOD BETWEEN SIGNALS			150
	BITS 14 AND 15 CONTAIN THE AXES INFORMATION			160
*				170
*				180
*				190
200	02E0	LWPI >1E0	INITIALISE WORK SPACE COUNTER	200
202	01E0			210
204	0202	LI R2,>300	DATA START AT LOCATION	220
206	0300		300 IN MEMORY	230
			START OF THE OUTPUT LOOP	240
208	020C	* ST LI R12,>00	SET BASE ADDRESS TO U10 9901	250
20A	0000			260
20C	3392	LDCR *R2,14	LOAD FIRST 14 BITS INTO CLOCK REGISTER	270
			AND START THE CLOCK	280
20E	1E00	SBZ 0	SWITCH 9901 TO INTERRUPT MODE	290
210	1D03	SBO 3	ENABLE U10 9901 TO INTERRUPT ON LEVEL 3	300
212	020C	LI R12>03C	SET POINTER TO BIT 14 OF THE CURRENT	310
214	003C		DATA WORD	320
216	0340	IDLE	PUT COMPUTER IN IDLE STATE, TO BE	330
			AWAKENED BY INTERRUPT	340
218	0340	* LWPI >1E0	INITIALIZE WORK SPACE, USED HERE	350
220	01E0		TO BALANCE TIMING OF THE LOOP TO MINIMUM	360
222	3062	LDCR *R2+,2	OUTPUT 2 BITS STARTING FROM THE	370
			LOCATION OF THE POINTER IN THE DATA WORD	380
21A	10F6	* JMP ST	GO TO BEGINING OF OUTPUT LOOP	390
			IF DATA STILL EXIST IN MEMORY	400
			PERIOD OF THE REAL TIME CLOCK	410

APPENDIX D
PERFORMANCE EVALUATION
OF THE TEMPLATE DIGITIZER

D.1 Introduction

The template digitizer is tested to evaluate both the digitization accuracy and the error in contouring speed. The hybrid computer EAI 680/640 is used as a means of collecting and preprocessing the radial and angular shaft encoder signals. The sequence of the radial and angular signals, as well as the time periods between these signals, are recorded. The sequence of the signals is used to evaluate the accuracy of the digitization process. The time periods between the signals are used to calculate the contouring speed.

The data collected on the hybrid computer is subsequently transmitted to the CDC CYBER 835 for processing.

D.2 Testing circuit

Figure D.1 shows a block diagram of the different components used to extract the required information and the flow of signals between these components. With reference to the figure, the four outputs generated by the digitizer encoders are combined into two signals using the recording circuit. The two signals are then recorded independently on two channels of an FM magnetic tape recorder. A high tape

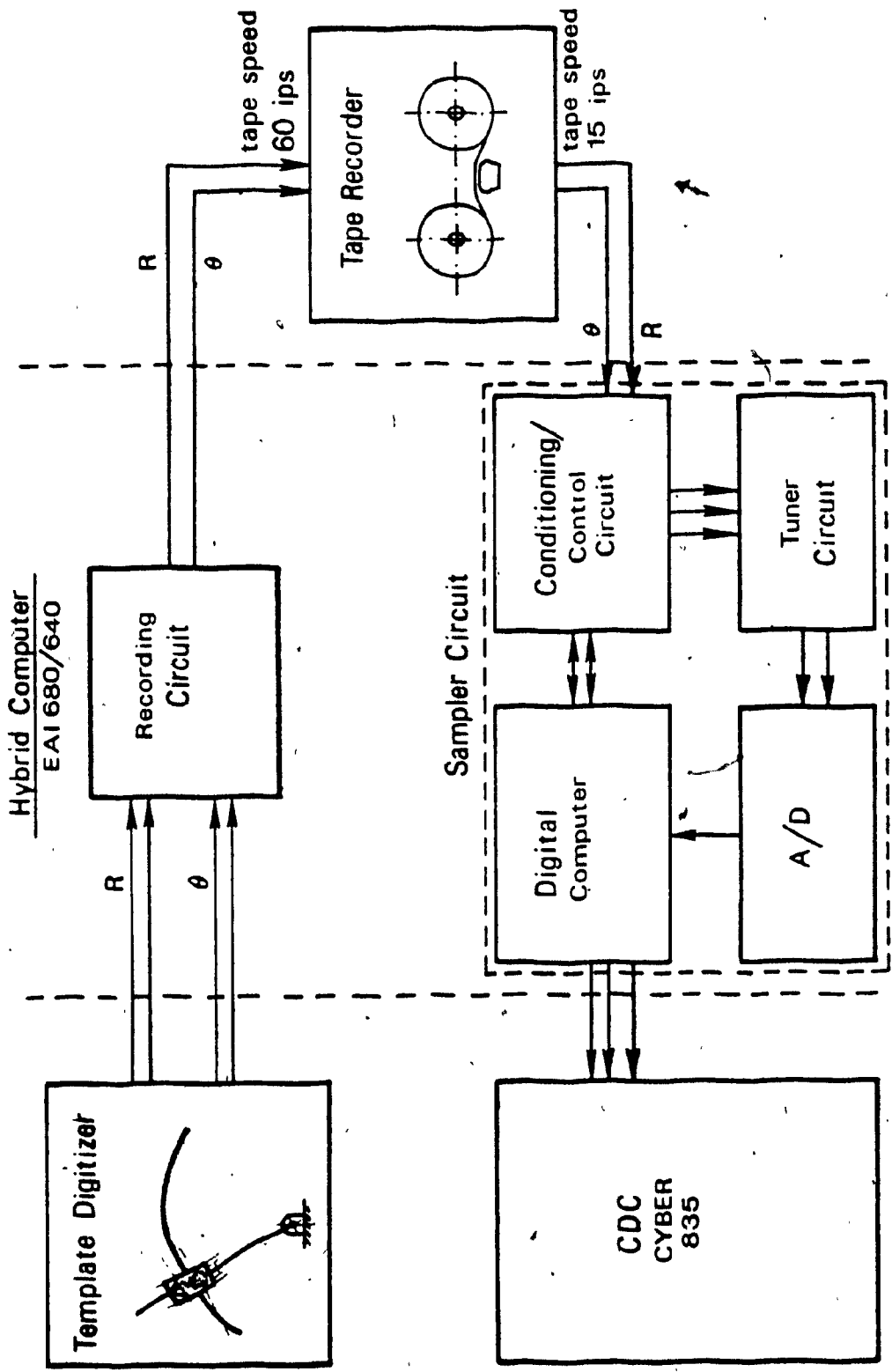


Figure D.1: Block Diagram of the Circuits Used in the Performance Evaluation of the Template Digitizer.

speed of 152.4 cm/s is used for recording. The recorded signals are then played back at a low tape speed of 38.1 cm/s and fed to the sampler circuit. Recording at high tape speeds and then playing back at low speeds scales up the time period between the signals, and allows more accurate time measurement. The sampler circuit processes the two incoming signals and generates two sets of digital output that feed into the digital computer part of the hybrid computer. One of these sets corresponds to the sequence of radial and angular signals, while the other set corresponds to the time period between the signals. The digital computer accumulates the data in a file until the end of the run. The file is then transferred to the CDC CYBER 835 for analysis.

The recording circuit is shown in Figure D.2: The circuit is a direct implementation of the one in Figure 2.9. The output of the circuit is scaled to 2 volts (p.p.) to match the maximum input signals level of the tape recorder. The digital components on the analog computer are synchronized to the computer clock, consequently the accuracy of timing between the recorded encoder signals is within one clock period, 1 μ s. At the beginning of each recording, an accurate reference signal is taped and is used later for calibration.

The recorded signals are slowed down when played back as has been mentioned earlier. The played back signals are fed to the sampler circuit. The circuit is shown in

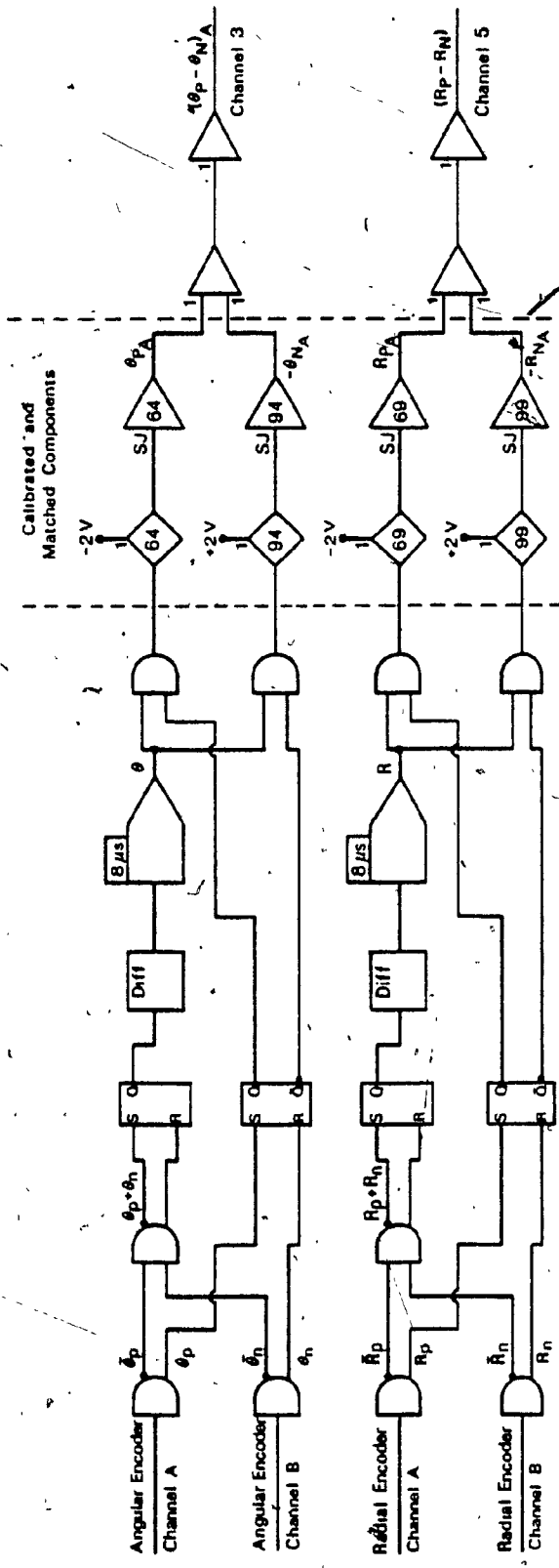


Figure D.2: Recording Circuit for the Encoder Signals.

Figure D.3. It consists essentially of two parts, these are:

Input part; this part uses threshold comparators to restore the played back signals to digital logic level and shape. The reconstructed signals are then processed by a digital part to give four logic signals. These signals indicate either the radial or angular axis indexed and its direction of motion. The four signals are stored temporarily in a register.

Timing part; the timing part of the circuit uses three operational amplifiers connected as integrators. The input to the integrators is a constant voltage. When the circuit is allowed to integrate, the voltage on the output of the integrator is proportional to time. Three integrators are used to circumvent the problem of the finite time required to sample an integrator output, and reset the integrator. The three integrators are operated in a cyclic order. While one integrator is integrating, the second is being sampled, and the third is being reset. The function of the three integrators is controlled by a logic circuit based upon the four signals generated by the input part of the sampler circuit. An integrator starts integrating the constant input voltage at the beginning of any transient indicating indexation, and is put in a hold state at the occurrence of the next such transient. The output of the integrator is converted into a digital equivalence using an A/D converter. The digital equivalence of time as well as the four signals

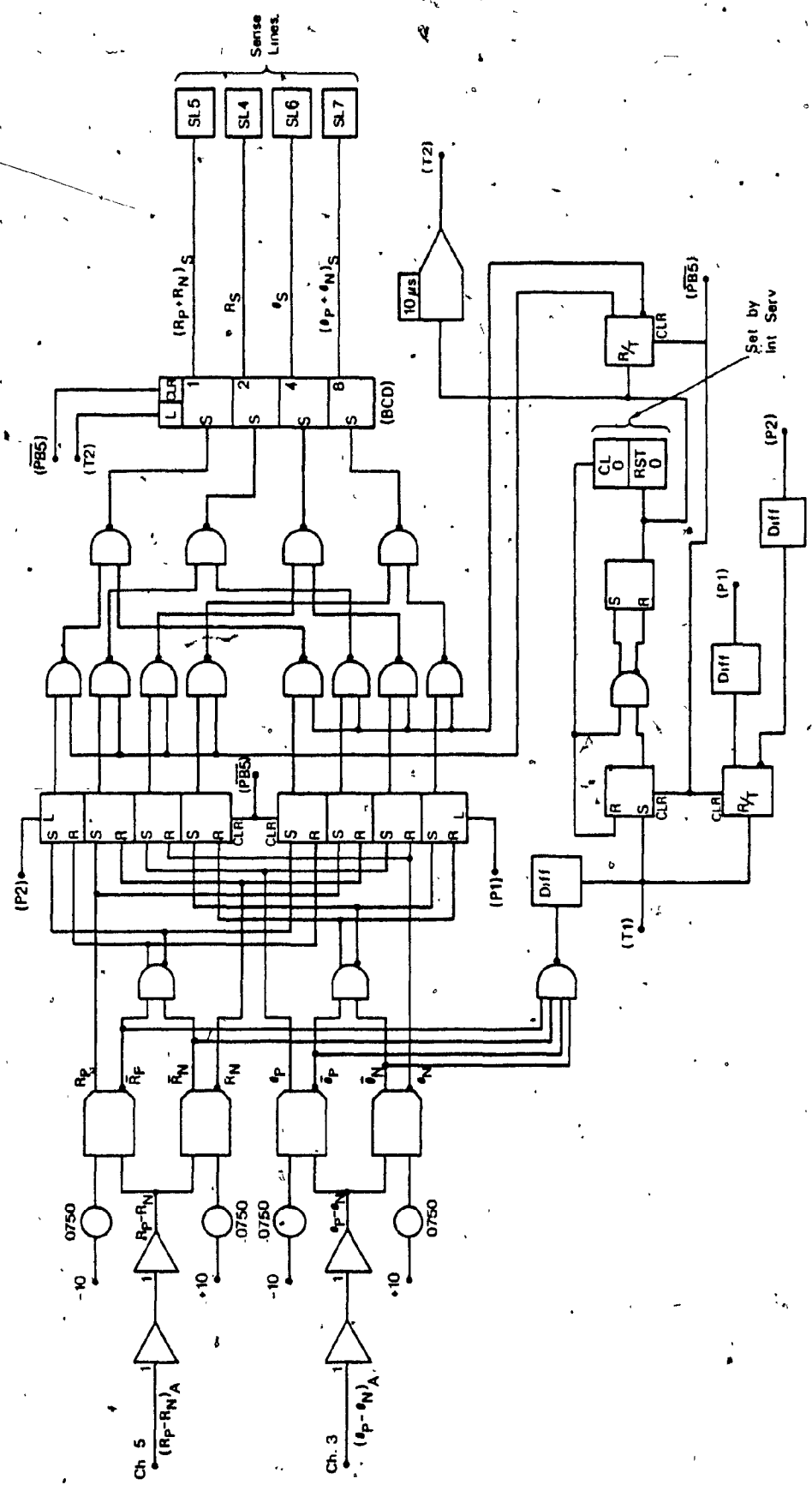


Figure D.3: Sampler Circuit for the Recorded Encoder Signals. (continued on D.7).

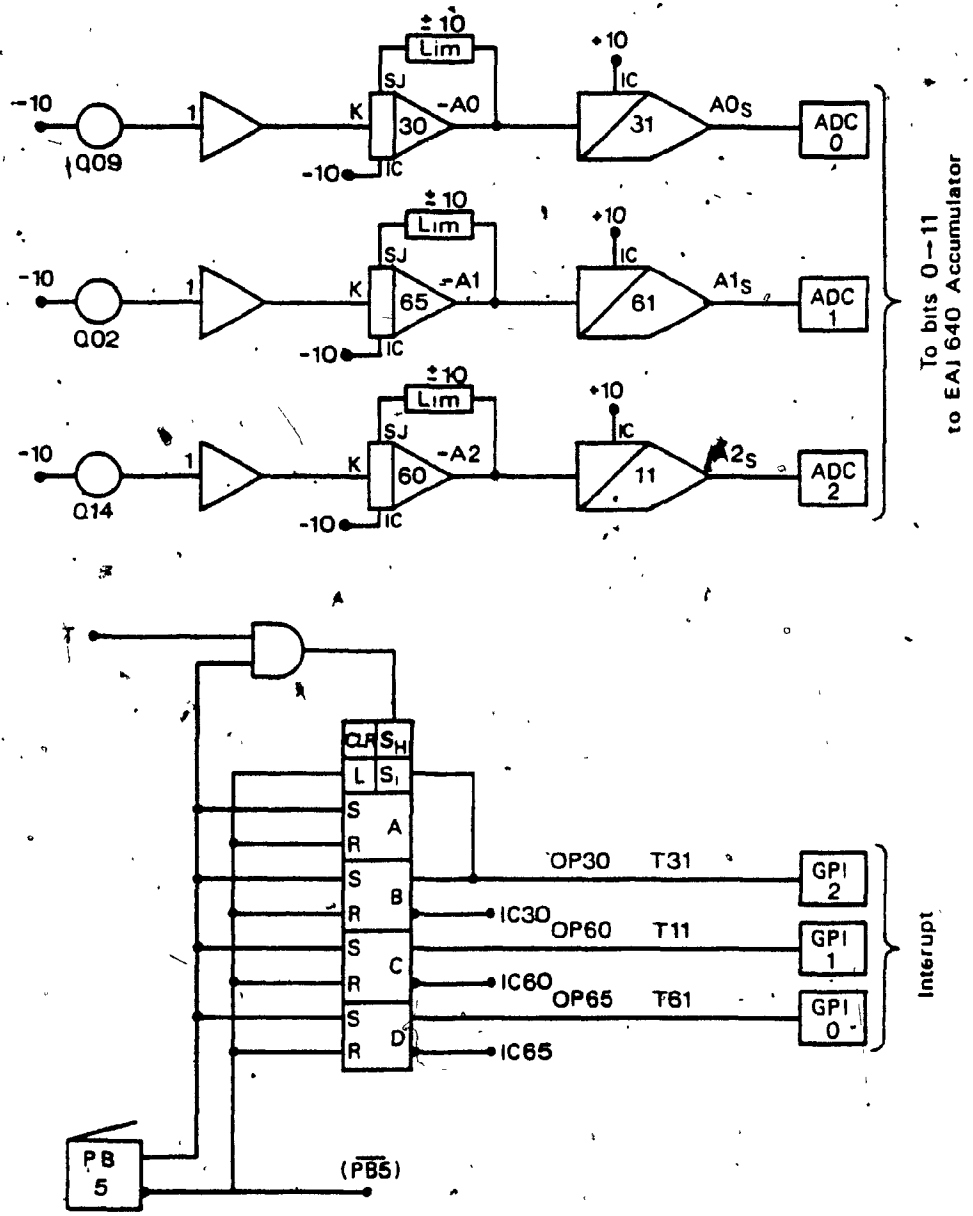


Figure D.3: Sampler Circuit for the Recorded Encoder Signals.

from the input part are compiled into one 16 bit computer word and transferred to the digital computer memory. The data are transferred from the analog part of the computer to the digital part in INTERRUPT mode of operation. Interrupts are generated when either the radial or angular template digitizer axes index.

An ASSEMBLER program executes on the EAI 640 and controls the hybrid computer operation to carry out the testing. A listing of this program is provided at the end of this appendix.

The data collected by the hybrid computer are subsequently transferred in ASCII code to the CYBER 835 for analysis. Two FORTRAN programs carry out a two stage decoding of the collected data and prepare them for analysis. Listings of the decoding programs are also provided at the end of this appendix.

D.3* Results of testing

An analysis of the collected data showed that the template digitizer perform the contour digitization process accurately for the three templates shown in the photograph in Figure 3.3. The data collected in testing of the line template were also used in verifying the objective function for area error minimization and are shown in Figure 4.8. The agreement between the theoretically and experimentally calculated objective functions serve as an implicit verification of the accuracy of digitization.

The analysis of the time signals collected, shows that for all practical purposes the contouring speed is found to be constant. At the beginning of motion, however, when power is switched on for the the roller mechanism motors, the contouring speed was found to oscillate for a short time. Furthermore, whenever the roller mechanism motion is disturbed by template imperfections in the form of indentations, oscillation starts again but lasts only or a short time.

* ACQUISITION SYSTEM MAIN PROGRAM.

* ----- ATEF -----

* VER. 1.4 APR. 28/1981 DRH

* ORIGINATED FROM AGO VER. 3.2

* AT PAUSE ENTER A=#OF POINTS.

* NAME ACQUIR
* ABS '1000

* ACQUIR EQU * SET UP REGISTER OPTIONS.
* P 0

* STA LENTH

* EX

* LA/ FWAD

* EG L,I ASAMPL

* L,X LENTH

* LA FWAD

* EG L,I

* J ASENDR

* ACQUIR

* LENTH OCT 0

* FWAD OCT 2000

* ASAMPL ADR SAMPLE

* ASENDR ADR SENDER

* BSS 3 KEEP BUFF ADD. AT 1030.

* BUFF BSS '634

* BUFO BSS 82

* EACB BSS 1

* SUBROUTINE SAMPLE

* USED TO SAMPLE ADC AT SPECIFIED RATES WITH
* SPECIFIED AMOUNTS OF DATA,
* DIRECTED TO A SPECIFIED BUFFER AREA.

* FIRST 12 BITS OF WORD IS ADC VALUE,
* LAST 4 BITS IS SL4,SL5,SL6,SL7.

* TO USE:

* L SAMPLE

* -X- CONTAINS NUMBER OF POINTS TO SAMPLE,
* RANGE IS FROM 1 TO 15000.

* -G- CONTAINS DATA BUFFER START ADDRESS,
* NORMALLY '2000.

* SAMPLER CLOCK FROM EA1680 - GP INTERRUPT 0.

** ABS '10

** SAMPLE ADR 0

** EG

** STA FFWA BUFFER FWA TO -A-

100
110
120
130
140
150
160
170
180
190
200
210
220
230
240
250
260
270
280
290
300
310
320
330
340
350
360
370
380
390
400
410
420
430
440
450
460
470
480
490
500
510
520
530
540
550
560
570
580
590
600
610
620
630
640
650
660
670
680
690
700
710
720
730
740
750
760
770
780
790
800
810

EQ					820
STX	LENGTH	SAVE	BUFFER	LENGTH.	830
EX					840
A	FFWA	ADD	FWA	TO	850
STA	BFPNT	SAVE	IN	BUFFER	860
LA	LENGTH	GET	BACK	LENGTH.	870
TCA					880
SSP					890
STA	LENGTH	FOR	NEG	VALUE	900
EX					910
LA	DF680				920
DO	'53	SELECT	ANALOG	CONSOLE.	930
LA	CLOT8				940
DF	'43	RESET	CL-0,CL2,CL4,CL6,CL8		950
LA	AGPI0				960
STA	'705	SET	UP	INT. POINTERS.	970
LA	AGPI1				980
STA	'706				990
LA	AGPI2				1000
STA	'707				1010
LA	NADC				1020
A	BFPNT	WILL	IGNORE	1ST	1030
STA	BFPNT				1040
LA	SLMASK	INITIALIZE	FIRST	SL	1050
STA	OLDSL				1060
J	SAM	START	SAMPLING.		1070
*					1080
*****					1090
*					1100
NADC	OCT	177777			1110
MSKGPI	OCT	160000			1120
LENGTH	OCT	0			1130
FFWA	OCT	0			1140
BFPNT	OCT	0			1150
DF680	OCT	40			1160
CLO	OCT	100000			1170
INT680	OCT	100000			1180
KREG	OCT	1000			1190
AGPI0	ADR	SERV0			1200
AGPI1	ADR	SERV1			1210
AGPI2	ADR	SERV2			1220
CLOT8	OCT	125200			1230
*					1240
*****					1250
*					1260
SAM	EQU	*			1270
LA	ES	KREG			1280
LA	INT680	ENABLE	CONSOLE	1	1290
DO	'54	INTERRUPT.			1300
LA	MSKGPI				1310
DO	'46	ENABLE	GPO-2	INTERRUPTS.	1320
CLR					1330
DF	'64	SELECT	ADC-0	AND	1340
LA	CLO	CONVERT.			1350
DF	'41	SET	CL-0.		1360
HWAIT	SMI				1370
J	*	WAIT	FOR	INTERRUPT.	1380
*					1390
*****					1400
*					1410
*	SERVICE	ROUTINES	SERV0,SERV1,SERV2		1420
*					1430
*	ADC	CHANNELS	0,1,2	ONLY.	1440
*					1450
SERV0	OCT	0			1460
OCT	0				1470
CLR		SET	UP	AD	1480
J	SAMP	CHAN	0.		1490
SERV1	OCT	0			1500
OCT	0				1510
LA	ADC1				1520
					1530

```

SERV2 J      SAMP      1540
      OCT      0      1550
      OCT      0      1560
      LA      ADC2     1570
      J      SAMP     1580
ADC1  OCT      1      1590
ADC2  OCT      2      1600
*                                           1610
* SAMPLE SELECTED ADC AND COMBINE WITH SL4-7. 1620
*                                           1630
SAMP  EG      '44      SAVE ADC CHANNEL NO.      1640
      SI      '45      READ SL'S 4,5,6,7 FOR      1650
      SI      '46      RESET TO ZERO.      1660
      SI      '47      1670
      DI      '65      READ CURRENT ADC VALUE(PREVIOUS CONVERT) 1680
      EG      '64      START NEXT CONVERSION.      1690
      DI      '42      READ ALL 8 SENSE LINES.      1700
      EG      AND      ADMASK      1710
      OR      OLDSSL      COMBINE DATA WITH PREVIOUS SENSE LINES. 1720
      STA,IX BFPNT      STORE LATEST VALUE IN BUFFER.      1730
      EG      AND      SLMASK      1740
      AND      OLDSSL      SAVE NEW SENSE LINES.      1750
      STA      CLOTB      1760
      LA      '41      TURN ON CL#0,CL#2,CL#4,CL#6,CL#8 1770
      DF      1      1780
      ICX     **2      1790
      J      **2      FINISHED SAMPLING.      1800
      J      **2      WAIT FOR NEXT INTERRUPT.      1810
      LA      WWAIT      1820
      DO      INT680     DISABLE 680 INT.      1830
      LA      '53      1840
      LA      MSKGPI     DISABLE GP INT.      1850
      DO      '40      1860
      J,I     SAMPLE     RETURN TO CALLER AT END OF BUFFER. 1870
SLMASK OCT      17      1880
ADMASK OCT      177760  1890
OLDSSL OCT      17      1900
*                                           1910
*****                                           1920
*                                           1930
*****                                           1940
*                                           1950
*                                           1960
*                                           1970
*                                           1980
* SUBROUTINE SENDER      1990
*                                           2000
* SENDS A SPECIFIC MEMORY BUFFER OF SPECIFIED      2010
* LENGTH TO DATA PHONE CONTROLLER.      2020
*                                           2030
* ASSUMES THAT PROTOCOL IS 6000 TEXT MODE,      2040
* THEREFOR SENDS 80 CHARS PLUS CR      2050
* WAITS FOR LF AND SENDS AGAIN.      2060
*                                           2070
* THE MOST SIGNIFICANT 12 BITS OF EACH MEMORY      2080
* IS THE ADC VALUE, WHILE THE LAST 4 BITS      2090
* REPRESENT THE RELATED SL SETTINGS (SL4-SL7).      2100
* THE COMPLETE 18-BIT WORD IS SENT AS 4 ASCII CHARS      2110
* IN THE RANGE '301 TO '320 (A TO P).      2120
*                                           2130
* TO RECOVER THE 12 BIT PORTION OF THE WORD, SUBTRACT 1      2140
* FROM EACH OF 1ST 3 CHARS IN EACH GROUP OF 4 AND      2150
* ASSEMBLE THE LEAST SIGNIFICANT 4 BITS OF      2160
* EACH OF 3 CHARS INTO A 12 BIT WORD.      2170
*                                           2180
* TO RECOVER THE 4-BIT SENSE-LINE WORD, SUBTRACT 1      2190
* FROM LAST CHAR IN EACH GROUP OF 4 AND KEEP LEAST      2200
* SIGNIFICANT 4 BITS OF THE CHARACTER.      2210
*                                           2220
*                                           2230
* TO USE      2240
*                                           2250

```

```

* L SENDER
*
* -X- CONTAINS BUFFER LENGTH
*
* -B- CONTAINS BUFFER FIRST WORD ADDRESS:
*
* WHEN IN TEXT MODE, START SENDING DATA
* BY ENTERING CNTRL R ON TTY.
*
* SSW A WILL SEND S CHAR TO COMM. MODULE.
*
*
* ACC OCT 0
* PSW OCT 100
* FWA ADR BUFF
* INP OCT 0
* OUTP OCT 0
*
*****
* ROC OCT 0
* STA ACC
* L FSTAT WAIT FOR WREG FROM COMM. MODULE.
* LA, I ACC
* OR FT
* DF '30 SEND OUT ONE LINE OF DATA.
* AOM ACC
* C CR
* SE
* J *-7
* LA FLAG
* SAE WAIT FOR LAST OUTPUT
* SKU INTERRUPT FLAG - COMM. MODULE.
* J, I *-3
* ROC
*
*****
* INITC OCT 0
* LA SFLAG RESET OUTPUT INTERRUPT
* STA FLAG FLAG FOR COMM. MODULE.
* LA DFON
* DF '30
* LA AINTC
* STA '674
* LA ASRV
* STA '646
* J, I INITC
* SFLAG OCT 0
*
*****
* DIAL OCT 0
* LA TTD
* DF 1
* L STAT
* LX D24
* DL1 LA, X MSG
* DO 1
* L STAT
* DCX 1
* J DL1
* LA TTD
* DF 2
* DI 2
* L SONE SEND ONE TTY CHAR TO COMM. MODULE.
* J, I DIAL
* MSG OCT 212, 215
* DATA S\NI GOL ,MEDOM NO NRUT\
* OCT 212, 215

```

2260
2270
2280
2290
2300
2310
2320
2330
2340
2350
2360
2370
2380
2390
2400
2410
2420
2430
2440
2450
2460
2470
2480
2490
2500
2510
2520
2530
2540
2550
2560
2570
2580
2590
2600
2610
2620
2630
2640
2650
2660
2670
2680
2690
2700
2710
2720
2730
2740
2750
2760
2770
2780
2790
2800
2810
2820
2830
2840
2850
2860
2870
2880
2890
2900
2910
2920
2930
2940
2950
2960
2970

Q24 DEC 24

```

*
*****
*
STAT  OCT      0
      SI      0
      ADA
      SAE
      J      *-3
      J, I    STAT
TTO   OCT      100012
TTI   OCT      100016
CR    OCT      50015
EOT   OCT      204
ESC   OCT      33
*
ASRV  ADR      SERV
DFON  OCT      130620
AINTC ADR      INTRC
*
***** SENDER *****
*
SENDER EQU      *
      OCT      0
      EQ
      STA      MP      GET BUFFER FIRST ADDRESS,
                          AND PUT IN MEMORY POINTER.
      EX
      A      MP      GET BUFFER LENGTH
                          ADD FIRST ADDRESS
      STA      ME      AND SET INTO MEMORY END- POINTER.
      L      INTC
      LA      FWA
      STA      INP      RESET IN BUFF POINTER.
      STA      OUTP     RESET -TTY BUFF POINTER.
      L      DIAL
      LA      TTI
      DF      2
LOGIN  L      BRIC
      SSW      A
      J      SENDS
      LA      OUTP
      C      INP
      SGE
      J      TYPE
      P      0      WAIT FOR, INTERRUPT OUT OF P.
      J      LOGIN+1
*
*****
*
SERV  OCT      0
      OCT      0
      DI      2
      C      EOT
      SNE
      LA      ESC
      C      CNTR
      SNE
      J      RREAD     CODE AND SEND LINE IF CNTRL-R-.
DOUT  EQ      FSTAT    WAIT FOR COMM. MODULE WREQ.
      EQ
      OR      FT
      DF      '30      OUT CHAR TO COMM. MODULE.
      LA      FWA
      STA      INP
      STA      OUTP
      J      LOGIN
CNTR  OCT      222
FLAG  BSS      1
FT    OCT      50000
*
*****

```

```

2980
2990
3000
3010
3020
3030
3040
3050
3060
3070
3080
3090
3100
3110
3120
3130
3140
3150
3160
3170
3180
3190
3200
3210
3220
3230
3240
3250
3260
3270
3280
3290
3300
3310
3320
3330
3340
3350
3360
3370
3380
3390
3400
3410
3420
3430
3440
3450
3460
3470
3480
3490
3500
3510
3520
3530
3540
3550
3560
3570
3580
3590
3600
3610
3620
3630
3640
3650
3660
3670
3680
3690

```

```

*
* TYPE LA DF TTO 3700
      L LA,I 3 3710
      DO 3 3720
      L AOM 3 3730
      LA DF 3 3740
      J LOGIN+1 2 3750
*
*****
* FSTAT OCT 0 3760
      STA 0 TEMP 3770
      LA FLAG 3780
      SAE COMM. MODULE READY FOR OUTPUT? 3790
      SKU *-3 3800
      CLR 3810
      STA FLAG RESET OUTPUT FLAG. 3820
      LA TEMP 3830
      J,I FSTAT 3840
      BSS 1 3850
*
*****
* INITIALIZE COMM. MODULE FOR INTERRUPTS. 3860
* 3870
* 3880
* 3890
* BRIC OCT 0 4000
      ES 0 4010
      OR PSM SET UP INT. MASK. 4020
      ES 4030
      LA FWA INITIALIZE INPUT 4040
      STA INP BUFFER POINTER. 4050
      SMI 4060
      J,I BRIC 4070
*
*****
* INTERRUPT SERVICE ROUTINE, COMM. MODULE. 4080
* 4090
* 4100
* 4110
* 4120
* INTRC OCT 0 4130
      OCT 0 4140
      SI '30 4150
      SKP IS RREG ON ? 4160
      J READ 4170
      LLS 1 4180
      SKN IS WREG ON ? 4190
      J ERROR 4200
      LA DFWR RESET WREG 4210
      DF '30 4220
      LA ONE TURN ON OUTPUT 4230
      STA FLAG INTERRUPT FLAG. 4240
      LA INTRC+1 4250
      SMI 4260
      J,I INTRC 4270
      AND RMASK GET INPUT CHAR. 4280
      OR BIT8 TURN ON PARITY BIT. 4290
      STA TEMP1 4300
      LA DFWR RESET RREG. 4310
      DF '30 4320
      LA TEMP1 4330
      STA,I INP SAVE IN CHAR. BUFFER 4340
      AOM INP 4350
      C BPNT CODING BUFFER ADDRESS 4360
      SGE EXCEEDED ? 4370
      J **4 4380
      LA FWA 4390
      STA INP RESET IN BUFF POINTER. 4400
      STA OUTP RESET TTY BUFF POINTER. 4410

```



```

LA          INTRC+1
SMI
J,I        INTRC
*
ERROR      LRS      1
           P        '77      NOT WREG OR RREG.
*
DFWR       OCT      10620
RMASK      OCT      377
TEMP1      BSS      1
DFWC       OCT      100620
BITS       OCT      200
ONE        OCT      1
*
DOC        EQU      ROC
*
*****
*
RREAD      SMI
           LA        BPNT
           STA       BI,BO
           LX        BPNT
           L         ROR
           LA        BPNT
           L         DOC
           L         WAIT
           J         RREAD+1
*
*****
*
WAIT       OCT      0
           LA        FWA
           STA       INP,OUTP
PAS        P        1      WAIT FOR INTERRUPT.
           LA,I      OUTP
           ADM       OUTP
           C         LF
           SE
           J         PAS
           L         DELAY ,DELAY 0.3 SEC.
           J,I      WAIT
LF         OCT      212
SAVE       OCT      0
*
*****
*
DELAY      OCT      0
           LA        NEG      GIVES 0.3 SEC DELAY.
           STA       NCNT
           LRS      '16
           NOP
           NOP
           ADM       NCNT
           J         *-4
           J,I      DELAY
NEG        DEC      -15384
NCNT       BSS      1
*
*****
*
ROR        OCT      0
           STX      SAVE
           STX      BP
           LX        DM20
AGN        LA        DM4
           STA      COUNT
           LA        MP
           S         ME      1ST WRD ADDRESS OF DATA BUFF.
           SNE      ME      LAST WRD ADD. OF DATA BUFFER.
           J         EXIT
           LA,I     MP
           ADM      MP
*

```

4420
4430
4440
4450
4460
4470
4480
4490
4500
4510
4520
4530
4540
4550
4560
4570
4580
4590
4600
4610
4620
4630
4640
4650
4660
4670
4680
4690
4700
4710
4720
4730
4740
4750
4760
4770
4780
4790
4800
4810
4820
4830
4840
4850
4860
4870
4880
4890
4900
4910
4920
4930
4940
4950
4960
4970
4980
4990
5000
5010
5020
5030
5040
5050
5060
5070
5080
5090
5100
5110
5120
5130

NXT	EQ				5140
	CLR				5150
	LLD	4			5160
	A	K301			5170
	STA,I	BP	SET UP TEMP. 80 CHAR BUFF.		5180
	ADM	BP			5190
	ADM	COUNT			5200
	J	NXT			5210
	ICX	I			5220
	J	AGN			5230
	LA	MCR			5240
	STA,I	BP	PUTS CR AT END OF BP BUFF.		5250
	LX	SAVE			5260
	J,I	RDR			5270
*					5280
*					5290
EXIT	EQU	*			5300
	LA	MCR			5310
	STA,I	BP			5320
	LA	BPNT			5330
	L	DOC			5340
	L	WAIT			5350
	LA	METX	THIS ETX CHAR, 'CNTRL-C',		5360
	DF	'30	GETS OUT OF TEXT MODE.		5370
	J	LOGIN			5380
*					5390

*					5400
SENDS	LA	SS			5410
	J	DDOUT	SEND S TO COMM. MODULE.		5420
SS	OCT	323			5430
*					5440
*					5450

*					5460
*					5470
*					5480
*					5490
*					5500
SONE	OCT	0			5510
	STA	ACC			5520
	LA	DFON			5530
	DF	'30	INITIALIZE COMM. MODULE.		5540
	LA	ACC			5550
	DR	FT			5560
	DF	'30	OUT 1ST CHAR TO COMM. MODULE.		5570
	J,I	SONE			5580
*					5590
***** MISC INTEGERS *****					
*					5600
METX	OCT	50003			5610
BI	OCT	0			5620
DM20	DEX	-20			5630
DM4	DEC	-4			5640
COUNT	OCT	0			5650
MP	OCT	0			5660
ME	OCT	0			5670
K301	OCT	301			5680
BP	OCT	0			5690
MCR	OCT	15			5700
BO	OCT	0			5710
BPNT	ADR	BUFO			5720
SENDXX	END	ACQUIR			5730
					5740

```
PROGRAM DECODE2(INPUT,OUTPUT,TAPE1=INPUT,TAPE2=OUTPUT) 100
-----
VER 1.4 APR 13/82 DRH 110
120
130
140
150
160
170
180
190
200
210
220
230
240
250
260
270
280
290
300
310
320
330
340
350
360
370
380
390
400
410
420
430
440
450
460
470
480
490
500
510
520
530
540
550
560
570
580
590
600
610
620
630
640
650
660
670
680
690
700
710
720
730
740
750
760
770
780
790
800
810
820
830
```

DECODE VER 2.7 USED AS STARTING BASIS.

DECODE 1ST 3 ASCII CHARS INTO 12 BIT INTEGER,
EACH ASCII CHAR CONTAINS FOUR BITS OF THE INTEGER,
SUBTRACT ONE FROM CHAR BEFORE DECODING, (F='306=5).

NOTE THAT CHARS ARE IN DISPLAY CODE (F='006=5).

NOTE THAT NEGATIVE INTEGERS FORMED ARE IN 2'S COMPLEMENT,
MUST BE CONVERTED TO ONE'S COMPLEMENT.

RESULTING SAMPLES ON TAPE2 IN VOLTS.
VOLTAGE READING REPRESENTS TIME BETWEEN PULSES.
(EXAMPLE: IN APR. 1982, 1 MICROSEC. = .01 VOLTS)

DECODE 4TH ASCII CHAR INTO POSITIVE INTEGER,
RESULT ON TAPE IN INTEGER RANGE 0-15.

DIMENSION CODE(80),DATA(20),IDAT(20)
INTEGER CODE

WILL READ LINES FROM TAPE1 UNTIL EOF.

OLDAT=0.0
3 CONTINUE
READ(1,120) (CODE(J),J=1,80)
120 FORMAT(BOR1)
IF(EOF(1).GT.0) GO TO 80

DO 5 I=1,80
5 CODE(I)=CODE(I)-1
JJ=0
DO 20 II=1,77,4
JJ=JJ+1
IDAT(JJ)=CODE(II+3)
DO 10 J=1,2
10 CODE(II) = CODE(II)*16 + CODE(II+J)
CONTINUE

CONVERT FROM TWO'S TO ONE'S COMPLEMENT.
FORM NUMBER EXPRESSED IN VOLTAGE.

IF(CODE(II).LE.2047) GO TO 15
CODE(II)=CODE(II).OR.77777777777777770000B
CODE(II)=CODE(II)-1
15 R=CODE(II)
DATA(JJ)=10.*R/2048.
IF(DATA(JJ).GE.(9.999)) DATA(JJ)=9.999
IF(DATA(JJ).LE.-9.999) DATA(JJ)=-9.999
DATA(JJ)=DATA(JJ)+10.0
20 CONTINUE

SHIFT DATA TO MATCH WITH PROPER SENSE-LINES.

TEMP=DATA(20)
KK=20
DO 30 I=1,19
KK=KK-1
DATA(KK+1)=DATA(KK)
30 CONTINUE
DATA(1)=OLDAT
OLDAT=TEMP
WRITE(2,130) (IDAT(I),DATA(I),I=1,10)
WRITE(2,130) (IDAT(I),DATA(I),I=11,20)
130 FORMAT(10(1X,I2,F5.2))
GO TO 3
80 STOP
END


```
DO 400 JJJ=1,56  
2000 WRITE(3,2000) (STD(JJ),IRS(JJ),ITHS(JJ),JJ=JJJ,336,56)  
400 FORMAT(1X,6(F10.6,2I4,4X))  
CONTINUE  
GO TO 200  
20 CONTINUE  
GO TO 50  
100 WRITE(3,130)IRN,IRP  
130 FORMAT(1H0,10X,*TOTAL R NEG= *,I5,*TOTAL R POS= *,I5)  
140 WRITE(3,140)ITHN,ITHP  
FORMAT(1H0,10X,*TOTAL THETA NEG= *,I5,*TOTAL THETA POS= *,I5)  
STOP  
END
```

820
830
840
850
860
870
880
890
900
910
920
930
940

APPENDIX E
ALGORITHMS USED FOR
AREA ERROR MINIMIZATION

```
BLOCK DATA
C-----
C ASSIGNMENT OF INPUT AND OUTPUT FILES
C-----
COMMON /IO/ IN,IOUT,IDATA
DATA IN,IOUT,IDATA /5,6,7/
END
C
C
C
PROGRAM CONTOUR(INPUT,OUTPUT=100B,TAPE7,TAPES=INPUT,TAPES=OUTPUT,
C-----
C MAIN PROGRAM TO CALCULATE AREA ERROR
C-----
+ DEBUG=OUTPUT)
COMMON /IO/ IN,IOUT,IDATA
COMMON /PIE/ TWOPI,PI
COMMON /PATH/ JRUTA,JROUTB
COMMON /SYSPAR/ DR,DTHETA,ORIGINR,ORIGINT,TMIN,TMAX,
1 XMIN,XMAX,TYPE,DT,DX,PX,PTHETA,ISECT,
2 TOTAL,ORIGINX,ORIGINY
C
INTEGER TYPE
LOGICAL ENDFLG,BWT
DIMENSION RADIUS(40),THETA(40)
DATA ESCAPE,EPSI /1.0E-06,0.6E-12/
C
C BEGIN (* MAIN *)
C
C
C
C* STORES(THETA,THE1)
C ARRAYS(RADIUS,THETA)
C PI=4.0*ATAN(1.)
C TWOPI=2.0*PI
C TOTAL=0.0
C JRUTA=0
C JROUTB=0
C-----
C INITIALIZE DATA AND GET INFORMATION REQUIRED TO
C CALCULATE THE AREA ERROR
C-----
CALL INIT
CALL SET(RADIUS(1),THETA(1),TYPE)
IF (TYPE.EQ.2) CALL FINDDX(THETA(1))
IF (TYPE.EQ.1) CALL FINDDT(THETA(1))
I=1
C-----
C OPERATING LOOP
C-----
110 I=I+1
IF (I .GT. 40) GOTO 9999
CALL POINT(RADIUS(I),THETA(I),ENDFLG)
IF (ENDFLG) GOTO 200
120 DDTHE=DIFF(THETA(I),THETA(1))
IF (DDTHE .LT. DTHETA) GOTO 110
THE1=THETA(1)
THE2=THETA(I)
IF (BWT(THETA(I),0.0,THETA(1))) GOTO 10
OMEGA=THETA(1)-DTHETA
IF (THETA(I) .GT. THETA(1))
1 OMEGA=THETA(1)+DTHETA
GOTO 20
10 IF (THETA(I) .GT. THETA(1)) GOTO 30
OMEGA=THETA(1)+DTHETA
IF (COSINE(THETA(I)) .GE. 0.0) OMEGA=THETA(1)-DTHETA
GOTO 20
30 OMEGA=THETA(1)-DTHETA
IF (COSINE(THETA(I)) .GE. 0.0) OMEGA=THETA(1)+DTHETA
20 CALL BIND(OMEGA,RADIUS(I-1),THETA(I-1),RADIUS(I),
1 THETA(I),RTEMP,TTEMP)
IF (ABS(THETA(I)) .LT. EPSI) THETA(I)=0.0
CALL FINDBAS(RBASE,RADIUS,THETA,I,RNXT,TNXT)
CALL FINDERR(RADIUS,THETA,I,RNXT,ERROR)
```

```
IF (ERROR .LT. 1.0E-02) GOTO 240 820
IF (TYPE .EQ. 2) GOTO 800 830
WRITE(6,230) ERROR,PTHETA 840
230 FORMAT(" ERROR FOR SECTOR ",G14.8,5X," PTHETA =",G14.8) 850
GOTO 820 860
800 WRITE(IOUT,810) ERROR,PX 870
810 FORMAT(" ERROR FOR SECTOR ",G14.8,5X," PX      =",G14.8) 880
820 CALL PRNT(RADIUS,THETA,RNXT,TNXT,4) 890
240 *TOTAL=TOTAL+ERROR 900
GOTO(440,550,660,660),TYPE 910
440 IF ((ABS(PTHETA-TMAX).LE.ESCAPE).OR.(PTHETA .GE. TMAX)) GOTO 200 920
GOTO 300 930
550 IF (PX.GT.XMAX) GOTO 200 940
GOTO 300 950
660 CONTINUE 960
300 RBASE=RNXT 970
RADIUS(1)=RADIUS(I) 980
THETA(1)=THETA(I) 990
RADIUS(2)=RTEMP 1000
THETA(2)=TTEMP 1010
I=2 1020
GOTO(700,701,120,120),TYPE 1030
700 CALL FINDDT(THETA(1)) 1040
GOTO 702 1050
701 CALL FINDDX(THETA(1)) 1060
702 I=1 1070
GOTO 110 1080
200 WRITE(6,220) TOTAL 1090
220 FORMAT(20H THE TOTAL ERROR IS , G14.8) 1100
WRITE(IOUT,290) JROUTA,JROUTB 1110
290 FORMAT(1X," JROUTA =",I7,5X," JROUTB =",I7) 1120
STOP 1130
9999 CALL PRNT(RADIUS,THETA,RNXT,TNXT,40) 1140
WRITE(IOUT,9998) PX,DX 1150
9998 FORMAT(5X," PX      =",G14.8,5X," DX      =",G14.8) 1160
STOP 1170
END 1180

C 1190
C 1200
C 1210
SUBROUTINE SET(RADIUS,THETA,ITYPE) 1220
C===== 1230
C SET STARTING POINT AT NEAREST GRID POINT OF R AND THETA 1240
C===== 1250
C 1260
COMMON /ID/ IN,IOUT,IDATA 1270
COMMON /SYSPAR/ DR,DTHETA,ORIGINR,ORIGINT,TMIN,TMAX, 1280
1 XMIN,XMAX,TYPE,DT,DX,PX,PTHETA,ISECT, 1290
2 TOTAL,ORIGINX,ORIGINY 1300
LOGICAL ENDFLG 1310
C 1320
GOTO(100,200,300,300),ITYPE 1330
100 PTHETA=TMIN-DT 1340
GOTO 400 1350
200 PX=XMIN-DX 1360
GOTO 400 1370
300 REWIND IDATA 1380
400 THETA=0.0 1390
CALL POINT(R1,T1,ENDFLG) 1400
IF (ENDFLG) GOTO 5000 1410
CALL POINT(R2,T2,ENDFLG) 1420
IF (ENDFLG) GOTO 5000 1430
IF (T2 .LT. T1) THETA=DTHETA 1440
THETA=THETA+INT(T1/DTHETA)*DTHETA 1450
RADIUS=INT(R1/DR)*DR 1460
GOTO(1000,2000,3000,3000),ITYPE 1470
1000 PTHETA=TMIN+DT 1480
RETURN 1490
2000 PX=XMIN+DX 1500
RETURN 1510
3000 REWIND IDATA 1520
READ(IDATA,*) SKP1,SKP2 1530
```



```

5000 RETURN
5010 WRITE(IOUT,5010)
5010 FORMAT(" *** INSUFFICIENT DATA *** ")
STOP
END
C
C
C SUBROUTINE POINT(RADIUS,THETA,ENDFLG)
C=====
C SUBROUTINE TO GENERATE THE CONTOUR DATA FROM EQUATION
C OR DISCRETE POINT INPUT.
C=====
COMMON /IO/ IN,IOUT,IDATA
COMMON /SYSPAR/ DR,DTHETA,ORIGINR,ORIGINT,TMIN,TMAX,
1 XMIN,XMAX,TYPE,DT,DX,PX,PTHETA,ISECT,
2 TOTAL,ORIGINX,ORIGINY
LOGICAL ENDFLG
INTEGER TYPE
ENDFLG=.FALSE.
GOTO(100,200,300,400),TYPE
100 PTHETA=PTHETA+DT
CALL GET1(RADIUS,THETA,PTHETA)
GOTO 700
200 PX=PX+DX
CALL GET2(RADIUS,THETA,PX)
GOTO 700
300 READ(IDATA,*) RADIUS,THETA
IF (EOF(IDATA).NE.0.0) GOTO 500
GOTO 700
400 READ(IDATA,*) RADIUS,THETA
IF (EOF(IDATA).NE.0.0) GOTO 500
700 CALL ADJUST(RADIUS,THETA,ORIGINX,ORIGINY,TYPE)
RETURN
500 ENDFLG=.TRUE.
RETURN
END
C
C
C
C SUBROUTINE FINDDX(ALPHA)
C=====
C FIND THE ANGLE WITH RESPECT TO THE MACHINE POLE
C FOR THE INCREMENTAL DISPLACEMENT DX.
C=====
COMMON /IO/ IN,IOUT,IDATA
COMMON /PIE/ TWOPI,PI
COMMON /SYSPAR/ DR,DTHETA,ORIGINR,ORIGINT,TMIN,TMAX,
1 XMIN,XMAX,TYPE,DT,DX,PX,PTHETA,ISECT,
2 TOTAL,ORIGINX,ORIGINY
INTEGER TYPE
C
DATA EPSI/1.0E-06/
C# STORES(ALPHA1,PXDBG)
ALPHA1=ALPHA * 180.0 / PI
PXDBG=PX
CALL SECOND(TSTRT)
100 CALL SECOND(TEND)
IF ((TEND-TSTRT) .GT. 5.0) GOTO 500
II=0
XVAL = PX + (ISECT-1) * DX
200 CALL GET2(RADIUS,THETA,XVAL)
CALL ADJUST(RADIUS,THETA,ORIGINX,ORIGINY,TYPE)
DDTHE = DIFF(THETA,ALPHA)
IF (DDTHE .GE. DTHETA) GOTO 300
XVAL = XVAL + DX
II = II + 1
IF (II .LE. 10 ) GOTO 200
IF (DDTHE.LT.EPSI) DDTHE=EPSI
DX = DX * (6 * DTHETA) / (5 * DDTHE)
GOTO 100
300 RJJ = DDTHE/DTHETA

```

```

1540
1550
1560
1570
1580
1590
1600
1610
1620
1630
1640
1650
1660
1670
1680
1690
1700
1710
1720
1730
1740
1750
1760
1770
1780
1790
1800
1810
1820
1830
1840
1850
1860
1870
1880
1890
1900
1910
1920
1930
1940
1950
1960
1970
1980
1990
2000
2010
2020
2030
2040
2050
2060
2070
2080
2090
2100
2110
2120
2130
2140
2150
2160
2170
2180
2190
2200
2210
2220
2230
2240
2250

```

```

JJ=RJJ
IF (JJ .EQ. 1) GOTO 400
IF (JJ .NE. 2) GOTO 350
IF (II .LE. 2) DX=DX/10.0
DX=DX*FLOAT(JJ)/3.0
GOTO 100
350 DX = DX/RJJ
GOTO 100
400 DX = ABS(XVAL-PX)/FLOAT(ISECT)
* WRITE(IOUT,450) ALPHA1,PX,XVAL,DX
*450 FORMAT(5X,"ALPHA1 =",G14.8,2X,"PX      =",G14.8,
*      1 2X,"XVAL  =",G14.8,2X,"DX      =",G14.8)
RETURN
500 WRITE(IOUT,510) ALPHA1,PXDBG,DDTHE,XVAL,RADIUS,
      1 THETA,DX
510 FORMAT(15X,"ALPHA1\ =",G14.8,15X,"PX      =",G14.8,/,
      1 15X,"DDTHE  =",G14.8,15X,"XVAL  =",G14.8,/,
      2 15X,"RADIUS  =",G14.8,15X,"THETA  =",G14.8,/,
      3 15X,"DX      =",G14.8)
WRITE(6,530) TOTAL
530 FORMAT(20H THE TOTAL ERROR IS , G14.8)
STOP
END
C
C
C
C
C
SUBROUTINE FINDDT(ALPHA)
C-----
C FIND THE ANGLE THETA WITH RESPECT TO THE MACHINE POLE
C FOR THE INCREMENTAL ANGULAR DISPLACEMENT WITH RESPECT
C TO THE CONTOUR POLE.
C-----
COMMON /IO/ IN,IOUT,IDATA
C
COMMON /SYSPAR/ DR,DTHETA,ORIGINR,ORIGINT,TMIN,TMAX,
      1 XMIN,XMAX,TYPE,DT,DX,PX,PTHETA,ISECT,
      2 TOTAL,ORIGINX,ORIGINY
C
INTEGER TYPE
C
DATA EPSI/1.0E-06/
PI=2 * ASIN(1.)
C
STORES(ALPHA1,RJJ,DT,PTHDBG,DDTDBG)
CALL SECOND(TSTRT)
ALPHA1=ALPHA * 180.0 / PI
PTHDBG=PTHETA * 180.0 / PI
100 CALL SECOND(TEND)
IF ((TEND-TSTRT) .GT. 5.0) GOTO 500
II=0
OMEGA = PTHETA + (ISECT-1) * DT
200 CALL GET1(RADIUS,THETA,OMEGA)
CALL ADJUST(RADIUS,THETA,ORIGINX,ORIGINY,TYPE)
DDTHE = DIFF(THETA,ALPHA)
IF (DDTHE .GE. DTHETA) GOTO 300
OMEGA = OMEGA + DT
II = II + 1
IF (II .LE. 10 ) GOTO 200
IF (DDTHE.LT.EPSI) DDTHE=EPSI
DT = DT * (6 * DTHETA) / (5 * DDTHE)
GOTO 100
300 RJJ = DDTHE/DTHETA
JJ=RJJ
IF (JJ .EQ. 1) GOTO 400
IF (JJ .NE. 2) GOTO 350
IF (II .LE. 2) DT=DT/10.0
DT=DT*FLOAT(JJ)/3.0
GOTO 100
350 DT = DT/RJJ
GOTO 100
400 DT = ABS(ABS(OMEGA)-ABS(PTHETA))/FLOAT(ISECT)
RETURN
500 WRITE(IOUT,510) ALPHA1,PTHDBG,DDTHE,OMEGA,RADIUS
      1 THETA,DT

```

```
510  FORMAT(15X,"ALPHA1 =",G14.8,15X,"PTHETA =",G14.8,/, 2980
      1 15X,"DDTHE =",G14.8,15X,"OMEGA =",G14.8,/, 2990
      2 15X,"RADIUS =",G14.8,15X,"THETA =",G14.8,/, 3000
      3 15X,"DT =",G14.8) 3010
520  WRITE(6,530) TOTAL 3020
530  FORMAT(20H THE TOTAL ERROR IS , G14.8) 3030
      STOP 3040
      END 3050
C 3060
C 3070
C 3080
      SUBROUTINE INIT 3090
C===== 3100
C INITIALIZATION AND INFORMATION INPUT SUBROUTINE. 3110
C NOTE "TYPE" IS PARAMETER THAT DEFINES TYPE OF CONTOUR 3120
C INFORMATION GIVEN, AND IS DEFINED AS FOLLOWS: 3130
C TYPE = 1 CONTOUR IS GIVEN IN POLAR COORDINATES 3140
C TYPE = 2 CONTOUR IS GIVEN IN CARTEZIEN COORDINATES 3150
C TYPE = 3 CONTOUR IS GIVEN AS DESCRETE POINTS IN POLAR 3160
C COORDINATES 3170
C TYPE = 4 CONTOUR IS GIVEN AS DESCRETE POINTS IN CARTEZIEN 3180
C COORDINATES 3190
C===== 3200
C 3210
C 3220
C----- 3230
C THE CONTOUR PARAMETERS ARE DEINED AS FOLLOWS 3240
C DR = SYSTEM RADIAL RESOLUTION 3250
C DTHETA = SYSTEM ANGULAR RESOLUTION 3260
C ORIGINX= MACHINE POLE LOCATION X AXIS 3270
C ORIGINY= MACHINE POLE LOCATION Y AXIS 3280
C TMIN = STARTING ANGULAR DISPLACEMENT OF THE CONTOUR 3290
C WITH RESPECT TO THE CONTOUR POLE 3300
C TMAX = MAXIMUM ANGULAR DISPLACEMENT OF THE CONTOUR 3310
C WITH RESPECT TO THE CONTOUR POLE 3320
C ISECT = NUMBER OF POINTS WITHIN ONE RESOLUTION TO 3330
C APPROXIMATE THE CONTOUR 3340
C COMMON /ID/ IN,IOUT,IDATA 3350
C COMMON /SYSPAR/ DR,DTHETA,ORIGINR,ORIGINT,TMIN,TMAX, 3360
      1 XMIN,XMAX,TYPE,DT,DX,PX,PTHETA,ISECT, 3370
      2 TOTAL,ORIGINX,ORIGINY 3380
C INTEGER TYPE 3390
C PI=4.0 * ATAN(1.) 3400
C READ(IN,*) TYPE 3410
C WRITE(IOUT,*) TYPE 3420
C GOTO(100,200,300,400),TYPE 3430
C 3440
C----- 3450
C FOR A CONTOUR IN POLAR COORDINATES 3460
100 READ(IN,*) DR,DTHETA,ORIGINX,ORIGINY,TMIN,TMAX,ISECT 3470
      TMIN=TMIN * PI / 180.0 3480
      TMAX=TMAX * PI / 180.0 3490
      ORIGINR=SQRT(ORIGINX**2+ORIGINY**2) 3500
      ORIGINT=0.0 3510
      IF ((ORIGINX.NE.0.0) .OR. (ORIGINY.NE.0.0)) 3520
        1 ORIGINT=ATAN2(ORIGINY,ORIGINX) 3530
      IF (ORIGINT .LT. -1.0E-200) ORIGINT=2.0*PI+ORIGINT 3540
      DTHETA=DTHETA * PI / 180.0 3550
      DT=DTHETA/FLOAT(ISECT) 3560
      PTHETA=TMIN 3570
      WRITE(IOUT,110) DR,DTHETA,ORIGINR,ORIGINT,ORIGINX,ORIGINY, 3580
      TMIN,TMAX,ISECT 3590
110  FORMAT(15X,"DR =",G14.8,15X,"DTHETA =",G14.8,/, 3600
      1 15X,"ORIGINR =",G14.8,15X,"ORIGINT =",G14.8,/, 3610
      1 15X,"ORIGINX =",G14.8,15X,"ORIGINY =",G14.8,/, 3620
      2 15X,"TMIN =",G14.8,15X,"TMAX =",G14.8,15X,/, 3630
      3 15X,"ISECT =",I2) 3640
      GOTO 500 3650
C----- 3660
C 3670
C 3680
C 3690
```

```
C-----3700
C OR A CONTOUR EQUATION IN CARTEZIEN COORDINATES 3710
200 READ(IN,*) DR,DTHETA,ORIGINX,ORIGINY,XMIN,XMAX,DX,ISECT 3720
    PX=XMIN 3730
    DTHETA=DTHETA * PI / 180.0 3740
    WRITE(IOUT,210) DR,DTHETA,ORIGINX,ORIGINY,XMIN,XMAX,ISECT 3750
210 FORMAT(15X,"DR      =",G14.8,15X,"DTHETA  =",G14.8,/, 3760
1      15X,"ORIGINX =",G14.8,15X,"ORIGINY =",G14.8,/, 3770
2      15X,"XMIN   =",G14.8,15X,"XMAX   =",G14.8,15X,/, 3780
3      15X,"ISECT  =",I2) 3790
    GOTD 500 3800
C-----3810
C-----3820
C-----3830
C-----3840
C-----3850
C OR A CONTOUR IN DESCRETE POINT FORM GIVEN IN POLAR 3860
C COORDINATES 3870
300 READ(IN,*) DR,DTHETA,ORIGINX,ORIGINY 3880
    ORIGINR=SQRT(ORIGINX**2+ORIGINY**2) 3890
    ORIGINT=0.0 3900
    IF ((ORIGINX.NE.0.0) .OR. (ORIGINY.NE.0.0)) 3910
1      ORIGINT=ATAN2(ORIGINY,ORIGINX) 3920
    IF (ORIGINT.LT. -1.0E-200) ORIGINT=2.0*PI+ORIGINT 3930
    DTHETA=DTHETA * PI / 180.0 3940
    WRITE(IOUT,*) DR,DTHETA,ORIGINR,ORIGINT 3950
    GOTD 500 3960
C-----3970
C-----3980
C-----3990
C-----4000
C-----4010
C FOR CONTOUR INORMATION IN DESCRETE POINT FORM GIVEN 4020
C IN CARTEZIEN COORDINATES 4030
400 READ(IN,*) DR,DTHETA,ORIGINX,ORIGINY 4040
    DTHETA=DTHETA * PI / 180.0 4050
    WRITE(IOUT,*) DR,DTHETA,ORIGINX,ORIGINY 4060
C-----4070
500 RETURN 4080
    END 4090
C-----4100
C-----4110
C-----4120
SUBROUTINE GET1(R,THETA,PHI) 4130
C-----4140
C SUBROUTINE TO GENERATE THE CONTOUR FROM AN EQUATION IN 4150
C POLAR COORDINATES 4160
C-----4170
    THETA=PHI 4180
    R=3.0+2.0*COS(THETA) 4190
    RETURN 4200
    END 4210
C-----4220
C-----4230
C-----4240
SUBROUTINE GET2(X,Y,XVAL) 4250
C-----4260
C SUBROUTINE TO GENERATE THE CONTOUR FROM AN EQUATION IN CARTEZIEN 4270
C COORDINATES. 4280
    DATA A,B /0.5,3.0/ 4290
    X=XVAL 4300
    Y=A*B*X/(A**2+X**2) 4310
    RETURN 4320
    END 4330
C-----4340
C-----4350
C-----4360
SUBROUTINE BIND(PHI,A,ALPHA,B,BETA,C,GAMMA) 4370
C-----4380
C SUBROUTINE TO FIND THE INTERSECTION BETWEEN THE CONTOUR 4390
C AND A GRID LINE WITHIN ONE INCREMENT. 4400
C-----4410
```

```
COMMON /PIE/ TWOPI,PI
C STORES(AX,BX,ALX,BEX,PHIX,T1,T2,T3,C) 4420
IF (ABS(PHI) .LT. PI) GOTO 10 4430
IF (PHI .GT. PI) GOTO 20 4440
IF (PHI .LT. -PI) PHIX=TWOPI+PHI 4450
GOTO 10 4460
20 PHI=PHI-TWOPI 4470
10 C= (A * B * SIN(DIFF(ALPHA,BETA)))/ 4480
1 (A * SIN(DIFF(ALPHA,PHI)) + B * SIN(DIFF(PHI,BETA))) 4490
GAMMA=PHI 4500
TMP=B 4510
B=C 4520
C=TMP 4530
TMP=GAMMA 4540
GAMMA=BETA 4550
BETA=TMP 4560
RETURN 4570
END 4580
4590
4600
4610
SUBROUTINE FINDBAS(A,RADIUS,THETA,LIMIT,C,GAMMA) 4620
===== 4630
C FIND NEAREST BASE POINT ON THE POLAR GRID 4640
===== 4650
COMMON /SYSPAR/ DR,DTHETA,ORIGINR,ORIGINT,TMIN,TMAX, 4660
1 XMIN,XMAX,TYPE,DT,DX,PX,PTHETA,ISECT, 4690
2 TOTAL,ORIGINX,ORIGINY 4700
INTEGER TYPE 4710
DIMENSION RADIUS(LIMIT),THETA(LIMIT) 4720
C=A 4730
DO 10 I=1,LIMIT 4740
C = C + INT((RADIUS(I)-C)/DR)*DR 4750
10 CONTINUE 4760
GAMMA=THETA(LIMIT) 4770
RETURN 4780
END 4790
4800
4810
4820
SUBROUTINE FINDERR(RADIUS,THETA,LIMIT,B,ERROR) 4830
===== 4840
C SUBROUTINE TO SET UP THE CONDITIONS AND ZONES TO 4850
C CALCULATE THE AREA ERROR. 4860
===== 4870
C 4880
COMMON /PATH/ JROUTA,JROUTB 4890
LOGICAL BWT,FLAG1 4900
DIMENSION RADIUS(LIMIT),THETA(LIMIT) 4910
4920
C AREA=0.0 4930
ERROR=0.0 4940
ANGINIT=THETA(1) 4950
LIM=LIMIT-1 4960
FLAG1=(THETA(1) .GT. THETA(2)) 4970
DO 300 K=2,LIM 4980
IF (FLAG1) GOTO 310 4990
IF (.NOT.(THETA(K).GT.THETA(K+1))) GOTO 300 5000
GOTO 350 5010
310 IF ((THETA(K).GT.THETA(K+1))) GOTO 300 5020
GOTO 350 5030
300 CONTINUE 5040
JROUTA=JROUTA+1 5050
DO 100 K=1,LIM 5060
IF (BWT(RADIUS(K),B,RADIUS(K+1))) GOTO 200 5070
AREA=AREA+RADIUS(K)*RADIUS(K+1) * SIN(DIFF(THETA(K),THETA(K+1))) 5080
GOTO 100 5090
200 CALL CALCANG(B,RADIUS(K),THETA(K),RADIUS(K+1),THETA(K+1),PHI) 5100
ARSCTR = DIFF(PHI,ANGINIT) * B * B 5110
AREA = AREA + RADIUS(K) * B * SIN(DIFF(THETA(K),PHI)) 5120
ERROR = ERROR + ABS(AREA-ARSCTR)/2.0 5130
```

```

    ANGINIT=PHI
    AREA = B * RADIUS(K+1) * SIN(DIFF(PHI,THETA(K+1)))
100 CONTINUE
    ARSCTR=DIFF(THETA(LIMIT),ANGINIT) * B * B
    ERROR = ERROR + ABS(AREA-ARSCTR)/2.0
    RETURN
350 JROUT9=JROUTB+1
    DO 400 K=1,LIM
        IF (BWT(RADIUS(K),B,RADIUS(K+1))) GOTO 500
        ERROR=ERROR+CALCERR(B,RADIUS(K),THETA(K),RADIUS(K+1),THETA(K+1))
500 GOTO 400
    CONTINUE
    CALL CALCANG(B,RADIUS(K),THETA(K),RADIUS(K+1),THETA(K+1),PHI)
    ERROR=ERROR+CALCERR(B,RADIUS(K),THETA(K),B,PHI)
    ERROR=ERROR+CALCERR(B,B,PHI,RADIUS(K+1),THETA(K+1))
400 CONTINUE
    RETURN
    END
C
C
C
C
    FUNCTION CALCERR(BASE,R,T,S,Q)
C=====
C FUNCTION TO CALCULATE THE AREA ERROR WITHIN A SMALL SEGMENT
C=====
C
    ARSCTR=DIFF(Q,T)*BASE*BASE
    ARTRI=R*S*SIN(DIFF(Q,T))
    CALCERR=ABS(ARSCTR-ARTRI)/2.0
    RETURN
    END
C
C
C
    SUBROUTINE CALCANG(BASE,A,ALPHA,B,BETA,PHI)
C=====
C THIS SUBROUTINE FINDS THE ANGLE WITH RESPECT TO THE
C MACHINE POLE, FOR THE INTERSECTION BETWEEN THE CONTOUR
C AND THE GRID LINE WITHIN THE INCREMENT.
C=====
C
    REAL IOTA,KAPPA
    DATA EPSI /1.0E-12/
C
    IF (ABS(BASE) .LT. EPSI) GOTO 300
    IF (DIFF(BETA,ALPHA) .GT. 1.0E-90) GOTO 200
    DELTA=0.0
    GOTO 10
200 C=SQRT(A**2+B**2-2*A*B*COS(DIFF(BETA,ALPHA)))
    TMP=B/C*SIN(DIFF(BETA,ALPHA))
    IF (ABS(TMP).LT. 1.0) GOTO 100
300 DELTA=DIFF(ALPHA,BETA)/2.0
    GOTO 110
100 IOTA=ASIN(TMP)
    KAPPA=ASIN(A/BASE*TMP)
    DELTA=DIFF(IOTA,KAPPA)
110 IF (ALPHA.GT.BETA) GOTO 10
    PHI=ALPHA+DELTA
    RETURN
10 PHI=ALPHA-DELTA
    RETURN
    END
C
C
C
    SUBROUTINE ADJUST(A,ALPHA,B,BETA,ITYPE)
C=====
C COORDINATE TRANSFORMATION SUBROUTINE.
C TRANSFORMS THE COORDINATES OF A POINT ON THE CONTOUR
C TO THE MACHINE POLE.
C=====
C
    STORES(ALPHA2,ALPDBG2,XA,YA)
5140
5150
5160
5170
5180
5190
5200
5210
5220
5230
5240
5250
5260
5270
5280
5290
5300
5310
5320
5330
5340
5350
5360
5370
5380
5390
5400
5410
5420
5430
5440
5450
5460
5470
5480
5490
5500
5510
5520
5530
5540
5550
5560
5570
5580
5590
5600
5610
5620
5630
5640
5650
5660
5670
5680
5690
5700
5710
5720
5730
5740
5750
5760
5770
5780
5790
5800
5810
5820
5830
5840
5850
```

```

IF ((B.EQ.0.0).AND.(BETA.EQ.0.0)) GOTO 300
IF ((ITYPE.NE.1) .AND. (ITYPE.NE.3)) GOTO 100
XA=A*COSINE(ALPHA)+B
YA=A*SINE(ALPHA)+BETA
GOTO 200
100 XA=A+B
YA=ALPHA+BETA
200 A=SQRT(XA**2+YA**2)
ALPHA = 0.0
IF ((XA.NE.0.0) .OR. (YA.NE.0.0)) ALPHA=ATAN2(YA,XA)
300 RETURN
END
C
C
C
C
FUNCTION SINE(ALPHA)
C=====
C FUNCTION TO HELP IN ELEMENATING OVERLOW OF COMPUTER
C WORD FOR SMALL VALUES OF THE INTRINSIC FUNCTIONS
C=====
DATA EPSI /6.87E-15/
SINE=SIN(ALPHA)
IF (ABS(SINE) .LT. EPSI) SINE=0.0
RETURN
END
C
C
C
C
FUNCTION COSINE(ALPHA)
C=====
C FUNCTION TO HELP IN ELEMENATING OVERLOW OF COMPUTER
C WORD FOR SMALL VALUES OF THE INTRINSIC FUNCTIONS
C=====
DATA EPSI /1.62E-14/
COSINE=COS(ALPHA)
IF (ABS(COSINE) .LT. EPSI) COSINE=0.0
RETURN
END
C
C
C
C
SUBROUTINE PRNT(RADIUS,THETA,A,ALPHA,LIMIT)
C=====
C PRINTING SUBROUTINE
C=====
COMMON /IO/ IN,IOUT,IDATA
DIMENSION RADIUS(LIMIT),THETA(LIMIT)
C
DO 100 I=1,LIMIT
WRITE(IOUT,110) I,RADIUS(I),THETA(I)
110 FORMAT(10X,I2,5X,"RADIUS =",F11.7,10X,"THETA =",F11.7)
100 CONTINUE
WRITE(IOUT,120) A,ALPHA
120 FORMAT(10X,"RBASE=",F11.7,10X,"TBASE =",F11.7)
RETURN
END
C
C
C
C
LOGICAL FUNCTION BWT(A,B,C)
C=====
C RETURNS A TRUE OR FALSE VALUE DEPENDING ON WIETHER
C A GIVEN VALUE LIES INBETWEEN TWO POINTS OR NOT
C=====
C BWT IS TRUE IF B IS BETWEEN A AND C
IF (A .GT. B) GOTO 10
IF (B. LT. C) GOTO 20
GOTO 30
10 IF (B .GT. C) GOTO 20
30 BWT=.FALSE.
RETURN

```

5860
5870
5880
5890
5900
5910
5920
5930
5940
5950
5960
5970
5980
5990
6000
6010
6020
6030
6040
6050
6060
6070
6080
6090
6100
6110
6120
6130
6140
6150
6160
6170
6180
6190
6200
6210
6220
6230
6240
6250
6260
6270
6280
6290
6300
6310
6320
6330
6340
6350
6360
6370
6380
6390
6400
6410
6420
6430
6440
6450
6460
6470
6480
6490
6500
6510
6520
6530
6540
6550
6560
6570

20 BWT=.TRUE.
RETURN
END

C
C
C

FUNCTION DIFF(KAPPA,LAMBDA)

C FUNCTION RETURNS THE VALUE OF THE DIFFERENCE BETWEEN
C TWO ANGLES IN THE ZONE FROM 0 TO 180 DEGREES.

COMMON /PIE/ TWOPI,PI
REAL KAPPA,LAMBDA
DIFF=ABS(KAPPA-LAMBDA)
IF (DIFF .GT. PI) DIFF=TWOPI-DIFF
RETURN
END

6580
6590
6600
6610
6620
6630
6640
6650
6660
6670
6680
6690
6700
6710
6720
6730
6740


```
PROGRAM HOKJEV(TAPES,INPUT=TAPES,TAPES,OUTPUT=TAPES) 100
C===== 110
C THIS PROGRAM FINDS THE RELATIVE LOCATION BETWEEN THE CONTOUR 120
C POLE AND THE MACHINE POLE, THAT WOULD RESULT IN A MINIMUM 130
C AREA ERROR. 140
C THE PROGRAM USES THE ALTERNATE OBJECTIVE FUNCTION BASED 150
C ON FSUM AND FDIF. 160
C HOOKE AND JEEVES OPTIMISATION ALGORITHM IS USED FOR THE 170
C MINIMIZATION. 180
C===== 190
C===== 200
C===== 210
C===== 220
C THE PROGRAM IS SET CURRENTLY TO OPERATE ON THREE TEST 230
C CONTOURS. 240
C===== 250
C===== 260
COMMON PI,NTP 270
DIMENSION EPS(2),RK(2),B(2),QG(2),W(2),PC(1000,2),URK(2),SRK(2) 280
C===== 290
C "NTP" IS AN INTEGER. IT DEFINES THE NUMBER OF DESCRETE DATA POINTS 300
C ON THE CONTOUR. 310
C ALSO USED HERE TO DEFINE THE TEST CONTOUR IN USE. 320
C===== 330
C 1=WHITCH OF AGNASI 340
C 2=SEPENTINE 350
C 3=LIMACON OF PASCAL 360
C READ *,NTP 370
C===== 380
C PI=2*ASIN(1.0) 390
C===== 400
C ENTER CONTOURING SYSTEM RESOLUTION (R=0.001,THETA=0.0225) 410
C FOR PROTOTYPE SYSTEM 420
C R =0.001 430
C THETA=0.0225 DEGREES 440
C PRINT *, 'ENTER SYSTEM RESOLUTIONS, RADIAL THEN ANGULAR' 450
C READ *,DEL R,DELTH 460
C===== 470
C DELTH=DELTH*ASIN(1.0)/90.0 480
C===== 490
C ENTER CONTOUR PARAMETERS. 500
C FOR TEST CONTOURS THE 510
C CURVE PARAMETERS ARE (1: A=8.5 520
C 2: A=0.5 D=3.0 530
C 3: A=2.0 B=3.0) 540
C N = NUMBER OF SEGMENTS APPROXIMATING THE CONTOUR 550
C READ *,N,K,L,A,B,C,D 560
C===== 570
C CALL CUREVA(N,K,L,A,B,C,D,PC,NP) 580
C===== 590
C ENTER MAXIMUM NUMBER OF ITERATIONS AND FUNCTION EVALUATIONS 600
C SUGGESTED VALUES: 610
C NUMBER OF ITERATIONS = 200 620
C NUMBER OF FUNC. EVALUATIONS = 50 630
C PRINT *, 'ENTER MAXIMUM NUMBER OF ITERATIONS' 640
C PRINT *, 'THEN NUMBER OF FUNCTION EVALUATIONS' 650
C READ *,ITMAX,NKAT 660
C===== 670
C===== 680
C===== 690
C ENTER INITIAL GUESS (Y THEN X) 700
C PRINT *, 'ENTER INITIAL GUESS Y, THEN X' 710
C READ *,(RK(II),II=1,2) 720
C===== 730
C===== 740
C===== 750
C ENTER INITIAL MOVE SIZE FOR EACH DIRECTION (Y, THEN X) 760
C SUGGESTED VALUES: 770
C Y = 0.125 780
C X = 0.125 790
C PRINT *, 'ENTER INITIAL MOVE SIZE (Y, THEN X)' 800
C READ *,(EPS(JJ),JJ=1,2) 810
```

```
-----
C-----
C ENTER SCALING FACTOR FOR MOVE SIZE, INCREASE THEN REDUCTION
C AND THE ERROR OR STOP CRITERION
C SUGGESTED VALUES:
C   ALPHA = 1.0
C   BETA  = 0.5
C   EPSY  = 1.0E-20
C   PRINT *, 'ENTER SCALING FACTORS, FOR INCREASE THEN DECREASE'
C   PRINT *, 'AND THE ERROR FOR STOPPING'
C   READ *, ALPHA, BETA, EPSY
C-----
C-----
C ENTER PARAMETRIC LIMITS, Y THEN X
C PARAMETRIC LIMITS ARE GOVERNED BY THE SIZE OF THE WORK AREA
C   PRINT *, 'ENTER SIZE OF THE WORK AREA, XMAX, XMIN, YMAX, YMIN'
C   READ *, ((URK(I),SRK(I)),I=1,2)
C-----
C-----
C ENTER CONTOUR DATA IF CONTOUR IS IN DESCRETE FORM
C FIRST X THE Y COORDINATES
C   READ *, ((PC(J,I),I=1,2),J=1,NP)
C READ INSTRUCTION IS COMMENTED OUT FOR THIS RUN
C-----
C
C   PRINT 001
001  FORMAT(1H1,/,/,20X,*PROGRAM INPUT DATA*,/20X,18(*-*))
C   PRINT 002
002  FORMAT(/,5X,*STRAIGHT LINE APPROXIMATION OF CURVE*,/5X,37(*-*))
C   PRINT 003
003  FORMAT(/,5X,*POINTS ORDINATES*,5X,*POINTS ABSCISSAE*,/2(5X,16(*-*)
C   $))
C   DO 10 I=1,NP
10   PRINT 004,(PC(I,J),J=1,2)
004  FORMAT(2(5X,F16.8))
100  CONTINUE
C   PRINT 005,ITMAX,NKAT
005  FORMAT(/,5X,*MAXIMUM NUMBER OF ITERATIONS AND STEP SIZE REDUCTIONS
C   $ ALLOWED RESPECTIVELY,ARE,*,5X,I4,*,*,I4)
C   PRINT 006,(RK(II),II=1,2)
006  FORMAT(/,5X,*INITIAL GUESS,ORDINATES AND ABSCISSA RESPECTIVELY,ARE
C   $*,2(5X,F16.8))
C   QD=0.0
C   CALL HOOKE(RK, EPS, ITMAX, NKAT, EPSY, ALPHA, BETA, QD, G, QG, W,
C   $NP, PC, URK, SRK, DELR, DELTH)
C   STOP
C   END
C-----
C-----
C SUBROUTINE HOOKE(RK, EPS, MAXK, NKAT, EPSY, ALPHA, BETA, QD, G, QG,
C   $W, NP, PC, URK, SRK, DELR, DELTH)
C-----
C-----
C THIS OPTIMIZATION ROUTINE IS BASED ON THE HOOKE AND JEEVES
C ALGORITHM.
C-----
C-----
C DIMENSION RK(2),EPS(2),Q(2),QG(2),W(2),PC(1000,2),URK(2),SRK(2)
C   PRINT 001
001  FORMAT(1H1,/,/,10X,*OPTIMUM POSITION OF CURVE W.R.T. ORIGEN FOR POL
C   $AR SCANING*,/9X,57(*-*))
C   PRINT 002
002  FORMAT(/,3X,*NUMBER OF*,6X,*ORIGEN ORDINATE*,7X,*ORIGEN ABSCISSA
C   $*,7X,*FUNCTION VALUE*,/3X,*FUNCTION*,/3X,*EVALUATIONS*,/3
C   $X,11(*-*),4X,2(15(*-*),7X),14(*-*))
C   KFLAG=0
C   DO 601 I=1,2
C   Q(I)=RK(I)
```

	W(I)=0.0	1540
601	CONTINUE	1550
	KAT=0.0	1560
	KK1=0	1570
70	KCOUNT=0	1580
	WBEST=W(2)	1590
	CALL OBJECT(SUM,SUM1,SUM2,RK,NP,PC,DELR,DELTH)	1600
	KK1=KK1+1	1610
	IF(KK1.EQ. 1) PRINT 100,KK1,(RK(I),I=1,2),SUM,SUM1,SUM2	1620
	BD=SUM	1630
	IF(KK1.NE. 1) GO TO 10	1640
	GD=SUM	1650
	ACC1=SUM1	1660
	ACC2=SUM2	1670
	GO TO 201	1680
10	CONTINUE	1690
	IF(BD-GD) 11,201,12	1700
11	CONTINUE	1710
	GD=BD	1720
	ACC1=SUM1	1730
	ACC2=SUM2	1740
	GO TO 201	1750
12	CONTINUE	1760
	KFLAG=1	1770
201	DO 55 I=1,2	1780
	QQ(I)=RK(I)	1790
	TSRK=RK(I)	1800
	RK(I)=TSRK+EPS(I)	1810
	CALL OBJECT(SUM,SUM1,SUM2,RK,NP,PC,DELR,DELTH)	1820
	KK1=KK1+1	1830
	W(I)=SUM	1840
	IF(W(I).LT. GD) GO TO 58	1850
	RK(I)=TSRK-EPS(I)	1860
	CALL OBJECT(SUM,SUM1,SUM2,RK,NP,PC,DELR,DELTH)	1870
	KK1=KK1+1	1880
	W(I)=SUM	1890
	IF(W(I).LT. GD) GO TO 58	1900
	RK(I)=TSRK	1910
	IF(I.EQ. 1) GO TO 513	1920
	W(I)=W(I-1)	1930
	GO TO 613	1940
513	W(I)=BD	1950
613	CONTINUE	1960
	KCOUNT=1+KCOUNT	1970
	GO TO 55	1980
58	GD=W(I)	1990
	ACC1=SUM1	2000
	ACC2=SUM2	2010
	QQ(I)=RK(I)	2020
55	CONTINUE	2030
	PRINT 100,KK1,(RK(I),I=1,2),GD,ACC1,ACC2	2040
100	FORMAT(/,5X,I5,5(5X,E16.8))	2050
	IF(KK1.GT. MAXK) GO TO 94	2060
	IF(KAT.GE. NKAT) GO TO 94	2070
	IF(ABS(W(2)-WBEST).LE. EPSY) GO TO 94	2080
	IF(KCOUNT.GE. 2) GO TO 28	2090
	DO 25 I=1,2	2100
	RK(I)=RK(I)+ALPHA*(RK(I)-Q(I))	2110
25	CONTINUE	2120
	DO 25 I=1,2	2130
	Q(I)=QQ(I)	2140
25	CONTINUE	2150
	GO TO 70	2160
28	KAT=KAT+1	2170
	IF(KFLAG.EQ. 1) GO TO 202	2180
	GO TO 204	2190
202	KFLAG=0	2200
	DO 203 I=1,2	2210
	RK(I)=Q(I)	2220
203	CONTINUE	2230
204	DO 80 I=1,2	2240
	EPS(I)=EPS(I)*BETA	2250

```
80 CONTINUE 2260
   PRINT 101,KAT 2270
101 FORMAT(/,I4,1X,*REDUCTION IN STEP SIZE UP TO TIME*) 2280
   GO TO 70 2290
94 PRINT 460,(EPS(I),I=1,2) 2300
460 FORMAT(///,5X,*FINAL STEP SIZES USED,ARE*,5X,*Y=*,F16.8,5X,*X=*,F1 2310
   $6.8) 2320
   PRINT 103,(RK(I),I=1,2) 2330
103 FORMAT(///,5X,*ORDINATE AND ABSCISSA FOR MINIMUM FUNCTION VALUE AR 2340
   $E,*,5X,*Y=*,F16.8,5X,*X=*,F16.8) 2350
   PRINT 462,GD,ACC1,ACC2 2360
462 FORMAT(///,5X,*THE MINIMUM FUNCTION VALUE IS,*,5X,F16.8,5X,2 2370
   $(3X,F16.8)) 2380
   RETURN 2390
   END 2400
C 2410
C 2420
C 2430
   SUBROUTINE OBJECT(SUMN,SUMF1,SUMF2,RKK,NP,PC,DELR,DELTH) 2440
C===== 2450
C 2460
C THIS ROUTINE SETS UP THE PARAMETERS FOR EVALUATING THE 2470
C OBJECTIVE FUNCTION OF THE LINE SEGMENTS APPROXIMATING 2480
C THE CONTOUR. 2490
C THE ROUTINE ALSO EVALUATES THE TOTAL OBJECTIVE FUNCTION 2500
C FOR THE CONTOUR. 2510
C ) 2520
C===== 2530
   DIMENSION RKK(2),PC(1000,2) 2540
   PI=2.0*ASIN(1.0) 2550
   NNP=NP-1 2560
   SUMF1=SUMF2=0.0 2570
   K=1 2580
   DO 10 J=1,NNP 2590
     Y1=PC(K,1)-RKK(1) 2600
     Y2=PC(J+1,1)-RKK(1) 2610
     X1=PC(K,2)-RKK(2) 2620
     X2=PC(J+1,2)-RKK(2) 2630
     XX=X2-X1 2640
     IF(XX .EQ. 0.0) XX=10.0**(-60) 2650
     SLOPE=(Y2-Y1)/XX 2660
     BINT=Y2-X2*SLOPE 2670
     THETU=ANGLE(X2,Y2) 2680
     THETL=ANGLE(X1,Y1) 2690
     IF(ABS(THETU)-ABS(THETL)) 11,10,12 2700
011 ACC=THETU 2710
     THETU=THETL 2720
     THETL=ACC 2730
012 CONTINUE 2740
     CALL XXINTT(SLOPE,BINT,THETU,THETL,SUMX1,SUMX2,DELR,DELTH,IFL) 2750
     IF(IFL .EQ. 1) GO TO 10 2760
     SUMF1=SUMF1+ABS(SUMX1) 2770
     SUMF2=SUMF2+ABS(SUMX2) 2780
     K=J+1 2790
010 CONTINUE 2800
     SUMN=SUMF1/SUMF2 2810
     SUMF2=SUMF2 2820
     RETURN 2830
     END 2840
C 2850
C 2860
C 2870
   SUBROUTINE XXINTT(SLOPE,BINT,THETU,THETL,SUMX1,SUMX2,DELR,DELTH 2880
   $,IFL) 2890
C===== 2900
C 2910
C THIS SUBROUTINE CALCULATES THE OBJECTIVE FUNCTION FOR THE 2920
C INDIVIDUAL LINE SEGMENTS APPROXIMATING THE CONTOUR. 2930
C 2940
C===== 2950
   SINU=SIN(THETU) 2960
   SINL=SIN(THETL) 2970
```

```

COSU=COS (THETU)
COSL=COS (THETL)
AU1=BINT / (SINU-SLOPE*COSU)
AL1=BINT / (SINL-SLOPE*COSL)
AU2=(COSU+SLOPE*SINU)/BINT
AL2=(COSL+SLOPE*SINL)/BINT
A1=ABS((AU1-AL1)/DELR)
A2=ABS(ABS(THETU)-ABS(THETL))/DELTH
IF(A1.GE. A2) A2=ABS((AU2-AL2)*DELR/DELTH**2)
IFL=0
IF(A1.EQ. 0.0 .OR. A2.EQ. 0.0) IFL=1
SUMX1=A1-A2
SUMX2=A1+A2
RETURN
END
2980
2990
3000
3010
3020
3030
3040
3050
3060
3070
3080
3090
3100
3110
3120
3130
3140
3150
3160
3170
3180
3190
3200
3210
3220
3230
3240
3250
3260
3270
3280
3290
3300
3310
3320
3330
3340
3350
3360
3370
3380
3390
3400
3410
3420
3430
3440
3450
3460
3470
3480
3490
3500
3510
3520
3530
3540
3550
3560
3570
3580
3590
3600
3610
3620
3630
3640
3650
3660
3670
3680
3690
=====
FUNCTION ANGLE(XXX,YYY)
=====
FUNCTION TO CALCULATE AN ANGLE BETWEEN 0 AND 360 DEGREAS,
GIVEN THE TANGENT OF THE ANGLE.
=====
PY=2.0*ASIN(1.0)
IF(YYY) 1,2,3
1 CONTINUE
ANGLE=3.0*PY/2.0-ATAN(XXX/YYY)
RETURN
2 CONTINUE
ANGLE=0.0
IF(XXX.LT. 0.0) ANGLE=PY
RETURN
3 CONTINUE
ANGLE=PY/2.0-ATAN(XXX/YYY)
RETURN
END
=====
SUBROUTINE XINTT (SLOPE,BINT,THETU,THETL,SUMX1,SUMX2,DELR,DELTH)
=====
INTEGRATION ROUTINE TO BE USED IN PLACE OF XXINTT SUBROUTINE,
AND CALLED FROM SUBROUTINE "OBJECT".
THE INTEGRATION IS CARRIED OUT USING GAUSS-LEGENDRE QUADRATURE.
=====
DIMENSION EPPS(12),WE(12)
DATA (EPPS(I),I=1,12)
$/0.0640568826,0.1911188675,0.3150426797,0.4337935076,0.5454214714,
$/0.6480936519,0.7401241916,0.8200019860,0.8864155270,0.9382745520,0
$/ .9747285560,0.9951872200/
DATA (WE(I),I=1,12)
$/0.1279381953,0.1258374563,0.1216704729,0.1155056681,0.1074442701,
$/0.0976186521,0.0861901615,0.0733464814,0.0592985849,0.0442774388,0
$/ .0285313886,0.0123412298/
DATA (EPPS(I),I=1,3)
$/0.2386191860,0.6612093864,0.9324691542/
DATA (WE(I),I=1,3)
$/0.4679139345,0.3607615730,0.1713244923/
X1=(THETU+THETL)/2.0
X2=(THETU-THETL)/2.0
SUMX1=0.0
SUMX2=0.0
DO 10 I=1,12
DO 10 I=1,3
XX1=X1+X2*EPPS(I)
CALL FUNC(XX1,BINT,SLOPE,FUN11,FUN21,DELR,DELTH)
XX2=X1-X2*EPPS(I)
CALL FUNC(XX2,BINT,SLOPE,FUN12,FUN22,DELR,DELTH)

```

```
10 SUMX1=SUMX1+(FUN11+FUN12)*WE(I) 3700
SUMX2=SUMX2+(FUN21+FUN22)*WE(I) 3710
SUMX1=SUMX1*X2 3720
SUMX2=SUMX2*X2 3730
RETURN 3740
END 3750
C 3750
C 3770
C 3780
SUBROUTINE FUNC(X,BINT,SLOPE,FUN1,FUN2,DELR,DELTH) 3790
C===== 3800
C SUBROUTINE TO CALCULATE THE OBJECTIVE FUNCTION, 3810
C AND IS CALLED ONLY WHEN "XINTT" IS USED. 3820
C===== 3830
R11=ABS(SIN(X)-SLOPE*COS(X)) 3840
R1=R11**2 3850
R2=ABS(BINT*(COS(X)+SLOPE*SIN(X))) 3860
R=R2/R1 3870
FUNY1=R/DELR 3880
FUNY2=DELR*R11/(DELTH**2*ABS(BINT)) 3890
FUN1=ABS(FUNY1-FUNY2) 3900
FUN2=FUNY1+FUNY2 3910
RETURN 3920
END 3930
C 3940
C 3950
C 3960
C 3970
C 3980
SUBROUTINE CUREVA(N,K,L,A,B,C,D,PC,NP) 3990
C===== 4000
C SUBROUTINE TO CALCULATE THE LINEAR SEGMENTS THAT APPROXIMATE 4010
C THE CONTOUR. 4020
C===== 4030
COMMON PI,NP 4040
DIMENSION PC(1000,2) 4050
NP=K+1 4060
IF(NP.EQ.3) GO TO 100 4070
DX=(C-B)/FLOAT(K) 4080
DO 10 I=1,NP 4090
PC(I,2)=XX=B+(I-1)*DX 4100
IF(NP.EQ.1) PC(I,1)=B.0*A**3.0/(XX*XX+4.0*A*A) 4110
IF(NP.EQ.2) PC(I,1)=A*D*XX/(A**2+XX**2) 4120
10 CONTINUE 4130
RETURN 4140
100 CONTINUE 4150
THE=2*PI/FLOAT(K) 4160
DO 11 I=1,NP 4170
TH=THE*(I-1) 4180
COSS=COS(TH) 4190
R=B+A*COSS 4200
PC(I,2)=R*COSS 4210
PC(I,1)=R*SIN(TH) 4220
11 CONTINUE 4230
RETURN 4240
END 4250
4260
```

APPENDIX F

STEPPING MOTOR

PULL-OUT TORQUE SPEED CHARACTERISTICS

F.1 Introduction

Electric stepping motors are electro magnetic actuators which convert digital pulse inputs to output shaft angular incrementations of equal magnitudes. Stepping motors are gaining ground in control applications over conventional AC and DC motors due to the following three reasons:

a) Stepping motors are inherently discrete motion devices and are more compatible with modern digital control techniques.

b) Positional errors of stepping motors are non-cumulative

c) Control systems employ stepping motors in an open loop configuration, yet achieve accurate position and speed control. In open loop control, costly transducers and feedback components are avoided. Furthermore, instability problems inherent in closed loop control systems are eliminated.

The stepping motors utilized in the prototype NC machine are of the DC permanent magnet type. Axial and sectional views of such motors are shown in Figures F.1 and F.2, respectively. The most common configuration of the motor consists of a toothed stator with teeth spaced at a 1/48 pitch. The stator has eight salient poles with two-phase four-pole bifilar windings. Bifilar windings are windings

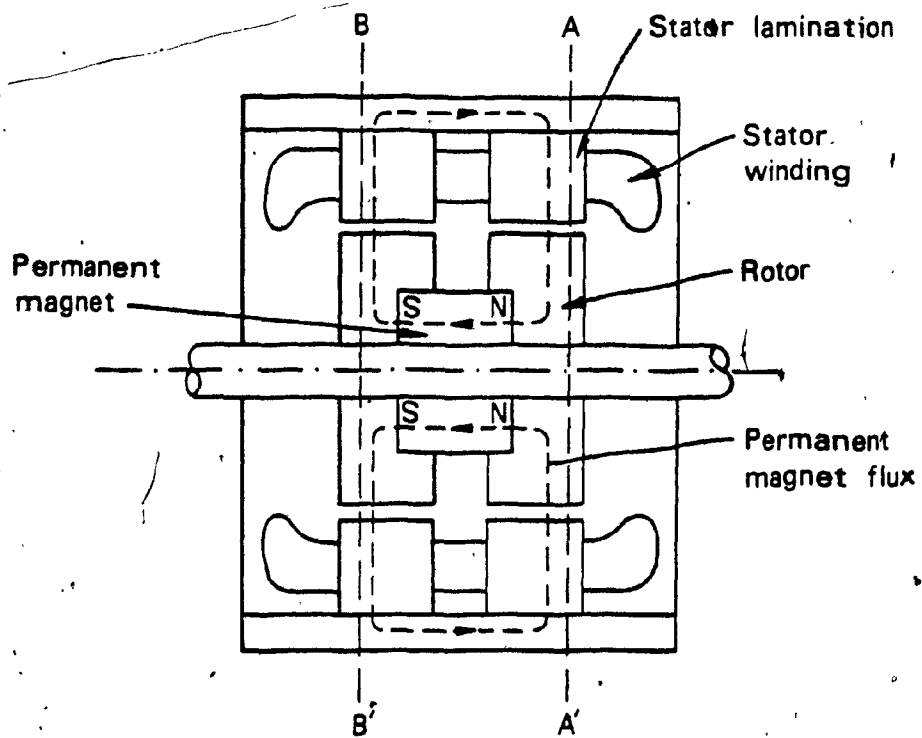


Figure F.1: Axial View of a D-C P-M Stepping Motor.

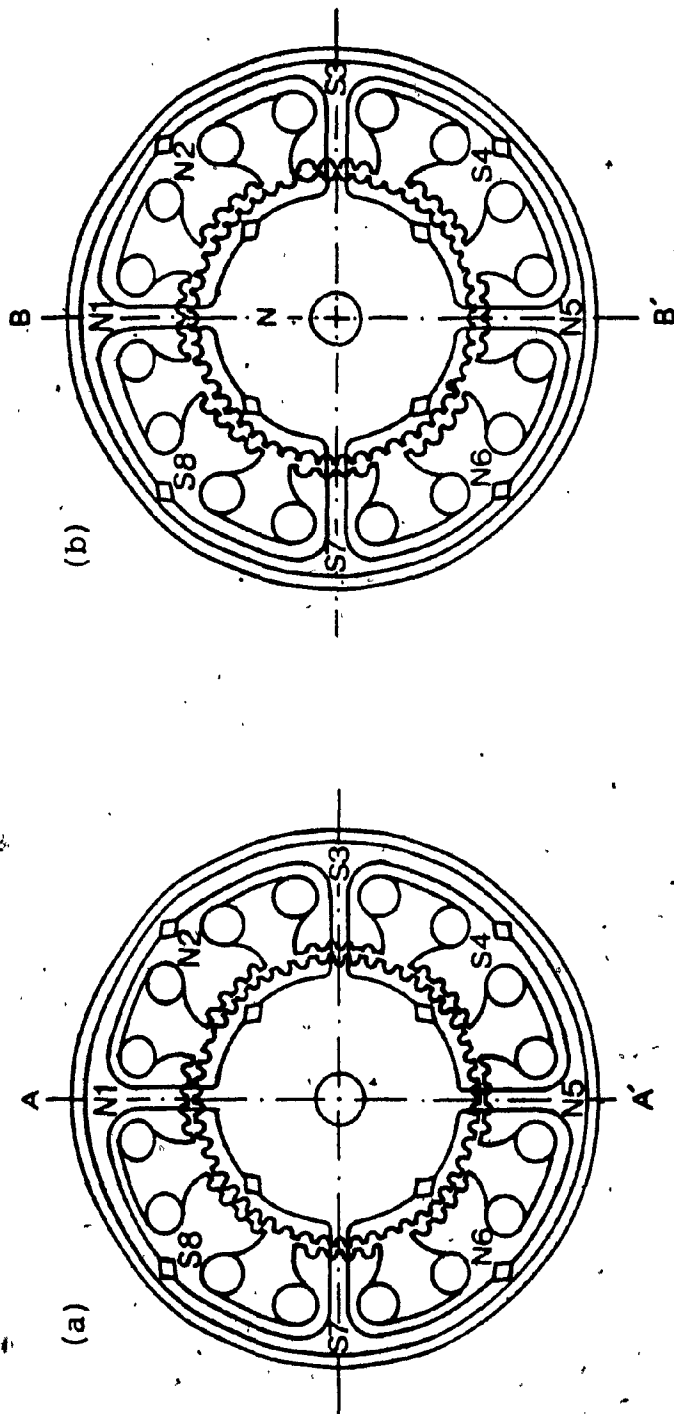


Figure F.2: Section View of a D-C.P-M Stepping Motor.

wound in opposite direction to each other on the same pole. Thus, instead of reversing the direction of the current in a winding, current in a bifilar winding is simply switched ON and OFF.

The stator houses a toothed rotor composed of two toothed plates each having 50 teeth. The plates sandwich a permanent magnet between them and are displaced angularly from each other by half a tooth as can be seen in Figures F.2.a and F.2.b.

Figure F.3 shows a simplified version of the motor with a four tooth stator and a 5 tooth rotor. A wiring diagram of the windings of the stepping motor and its drive circuit is shown Figure F.4. Torque develops in a stepping motor based upon the principle that, when the stator windings are energized, a magnetic flux pattern is set which interacts with the permanent magnet field so as to move the motor and line up the two fields.

Three energization (switching) schemes are used to drive stepping motors. These are: full step two windings ON, full step one winding ON, and half step (also known as wave) schemes. Table F.1 shows the states of the four switches in Figure F.3 that are required to drive the motor using these three schemes.

Figures F.5.a to F.5.e show the alignment of the rotor as current is sequenced according to the most commonly used full step two windings ON scheme. The polarity of the stator poles is indicated on each of the figures. The se-

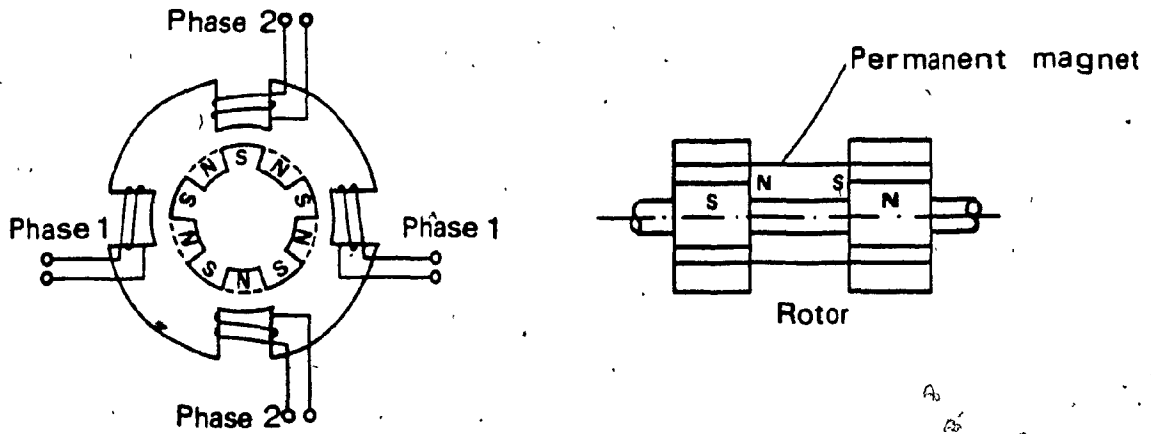


Figure F.3: Stepping Motor with 5 Teeth on the Rotor.

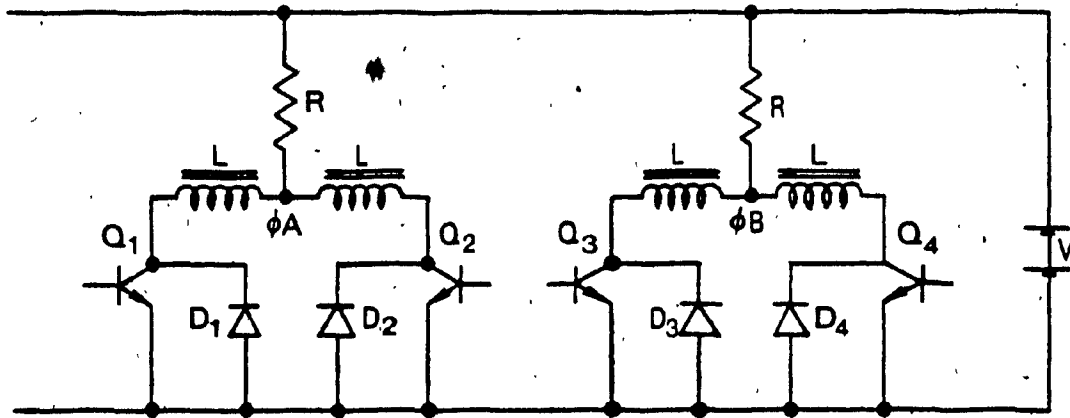


Figure F.4: Drive Circuit for Stepping Motor.

Table F.1: Switching Sequences for D-C P-M Stepping Motors

Full-Step, One Winding On

Step Number	Motor Coil Switch			
	SW1	SW2	SW3	SW4
1	OFF	OFF	OFF	ON
2	ON	OFF	OFF	OFF
3	OFF	OFF	ON	OFF
4	OFF	ON	OFF	OFF
1	OFF	OFF	OFF	ON

Full-Step, Two Windings On

Step Number	Motor Coil Switch			
	SW1	SW2	SW3	SW4
1	ON	OFF	OFF	ON
2	ON	OFF	ON	OFF
3	OFF	ON	ON	OFF
4	OFF	ON	OFF	ON
1	ON	OFF	OFF	ON

Half Step

Step Number	Motor Coil Switch			
	SW1	SW2	SW3	SW4
1	OFF	OFF	OFF	ON
2	ON	OFF	OFF	ON
3	ON	OFF	OFF	OFF
4	ON	OFF	ON	OFF
5	OFF	OFF	ON	OFF
6	OFF	ON	ON	OFF
7	OFF	ON	OFF	OFF
8	OFF	ON	OFF	ON
1	OFF	OFF	OFF	ON

quence of switching shown in Figures F.5.a to F.5.e, respectively, results in a clockwise rotation of the rotor. Counter-clockwise rotation is achieved by reversing the sequence shown in the figure.

The full step one winding ON scheme results in similar stepping sequence to that shown in Figure F.5. The control logic required for such an energization scheme is less complex than the one required for the full step two windings ON scheme. The output torque is 60% to 70% of that provided by the two windings ON scheme, and step accuracy may be slightly degraded. This mode however, requires only 50% of the power required for the full step two windings ON scheme.

The half step scheme requires a more complex control logic than that required by the other two schemes. Energization of the motor windings alternates between two windings ON and one winding ON, hence the name wave energization scheme. As a result of the wave energization, the motor output torque alternates between "strong steps", when two windings are ON, and "weak steps", when one winding only is ON. This energization scheme provides a finer resolution, half the step size obtained from the other schemes. In addition it permits starting at higher stepping rates. The alternating torque values, strong and weak steps, result in better resonance characteristics of the stepping motor [21].

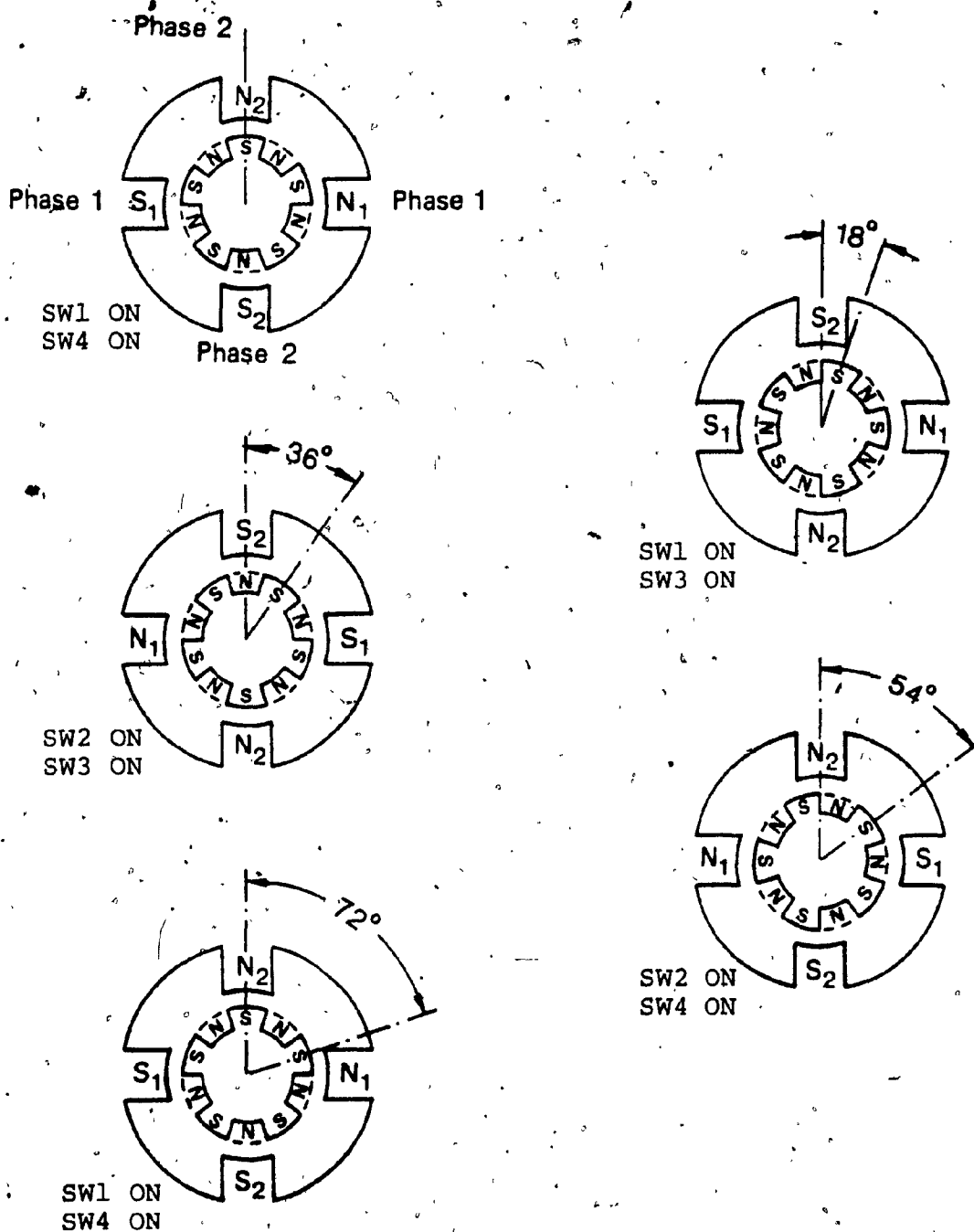


Figure F.5: Stepping Motor Rotor Positions in Sequential Stepping.

F.2 Derivation of the pull-out torque speed relationship

The phase voltage pattern for the wave energization scheme is shown in Figure F.6. This voltage pattern can be decomposed, using Fourier Series, to its sinusoidal constituents and are given by:

$$V(t) = \frac{2V}{(2n+1)} \cdot \sum_{n=0}^{\infty} \left\{ K_n \cos [(2n+1) (\omega t - \epsilon_1)] + (1+k_n) \sin [(2n+1) (\omega t - \epsilon_1)] \right\} \quad \text{F.1}$$

where,

$$K_n = (-1)^{\text{Int} \left(\frac{2n+1}{4} \right)} / \sqrt{2}$$

$$\epsilon_1 \begin{cases} = 0 & \text{for phase A} \\ = \frac{3\pi}{2} & \text{for phase B} \end{cases}$$

where ω is the frequency of the stepping signals.

The drive circuit shown in Figure F.4 is a unipolar, low L/R type. The circuit used to drive the motor is similar to the one shown in the figure. With reference to Figure F.4 the voltage-time relation for the phases is given by:

$$V(t) = i(t)R_a + L_a \frac{di(t)}{dt} - K_V \sin (N_s \sigma - \epsilon_2) \quad \text{F.2}$$

where,

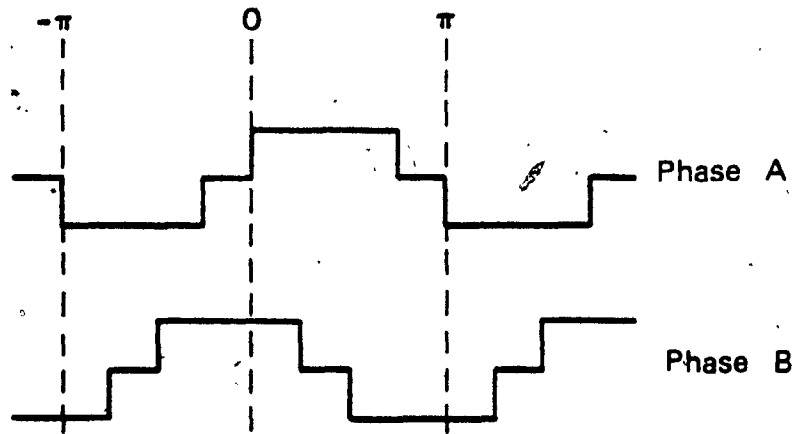


Figure F.6: Stepping Voltage Pattern for Wave Energization.

$$\epsilon_2 \begin{cases} = \frac{\pi}{4} & \text{for phase A} \\ = -\frac{\pi}{4} & \text{for phase B} \end{cases}$$

where L_a is the motor winding inductance,
 N_s is the number of teeth on the motor rotor,
 K_V is the voltage constant of the motor winding,
and σ is the angular displacement of the motor shaft measured from a stable position.

Stepping motors are essentially synchronous machines, thus when operated at a constant angular velocity ω the angle σ can be expressed as:

$$\sigma = \omega_0 t - \phi$$

where ϕ is the load angle,
and ω_0 is the angular velocity of the motor shaft.

Combining Equations F.1 and F.2 and solving the resulting differential equation yields:

$$i(t) = C_0 e^{-R_a t / L_a} + \sum_{n=0}^{\infty} \frac{2V \sqrt{2K_n + 2k_n + 1}}{(2n+1) \pi \sqrt{R_a^2 + [(2n+1) \omega L_a]^2}} \cos \left[(2n+1) (\omega t - \epsilon_1) + \lambda_n - \Delta \right] + \frac{K_V \omega_0}{\sqrt{R_a^2 + L_a^2 \omega^2}} \cdot \cos \left[\omega t + N_S \phi - \epsilon_2 + \lambda_1 \right] \quad \text{F.3}$$

where,

$$\omega = N_S \omega_0$$

$$\lambda_n = \tan^{-1} \left[\frac{R_a}{(2n+1) L_a \omega} \right]$$

$$\Delta = \tan^{-1} \left[\frac{K_n}{1+K_n} \right]$$

The constant of integration C_0 is evaluated at $t=0$ where;

$$i(0) = \frac{V}{R_a} + \frac{K_V \omega_0}{R_a} \sin(N_S \phi + \epsilon_2)$$

and is given by:

$$C_0 = \frac{V}{R_a} + \frac{K_V \omega_0}{R_a} \sin(N_S \phi + \epsilon_2) - \sum_{n=0}^{\infty} \frac{2V \sqrt{2K_n + 2K_n + 1}}{(2n+1) \pi \sqrt{R_a^2 + [(2n+1) \omega L_a]^2}} \cos \left[\lambda_n - (2n+1) \epsilon_1 - \Delta \right] + \frac{K_V \omega_0}{\sqrt{R_a^2 + \omega^2 L_a^2}} \cos(N_S \phi + \epsilon_2 + \lambda_1)$$

The torque equation for permanent magnet stepping mo-

tor is given [24] by:

$$T = -K_T i(t) \sin(\omega t - N_s \phi - \epsilon_2) \quad \text{F.4}$$

where K_T is the torque constant of the stepping motor.

Solving Equations F.3 and F.4 results in a torque expression which consists of the following groups of terms:

- a) Non-sinusoidal decaying components resulting from terms in C_0 with $n=0$.
- b) Decaying sinusoidal components resulting from the remaining terms in C_0 ,
- c) Constant components resulting from terms with $n=0$ excluding those in C_0 ; time does not appear in these components and
- d) Sinusoidal components resulting from all the remaining terms in the torque expression.

It is of interest in this analysis to calculate the pull-out torque, i.e. the maximum average torque [24], that the motor can develop at different speeds. Due to the small time constant of the drive circuit used, the exponential terms decay rapidly and can be ignored. Furthermore the sinusoidal terms have an average torque of zero and can also be ignored. Thus the remaining terms, having constant magnitude, are:

$$T_{\text{const.}} = \frac{(1.17632) V K_T}{\sqrt{R_a^2 + \omega^2 L_a^2}} \sin\left(N_s \phi - \lambda_1 + \Delta + \frac{3\pi}{4}\right) -$$

$$\frac{K_V \omega_o K_T}{\sqrt{R_a^2 + \omega^2 L_a^2}} \sin \lambda_1 \quad \text{F.5}$$

The pull-out torque is the maximum of this constant torque and is thus given by:

$$T_P = \frac{(1.17632) V K_T}{\sqrt{R_a^2 + \omega^2 L_a^2}} - \frac{K_V \omega R K_T}{N_s (R_a^2 + \omega^2 L_a^2)} \quad \text{F.6}$$

At any given stepping frequency the pull-out torque can be calculated using this equation.

F.3 Experimental verification of the pull-out torque relationship

The pull-out torque speed characteristics of the stepping motors used in the prototype NC machine were measured and compared to the published and to the calculated data. Two tests were conducted. In the first, the motor losses due to friction, windage, and damping were measured, using a torque transducer, while the motor is being driven by another motor.

In the second test the stepping motor is energized at a constant rate. The load on the motor is then gradually increased until failure to register step commands starts to

occur. The load is varied by means of a friction brake and flywheel discs. The torque delivered by the motor is measured using a torque transducer inserted between the motor and the load. Failure to register step commands is detected by calculating the theoretical motor shaft position for a preset number of stepping commands, and comparing that position with the actual position of the motor shaft. A logic counter is used to mark the theoretical position on an oscilloscope screen. The actual motor shaft position is displayed on the oscilloscope screen by means of a rotational variable differential transformer (RVDT) coupled to the stepping motor shaft.

Figure F.7 shows the experimental results, the theoretical results, the manufacturer published data, as well as the measured motor losses. The figure shows that the theoretical torque value have a maximum deviation of 10% from the measured torque values at very low stepping speeds. This is mainly due to the inaccuracy in measuring the motor losses at such low speeds, and the use of a linear regression to approximate the losses. At high stepping speeds there is good correlation between the theoretical and measured data.

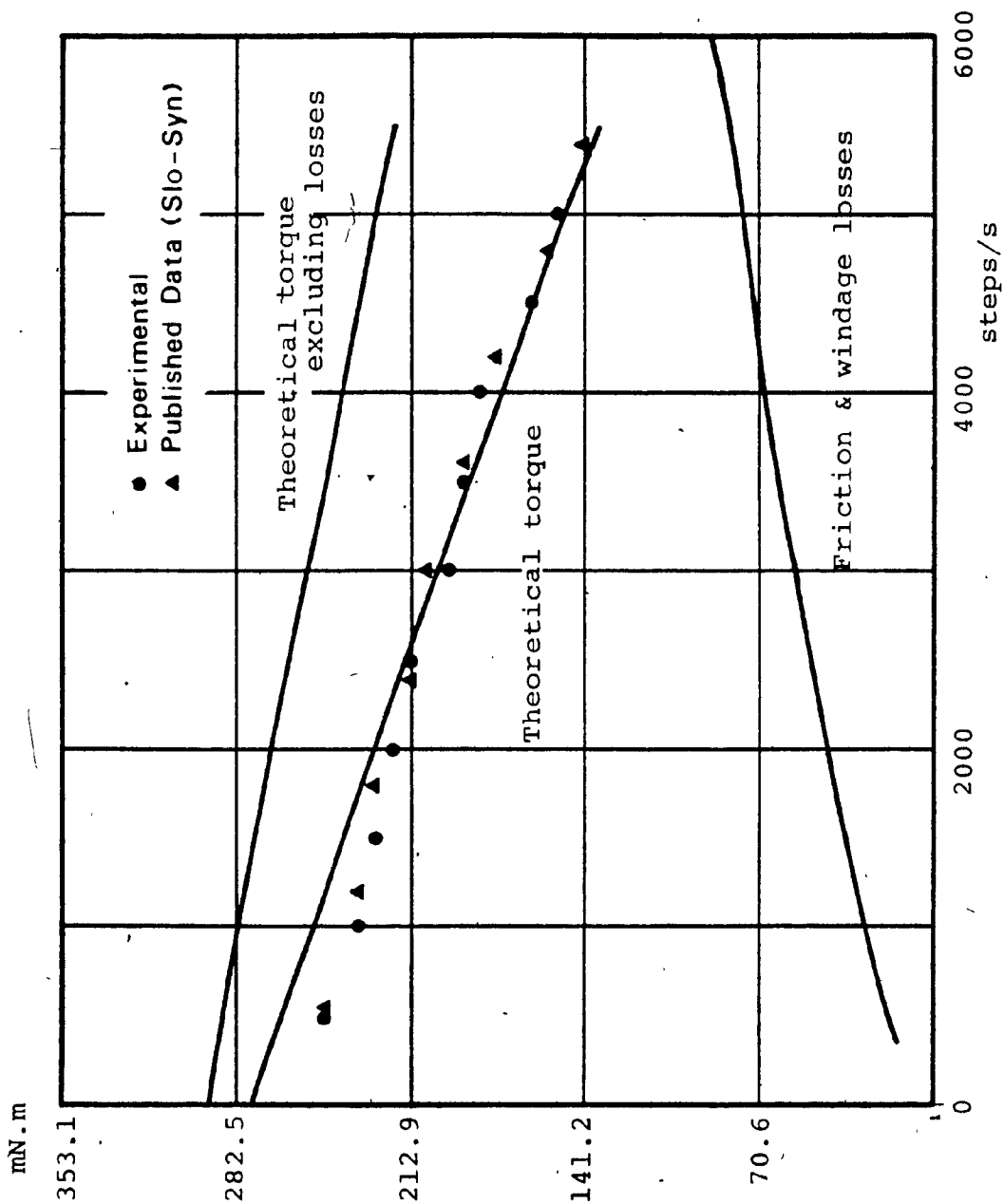


Figure F.7: Experimental and Theoretical Results for the Pull-Out Torque of a Stepping Motor.